Funktionelle Charakterisierung und Positionierung von *Drosophila* Cenp-C im Zentromer/Kinetochor-Komplex

Dissertation

zur Erlangung des Grades eines

Doktors der Naturwissenschaften

-Dr. rer. nat.-

der Fakultät für Biologie, Chemie und Geowissenschaften

der Universität Bayreuth

vorgelegt von

Sebastian Heeger

2006

Die vorliegende Arbeit wurde in der Zeit von Januar 2003 bis Dezember 2006 an der Universität Bayreuth am Lehrstuhl für Genetik unter der Betreuung von Prof. Dr. Christian F. Lehner angefertigt.

Vollständiger Abdruck der von der Fakultät für Biologie, Chemie und Geowissenschaften der Universität Bayreuth genehmigten Dissertation zur Erlangung des akademischen Grades eines Doktors der Naturwissenschaften (Dr. rer. nat.).

Promotionsgesuch eingereicht am: 06.12.2006

Erstgutachter: Prof. Dr. Christian F. Lehner

Zweitgutachter: Prof. Dr. Benedikt Westermann

Tag der mündlichen Prüfung: 05.02.2007

Danksagung

Diese Arbeit wurde am Lehrstuhl für Genetik der Universität Bayreuth unter der Anleitung von Prof. Dr. Christian F. Lehner angefertigt.
Bei Christian F. Lehner bedanke ich mich für die Betreuung meiner Promotion, für seine Anleitung zum selbständigen wissenschaftlichen Arbeiten, seine Hilfsbereitschaft und seinen Ideenreichtum in theoretischen und praktischen Aspekten der Arbeit sowie für seinen Enthusiasmus, der mir immer eine Motivation und ein Vorbild war.
Besonderer Dank gilt auch den derzeitigen und ehemaligen Mitarbeitern des Lehrstuhls für Genetik für ihre Diskussionsbereitschaft und Zusammenarbeit. Stefan Heidmann, Alf Herzig, Hubert Jäger und besonders Oliver Leismann haben mir immer hilfreich zur Seite gestanden. Rahul Pandey, Friederike Althoff, André Koch, Sebastian Götz und Ralf Schittenhelm danke ich für die Hilfe bei der Ausarbeitung dieses Manuskriptes. Brigitte Jaunich, Petra Helies und Katharina Neugebauer haben mir bei technischen Aspekten Hilfe geleistet.

Sehr dankbar bin ich des weiteren meinen Eltern Peter und Marianne Heeger für ihre stetige Unterstützung und Motivation.

Inhaltsverzeichnis

1 Summary

Faithful distribution of genetic information during mitosis is essential for the maintenance of genetic stability. In eukaryotes, sister chromatids of linear chromosomes are distributed to opposite poles by the mitotic spindle during anaphase. For this purpose, the spindle has to attach to specialized structures within the sister chromatids. In the following, these structures which are formed by centromeric DNA sequences and associated centromere/kinetochore proteins will be designated as the centromere kinetochore complex (CKC).

The basis of the CKC is formed by constitutive centromere proteins, which localize to the CKC throughout the cell cycle. A centromere-specific histone H3 variant, Cenp-A, has been the only known ubiquitous constitutive component until recently. With the identification of the strongly diverged *Drosophila* Cenp-C, an additional constitutive component was revealed here. The Cenp-C motif, the only brief stretch of amino acids present in all known Cenp-C homologs, was shown to be required for CKC localization. Analysis of the Cenp-C mutant phenotype demonstrated its essential role for the formation of a functional CKC.

During mitosis, the constitutive CKC components serve as a platform for the recruitment of the transient CKC components, which mediate the attachment to the spindle. Transient CKC components include the Ndc80 and MIND complexes. With the identification of *Drosophila* Ndc80 and MIND complex subunits (Ndc80, Nuf2, Spc25, Mis12, Nsl1, Nnf1a, Nnf1b) the notion of a conserved CKC design principle was further enforced here. Moreover, fluorescent fusion proteins of various CKC components were used to generate a CKC map at unprecedented resolution by microscopic analyses of novel preparations of native mitotic chromosomes.

The interaction between CKCs and the spindle is monitored by a surveillance mechanism called mitotic spindle checkpoint. Mitotic spindle checkpoint proteins concentrate on CKCs which have not yet been integrated properly into the mitotic spindle. Here, in vivo imaging was used to characterize the localization of the mitotic spindle checkpoint component Mps1 on the CKC. Moreover, the behavior of Cenp-C, the Ndc80 component Nuf2 and Mps1 was analyzed in response to spindle damage resulting from oxygen deprivation.

2 Zusammenfassung

Die korrekte Verteilung der genetischen Information während der Mitose ist wesentlich für den Erhalt der genetischen Stabilität. Die Chromatiden der linearen Chromosomen der Eukaryoten werden in der Anaphase durch die mitotische Spindel zu gegenüberliegenden Polen transportiert. Die Spindel greift hierbei an spezialisierten Strukturen der Schwesterchromatiden an. Diese Strukturen, bestehend aus der zentromeren DNS und angelagerten Zentromer- und Kinetochorproteinen, werden im Folgenden Zentromer/Kinetochor-Komplex (kurz CKC für "centromere kinetochore complex") genannt.

Die Basis des CKC bilden die konstitutiven Komponenten, welche während des gesamten Zellzyklus am CKC lokalisieren. Cenp-A, eine für das Zentromer spezifische Variante des Histon H3, war bis vor Kurzem die einzige bekannte ubiquitäre konstitutive Komponente des CKC. Mit der Identifizierung des stark abgeleiteten Cenp-C von *Drosophila* wurde eine weitere konstitutive Komponente enthüllt. Das Cenp-C-Motiv, das einzige kurze Stück mit konservierter Aminosäuresequenz unter den bekannten Cenp-C-Homologen, konnte als notwendig für die CKC-Lokalisierung bestätigt werden. Untersuchungen des Cenp-C-mutanten Phänotyps belegten die essentielle Rolle von Cenp-C beim Aufbau eines funktionellen CKC.

Während der Mitose dienen die konstitutiven CKC-Komponenten als Plattform für die Anlagerung transienter CKC-Komponenten, welche die Interaktion mit der Spindel vermitteln. Zu den transienten CKC-Komponenten gehören der Ndc80- und der MIND-Komplex. Die Identifizierung der Drosophila Ndc80- und MIND-Komplex-Untereinheiten (Ndc80, Nuf2, Spc25, Mis12, Nsl1, Nnf1a, Nnf1b) in dieser Arbeit bekräftigt die Existenz einer konservierten CKC-Struktur. Überdies wurden verschiedene fluoreszierende Fusionsproteine von CKC-Komponenten verwendet, um, nach mikroskopischer Untersuchung neuartig präparierter nativer mitotischer Chromosomen, eine Karte des CKC mit bisher ungekannter Auflösung zu erstellen.

Die Interaktion der CKC mit der Spindel wird von einem komplizierten Mechanismus überwacht, der Spindelkontrollpunkt genannt wird. Die Proteine des Spindelkontrollpunktes reichern sich an den CKC an, welche noch nicht korrekt in die Spindel integriert wurden. In vivo Mikroskopie wurde benutzt, um die CKC-Lokalisierung des Spindelkontrollpunktproteins Mps1 zu charakterisieren. Zudem wurde das Verhalten von Cenp-C, der Ndc80-Komplex-Komponente Nuf2 und Mps1 als Antwort auf eine beschädigte Spindel nach Sauerstoffentzug untersucht.

3 Einleitung

Die exakte Regulierung des Zellzyklus ist von entscheidender Bedeutung für die Erhaltung der genetischen Stabilität. Während der Synthese-Phase (S-Phase) wird die genetische Information verdoppelt, um in der Mitose gleichmäßig auf die beiden neu entstehenden Tochterzellen verteilt werden zu können. S-Phase und Mitose müssen für gewöhnlich strikt alternieren und keine der beiden darf stattfinden, ohne dass die vorherige korrekt beendet wurde.

In eukaryotischen Zellen kommt es in der S-Phase zur Beladung der DNS mit dem sogenannten Kohäsin (Michaelis et al., 1997; Uhlmann und Nasmyth, 1998; Toth et al., 1999). Dieses ist bis zur Mitose verantwortlich dafür, dass die Schwesterchromatiden eines Chromosoms miteinander verbunden bleiben. Während der Prophase wird in höheren Eukaryoten der Großteil des Kohäsins von den Chromosomen entfernt (Sumara et al., 2002). Verbleibendes Kohäsin befindet sich nun vornehmlich in der zentromeren Region (Abb. 1, Prophase). Die Kohäsion zwischen den Schwesterchromatiden ist wichtig für die Etablierung einer bipolaren Orientierung der Chromosomen in der mitotischen Spindel. Beide Schwesterchromatiden müssen mit Spindelfasern von gegenüberliegenden Polen verbunden sein (Abb. 1, Metaphase), um die korrekte Aufteilung der genetischen Information zu gewährleisten. Die Folge der bipolaren Orientierung des Chromosoms ist eine mechanische Spannung zwischen den verbunden Schwesterchromatiden. Ein komplexes regulatorisches System, der sogenannte Spindelkontrollpunkt ("spindle assembly checkpoint", SAC), kontrolliert sowohl, ob alle Chromatiden mit Spindelfasern verbunden sind, als auch, ob Spannung zwischen den Schwesterchromatiden wirkt. Nach Erfüllung dieser Kriterien wird das Protein Cdc20 (Fzy in *Drosophila melanogaster*) frei, um den APC/C ("anaphase promoting complex/cyclosome") zu aktivieren. Der APC/C ist eine Ubiquitin-Ligase und vermittelt den Abbau verschiedener Proteine. Eines der Zielproteine des APC/C ist das Securin (PIM in *D. melanogaster*). Der Abbau des Securins führt zur Aktivierung der Protease Separase (SSE in *D. melanogaster*). Separase spaltet eine Untereinheit des Kohäsins (Uhlmann et al., 1999), so daß die Schwesterchromatiden durch die Spindel zu den gegenüberliegenden Polen transportiert werden können (Abb. 1, Anaphase). PIM ist also verantwortlich, eine frühzeitige Aktivierung der Separase zu verhindern. Neben dem Securin verfügt

die Separase in *D. melanogaster* über eine weitere regulatorische Untereinheit, das Protein THR ("Three Rows"). Eine Aufgabe von THR hängt mit der Deaktivierung der Separase nach dem Meta-/Anaphasenübergang zusammen (Herzig et al., 2002).

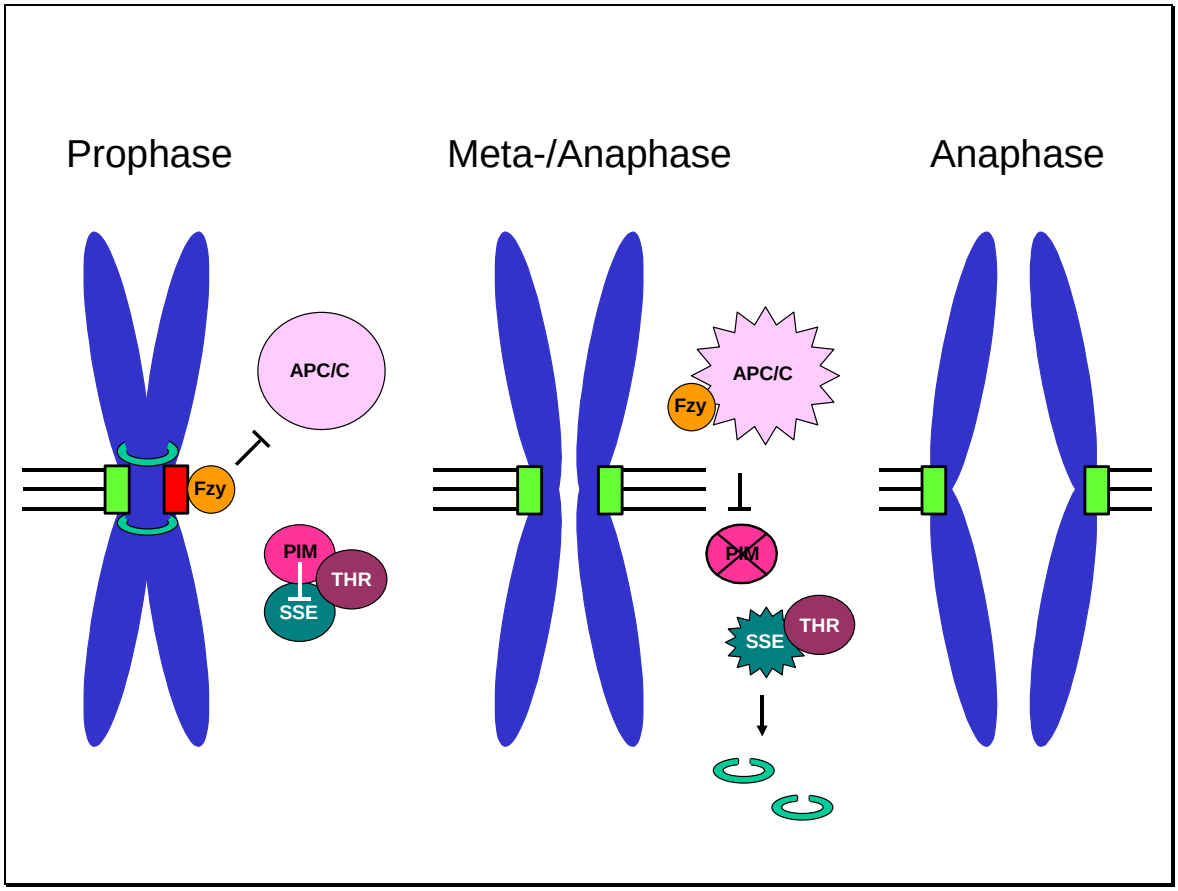

Abbildung 1. Schematische Darstellung eines mitotischen Chromosoms
Gezeigt ist ein Chromosom (blau) in der Prophase, an dem Meta-/Anaphasen-Übergang und in der Anaphase. Nicht bezeichnete Strukturen erklären sich wie folgt: grüne Ringe symbolisieren Kohäsin, schwarze Linien Mikrotubuli, hellgrün Rechtecke mit Mikrotubuli besetzte CKC und rote Rechtecke nicht besetzte CKC. Eine ausführliche Erklärung, unter anderem der Rollen der verschiedenen angedeuteten Proteine, findet sich im Text.

Eine zentrale Rolle bei der Schwesterchromatidentrennung kommt dem Zentromer oder auch Kinetochor zu, den Strukturen, welche Interaktion mit der mitotischen Spindel vermitteln. Die beiden Begriffe sind nicht klar voneinander zu unterscheiden und werden teils synonym, aber auch mit unterschiedlicher Bedeutung verwendet. Oft wird die grundlegende Struktur um die DNS als Zentromer und der Multiproteinkomplex, der während der Mitose hier assoziiert, als Kinetochor bezeichnet. Im Folgenden soll der Begriff CKC (für "centromere kinetochore complex", Zentromer/Kinetochor-Komplex) verwendet werden. Der CKC hat verschiedene Aufgaben. An ihm findet die Wechselwirkung der

gepaarten Schwesterchromatiden mit der mitotischen Spindel statt (Abb. 1). Zudem koppelt der CKC die Dynamik der Mikrotubuli-(+)-Enden mit der Bewegung der Chromatiden in der Mitose (Abb. 1, Anaphase). Obendrein werden hier die Spindelkontrollpunktsignale generiert, die den Eintritt in die Anaphase bis zum Zeitpunkt der bipolaren Orientierung aller Chromosomen in der mitotischen Spindel verzögern (Abb. 1, vergleiche Prophase und Meta-/Anaphase).

Strukturell beinhaltet der CKC den Teil der DNS, der als zentromere DNS (CEN DNS) bezeichnet wird und die Proteine, welche zwischen der CEN DNS und der Spindel vermitteln.

Soweit bekannt, gibt es im Reich der Eukaryoten zwei grundsätzlich verschiedene Arten von CEN DNS (für einen Überblick siehe Meraldi et al., 2006). In *Saccharomyces cerevisiae* und wenigen nah verwandten Spezies sind sehr kurze (~125 bp) und hoch konservierte CEN DNS (Punkt-CEN, "point CEN") notwendig und ausreichend, um einen CKC zu organisieren (Fitzgerald-Hayes et al., 1982). Im Gegensatz hierzu ist die Mehrzahl der bisher beschriebenen CEN DNS sehr viel länger und komplexer (regionale CEN, "regional CEN") und sehr viel weniger konserviert. Eine besondere Stellung nehmen hier Spezies wie z.B. *Caenorhabditis elegans* mit holozentrischen Chromosomen ein, deren CEN DNS über das ganze Chromosom verteilt ist (Maddox et al., 2004).

Die CEN DNS rekrutiert die CKC-Proteine. Die Proteinkomponenten des CKC können in mehrere Klassen unterteilt werden. Es gibt DNS-bindende und mit diesen assoziierte Proteine, welche während des gesamten Zellzyklus an der CEN DNS lokalisieren und daher konstitutiv genannt werden. Diesen gegenüber stehen die sogenannten transienten CKC-Komponenten, deren CKC-Lokalisierung vornehmlich während der Mitose stattfindet. Zu den transienten CKC-Komponenten gehören die Mikrotubuli-bindenden Proteine und solche, welche zwischen diesen und den konstitutiven CKC-Komponenten vermitteln. Die Proteine des Spindelkontrollpunktes lokalisieren ebenfalls transient am CKC.

In den letzten Jahren wurden bedeutende Fortschritte in der Aufklärung der CKC-Struktur erzielt. Eine ganze Reihe von CKC-Komponenten wurde identifiziert und Homologe von vielen dieser Komponenten wurden in verschiedenen Spezies nachgewiesen (für einen Überblick siehe Chan et al., 2005; Vos et al., 2006). Zur Zeit sind über 100 CKC-Komponenten bekannt und man geht davon aus, daß trotz

der unterschiedlichen Organisation der CEN DNS, der Satz und die Architektur der CKC-Komponenten im höchsten Maße konserviert ist.

Zu den konstitutiven CKC-Komponenten in Vertebraten gehört unter anderem Cenp-A (centromere protein A). Cenp-A ist ein Homolog des Histon-H3 und wird an dessen Stelle in die Nukleosomen der CEN DNS integriert. Cenp-A zeigt in der C-terminalen, sogenannten HFD ("histone fold domain") hohe Sequenzähnlichkeit mit Histon-H3. Im Gegensatz zum Histon-H3 hat es aber eine größere N-terminale Domäne, welche basierend auf Strukturanalysen aus dem Nukleosom herausragt (Luger et al., 1997) und als Plattform für die Interaktion mit weiteren CKC-Komponenten dient (Abb. 2). Cenp-A wurde in verschiedenen Spezies nachgewiesen (Cse4 in *S. cerevisiae*, Cnp1 in *Schizosaccharomyces pombe,* HCP-3 in *C. elegans* und Cid in *D. melanogaster* (Stoler et al., 1995; Takahashi et al., 2000; Buchwitz et al., 1999; Henikoff et al., 2000)). Es hat als grundlegendes Strukturelement des CKC viele Aufgaben, wie epigenetische Markierung der CEN DNS in Organismen mit regionaler CEN DNS und Rekrutierung weiterer CKC-Komponenten.

Eine weitere konstitutive CKC-Komponente ist Cenp-C. Cenp-C wird durch Cenp-A an den CKC rekrutiert (Liu et al., 2006; Abb. 2). Cenp-C wurde wie Cenp-A ursprünglich als humanes Autoantigen (Earnshaw und Rothfield, 1985; Saitoh et al., 1992) identifiziert. Humanes Cenp-C zeigt Sequenzhomolgie zu Proteinen anderer Spezies (Mif2 in *S. cerevisiae*, Cnp3 in *S. pombe,* HCP-4 in *C. elegans* und Cenp-C in Arabidopsis thaliana und Zea mays (Moore und Roth, 2001; Oegema et al., 2001; Dawe et al., 1999; Shibata und Murata 2004; Brown, 1995; Meluh und Koshland, 1995; Talbert et al., 2004)). Cenp-C in *D. melanogaster* war bis zum Beginn dieser Arbeit nicht identifiziert.

Neuere Studien (Cooper und Henikoff, 2004; Talbert et al., 2004) haben einen interessanten Aspekt bezüglich dieser beiden sehr basalen CKC-Komponenten aufgetan. Es scheint, als ob die schnelle Evolution der CEN DNS Sequenzen mit einer adaptiven Evolution von Cenp-A und/oder Cenp-C einhergeht. Diese Theorie bringt die vergleichsweise geringe Konservierung der CKC-Komponenten mit ihrer Funktion in dem so ursprünglichen und wichtigen Vorgang der Mitose in Eintracht. Genau dieser Umstand ist auch ursächlich für die Nichtidentifizierung von Cenp-C in *D. melanogaster* bis zum Beginn dieser Arbeit.

Zu den transienten CKC-Komponenten mit Vermittlerfunktion zwischen den konstitutiven und den Mikrotubuli-bindenden Proteinen zählen der Ndc80- und der MIND-Komplex.

Der Ndc80-Komplex besteht aus vier Untereinheiten und wurde in *S. cerevisiae* und humanen Zellkulturen am eingehendsten untersucht (Ciferri et al., 2005; Wei et al., 2005; Wei et al., 2006). Die vier Untereinheiten sind Ndc80/Hec1, Nuf2, Spc25 und Spc24. Der Ndc80-Komplex bildet eine längliche hantelähnliche Struktur aus, wobei Ndc80 und Nuf2 das eine und Spc25 und Spc24 das andere Ende formen. Die Dimension dieser Struktur beträgt nach elektronenmikroskopischen (EM-) und "scanning force"-mikroskopischen (SFM-) Analysen etwa 50 nm (Ciferri et al., 2005; Wei et al., 2005). Es gibt Indizien für eine polarisierte Integration dieses Komplexes in den CKC. So lokalisiert humanes Hec1 in der äußeren Platte (Abb. 3) des CKC (DeLuca et al., 2005) und Nuf2 bindet an Dam1 in *S. cerevisiae* (Shang et al., 2003), einem Mikrotubuli-assoziierten Protein. Zudem ist nach RNAi-vermittelter Depletion ("RNA interference") von humanem Spc25 in Zellkultur keine CKC-Lokalisierung von Hec1 mehr nachweisbar (Bharadwaj et al., 2004). Diese Ergebnisse unterstützen die Hypothese, der Ndc80-Komplex läge mit Spc24 und Spc25 in Richtung des Chromatins und mit Ndc80/Hec1 und Nuf2 in Richtung der Mikrotubuli polar im CKC, beweisen diese Hypothese aber nicht.

Ein weiterer Proteinkomplex mit transienter CKC-Lokalisierung ist der MIND-Komplex. Er besteht ebenfalls aus vier Untereinheiten. Mis12/Mtw1, Nsl1, Nnf1, Dsn1 konnten mittlerweile in *S. cerevisiae* (Euskirchen, 2002; De Wulf et al., 2003), *S. pombe* (Obuse et al., 2004) und in *Homo sapiens* (Kline et al., 2006). identifiziert werden. Während der Ndc80-Komplex wie die meisten der transienten CKC-Komponenten nur während der Mitose am CKC lokalisiert ist, zeigt der MIND-Komplex CKC-Lokalisierung während des gesamten Zellzyklus außer in der Telophase der Mitose (Kline et al., 2006; McAinsh et al., 2006). Des weiteren nimmt der MIND-Komplex eine Sonderstellung ein, insofern eine seiner Untereinheiten Mis12 in ihrer Lokalisierung als abhängig von HP1 (Heterochromatinprotein 1) und Cenp-A beschrieben wurde (Obuse et al., 2004; Liu et al., 2006) während alle anderen CKC-Komponenten nicht auf HP1 angewiesen sind.

Neben diesen transienten Strukturproteinen des CKC sind auch die Proteine des Spindelkontrollpunktes transient CKC-lokalisiert. Eines der Spindelkontrollpunkt-proteine ist Mps1 (monopolar spindle 1). Mps1 wurde in *S. cerevisiae* entdeckt (Winey et al., 1991). Mps1-Funktionen wurden diskutiert im Zusammenhang mit dem Zentrosomenzyklus. Es hat eine entscheidende Rolle im Spindelkontrollpunkt und ihm werden auch noch bislang unbekannte, kontrollpunktunabhängige Funktionen zugesprochen. Die wichtige Stellung von Mps1 im Spindelkontrollpunkt wird verdeutlicht durch den Metaphasenarrest infolge von Überexpression des Proteins (Hardwick et al., 1996). Da dieser Arrest abhängig von anderen Kontrollpunktproteinen ist, kommt Mps1 wahrscheinlich eine Rolle am Anfang der Signalkette zu, die zum Arrest führt.

Neben der Identifizierung und Charakterisierung der einzelnen CKC-Komponenten ist von entscheidendem Interesse, wie diese Komponenten zusammenwirken, um den CKC aufzubauen. Um die Struktur des CKC aufzuklären, wurden verschiedene Experimente durchgeführt. Genaue Analysen über die Zeitfenster der CKC-Lokalisierung der verschiedenen transienten CKC-Komponenten und Untersuchungen über gegenseitige Abhängigkeiten in der Lokalisierungs-kompetenz der Komponenten vermittelten ein hierarchisches Bild der CKC-Struktur (für einen Überblick siehe Liu et al., 2006). Cenp-A steht demnach an der Spitze der Hierarchie und rekrutiert über verschiedene Wege alle anderen CKC-Komponenten. Die anderen konstitutiven CKC-Komponenten folgen Cenp-A in der Hierarchie. Die verschiedenen Rekrutierungswege verzweigen sich zusehends und bilden gelegentlich auch Verbindungen untereinander aus. Abbildung 2 zeigt eine CKC-Karte, die mit Hilfe solcher Untersuchungen erstellt wurde. Einbezogen einige der in dieser Arbeit behandelten Proteine und jene, die für deren Vernetzung wichtig sind.

Diese Daten können allerdings nur bedingt in eine räumliche Struktur übersetzt werden. Das zeitlich versetzte Auftreten der verschiedenen Komponenten am CKC sowie die Abhängigkeiten bei der Lokalisierung verschiedener Komponenten voneinander suggerieren ihre räumliche Anordnung, beweisen sie aber nicht. Im besten Falle sind sie korrekt im Bezug auf die Abfolge der Proteine im CKC entlang einer Achse für einen der verschiedenen Rekrutierungswege. Sie geben aber keinesfalls eine Auskunft über die Abundanz der einzelnen Proteine, ihre

Entfernungen zueinander oder eine eventuell sehr komplexe räumliche Anordnung der Komponenten.

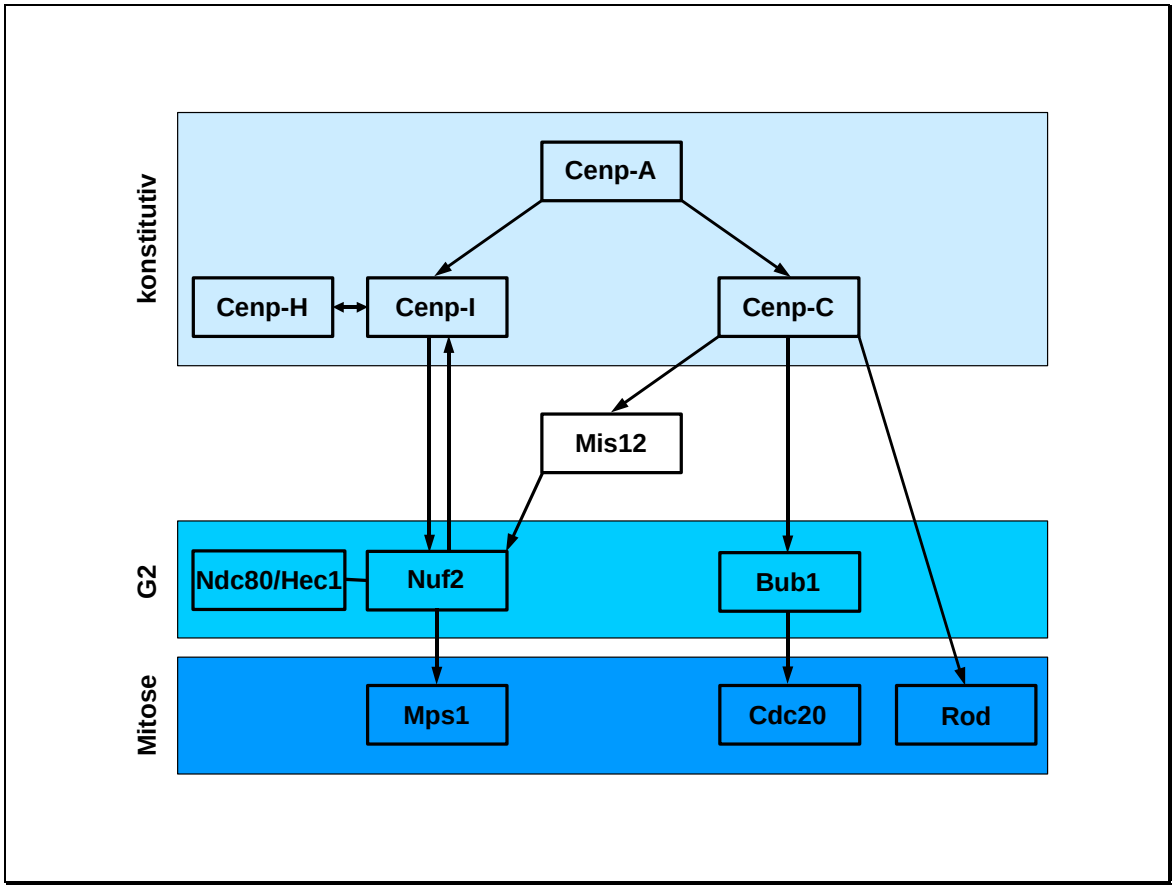

Abbildung 2. Schematische Darstellung einer CKC-Karte

Untersuchungen der gegenseitigen Abhängigkeiten bei der Lokalisierung sowie der Zeitfenster der CKC-Lokalisierung verschiedener CKC-Komponenten ergeben ein hierarchisches Bild. Die konstitutiven CKC-Komponenten stehen dabei an erster Stelle und rekrutieren über vielfältige, sich verzweigende und wieder zusammenlaufende Wege alle anderen CKC-Komponenten. Dargestellt sind einige der in dieser Arbeit besprochenen und die für deren Rekrutierung wichtigen Proteine. Die Pfeile geben Abhängigkeiten an und die farbigen Boxen symbolisieren den Beginn der CKC-Lokalisierung der CKC-Komponenten. (verändert nach Liu et al., 2006)

Von großer Hilfe bei der Aufklärung der CKC-Struktur waren den bereits beschriebenen auch EM-Analysen. Diese sind vornehmlich im Vertebratensystem durchgeführt worden und vermitteln eine Vorstellung vom strukturellen Auf-, Um- und Abbau des CKC im Verlauf der Mitose (für einen Überblick siehe Rieder, 1982). Die Abbildung 3 dokumentiert schematisch die im EM sichtbaren Strukturen in verschiedenen Phasen der Mitose. Während der Prophase bildet sich an der primären Einschnürung der Chromosomen eine kugelförmige Struktur, welche als Kinetochorball bezeichnet wird (Abb. 3, Prophase, grüner Kreis). Nach dem Zusammenbruch der Kernhülle in der Prophase differenziert sich eine elektronendichte Kinetochorplatte mit einer Schichtdicke von etwa 25-40 nm (Abb.

3, Prometaphase, grünes Rechteck). Diese ist durch eine etwa genauso breite, aber weniger elektronendichte Zone (schraffiert Rechteck) von dem ebenfalls sehr elektronendichten Chromatin (blau) getrennt. Von der Platte aus erstreckt sich die wenig geordnete, sogenannte fibrilläre Corona, die bis zu 250 nm dick sein kann (gelb). Nach dem Anheften der mitotischen Spindel am CKC in der Metaphase verkleinert sich die fibrilläre Corona und eine trilaminare Struktur wird erkennbar (Abb. 3, Metaphase). Auf das Chromatin folgt die elektronendichte innere Platte mit etwa 40 nm Dicke (rot) dann eine weniger dichte Zwischenzone (kariert) mit etwa 40 nm Dicke und schließlich die äußere elektronendichte Platte mit nochmals etwa 40 nm Dicke (dunkelgrün). Die angreifenden Mikrotubuli enden in der äußeren Platte (schwarze Linien).

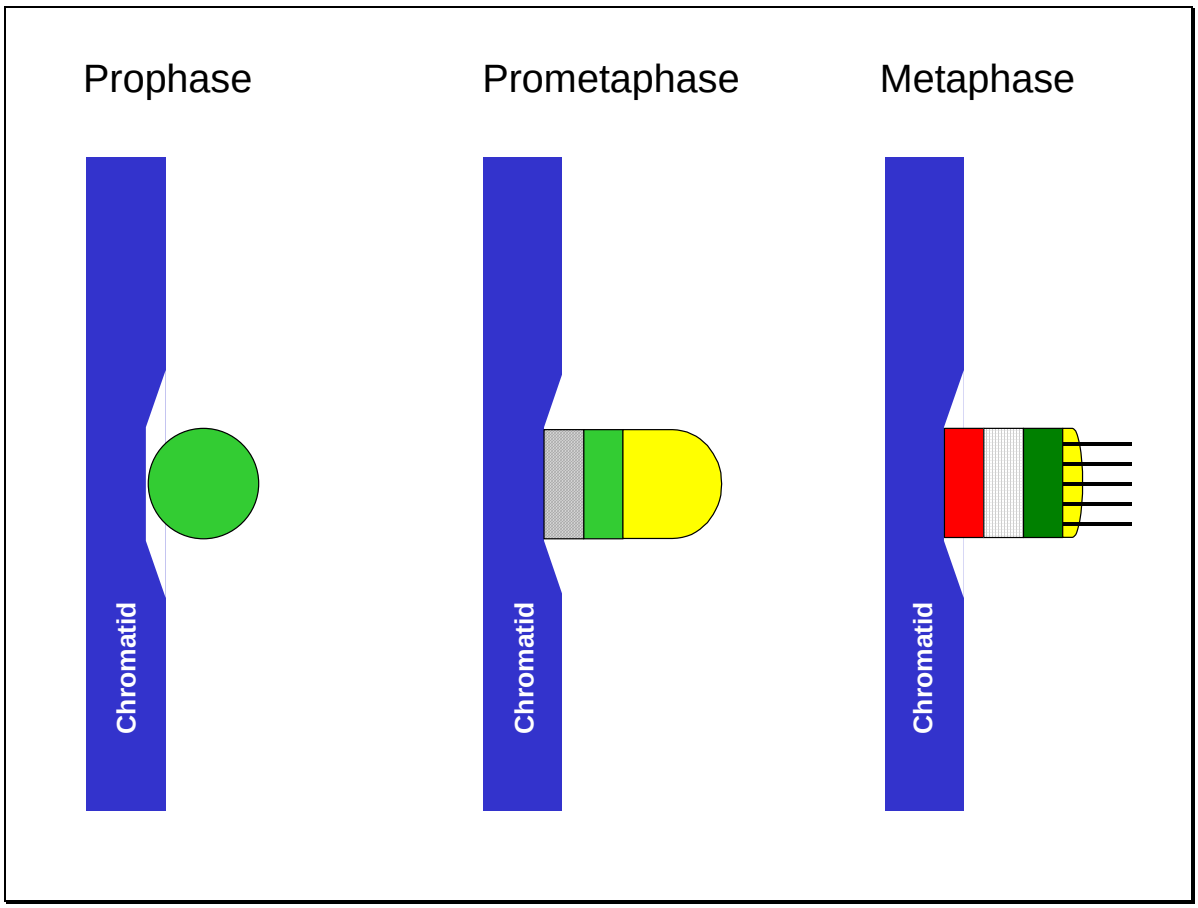

Abbildung 3. Schematische Darstellung der im EM sichtbaren CKC-Strukturen

Dargestellt ist ein einzelnes Chromatid (blau) in der Pro-, Prometa- und Metaphase. Die Formation und Reifung der CKC-Strukturen geschieht an der primären Einschnürung des Chromatids. Die schwarzen Linien in der Metaphasenabbildung repräsentieren Mikrototubuli, die farbigen und gemusterten Elemente deuten die im EM sichtbaren Strukturen an. Eine ausführliche Erklärung findet sich im Text. (frei nach Rieder, 1982)

Mit Hilfe von Immun-EM-Untersuchungen konnten verschiedene CKC-Komponenten in den unterschiedlichen Bereichen der trilaminaren Struktur der Metaphasen-CKC lokalisiert werden. Dies führte zur Einteilung der CKC-Proteine

in innere und äußere CKC-Komponenten. Ndc80/Hec1 gehört so zum Beispiel zu den äußeren Komponenten (DeLuca et al., 2005).

Neuere EM-Untersuchungen beschreiben die Verhältnisse in *D. melanogaster* als vergleichbar mit den hier dargestellten Ergebnissen in Vertebraten (Maiato et al., 2006).

Viele der CKC-Komponenten sind in Organismen wie *S. cerevisiae*, *S. pombe* und im Menschen entdeckt und untersucht worden. Ihre Homologen in *D. melanogaster* blieben lange unentdeckt. Mittlerweile haben bioinformatische Methoden zur Identifizierung einiger CKC-Komponenten in *D. melanogaster* geführt (Meraldi et al., 2006). Dennoch sind hier viele der bekannten CKC-Komponenten noch unentdeckt, da sich die Homologen bioinformatisch nicht identifizieren lassen. Der Grund hierfür ist eine starke Ableitung der CKC-Komponenten in *D. melanogaster*.

4 Problemstellung

Der CKC ist eine essentielle chromosomale Struktur. In jeder mitotischen und meiotischen Teilung aller eukaryotischen Zellen greift die Spindel am CKC an, um die erforderliche Verteilung der genetischen Information zu vollziehen. Trotz der fundamentalen Bedeutung des CKC für die Erhaltung der genetischen Stabilität sind seine Komponenten nur wenig konserviert. Eine adaptive Evolution der CKC-Komponenten gegenüber den ihnen zugrunde liegenden DNS-Sequenzen hat zu einer ungewöhnlich hohen Abweichung in den Sequenzen der Gene und Proteine geführt. Dennoch scheint die Architektur des CKC in allen Eukaryoten grundsätzlich gleich.

Ziel dieser Arbeit war die Identifizierung von bisher in *D. melanogaster* unbekannten CKC-Komponenten und die Ergründung ihrer funktionellen und strukturellen Eigenschaften. Aufbauend auf diesen Erkenntnissen galt es, die Architektur und Funktion des CKC von *D. melanogaster* besser zu verstehen und Parallelen und Abweichungen zu anderen Modellorganismen zu beschreiben.

Zum Beginn dieser Arbeit waren viele der Spindelkontrollpunktproteine aber unter den konstitutiven CKC-Komponenten nur Cenp-A in *D. melanogaster* bekannt. Die Identifizierung und detaillierte Charakterisierung von *D. melanogaster* Cenp-C ist Gegenstand der Teilarbeit A.

Aus der Gruppe der transienten strukturellen CKC-Komponenten ist zu Beginn dieser Arbeit kein einziger Vertreter in *D. melanogaster* bekannt gewesen. Die Identifizierung von Untereinheiten des *D. melanogaster* Ndc80- und MIND-Komplexes sowie die Anwendung einer neuartigen Kombination von Präparation und Mikroskopie von nativen mitotischen Chromosomen zur Vermessung des CKC mit einer Auflösung im Nanometerbereich ist beschrieben in der Teilarbeit B.

Auf die Rolle des transienten CKC- und Spindelkontrollpunktproteins Mps1 von *D. melanogaster* bei der Arretierung der Metaphase in den drei nichtgenutzten Produkten der weiblichen Meiose und nach Sauerstoffentzug während der Embryonalentwicklung wird eingegangen in der Teilarbeit C.

Eine Beschreibung der Vorgänge, Zusammenstellung der einbezogenen Proteine und Darstellung des Mechanismus, welche zu dem Metaphasenarrest nach Sauerstoffentzug führen wird gegeben in der Teilarbeit D.

5 Ausführliche Darstellung der Ergebnisse und Diskussion

5.1 Identifizierung genetischer Interaktionspartner der regulatorischen Untereinheiten der Separase

Die Separase in *D. melanogaster* hat zwei bekannte regulatorische Untereinheiten, die Proteine PIM und THR. Das Securin PIM verhindert eine vorzeitige Aktivierung der Separase. Das Protein THR, welches nur in *D. melanogaster* vorkommt, zeigt Übereinstimmungen mit der N-terminalen Region anderer bekannter Separasen und hilft bei der Inaktivierung der Separase nach dem Meta-/Anaphasenübergang. Beide Proteine sind allerdings auch notwendig für die Aktivierung der Separase (Funabiki et al., 1996; Stratmann und Lehner, 1996). Dieser positive Effekt der regulatorischen Untereinheiten auf die Separase ist bislang unverstanden und es galt, die Frage nach weiteren involvierten Proteinen zu beantworten.

Hierzu wurde nach genetischer Interaktion von *pim* und *thr* mit anderen chromosomalen Bereichen gesucht (A, Fig. 1A). Die ektopische Expression von PIM oder THR∆C, einer C-terminal verkürzten Version von THR, im Auge von *D. melanogaster* verursacht einen anomalen Phänotyp. Nach Herabsetzen der Gendosis bestimmter Loci durch Einkreuzen von Defizienzen wird nach Verstärkung oder Abschwächung des ursprünglichen Augenphänotyps gesucht. Im Zuge dieser Arbeiten wurde die Defizienz *Df(3R)p-XT103* als dominanter Verstärker des Überexpressionsphänotyps von PIM und THR∆C gefunden. Komplementationsanalysen mit überlappenden Defizienzen führten zur Eingrenzung der interagierenden Region (A, Fig. 1B). Zur Identifizierung des genauen Lokus wurden Letalmutationen, welche in die entsprechende Region kartiert worden waren (Jones und Rawls, 1988) auf Modifizierung getestet. Die Letalmutation *l(3)85Aa*^{prl41} wurde so als verantwortlicher Lokus identifiziert. Positionelle Klonierung bestätigte *CG31258* als das Gen mit wildtypischer *l(3)85Aa*^{prl41} -Funktion.

5.2 Identifizierung von *D. melanogaster* Cenp-C

Zur Untersuchung der zellulären Funktion von *CG31258* wurde zuerst die Lokalisierung des Proteins festgestellt. Hierzu wurden Antikörper gegen das Protein generiert und Transgene etabliert, welche detektierbare Fusionsproteine kodieren. Als Epitopmarkierungen wurden EYFP und EGFP ("enhanced yellow/green fluorescent protein") verwendet. Immunfluoreszenzmarkierungen des endogenen Proteins sowie der Transgenprodukte und *in vivo*-Mikroskopie von Embryonen, die ein funktionelles EYFP-Fusionsprotein exprimierten, zeigten, daß es sich bei CG31258 um eine konstitutive CKC-Komponente handelt (A, Fig. 2A).
Vergleiche mit den Sequenzen anderer Drosophiliden ließen einige konservierte Bereiche erkennen. Einer dieser Bereiche erwies sich als abgeleitetes Cenp-C-Motiv (A, Fig. 4B).
Aufgrund dieser Erkenntnisse und unter Beachtung der folgenden funktionellen Untersuchungen wurde das Protein *Drosophila* Cenp-C genannt.

5.3 Homologien und funktionelle Bereiche von *D. melanogaster* Cenp-C

Vergleiche der DNS- und Proteinsequenzen von *D. melanogaster* Cenp-C mit denen anderer Drosophiliden zeigten einige konservierte Bereiche. Die Konservierung gegenüber Cenp-C anderer Metazoen ist wesentlich geringer. Zum Teil waren die konservierten Bereiche konsistent mit Vorhersagen über funktionelle Bereiche, welche aufgrund der Primärsequenz getroffen werden konnten (Übersicht in A, Fig. 4A).
So findet sich im N-Terminus eine Arginin-reiche Region (RRR, R reiche Region). Diese ist charakteristisch für Cenp-C in Drosophiliden und könnte DNS-bindende Eigenschaften haben. Eine weitere Region im N-terminalen Drittel des Proteins ist für die Drosophiliden charakteristisch. Für diese gab es keine funktionelle Vorhersage. Sie wurde als Drosophila-Homologie-Region (DH) bezeichnet. *D. melanogaster* Cenp-C weist zwei vorhergesagte "AT hooks" (AT) auf, die selbst unter den Drosophiliden wenig konserviert sind. Diese Motive könnten Bindung an die kleine Furche AT-reicher DNS-Sequenzen vermitteln, die im zentromeren Heterochromatin vorkommen. Im C-Terminus wird eine NLS (Nukleus-Lokalisierungs-Sequenz) vorhergesagt, die ebenfalls nur unter den Drosophiliden

konserviert ist. Außerdem befindet sich hier das abgeleitete Cenp-C-Motiv, das in allen bisher identifizierten Cenp-C-Proteinen hoch konserviert ist. Im C-Terminus weicht die Drosophiliden-Konsensussequenz des Cenp-C-Motivs allerdings von der anderer Spezies ab (A, Fig. 4B). Der äußerste C-Terminus des Proteins zeigt beträchtliche Konservierung unter den Drosophiliden und auch zu den Cenp-C-Proteinen anderer Metazoen. Funktionelle Vorhersagen für diese Domäne gibt es nicht.

Eine funktionelle Bedeutung der erwähnten Elemente wurde mittels ektopischer Expression getestet (A, Fig. 5). Ein Überschuß an funktionellem oder nur bedingt funktionellem Protein am falschen Ort verursacht einen anomalen Phänotyp. Nach ektopischer Expression des intakten Cenp-C-Proteins ergab sich ein anomaler Phänotyp im Flügel nicht aber im Auge (A, Fig. 5, FL ("full length"). Dies spricht eventuell für eine Titration von Bindungspartnern durch nicht CKC-gebundenes Cenp-C. Da kein Unterschied zwischen den Phänotypen, verursacht durch ektopische Expression von Cenp-C und EGFP-Cenp-C, zu erkennen war (A, Fig. 5, vergleiche FL und E-FL), scheint der Anteil der EGFP-Markierung an diesem Effekt gering zu sein. Die ektopische Expression des nicht konservierten zentralen Teils des Proteins hatte keinen Effekt (A, Fig. 5, E-M). Den anomalsten Phänotyp verursachte die ektopische Expression des C-terminalen Drittels von Cenp-C und eines kleineren Teils des C-Terminus, welche beide das Cenp-C-Motiv umfassen (A, Fig. 5, E-C und E-CN), das, wie später beschrieben, die CKC-Lokalisierung verursacht. Dies spricht für eine Besetzung der Cenp-C-Bindungsstellen im CKC durch nicht vollständig funktionelles Protein. Einen ebenfalls deutlichen Phänotyp verursachte die ektopische Expression des N-terminalen Drittels (A, Fig. 5, E-N), welche die konservierten RRR- und DH-Motive umfaßt. Hierbei könnte es sich ebenfalls um einen Effekt durch Titration handeln, was für eine Protein-Protein-Wechselwirkung in dieser Domäne spräche. Zusammengefaßt deuten diese Ergebnisse auf eine Dreiteilung des Proteins in die C-terminale Region mit CKC-Bindungsfunktion, die zentrale Region mit Brückenfunktion und die N-terminale Region mit Rekrutierungsfunktion hin.

5.4 Identifizierung der CKC-Lokalisierungsdomäne von Cenp-C

Wie bereits beschrieben, wurden verschiedene induzierbare Transgene produziert, die Fusionsproteine von EGFP mit Teilen des Cenp-C-Proteins kodieren. Diese wurden verwendet, um die CKC-Lokalisierungsdomäne von Cenp-C einzugrenzen. Nach Expression in der Epidermis von *D. melanogaster*-Embryonen wurde die CKC-Lokalisierung der Produkte untersucht (A, Fig. 3).
Der N-terminale und der zentrale Teil des Cenp-C-Proteins zeigten keine CKC-Lokalisierung. Das intakte Protein und der C-terminale Teil hingegen konnten am CKC nachgewiesen werden (A, Fig. 3B, C+). Eine weitere Eingrenzung gelang mit der Untersuchung von drei Teilen des C-Terminus, bei der nur der N-terminale Teil des C-Terminus CKC-Lokalisierung zeigte (A, Fig. 3B, CN+). Cenp-C-Versionen, denen der N-Terminus, AT1, NLS oder AT2 fehlen, konnten alle noch an den CKC binden. C-terminal verkürzte Versionen, welche die vorzeitigen Stop-Mutationen in den beiden bekannten Allelen *Cenp-C*^{prl41} und *Cenp-C*^{IR35} repräsentieren, verloren ihre Fähigkeit, an den CKC zu binden. Somit liegt die CKC-Lokalisierungsdomäne in der N-terminalen Hälfte des C-terminalen Drittels des Proteins (CN).
Um diesen Bereich noch weiter eingrenzen zu können, wurde eine sättigende Zufallsmutagenese der CN-Region vorgenommen (A, Fig. 3C und D). Alle gefundenen vorzeitigen Stop-Mutationen bis zu der Aminosäureposition 1084 führten zum Verlust der CKC-Bindung. Ein Stop an Position 1192 hatte hingegen keinen Effekt. Somit konnte die CKC-Lokalisierungsdomäne von *D. melanogaster* Cenp-C auf die Aminosäuren 1085 bis 1191 bestimmt werden. Die einzige Punktmutation, die zum Verlust der CKC-Bindung führte, resultierte in einem Austausch des Arginin 1101 zu Glutamat. Dieser Rest ist in allen bekannten Cenp-C-Motiven invariabel. Somit kommt dem Cenp-C-Motiv die Rolle der CKC-Bindung zu, was auch dessen hohe Konservierung erklären könnte.

5.5 Phänotypische Konsequenzen von *Cenp-C*-Mutationen

Beide verfügbaren Allele von Cenp-C, *Cenp-C*^{prl41} und *Cenp-C*^{IR35}, kodieren verkürzte Proteine durch vorzeitige Stopkodons. Statt für die 1411 Aminosäuren des wildtypischen Cenp-C kodieren die offen Leseraster der Allele nur 1106 bzw.

857 Aminosäuren. Lokalisierungsexperimente mit analogen EGFP-markierten Transgenen zeigten keine CKC-Lokalisierung der entsprechenden Produkte.

Erste augenscheinliche Defekte treten in homo- und transheterozygoten Embryonen in der epidermalen Mitose 16 auf. Bis zu diesem Zeitpunkt ist die maternale Kontribution im Embryo wahrscheinlich ausreichend für einen problemfreien Ablauf der Mitosen. Die Defekte in Abwesenheit von Cenp-C äußern sich in Chromatinbrücken während Ana- und Telophasen. Diese Brücken zeigen meist ein bis wenige CKC-Signale in ihrer Mitte (A, Fig. 6C). Eine genauere Untersuchung der Mitose 16 mittels *in vivo*-Mikroskopie (A, Fig. 7A) ergab eine verlängerte Zeitspanne von der Pro- bis zum Ende der Metaphase (A, Fig. 7B) und einen verkleinerten Zwischen-CKC-Abstand, was auf einen Defekt während der Anheftung der Spindel an den CKC und somit in der Kongression der Chromosomen hindeutet (A, Fig. 7C). Nur einige der epidermalen Zellen zeigen phänotypische Veränderungen. Ein klar anomaler Phänotyp tritt später während der Embryonalentwicklung im zentralen Nervensystem (ZNS) auf. Einige Zellen des Nervensystems durchlaufen noch Mitosen, wenn der überwiegende Teil der anderen Zellen bereits postmitotisch ist. Dieser Umstand wird im Wildtyp begleitet von einem Rückgang des nachweisbaren Proteins (A, Fig. 2B und C). In der Mutante ist der Pegel an Cenp-C während der späteren Mitosen im ZNS so weit herabgesetzt, daß ein anomaler Phänotyp auftritt. Dieser äußert sich in einer großen Anzahl sehr kleiner Kerne, welche typisch für Apoptose sind. Außerdem scheint der DNS-Gehalt der Zellen sehr unterschiedlich zu sein, was auf eine Fehlverteilung der DNA in vorherigen Zyklen zurückzuführen ist. Des weiteren reichern die Zellen Cyclin B an und die Kerndichte ist herabgesetzt (A, Fig. 6A).

Expression von wildtypischem und EGFP-markiertem Cenp-C im ZNS von mutanten Embryonen vermag diesen Phänotyp zu revertieren (Daten nicht gezeigt). Dies ist auch der Fall für die Expression einer Cenp-C-Variante, die das vorhergesagte AT1-Motiv nicht beinhaltet (A, Fig 2A).

Expression von Transgenen mit fehlendem N-Terminus, AT2-Motiv oder NLS, sowie Expression des N- oder C-terminalen und mittleren Drittels von Cenp-C führen nicht zu einer Reversion des mutanten Phänotyps im ZNS. Daraus kann geschlußfolgert werden, daß ihnen wichtige Elemente fehlen. Der N-Terminus, das AT2-Motiv sowie das NLS haben also essentielle Funktionen.

5.6 Genetische Interaktion mit *D. melanogaster Cenp-A* und *Cenp-C*

Da Vertebraten-Cenp-C als in seiner Lokalisierung abhängig von Cenp-A beschrieben wurde (Liu et al., 2006), wurde diese Anhängigkeit in *D. melanogaster* getestet. Cenp-A mutante Embryonen entwickeln aufgrund der maternalen Kontribution ebenfalls erst gegen Ende der Embryogenese einen Phänotyp. Zum Zeitpunkt der epidermalen Mitose 16 gibt es keine phänotypischen Auffälligkeiten, und doch ist die Intensität der Cenp-C Signale bereits um ein Vielfaches geringer als in wildtypischen Embryonen (A, Fig. 2E, vergleiche cid^+ und cid^-). Die Cenp-A- Signale in Cenp-C-Mutanten waren hingegen stabil (Daten nicht gezeigt). Die CKC-Lokalisierung von Cenp-C ist also auch in *D. melanogaster* von Cenp-A abhängig und die CKC-Lokalisierung von Cenp-A ist unabhängig von Cenp-C.

Zusätzlich wurde auch eine genetische Interaktion von *Cenp-A* und *Cenp-C* nachgewiesen. Analog der ektopischen Expression von PIM und THRΔC verursacht auch eine ektopische Expression von Cenp-A im Auge von *D. melanogaster* einen anomalen Phänotyp. Die Herabsetzung der Kopienzahl an wildtypischem *Cenp-C* bedingt eine Verstärkung dieses Phänotyps (A, Fig. 2F).

Dieses Ergebnis wird im Lichte der Abhängigkeit der Cenp-C-Lokalisierung von Cenp-A erwartet. Warum jedoch *Cenp-C* als mit *pim* und *thr* interagierender Lokus identifiziert wurde, ist nicht offensichtlich. Eine mögliche Erklärung ist, daß eine von Cenp-C abhängige CKC-Lokalisierung der Separase in der Metaphase nötig ist, um die Spaltung des verbliebenen zentromeren Kohäsins zu ermöglichen. Diese Theorie würde auch den positiven Effekt von PIM und THR auf die Aktion der Separase erklären, wenn diese regulatorischen Untereinheiten Vermittler einer von Cenp-C abhängigen Lokalisierung der Separase wären.

5.7 Identifizierung transienter CKC-Komponenten in *D. melanogaster*

Bis zu dem Zeitpunkt dieser Analysen waren nur wenige der CKC-Komponenten von *D. melanogaster* bekannt. Cenp-A und Cenp-C sowie viele der Spindel-kontrollpunktproteine waren beschrieben. Es gab jedoch keine Kenntnis von den Homologen der Komponenten des Ndc80- und MIND-Komplexes. Bioinformatische Methoden waren wegen der hohen Divergenz in den

Primärsequenzen nur begrenzt hilfreich beim Auffinden von CKC-Komponenten in *D. melanogaster*. Neuerliche Versuche, bei denen nur konservierte Blöcke bekannter Homologe als Matrize verwendet wurden, waren erfolgreich bei der Identifizierung der Ndc80-Komplex-Untereinheiten Ndc80, Nuf2 und Spc25 sowie der MIND-Komplex-Untereinheit Mis12 (Meraldi et al., 2006).

CG9938, *CG8902* und *CG7242,* welche so als die Homologen von *D. melanogaster* Ndc80, Nuf2 und Spc25 postuliert wurden, zeigten auch in einem genomweiten "Yeast Two Hybrid" Experiment in *D. melanogaster* die somit erwartete Interaktion (Giot et al., 2003). Da Ndc80, Nuf2 und Spc25 Untereinheiten des Ndc80-Komplexes sind, dessen Lokalisationsverhalten in verschiedenen Vertebratensystem bereits beschrieben war, wurde die intrazelluläre Lokalisierung dieser *D. melanogaster*-Proteine untersucht. In Schneiderzellen und Embryonen konnten die Produkte fluoreszenzmarkierter Transgene als nur während der Mitose CKC-lokalisiert nachgewiesen werden (B, Fig. 1A, B, C und Daten nicht gezeigt). Diese Beobachtungen lassen schließen, daß es sich tatsächlich bei *CG9938*, *CG8902* und *CG7242* um *D. melanogaster-Ndc80*, *-Nuf2* und *-Spc25* handelt.

Das von Meraldi et al. (2006) postulierte *D. melanogaster*-Homolog von Mis12, *CG18156,* zeigte konstitutive CKC-Lokalisierung in Schneiderzellen (B, Fig. S1A). In Embryonen hingegen konnte lediglich CKC-Lokalisierung während der Mitose nachgewiesen werden (B, Fig. 1D). *CG18156* kodiert demnach für *D. melanogaster*-Mis12.

Um weitere CKC-Komponenten zu identifizieren, wurden Koimmunopräzipitations-experimente durchgeführt. Nach Präzipitation von EGFP-Nuf2 bzw. Spc25-mRFP (monomeric red fluorescent protein) mit Antikörpern gegen EGFP oder mRFP wurde eine massenspektrometrische Untersuchung der spezifisch kopräzipitierten Proteine durchgeführt (B, Fig. 2). Wie erwartet, konnten die bekannten Untereinheiten des Ndc80-Komplexes wie auch Mis12 kopräzipitiert werden. Wechselwirkungen zwischen den Proteinen des MIND- und Ndc80-Komplexes konnten bereits in anderen Organismen nachgewiesen werden (Cheeseman et al., 2004; Obuse et al., 2004; Liu et al., 2005). Des weiteren wurden bei diesen Koimmunopräzipitationsexperimenten potentielle *D. melanogaster*-Homologe von Nsl1 und Nnf1 gefunden, welche zu den MIND-Komplex-Untereinheiten gehören. *CG1558* zeigt geringe Ähnlichkeit zu *Nsl1* und *CG13434* zu *Nnf1*. Auch in diesen

Fällen konnte die Identität der Homologen durch Lokalisierungsstudien in Schneiderzellen bewiesen werden (B, Fig. S1B, C).
Die Koimmunopräzipitationen mit EGFP-Nuf2 und Spc25-mRFP führten allerdings weder zur Identifizierung der vierten Ndc80-Komplex-Untereinheit Spc24 noch zur Identifizierung der vierten MIND-Komplex-Untereinheit Dsn1 in *D. melanogaster*.
Die Transgene, welche die Expression von den fluoreszenzmarkierten Fusionsproteinen EGFP-Nuf2, Spc25-mRFP und EGFP-Mis12 unter der Kontrolle der jeweiligen genomischen Elemente erlauben, wurden auf Funktionalität getestet. Verfügbare mutante Allele wurden phänotypisch charakterisiert und deren Letalität durch die entsprechenden Transgene revertiert. Diese Untersuchungen zeigen, daß die *D. melanogaster*-Gene *Nuf2*, *Spc25* und *Mis12* essentiell und die entsprechenden Transgene funktionell sind.

5.8 Vermessung des CKC

Die momentanen Vorstellungen über die Struktur des CKC beruhen auf Ergebnissen aus EM-Experimenten, Untersuchungen über die gegenseitige Abhängigkeit von Proteinen bei ihrer Lokalisierung im CKC und die zeitlichen Unterschiede beim Auftreten der CKC-Lokalisierung der Komponenten. Experimentelle Prozeduren wie Fixierungen und Immunmarkierung wie sie z.B. bei EM notwendig sind, führen zu artifiziellen Bedingungen und verringern die Auflösung drastisch. Die Verwendung von Antikörpern bedingt allein durch deren Größe einen Auflösungsverlust. Außerdem kann man nicht ohne weiteres von einer gleichen Zugänglichkeit unterschiedlicher Epitope ausgehen. Daten über gegenseitige Abhängigkeiten und zeitlichen Unterschiede bei der Lokalisierung geben bestenfalls eine Vorstellung über die relative Position der Proteine im CKC. Um eine genauere Vorstellung von der Architektur des CKC zu bekommen, wurden mikroskopische Analysen von nativen, mitotischen Chromosomen durchgeführt (B, Fig. 3A, B, C).
Für die Präparation der nativen Chromosomen wurden Embryonen im syncitialen Blastoderm verwendet. In diesen Embryonen liegen Tausende von Zellkernen ohne trennende Zellmembranen vor. Die verwendeten Embryonen exprimierten eine rot fluoreszierende CKC-Komponente und eine grün fluoreszierende. Die Embryonen wurden in einem Puffer mit DNS-Farbstoff zwischen einem

Objektträger und einem Deckglas durch Kapillarkräfte aufgebrochen, so daß die Chromosomen freigesetzt wurden. Die minimale Schichtdicke des Präparates garantierte somit ein ebenfalls minimales Hintergrundsignal. Mitotische Chromosomen mit roten und grünen CKC-Signalen wurden dann mikroskopiert (B, Fig. 3A, B, C).

Mit Hilfe des ImageJ Programms wurde dann die Signalintensität beider Kanäle über einer Verbindungslinie zwischen den beiden Schwester-CKC eines Chromosoms ermittelt (B, Fig. 3C, D). Der Abstand der Maxima der beiden grünen Signale wurde als Inter-CKC-Abstand der grün fluoreszierenden CKC-Komponente (dGGinter) und der der roten Maxima als dRRinter bezeichnet (B, Fig. 3D). Um von diesen über der Auflösungsgrenze des Lichtmikroskops liegenden Abständen auf den Intra-CKC-Abstand zwischen der rot und grün fluoreszierenden CKC-Komponente eines Schwester-CKC (dRGintra) zu schließen, welche beträchtlich unter der Auflösungsgrenze des Lichtmikroskops liegt, wurde dGGinter von dRRinter subtrahiert und die erhaltene Differenz durch zwei geteilt (B, Fig. 3D).

Für jedes untersuchte Paar von CKC-Komponenten wurde dRGintra für 100 Schwester-CKC-Paare ermittelt. Mit Hilfe von MS Excel wurde anschließend der Mittelwert der 100 Messungen bestimmt (B, Tab. 1). Die so erhaltenen Abstände der CKC-Komponenten innerhalb eines CKC sind in Fig. 3E der Teilarbeit B als Doppelpfeile dargestellt.

Eine andere Art der Auswertung der Daten beruht auf der Mittelung aller in den verschiedenen Experimenten erhaltenen Inter-CKC-Abstände für eine bestimmte CKC-Komponente. So wurden im Fall von Cenp-A 500 dRRinter und 200 dGGinter gemessen und ein Mittelwert für den Inter-CKC-Abstand (dinter(Cenp-A)) von 460 nm bestimmt. Der Intra-CKC-Abstand zwischen den CKC-Komponenten eines CKC geht auf die äquivalente Berechnung zurück (B, Tab. 2). In der Tabelle sind die relativen Positionen der CKC-Komponenten zu Cenp-A angegeben, welches als innerste Komponente den Bezugswert null besitzt. Diese relativen Positionen sind in der Fig. 3E der Teilarbeit B durch die vertikalen farbigen Linien dargestellt.

Mathematisch lassen sich die beiden Methoden wie folgt darstellen, wobei x und y beliebige CKC-Komponenten bezeichnen:

I $\overline{dintra(xy)} = \overline{(dinter(x) - dinter(y))/2}$

II $\overline{dintra(xy)} = (\overline{dinter(x)} - \overline{dinter(y)})/2$

Der gemittelte Inter-CKC-Abstand von Cenp-A betrug 460 nm. Dies entspricht in etwa bereits für Prophasen-Chromosomen publizierten Werten (Logarinho et al., 2004). Nach bipolarer Orientierung der Chromosomen kommt es zu einer Vergrößerung dieses Abstandes. Dies legte nahe, daß auf die nativen mitotischen Chromosomen kein Zug durch die Spindel ausgeübt wird. Um dies zu bestätigen wurden Präparationen von Embryonen vorgenommen, welche rot fluoreszierendes Cenp-A und ein grün fluoreszierendes Mikrotubuli-assoziiertes Protein (G147, Morin et al., 2001) exprimierten (B, Fig. S4). Auszählungen ergaben, daß 82,4% der CKC-Signale nicht mit Mikrotubuli assoziiert waren, 16,6% lateralen Kontakt hatten und 1% mono- oder bipolar mit Mikrotubuli besetzt war (n = 319). Allerdings ist aufgrund der unstrukturierten Mikrotubulisignale davon auszugehen, daß die Spindel bei der Präparation zerstört wird und auf keines der Chromosomen Zug wirkt.

Des weiteren konnte auch starkes Signal der Spindelkontrollpunktproteine an den CKC der nativen mitotischen Chromosomen nachgewiesen werden, was eine fehlende Interaktion der CKC mit der Spindel bestärkt. So war die Verteilung von grün fluoreszierendem Bub3 sehr variabel, was eine Einbeziehung der Spindelkontrollpunktproteine in die Abstandsmessungen unmöglich machte (B, Fig. 5). Die Spindelkontrollpunktproteine Polo und Rod zeigten ein vergleichbares Verhalten (Daten nicht gezeigt).

Um die Korrektheit der Messungen zu demonstrieren, wurden Kontrollen mit rot bzw. grün fluoreszierenden Versionen von einem Protein durchgeführt. Für Cenp-A ergaben diese Messungen einen Abstand von 5 nm und für Spc25 0 nm. Als weiteres Indiz für die Korrektheit kann angeführt werden, daß das additive Verhalten gemessener Teilabstände den Erwartungen entspricht.

Diese Untersuchung erlaubt die Einsicht in strukturelle Eigenschaften mit bisher unbekannter Auflösung. Eine Hierarchie im Aufbau des CKC war lange bekannt und die gewonnenen Daten bestätigen einige der bekannten und postulierten

Aspekte. So ist Cenp-A das basalste, dem Chromatin naheste der CKC-Proteine, gefolgt von Cenp-C und den Proteinen mit Brückenfunktion zwischen DNS und Mikrotubuli. Mis12 und Spc25 sind Cenp-C sehr nah. Nuf2 ist das dem Chromatin fernste der untersuchten Proteine.

Die Plazierungen von Spc25 und Nuf2 sprechen in der Tat für eine polare Orientierung des Ndc80-Komplexes im CKC. Allerdings ist der ermittelte Abstand zwischen den beiden mit etwa 20 nm mehr als zwei mal kleiner als die Ausdehnung des Komplexes nach EM- und SFM-Untersuchungen von etwa 50 nm (Ciferri et al., 2005; Wei et al., 2005). Da bei der Präparation der nativen mitotischen Chromosomen die Interaktion mit der Spindel verloren geht und so kein Zug zwischen den Schwester-CKC wirkt, ist vorstellbar, daß die gestreckten Ndc80-Komplexe in einer nicht vollständig geordneten Konformation vorliegen. Eine andere Erklärung könnte sein, daß die Ndc80-Komplexe auf einen Zug mit Streckung reagieren und in den Präparaten gebogen oder geknickt vorliegen. Dies könnte bedeuten, daß die Ndc80-Komplexe den Zug, der nach bipolarer Orientierung zwischen den Schwester-CKC wirkt, zu detektieren vermögen. So könnte neben Aurora B (für eine Übersicht siehe Tanaka, 2005) auch der Ndc80-Komplex bei der Registrierung der bipolaren Orientierung der Chromosomen eine Rolle spielen.

Neben der polaren Orientierung des Ndc80-Komplexes scheint auch Cenp-C polar orientiert zu sein. So zeigt seine C-terminale Domäne mit dem Cenp-C-Motiv zum Chromatin und die N-terminale Domäne mit den RRR- und DH-Motiven zu den Mikrotubuli. Diese Ergebnisse unterstützen die Vorstellung, daß der am wenigsten konservierte Mittelteil des Proteins als Brücke zwischen dem C-Terminus, der notwendig für die CKC-Lokalisierung ist, und den möglicherweise Ndc80- und MIND-Komplex-bindenden N-terminalen konservierten Motiven wirkt. Der beträchtliche Raum zwischen Cenp-A und Cenp-C könnte durch die kürzlich identifizierten Proteine Cenp-M, -N, -T, -U und -H ausgefüllt sein, welche neben Cenp-C mit Cenp-A-Nukleosomen präzipitiert werden können (Foltz et al., 2006).

Da Cenp-C bereits als Protein der innern Platte beschrieben wurden (Saitoh et al., 1992), liegt nahe, daß Spc25 und Mis12 ebenfalls innere CKC-Komponenten sind. Die Lokalisierung von humanem Hec1 in der äußeren Platte (DeLuca et al., 2005) würde demnach die These unterstützen, daß die weniger elektronendichte

Interzone des Metaphasen-CKC von den "Coiled-Coil"-Regionen des Ndc80-Komplexes gebildet wird.
Neben der Reihenfolge der CKC-Komponenten im CKC geben die hier beschriebenen Ergebnisse auch Aufschluß über die relativen Entfernungen der Proteine zu einander und somit über Orte an denen man eventuell noch nicht entdeckte Strukturproteine finden könnte.

5.9 Charakterisierung von *D. melanogaster* Mps1

Mps1 wurde in verschiedenen Organismen als Spindelkontrollpunktprotein beschrieben (Fisk und Winey, 2004). Demnach gehört es zu den transienten CKC-Komponenten.
Um die Lokalisierung von *D. melanogaster* Mps1 zu untersuchen, wurde ein funktionelles EGFP-markiertes Transgen etabliert (C, Fig 1A). Die Lokalisierung von EGFP-Mps1 in der Interphase ist zytoplasmatisch mit Anreicherung an den Zentrosomen (C, Fig. 1C und 1D). In der Prophase nimmt das Zentrosomensignal ab und eine CKC-Lokalisierung kann beobachtet werden. Bis Beginn der Anaphase verschwindet EGFP-Mps1 zusehends vom CKC und reichert sich an der Spindel und den Spindelpolen an. In der Anaphase ist keine CKC-Lokalisierung mehr nachweisbar. *D. melanogaster* Mps1 zeigt demnach ein Lokalisierungsverhalten, wie es für ein Spindelkontrollpunktprotein zu erwarten war.
Als Spindelkontrollpunktprotein ist Mps1 beteiligt an der Verzögerung der Anaphase bis alle Chromosomen bipolar in der mitotischen Spindel angeordnet sind. Ist dies nicht der Fall, arretiert der Spindelkontrollpunkt den Zellzyklus in der Metaphase.
In *D. melanogaster* arretiert die reife Oozyte in der Metaphase der Meiose I. Dieser Arrest scheint jedoch nicht abhängig von Mps1 zu sein, da Oozyten ohne maternale Kontribution an Mps1 einen augenscheinlich normalen Arrest und keinerlei Probleme in den nachfolgenden meiotischen Teilungen haben (Daten nicht gezeigt).
Nach Fertilisierung der Oozyte finden beide meiotischen Teilungen ohne eine Zytokinese statt, und die vier haploiden Meioseprodukte verbleiben in einem gemeinsamen Zytoplasma. Nur eines dieser Meioseprodukte entwickelt sich zum

weiblichen Vorkern und verschmilzt mit dem männlichen Vorkern zum Kern der Zygote. In der ersten S-Phase der Zygote wird auch die DNS der drei nicht genutzten Meioseprodukte repliziert. Im Gegensatz zum zygotischen Kern arretiert dieses Chromatin in der ersten Mitose mit radial angeordneten, kondensierten Chromosomen und verbleibt als sogenanntes Bouquet im Zytoplasma.

Es konnte nachgewiesen werden, daß dieser Arrest abhängig von Mps1 ist. Zum einen findet eine Anreicherung von verschieden Spindelkontrollpunktproteinen wie Mps1, Mad2 und BubR1 an den CKC der Chromosomen statt (C, Fig. 3C, 3D und nicht gezeigt). Andererseits zeigen Embryonen ohne maternale Mps1-Kontribution einen auffälligen Phänotyp des Bouquets (C, Fig. 3, vergleiche A und B). In diesem Fall bleibt eine Anreicherung von Mad2 am CKC aus (C, Fig. 3G), das Chromatin ist dekondensiert (C, Fig. 3H) und eine erhöhte Anzahl an CKC-Signalen (C, Fig. 3I) deutet auf eine Überreplizierung der DNS hin. Die Chromosomen des Bouquets arretieren also nicht.

Ein weiterer physiologischer Metaphasenarrest wurde auf Abhängigkeit von Mps1 getestet. In *C. elegans* wurden die Spindelkontrollpunktgene *san-1* (*Mad3*) und *mdf-2* (*Mad2*) als wichtig für den Metaphasenarrest nach Sauerstoffentzug beschrieben (Nystul et al., 2003). Da auch in *D. melanogaster* ein reversibler Metaphasenarrest nach Sauerstoffentzug beobachtet werden kann, sollte dessen Abhängigkeit von Mps1 untersucht werden. Synzytiale Embryonen von *D. melanogaster* verbleiben nach Sauerstoffentzug entweder in einem Interphasenarrest mit kondensierten Chromosomen (C, Fig. 2A) oder in einem Metaphasenarrest mit stark kondensierten Chromosomen (C, Fig. 2B). Ausschlaggebend dafür, welcher Arrest auftritt, ist die Zellzyklusphase, in der sich die Kerne des Embryos zum Zeitpunkt des Sauerstoffentzuges befanden. Embryonen mit überwiegend Ana- und Telophasenfiguren sind nicht zu finden. Im Gegensatz hierzu sind in Embryonen ohne maternale Mps1-Kontribution solche Figuren nachweisbar (C, Fig. 2D), was darauf schließen läßt, daß Mps1 für den Metaphasenarrest notwendig ist. Die beobachteten späten mitotischen Figuren waren, vermutlich in Folge von Fehlern in der Mitose unter Sauerstoffentzug, anomal mit Chromatinbrücken und welligen Chromosomenarmen (C, Fig. 2E-H). Da der Interphasenarrest infolge verminderter Sauerstoffzufuhr in Embryonen ohne maternale Mps1-Kontribution vergleichbar mit dem des Wildtyps war (C, Fig. 2C), liegt es nahe, daß Mps1 keinen Einfluß auf diesen hat.

Nach *C. elegans* Mad2 und Mad3 wurde hier also auch *D. melanogaster* Mps1 als drittes Spindelkontrollpunktprotein mit Funktion im Metaphasenarrest infolge von Sauerstoffentzug beschrieben. Daß der Metaphasenarrest infolge von Sauerstoffentzug neben in *C. elegans* auch in *D. melanogaster* von Spindelkontrollpunktproteinen abhängig ist, weist auf eine Konservierung dieses Mechanismus unter den Metazoen hin.

5.10 Verhalten der Spindel und des CKC nach Sauerstoffentzug

Da also nach Sauerstoffentzug der Spindelkontrollpunkt aktiviert wird, um eine fehlerhafte Mitose zu vermeiden war von Interesse, ob der Spindelkontrollpunkt eventuell auf ein spezifisches Signal reagiert. Einerseits könnte ein Sauerstoffentzug zu gestörter Interaktion der CKC mit der Spindel und so zu Fehlern in der bipolaren Orientierung der Chromosomen führen und folglich den Spindelkontrollpunkt aktivieren. Andererseits könnte ein Sauerstoffentzug auch aktiv detektiert und ein Signal an den Spindelkontrollpunkt weitergegeben werden. Um zwischen diesen beiden Möglichkeiten zu unterscheiden, wurde nach den frühesten Veränderungen nach einem Sauerstoffentzug gesucht und das Augenmerk auf die Spindel und den CKC gerichtet.

Mittels Immunfluoreszenzmarkierung von Tubulin in *D. melanogaster*-Embryonen und *in vivo*-Mikroskopie von Embryonen, welche GFP-markiertes Tubulin exprimierten, konnte gezeigt werden, daß die mitotische Spindel sehr schnell und reversibel auf einen Sauerstoffentzug reagiert (D, Fig. 1). In der Metaphase arretierte Embryonen zeigten bereits nach einem zweiminütigen Sauerstoffentzug eine Reduktion der Spindelastern und der zentrosomenproximalen Spindelfasern. Die Verbindung zwischen dem Zentrosom und der Spindel war geschwächt. Diese Effekte wurden nach länger andauerndem Sauerstoffentzug drastischer (D, Fig. 1A). Die Spindellänge nahm nach Sauerstoffentzug leicht zu (D, Fig. 1B) und ihre Breite nahm ab (D, Fig. 1C).

Die Spindel in Embryonen ohne maternale Mps1-Kontribution zeigte nach Sauerstoffentzug vergleichbare Effekte (D, Fig. 2A). Damit ist bewiesen, daß die Effekte auf die Spindel nicht vom Spindelkontrollpunkt abhängig sind.

Immunfluoreszenzmarkierung von Cenp-A zeigte keine Auffälligkeiten in der CKC-Lokalisierung von Cenp-A nach Sauerstoffentzug (D, Fig. 2C) wiesen aber auf

einen verminderten Zwischen-CKC-Abstand hin (D, Fig. 2D), was einen verminderten Zug auf die Schwester-CKC vermuten läßt.

Interessanterweise veränderte jedoch Cenp-C drastisch sein Lokalisierungsverhalten nach Sauerstoffentzug. Ein kleiner Teil des Cenp-C zeigt auch unter normoxischen Bedingungen Spindelassoziation (D, Fig. 5A). Nach Sauerstoffentzug ist das Spindelsignal erheblich verstärkt und konzentriert in der Region am Zentrosom. Die CKC-Lokalisierung von Cenp-C bleibt bestehen (D, Fig. 5A). Die Ergebnisse nach Immunfluoreszenzmarkierung mit Antikörpern und *in vivo*-Mikroskopie mit Embryonen, die ein EYFP-markiertes, funktionelles Cenp-C exprimieren, waren vergleichbar. Ähnliche Verhältnisse wurden bei der Beobachtung einer EGFP-markierten Version der äußeren CKC-Komponente Nuf2 gefunden (D, Fig. 5B). Somit hat Sauerstoffentzug einen Effekt auf einige wichtige CKC-Komponenten.

Da dem Spindelkontrollpunkt eine entscheidende Rolle bei der Induktion des Metaphasenarrests nach Sauerstoffentzug zukommt, wurde das Verhalten von mehreren Spindelkontrollpunktproteinen nach Sauerstoffentzug untersucht. Mps1, BubR1, Bub3, Rod, Mad2 und Cdc20/Fzy zeigten nach Sauerstoffentzug alle eine veränderte Lokalisierung (D, Fig. 6, vergleiche jeweils + O_2 und -O_2).

Eine Folge des Sauerstoffentzuges ist ein verminderter zellulärer ATP-Spiegel. Es wurde beschrieben, daß in den ersten Minuten nach Sauerstoffentzug nur ein 10%-iger Abfall des ATP-Spiegels resultiert (DiGregorio et al., 2001). Dieser moderate Rückgang wurde als unwahrscheinlicher Grund für die beschrieben Resultate erachtet. Dennoch wurde getestet, ob metabolische Inhibitoren ähnliche Veränderungen bewirken wie der Sauerstoffentzug. *D. melanogaster*-Embryonen, die in einem Medium mit Azid oder Cyanid inkubiert wurden, zeigten, wider Erwarten, Effekte auf die Spindel, das Chromatin und Mps1 (D, Fig. 8), die von den in Folge des Sauerstoffentzuges beobachteten Effekten nicht unterscheidbar waren.

Zusammengefaßt läßt sich sagen, daß die Aktivierung des Spindelkontrollpunktes nach Sauerstoffentzug wahrscheinlich auf die Inhibition der oxidativen Phosphorylierung zurückgeht und daß der herabgesetzte ATP-Spiegel einen sehr schnellen und reversiblen Einfluß auf die Mikrotubulidynamik und somit die Spindel und die von ihr abhängigen CKC-Komponenten hat. Da die Interaktion von

Spindel und CKC klar gestört ist nach einem Sauerstoffentzug, ist anzunehmen, daß dies den Spindelkontrollpunkt aktiviert.

Der Umstand, daß auch die konstitutive CKC-Komponente Cenp-C drastische Lokalisierungsveränderungen nach Sauerstoffentzug zeigt, war überraschend. Dennoch blieb ein Teil des Cenp-C CKC-lokalisiert und die Anreicherung von zusätzlichem Cenp-C an der Spindel, weist möglicherweise auf den Mechanismus hin, über den Cenp-C am CKC lokalisiert wird.

6 Literaturverzeichnis

Bharadwaj, R., W. Qi und H. Yu. 2004. Identification of two novel components of the human NDC80 kinetochore complex. *J Biol Chem* **279**: 13076-85.

Brown, M. T. 1995. Sequence similarities between the yeast chromosome segregation protein Mif2 and the mammalian centromere protein CENP-C. *Gene* **160**: 111-6.

Buchwitz, B. J., K. Ahmad, L. L. Moore, M. B. Roth und S. Henikoff. 1999. A histone-H3-like protein in *C. elegans*. *Nature* **401**: 547-8.

Chan, G. K., S. T. Liu und T.J. Yen. 2005. Kinetochore structure and function. *Trends Cell Biol* **15**: 589-98.

Cheeseman, I. M., S. Niessen, S. Anderson, F. Hyndman, J. R. 3rd. Yates, K. Oegema und A. Desai. 2004. A conserved protein network controls assembly of the outer kinetochore and its ability to sustain tension. *Genes Dev* **18**(18): 2255-68.

Ciferri, C., J. De Luca, S. Monzani, K. J. Ferrari, D. Ristic, C. Wyman, H. Stark, J. Kilmartin, E. D. Salmon und A. Musacchio. 2005. Architecture of the human ndc80-hec1 complex, a critical constituent of the outer kinetochore. *J Biol Chem* **280**: 29088-95.

Cooper, J. L. und S. Henikoff. 2004. Adaptive evolution of the histone fold domain in centromeric histones. *Mol Biol Evol* **21**: 1712-8.

Dawe, R. K., L. M. Reed, H. G. Yu, M. G. Muszynski und E.N. Hiatt. 1999. A maize homolog of mammalian CENPC is a constitutive component of the inner kinetochore. *Plant Cell* **11**:1227-38.

DeLuca, J. G., Y. Dong, P. Hergert, J. Strauss, J. M. Hickey, E. D. Salmon und B. F. McEwen. 2005. Hec1 and nuf2 are core components of the kinetochore outer plate essential for organizing microtubule attachment sites. *Mol Biol Cell* **16**(2): 519-31

De Wulf, P., A. D. McAinsh und P.K. Sorger. 2003. Hierarchical assembly of the budding yeast kinetochore from multiple subcomplexes. *Genes Dev* **17**: 2902-21.

DiGregorio, P.J., J.A. Ubersax und P.H. O'Farrell. 2001. Hypoxia and nitric oxide induce a rapid, reversible cell cycle arrest of the Drosophila syncytial divisions. *J Biol Chem* **276**: 1930-7.

Earnshaw, W. C. und N. Rothfield. 1985. Identification of a family of human centromere proteins using autoimmune sera from patients with scleroderma. *Chromosoma* **91**: 313-21.

Euskirchen, G. M. 2002. Nnf1p, Dsn1p, Mtw1p, and Nsl1p: a new group of proteins important for chromosome segregation in *Saccharomyces cerevisiae*. *Eukaryot Cell* **1**: 229-40.

Fisk, H. A. und M. Winey. 2004. Spindle regulation: Mps1 flies into new areas. *Curr Biol* **14**: R1058-60.

Fitzgerald-Hayes, M., L. Clarke und J. Carbon. 1982. Nucleotid sequence comparisons and functional analysis of yeast centromere DNAs. *Cell* **29**(1): 235-44.

Foltz, D. R., L. E. Jansen, B. E. Black, A. O. Bailey, J. R. 3rd. Yates und D. W. Cleveland. 2006. The human CENP-A centromeric nucleosome-associated complex. *Nat Cell Biol* **8**(5): 458-69.

Funabiki, H., H. Yamano, K. Kumada, K. Nagao, T. Hunt und M. Yanagida. 1996. Cut2 proteolysis required for sister-chromatid separation in fission yeast. *Nature* **381**: 438-41.

Giot, L., J. S. Bader, C. Brouwer, A. Chaudhuri, B. Kuang, Y. Li, Y. L. Hao, C. E. Ooi, B. Godwin, E. Vitols, G. Vijayadamodar, P. Pochart, H. Machineni, M. Welsh, Y. Kong, B. Zerhusen, R. Malcolm, Z. Varrone, A. Collis, M. Minto, S. Burgess, L. McDaniel, E. Stimpson, F. Spriggs, J. Williams, K. Neurath, N. Ioime, M. Agee, E. Voss, K. Furtak, R. Renzulli, N. Aanensen, S. Carrolla, E. Bickelhaupt, Y. Lazovatsky, A. DaSilva, J. Zhong, C. A. Stanyon, R. L. Finley Jr, K. P. White, M. Braverman, T. Jarvie, S. Gold, M. Leach, J. Knight, R. A. Shimkets, M. P. McKenna, J. Chant und J. M. Rothberg. 2003. A protein interaction map of *Drosophila melanogaster*. *Science* **302**: 1727-36.

Hardwick, K. G., E. Weiss, F. C. Luca, M. Winey und A.W. Murray. 1996. Activation of the budding yeast spindle assembly checkpoint without mitotic spindle disruption. *Science* **273**: 953-6.

Henikoff, S., K. Ahmad, J. S. Platero und B. van Steensel. 2000. Heterochromatic deposition of centromeric histone H3-like proteins. *Proc Natl Acad Sci U S A* **97**: 716-21.

Herzig, A., C. F. Lehner und S. Heidmann. 2002. Proteolytic cleavage of the THR subunit during anaphase limits *Drosophila* separase function. *Genes Dev* **16**: 2443-54.

Jones, W. K und J. M. Rawls Jr. 1988. Genetic and molecular mapping of chromosome region 85A in *Drosophila melanogaster*. *Genetics* **120**: 733-42.

Kline, S. L., I. M. Cheeseman, T. Hori, T. Fukagawa und A. Desai. 2006. The human Mis12 complex is required for kinetochore assembly and proper chromosome segregation. *J Cell Biol* **173**: 9-17.

Liu, X., I. McLeod, S. Anderson, J. R. Yates 3rd und X. He. 2005. Molecular analysis of kinetochore architecture in fission yeast. *EMBO J* **24**: 2919-30.

Liu, S. T., J. B. Rattner, S. A. Jablonski und T.J. Yen. 2006. Mapping the assembly pathways that specify formation of the trilaminar kinetochore plates in human cells. *J Cell Biol* **175**: 41-53.

Logarinho, E., H. Bousbaa, J. M. Dias, C. Lopes, I. Amorim, A. Antunes-Martins und C. E. Sunkel. 2004. Different spindle checkpoint proteins monitor microtubule attachment and tension at kinetochores in Drosophila cells. *J Cell Sci.* **117**(9): 1757-71

Luger, K., A. W. Mader, R. K. Richmond, D. F. Sargent und T.J. Richmond. 1997. Crystal structure of the nucleosome core particle at 2.8 A resolution. *Nature* **389**: 251-60.

Maddox, P. S., K. Oegema, A. Desai und I.M. Cheeseman. 2004. "Holo"er than thou: chromosome segregation and kinetochore function in *C. elegans. Chromosome Res* **12**: 641-53.

Maiato, H., P. J. Hergert, S. Moutinho-Pereira, Y. Dong, K. J. Vandenbeldt, C. L. Rieder und B. F. McEwen. 2006. The ultrastructure of the kinetochore and kinetochore fiber in *Drosophila* somatic cells. *Chromosoma* **115**: 469-80.

McAinsh, A. D., P. Meraldi, V. M. Draviam, A. Toso und P.K. Sorger. 2006. The human kinetochore proteins Nnf1R and Mcm21R are required for accurate chromosome segregation. *EMBO J* **25**: 4033-49.

Meluh, P. B. und D. Koshland. 1995. Evidence that the MIF2 gene of *Saccharomyces cerevisiae* encodes a centromere protein with homology to the mammalian centromere protein CENP-C. *Mol Biol Cell* **6**: 793-807.

Meraldi, P., A. D. McAinsh, E. Rheinbay und P. K. Sorger. 2006. Phylogenetic and structural analysis of centromeric DNA and kinetochore proteins. *Genome Biol* **7**(3): R23.

Michaelis, C., R. Ciosk und K. Nasmyth. 1997. Cohesins: Chromosomal proteins that prevent premature separation of sister chromatids. *Cell* **91**: 35-45.

Moore, L. L. und M. B. Roth. 2001. HCP-4, a CENP-C-like protein in Caenorhabditis elegans, is required for resolution of sister centromeres. *J Cell Biol* **153**: 1199-208.

Morin, X., R. Daneman, M. Zavortink und W. Chia. 2001. A protein trap strategy to detect GFP-tagged proteins expressed from their endogenous loci in Drosophila. *Proc Natl Acad Sci U S A* **98**(26): 15050-55.

Nystul, T.G., J.P. Goldmark, P.A. Padilla and M.B. Roth. 2003. Suspended animation in C. elegans requires the spindle checkpoint. *Science* **302**: 1038-41.

Obuse, C., O. Iwasaki, T. Kiyomitsu, G. Goshima, Y. Toyoda und M. Yanagida. 2004. A conserved Mis12 centromere complex is linked to heterochromatic HP1 and outer kinetochore protein Zwint-1. *Nat Cell Biol* **6**: 1135-41.

Oegema, K., A. Desai, S. Rybina, M. Kirkham und A.A. Hyman. 2001. Functional analysis of kinetochore assembly in *Caenorhabditis elegans*. *J Cell Biol* **153**: 1209-26.

Rieder, C.L. The formation, structure, and composition of the mammalian kinetochore and kinetochore fiber. 1982. *Int Rev Cytol* **79**: 1-58.

Saitoh, H., J. Tomkiel, C. A. Cooke, H. Ratrie, M. Maurer, N. F. Rothfield und W. C. Earnshaw. 1992. CENP-C, an autoantigen in scleroderma, is a component of the human inner kinetochore plate. *Cell* **70**: 115-25.

Shang, C., T. R. Hazbun, I. M. Cheeseman, J. Aranda, S. Fields, D. G. Drubin und G. Barnes. 2003. Kinetochore protein interactions and their regulation by the Aurora kinase Ipl1p. *Mol Biol Cell* **14**: 3342-55.

Shibata, F. und M. Murata. 2004. Differential localization of the centromere-specific proteins in the major centromeric satellite of *Arabidopsis thaliana*. *J Cell Sci* **117**: 2963-70.

Stoler, S., K. C. Keith, K. E. Curnick und M. Fitzgerald-Hayes. 1995. A mutation in CSE4, an essential gene encoding a novel chromatin-associated protein in yeast, causes chromosome nondisjunction and cell cycle arrest at mitosis. *Genes Dev* **9**: 573-86.

Stratmann, R. und C.F. Lehner. 1996. Separation of sister chromatids in mitosis requires the *Drosophila pimples* product, a protein degraded after the metaphase anaphase transition. *Cell* **84**: 25-35.

Sumara, I., E. Vorlaufer, P.T. Stukenberg, O. Kelm, N. Redemann, E. A. Nigg und J.M. Peters. 2002. The dissociation of cohesin from chromosomes in prophase is regulated by Polo-like kinase. *Mol Cell* **9**: 515-25.

Takahashi, K., E. S. Chen und M. Yanagida. 2000. Requirement of Mis6 centromere connector for localizing a CENP-A-like protein in fission yeast. *Science* **288**: 2215-9.

Talbert, P. B., T. D. Bryson und S. Henikoff. 2004. Adaptive evolution of centromere proteins in plants and animals. *J Biol* **3**:18.

Tanaka, T. U. 2005. Chromosome bi-orientation on the mitotic spindle. *Phil. Trans. R. Soc. B* **360**: 581-589.

Toth, A., R. Ciosk, F. Uhlmann, M. Galova, A. Schleiffer und K. Nasmyth. 1999. Yeast cohesin complex requires a conserved protein, Eco1p(Ctf7), to establish cohesion between sister chromatids during DNA replication. *Genes Dev* **13**: 320-33.

Uhlmann, F. und K. Nasmyth. 1998. Cohesion between sister chromatids must be established during DNA replication. *Curr Biol* **8**: 1095-101.

Uhlmann, F., F. Lottspeich und K. Nasmyth. 1999. Sister-chromatid separation at anaphase onset is promoted by cleavage of the cohesin subunit Scc1. *Nature* **400**: 37-42.

Vos, L. J., J. K. Famulski und G.K. Chan. 2006. How to build a centromere: from centromeric and pericentromeric chromatin to kinetochore assembly. *Biochem Cell Biol* **84**: 619-639.

Wei, R. R., P. K. Sorger und S.C. Harrison. 2005 . Molecular organization of the Ndc80 complex, an essential kinetochore component. *Proc Natl Acad Sci U S A* **102**: 5363-7.

Wei, R. R., J. R. Schnell, N. A. Larsen, P. K. Sorger, J. J. Chou und S.C. Harrison. 2006. Structure of a central component of the yeast kinetochore: the Spc24p/Spc25p globular domain. *Structure* **14**: 1003-9.

Winey, M., L. Goetsch, P. Baum und B. Byers. 1991. MPS1 and MPS2: novel yeast genes defining distinct steps of spindle pole body duplication. *J Cell Biol* **114**: 745-54.

7 Anhang

Teilarbeit A

Darstellung des Eigenanteils

Teilarbeit B

Darstellung des Eigenanteils

Teilarbeit C

Darstellung des Eigenanteils

Teilarbeit D

Darstellung des Eigenanteils

Erklärung

Teilarbeit A

Sebastian Heeger*, Oliver Leismann*, Ralf Schittenhelm, Oliver Schraidt, Stefan Heidmann and Christian F. Lehner (2005)

Genetic interactions of separase regulatory subunits reveal the diverged *Drosophila* Cenp-C homolog

Genes Dev **19**: 2041–2053

* beide Autoren haben im selben Maße zu dieser Arbeit beigetragen

Darstellung des Eigenanteils

Die Arbeiten, die zu den Abbildungen (Fig. 2, 3 und 5) führten, stammen von mir. Die Zufallsmutagenese, dargestellt in der Abbildungen 3C und 3D wurde von Ralf Schittenhelm während seiner Diplomarbeit unter meiner Anleitung vorgenommen.

Die Beschreibung der funktionellen Domänen von Cenp-C mittels Reversion des ZNS-Phänotyps stammt von mir (unterer Teil der Fig. 6A).

Geschrieben wurde diese Teilarbeit von Christian F. Lehner mit Beiträgen der anderen Autoren.

Genetic interactions of separase regulatory subunits reveal the diverged *Drosophila* Cenp-C homolog

Sebastian Heeger,[1] Oliver Leismann,[1,2] Ralf Schittenhelm, Oliver Schraidt, Stefan Heidmann, and Christian F. Lehner[3]

Department of Genetics, BZMB, University of Bayreuth, 95440 Bayreuth, Germany

Faithful transmission of genetic information during mitotic divisions depends on bipolar attachment of sister kinetochores to the mitotic spindle and on complete resolution of sister-chromatid cohesion immediately before the metaphase-to-anaphase transition. Separase is thought to be responsible for sister-chromatid separation, but its regulation is not completely understood. Therefore, we have screened for genetic loci that modify the aberrant phenotypes caused by overexpression of the regulatory separase complex subunits Pimples/securin and Three rows in *Drosophila*. An interacting gene was found to encode a constitutive centromere protein. Characterization of its centromere localization domain revealed the presence of a diverged CENPC motif. While direct evidence for an involvement of this *Drosophila* Cenp-C homolog in separase activation at centromeres could not be obtained, in vivo imaging clearly demonstrated that it is required for normal attachment of kinetochores to the spindle.

[*Keywords*: Centromere; Cenp-A; Cenp-C; kinetochore; separase]

Supplemental material is available at http://www.genesdev.org.

Received April 22, 2005; revised version accepted June 29, 2005.

Separase functions as a protease at the metaphase-to-anaphase transition of mitosis (for review, see Nasmyth 2002). At this crucial cell cycle transition, separase cleaves the α-kleisin subunit (Scc1/Mcd1/Rad21) of the cohesin complex and thereby promotes the final release of sister-chromatid cohesion. The careful control of separase activity during the cell division cycle involves regulatory subunits. Securin is a subunit that accumulates and associates with separase during interphase. It acts as an inhibitor of separase activity. Thus, the rapid degradation of securin at the metaphase-to-anaphase transition via the anaphase-promoting complex/cyclosome (APC/C) pathway of ubiquitin-dependent proteolysis results in separase activation. In *Drosophila*, securin is encoded by the *pimples* (*pim*) gene (Leismann et al. 2000) and the catalytic protease subunit by the *Separase* (*Sse*) gene (Jäger et al. 2001). *Drosophila* Sse lacks the extensive N-terminal regulatory domain that is present in separases outside the dipterans because the corresponding gene region appears to have evolved into an independent gene, *three rows* (*thr*) (Herzig et al. 2002; Jäger et al. 2004). *Drosophila* Thr binds to Sse and is required for sister-chromatid separation during mitosis (Jäger et al. 2001).

The precise role of Thr and the corresponding N-terminal domains in nondipteran separases is not understood. Moreover, Pim and other securins are not just separase inhibitors but also contribute in an unknown positive manner to sister-chromatid separation. In fission yeast, securin recruits separase to the mitotic spindle, and similar observations have been described in other organisms (Funabiki et al. 1996; Ciosk et al. 1998; Kumada et al. 1998; Jensen et al. 2001; Herzig et al. 2002; Chestukhin et al. 2003). Separase activation and transport on spindle microtubules might confine its action to the congressed chromosomes in metaphase plates and in particular to the pericentromeric region. This hypothetical scenario might explain why only a minute and preferentially pericentromeric pool of Scc1 appears to be cleaved by separase during mitosis of higher eukaryotic cells, while the large majority of Scc1 remains intact.

To identify additional genes that might contribute to separase regulation and function, we have screened for chromosomal regions that act as genetic modifiers of the aberrant phenotypes resulting from overexpression of Pim or a dominant-negative Thr fragment during *Drosophila* eye development. Molecular characterization of an interacting locus revealed that it encodes a constitutive centromere protein. Mapping of its centromere localization domain in combination with sequence com-

[1]These authors contributed equally to this work.
[2]Present address: Laboratory of Chromosome and Cell Biology, Rockefeller University, 1230 York Avenue, New York, NY 10021, USA.
[3]Corresponding author.
E-MAIL chle@uni-bayreuth.de; FAX 49-921-55-2710.
Article and publication are at http://www.genesdev.org/cgi/doi/10.1101/gad.347805.

parisons among Drosophilid orthologs allowed its identification as the most diverged Cenp-C homolog. Cenp-C was originally identified as a human autoantigen localized to centromeres (Earnshaw and Rothfield 1985; Saitoh et al. 1992) and found to display limited sequence similarity to budding yeast Mif2 (Brown 1995; Meluh and Koshland 1995), which was identified by mutations affecting the fidelity of chromosome transmission during mitosis (Meeks-Wagner et al. 1986). Homologs have also been described in nematodes (HCP-4) and plants (Dawe et al. 1999; Moore and Roth 2001; Oegema et al. 2001; Shibata and Murata 2004; Talbert et al. 2004). For simplicity, we use Cenp-C as a designation for all these homologs. Interestingly, recent analyses have demonstrated that Cenp-C, as well as Cenp-A, a histone H3 variant present in centromeric nucleosomes, evolve rapidly and adaptively in many lineages, perhaps driven by the rapid evolution of centromeric satellite sequences, and in *Drosophila*, Cenp-C was supposed to be absent (Talbert et al. 2004). Apart from providing further support for the striking sequence divergence of ubiquitous eukaryotic centromere components, our findings also raise the possibility that separase activity might be enhanced by such components.

Results

Mutations in Cenp-C *modify phenotypic consequences resulting from separase dysregulation*

Overexpression of *pim* during *Drosophila* eye development results in an aberrant rough eye phenotype in adults (Fig. 1A, *GMR > pim*). Although we have not characterized this phenotype at a cellular level, we assume that it results primarily from inhibition of sister-chromatid separation during mitotic divisions of eye imaginal disc cells, because *pim* overexpression during embryogenesis is known to have this effect (Leismann et al. 2000). Moreover, analyses in salivary glands indicated that *pim* overexpression does not have obvious effects in cells progressing through endoreduplication cycles that lack mitotic divisions (data not shown).

When expressed during eye development, a mutant *thr* version lacking C-terminal sequences (*thrΔC*) resulted in a phenotype very similar to that caused by eye-specific *pim* overexpression (Fig. 1A, *GMR-thrΔC*). The effect of *thrΔC* was suppressed by concomitant expression of wild-type *thr*, suggesting that *thrΔC* acts in a dominant-negative manner. The severity of the aberrant phenotypes resulting from *pim* and *thrΔC* overexpression during eye development was correlated with transgene copy numbers (data not shown).

To identify loci interacting with *pim* and *thr*, we crossed a collection of chromosomal deficiencies into the backgrounds with the transgenes resulting in *pim* or *thrΔC* overexpression during eye development. Heterozygosity for the deficiency *Df(3R)p-XT103*, which deletes the chromosomal interval 85A–85C, was found to enhance the rough eye phenotypes caused by *pim* and *thrΔC* overexpression. Based on analyses with additional deficiencies, the interacting region could be narrowed down (Fig. 1B). Moreover, heterozygosity for the EMS-induced, recessive lethal mutation *l(3)85Aa*^{prl41}, which had previously been mapped to this chromosomal region (Jones and Rawls 1988), was also found to enhance the aberrant eye phenotype resulting from *pim* and *thrΔC* overexpression (Fig. 1A, *GMRpim prl41* and *GMR-thrΔC*

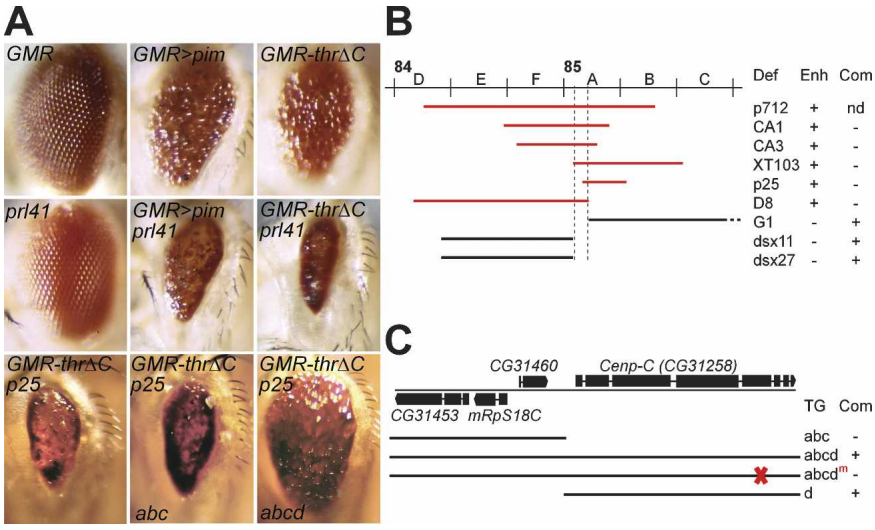

Figure 1. Separase regulatory subunits encoded by *pim* and *thr* interact genetically with *Cenp-C*. (*A*) Overexpression of *pim* and C-terminally truncated *thr* during eye development results in an aberrant eye phenotype that is enhanced by mutations in *Cenp-C*. The eyes shown are from flies with the following genotypes: *GMR-GAL4/+* (*GMR*), *GMR-GAL4 UAS-pim-myc* II.3/+ (*GMR > pim*), *GMR-thrΔC* III.1/+ (*GMR-thrΔC*), *Cenp-C*^{prl41}/+ (*prl41*), *GMR-GAL4 UAS-pim-myc* II.3/+; *Cenp-C*^{prl41}/+ (*GMR > pim prl41*), *GMR-thrΔC* III.1/*Cenp-C*^{prl41} (*GMR-thrΔC prl41*), *GMR-thrΔC* III.1/*Df(3R)p25* (*GMR-thrΔC p25*), *abc* II.1/+; *GMR-thrΔC* III.1/*Df(3R)p25* (*GMR-thrΔC p25 abc*), *abcd* II.2/+; *GMR-thrΔC* III.1/*Df(3R)p25* (*GMR-thrΔC p25 abcd*). *Df(3R)p25* deletes *Cenp-C* (see panel *B*), and the transgene insertions *abc* II.1 and *abcd* II.2 carry genomic fragments without and with *Cenp-C*, respectively (see panel *C*). The latter but not the former transgene reverses the enhancement that *Df(3R)p25* contributes to the phenotype induced by *GMR-thrΔC* III.1. (*B*) Red lines indicate the chromosomal regions deleted by deficiencies (Def) that scored as enhancers (Enh, +) of the aberrant eye phenotype resulting from overexpression of *pim* or *thrΔC* and that failed to complement *Cenp-C*^{prl41} (Com, –), while black lines represent deficiencies with the opposite behavior (Enh, –; Com, +). A locus interacting with *pim* and *thr* is therefore located between the vertical dashed lines. (nd) Not done. (*C*) Black lines indicate the chromosomal regions and the annotated genes (*CG31453*, *mRpS18C*, *CG31460*, *Cenp-C*) present in transgenes (TG) that were assayed in complementation tests (Com) for their ability to prevent the recessive lethality resulting from *Cenp-C*^{prl41} hemizygosity. The frameshift mutation introduced in the *Cenp-C* region of transgene *abcd*^{m} is indicated by the red ×.

prl41). Complementation tests with *l(3)85Aa*^{prl41} and deficiencies breaking within 85A–85C revealed noncomplementation in case of deficiencies that enhanced the *pim* and *thr*Δ*C* overexpression phenotype and, conversely, complementation for deficiencies that did not modify this phenotype (Fig. 1B). After molecular mapping of selected deficiency breakpoints, a series of transgenic strains carrying genomic DNA fragments with some of the genes predicted within the identified chromosomal region was generated and used for complementation tests with *l(3)85Aa*^{prl41}. Only DNA fragments containing the intact gene *CG31258* were found to prevent the developmental lethality of *l(3)85Aa*^{prl41} hemi- and homozygotes (Fig. 1C). Moreover, these fragments also suppressed the enhancing effect of heterozygosity for *l(3)85Aa*^{prl41} or noncomplementing deficiencies on the aberrant phenotype caused by *pim* and *thr*Δ*C* overexpression during eye development (Fig. 1A; data not shown). In addition, molecular analyses of the *CG31258* sequence isolated from the *l(3)85Aa*^{prl41} chromosome revealed the presence of a premature stop codon instead of a glutamine codon at position 1107 of the predicted protein. Therefore, we conclude that *l(3)85Aa*^{prl41} represents a mutant allele of *CG31258* that interacts genetically with *pim* and *thr*.

Furthermore, in a screen for recessive lethals resulting in cell cycle progression defects during embryogenesis, another mutation was subsequently identified that was characterized by a similar embryonic mutant phenotype and map location (K. Dej and T. Orr-Weaver, pers. comm.) and eventually was found to be allelic to *l(3)85Aa*^{prl41}. This second allele *l(3)85Aa*^{IR35} enhanced the rough eye phenotype resulting from *pim* and *thr*Δ*C* overexpression to the same extent as *l(3)85Aa*^{prl41}, and its recessive lethality was also fully complemented by *CG31258* transgenes (data not shown). Sequence analysis of *l(3)85Aa*^{IR35} revealed a premature stop codon instead of the glutamine codon at position 858 of the predicted *CG31258* protein.

The most recent gene model of *CG31258* annotated by the *Drosophila* Genome Project agrees with our independent cDNA sequence analyses except for the position of the intron–exon junction at the start of exon 4. Initial database searches with the predicted amino acid sequence did not reveal statistically significant similarities to other genes until sequence traces of various Drosophilid genome projects were deposited in the public domain. The sequence comparisons with these Drosophilid orthologs in combination with the results of our functional characterizations described below eventually allowed an identification of *CG31258* as the *Drosophila Cenp-C* homolog. In the following, therefore, we designate this gene as *Cenp-C*, even though its identity was recognized only after and because of our functional characterization.

Identification of a centromere localization domain in Cenp-C

To evaluate the intracellular localization of *Drosophila* Cenp-C, we produced transgenic lines expressing Cenp-C variants fused either to the enhanced yellow fluorescent protein (EYFP) or to myc epitope copies at the N or C terminus. In addition, affinity-purified rabbit antibodies were generated. Both immunolabeling of wild-type Cenp-C or tagged variants as well as in vivo imaging of EYFP fusions in *Drosophila* embryos (Fig. 2A,D) indicated that Cenp-C is a constitutive centromere protein. This notion was confirmed by comparing the localization of Cenp-C with that of the centromere protein Cid, the *Drosophila* Cenp-A homolog. The comparison revealed colocalization during interphase (Fig. 2D) and mitosis (data not shown).

Analysis of Cenp-C expression during development by immunoblotting (Fig. 2B) and immunofluorescence (Fig. 2C) revealed a correlation with mitotic proliferation. Anti-Cenp-C signals declined rapidly in the embryonic epidermis after the final mitotic division, while they were still intense in central nervous system cells that proliferate mitotically. In late embryos, where mitotic proliferation is restricted to only very few cells mainly in the brain, Cenp-C levels were found to be minimal. Moreover, neither immunoblotting (Fig. 2B) nor immunofluorescence and EYFP-Cenp-C fluorescence (data not shown) revealed Cenp-C in the endoreduplicating salivary glands from third instar larvae.

Consistent with the shared intracellular localization of Cid/Cenp-A and Cenp-C, we observed genetic interactions between *cid* and *Cenp-C*. The aberrant rough eye phenotype caused by *cid* overexpression during eye development (Jäger et al. 2005) was found to be enhanced by lowering the number of functional *Cenp-C* gene copies from two to one (Fig. 2F). A noncentromeric excess of overexpressed Cid/Cenp-A, therefore, might titrate limiting amounts of Cenp-C away from the centromere.

Consistent with the idea that Cid/Cenp-A and Cenp-C are in close association, immunolabeling of *cid* mutant embryos with antibodies against Cenp-C revealed that Cid/Cenp-A is required for normal centromeric Cenp-C localization. In *cid* mutant embryos, the presence of a maternal contribution prevents mitotic abnormalities until late in embryogenesis. However, already at earlier developmental stages when maternally contributed Cid/Cenp-A was still detectable (data not shown) and mitotic defects were not yet apparent, anti-Cenp-C signals were clearly weaker in *cid* mutants compared with sibling control embryos (Fig. 2E). Immunolabeling of *Cenp-C* mutant or deficient embryos with anti-Cid/Cenp-A did not reveal a reciprocal dependence of Cid/Cenp-A localization on normal Cenp-C expression and function (see below).

To define centromere localization domains in Cenp-C, we expressed various Cenp-C fragments fused to enhanced green fluorescent protein (EGFP) in *Drosophila* embryos from appropriate transgenes (Fig. 3A). The N-terminal third of Cenp-C (amino acids 1–575) and the central third (amino acids 558–1038) failed to localize the fused EGFP to the centromere (Fig. 3B, N+ and M+). In contrast, the C-terminal third (amino acids 1009–1411) was sufficient to direct efficient centromere localization (Fig. 3B, C+). Further analysis of this region

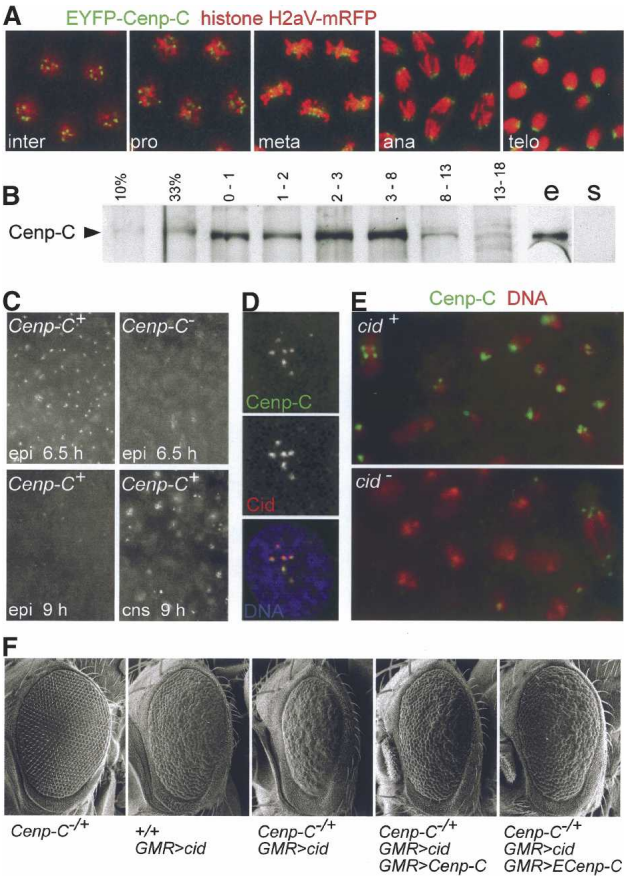

Figure 2. *Drosophila* Cenp-C is a constitutive centromere protein colocalizing and interacting with Cid/Cenp-A. (*A*) In vivo imaging of syncytial embryos, which express EYFP-Cenp-C (green) and histone H2Av-mRFP (red), indicates that Cenp-C is centromeric during interphase (inter), prophase (pro), metaphase (meta), anaphase (ana), and telophase (telo). (*B*) Immunoblotting with embryo extracts prepared at different developmental ages (0–1, 1–2, 2–3, 3–8, 8–13, and 13–18 h after egg deposition) revealed high levels of Cenp-C during stages with intense mitotic cell proliferation (0–8 h) and decreasing levels during late embryogenesis when few cells proliferate mitotically (8–18 h). Thirty embryos were loaded per lane except in the first two where three (10%) and 10 (33%) 0–1-h embryos were loaded. Moreover, while Cenp-C was clearly detected in an extract prepared from 20 6–8-h embryos (e), it could not be detected in a comparable amount of protein in an extract prepared from 30 salivary glands of third instar larvae (s). (*C*) Immunofluorescence experiments with embryos homozygous for *Df(3R)Exel6149*, which deletes *Cenp-C* (*Cenp-C*$^{-}$), and sibling control embryos (*Cenp-C*$^{+}$) revealed strong anti-Cenp-C signals in the epidermis of *Cenp-C*$^{+}$ embryos at the stage of mitosis 16 (epi 6.5 h) and in the central nervous system, where mitotic proliferation occurs also at 9 h (cns 9 h). In contrast, weak signals were observed in the post-mitotic epidermis of *Cenp-C*$^{+}$ embryos at 9 h (epi 9 h) and already at the stage of mitosis 16 in *Cenp-C*$^{-}$ embryos (epi 6.5). (*D*) An interphase nucleus from a syncytial embryo expressing Cenp-C-myc is shown at high magnification after labeling with anti-myc (*top* panel and green in *bottom* panel), anti-Cid/Cenp-A (*middle* panel and red in *bottom* panel), and a DNA stain (blue in *bottom* panel). (*E*) Labeling of *cid* mutant embryos (*cid*$^{-}$) and sibling control embryos (*cid*$^{+}$) with anti-Cenp-C (green) and a DNA stain (red) indicates that Cid/Cenp-A is required for normal Cenp-C localization at the centromere. High-magnification views of epidermal regions at the stage of mitosis 16 show reduced centromeric anti-Cenp-C signals in *cid* mutants. (*F*) Overexpression of *cid*/*Cenp-A* results in an aberrant eye phenotype that is enhanced by mutations in *Cenp-C*. The eyes shown are from flies with the following genotypes: *Cenp-C*^{IR35}/+ (*Cenp-C*$^{-/+}$), *GMR-GAL4 UAS-cid* II.3B/+ (+/+ *GMR > cid*), *GMR-GAL4 UAS-cid* II.3B/+; *Cenp-C*^{IR35}/+ (*Cenp-C*$^{-/+}$ *GMR > cid*), *GMR-GAL4 UAS-cid* II.3B/*UAS-Cenp-C* II.1; *Cenp-C*^{IR35}/+ (*Cenp-C*$^{-/+}$ *GMR > cid GMR > Cenp-C*), *GMR-GAL4 UAS-cid* II.3B/+; *Cenp-C*^{IR35}/*UAS-EGFP-Cenp-C* III.2 (*Cenp-C*$^{-/+}$ *GMR > cid GMR > ECenp-C*).

indicated that the subregion from amino acids 1009–1205 was also sufficient to confer centromere localization (Fig. 3B, CN+), while two other subregions (amino acids 1094–1306 and 1204–1411) were not sufficient (Fig. 3B, CM+ and CC+).

To identify amino acid positions crucial for centromere localization, we randomly mutagenized the sequences encoding the region sufficient for centromere localization in vitro by error-prone PCR and used these mutated sequences to replace the corresponding wild-type sequence in a construct allowing expression of the C-terminal third of Cenp-C fused to EGFP. Three-hundred-ninety-four mutagenized clones were analyzed for their ability to localize to the centromere after transfection of *Drosophila* SR+ cultured cells. All 50 mutants that had lost centromere localization were subjected to DNA sequence analysis. In addition, 25 randomly selected mutants that localized to the centromere were sequenced as well. These sequences revealed that mutant constructs contained on average 1.9 mutations and that every amino acid position within the region sufficient for centromere binding should have been covered by about two missense mutations in our mutagenesis experiment. Yet only a single-point mutation (R1101G) that abolished centromere localization in the transfection assay was identified (Fig. 3C,D). R1101, therefore, appears to be of special importance for centromere localization. All other mutants that failed to localize to the centromere were characterized by the presence of premature stop codons. The location of these stop codons in combination with the location of a premature stop codon (1192stop) that did not abolish centromere localization in the transfection assay indicated that the region between amino acids 1084 and 1192 is important for centromere localization (Fig. 3C,D).

Drosophilid Cenp-C homologs contain a diverged CENPC motif

The deposition of Drosophilid genome sequences in the public internet domain allowed the identification of *Cenp-C* orthologs from *Drosophila simulans*, *Drosophila yakuba*, *Drosophila erecta*, *Drosophila ananassae*, *Drosophila pseudoobscura*, and *Drosophila virilis*. Amino acid comparisons between the predicted proteins revealed the presence of conserved blocks (Fig. 4A). Sev-

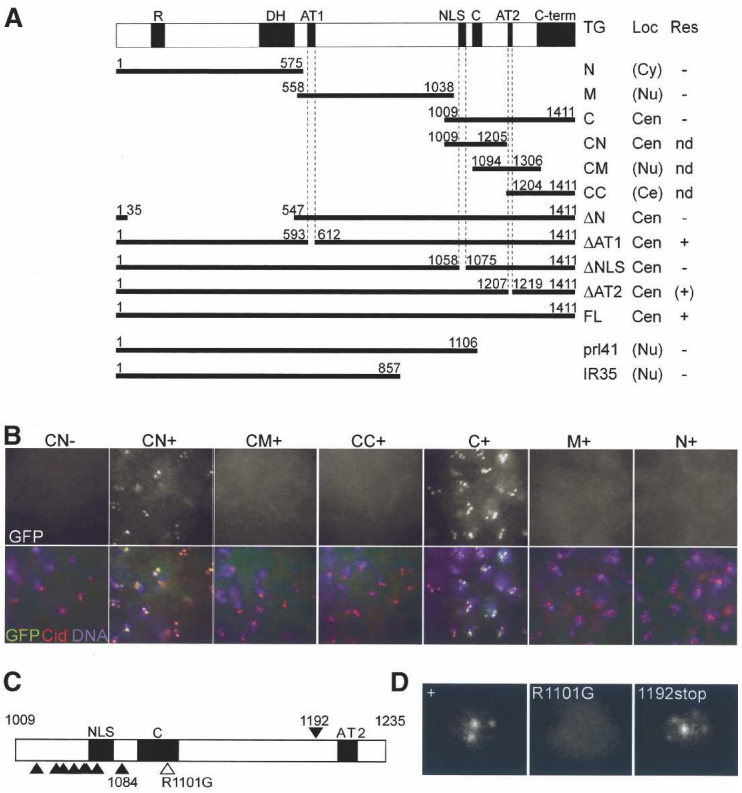

Figure 3. Identification of the Cenp-C centromere localization domain. (*A*) The Cenp-C regions present in *UAS-EGFP* transgene variants (TG) are indicated by black horizontal lines with numbers indicating amino acid positions. The intracellular localization of the EGFP-Cenp-C variants expressed from these transgenes is listed (Loc) and was found to be either cytoplasmic (Cy), nuclear (Nu), centromeric (Cen), or all over the cell (Ce). Brackets indicate results that were observed only after strong expression. The ability of these transgenes to prevent phenotypic abnormalities after expression in *Cenp-C* mutant embryos is also listed (Res) with + or – indicating those that did or did not rescue, respectively. (nd) Not done. The two black horizontal lines at the *bottom* represent the Cenp-C fragments expressed from the *Cenp-C*^{prl41} and *Cenp-C*^{IR35} alleles, which both carry premature stop codons after codons 1106 and 857, respectively. Black boxes on *top* indicate the following Cenp-C regions: arginine-rich region (R), a region highly conserved in the Drosophilid Cenp-C homologs (DH), predicted AT hooks (AT1 and AT2) and nuclear localization signal (NLS), the CENPC motif (C), and the metazoan-like C-terminal region (C-term). (*B*) High-magnification views from the epidermis of embryos with a heat-inducible *GAL4* transgene and *UAS-EGFP-Cenp-C* transgene variants (CN, CM, CC, C, M, N) (see *A*). The embryos were either heat-treated (+) or not (–), fixed, and labeled with anti-GFP (GFP, green in *bottom* panel), anti-Cid/Cenp-A (Cid, red in *bottom* panel), and a DNA stain (DNA, blue in *bottom* panel). (*C*) Variants of EGFP-Cenp-C-C obtained after random mutagenesis of the region from amino acids 1009–1235 of Cenp-C were expressed after transfection of *Drosophila* SR+ cells and analyzed for their ability to localize to the centromere. The arrowhead pointing down to position 1192 indicates a premature stop codon that does not interfere with centromere localization. The filled arrowheads pointing up indicate premature stop codons that abolish centromere localization. The open arrowhead pointing up indicates the single identified point mutation (R1101G) that prevents centromere localization. (*D*) GFP signals in representative transfected SR+ cells expressing EGFP-Cenp-C variants. The following variants were expressed: *EGFP-Cenp-C-C* (+), *EGFP-Cenp-C-C* with G instead of R at position 1101 (R1101G), *EGFP-Cenp-C-C* with a premature stop codon at position 1192 (1192stop).

eral blocks of relatively high conservation were found within the region important for centromere localization (Fig. 4A, Cen). R1101, which is crucial for centromere localization, is present within the largest of these blocks, and the corresponding position was found to be invariant in all of the Drosophilid sequences. Moreover, comparison of the consensus sequence of this block with the consensus sequence of the CENPC motif that has recently been shown to be the only shared element in the Cenp-C proteins of yeast, plants, and vertebrates (Talbert et al. 2004) revealed strong similarities (Fig. 4B). R1101 corresponds to a position in the CENPC motif that is identical in all Cenp-C proteins (Fig. 4B, see arrow). While the C-terminal part of the Drosophilid CENPC motif is different from that of other eukaryotes, we emphasize that similarities between the Cenp-C proteins of *Drosophila*, fungi, and vertebrates are also detectable in the very C-terminal region (Fig. 4A, C-term). The human Cenp-C region encompassing the CENPC motif to the C terminus is known to be sufficient for centromere targeting (Lanini and McKeon 1995; Song et al. 2002). Based on the very limited but distinct sequence similarities in functionally identical centromere localization domains, therefore, the Drosophilid proteins appear to be strongly diverged Cenp-C orthologs.

Independent functional domains in Cenp-C

The Drosophilid Cenp-C proteins share some regions of high similarity. As discussed above, the C-terminal region and the CENPC motif within the region sufficient for centromere localization are well conserved (Fig. 4A, C and C-term). However, the most extensive conservation is present within the N-terminal third in an arginine-rich region (Fig. 4A, R) and in another region unique to the Drosophilid Cenp-C proteins (Fig. 4A, DH, for Drosophilid homology region). Fragments of human Cenp-C encompassing the equivalent positions can function as a second centromere localization domain, independent of the previously mentioned C-terminal centromere localization domain (Yang et al. 1996; Song et al. 2002). In the case of *Drosophila melanogaster* Cenp-C, the highly conserved N-terminal block does not confer normal centromere localization. Fused to EGFP, the N-terminal region including DH is not sufficient for centromere localization (Fig. 3B, N+), nor does Cenp-C lack-

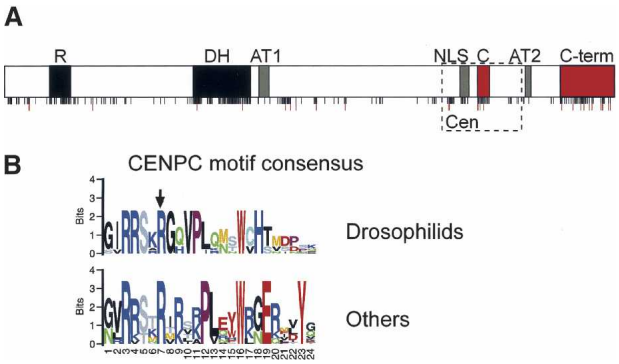

Figure 4. Comparison of Cenp-C from *Drosophila* and other metazoans. (*A*) Identical positions present in an alignment of the amino acid sequences of Cenp-C from *D. melanogaster*, *D. pseudoobscura*, and *D. virilis* are indicated by black lines. Positions that are also identical in an alignment including Cenp-C from *Homo sapiens*, *Mus musculus*, and *Rattus norvegicus* in addition to the three *Drosophila* species are indicated by red lines. The boxes indicating the CENPC motif (C) and the C-terminal region (C-term), which appear to be conserved in all metazoans, are filled in red. The arginine-rich region (R) and another region (DH) that were found to be maximally conserved among *Drosophila* species are illustrated by black boxes. Gray boxes indicate the poorly conserved predicted AT hooks (AT1 and AT2) and nuclear localization signal (NLS). The region sufficient for centromere localization is indicated by a dashed rectangle (Cen). (*B*) A CENPC motif consensus sequence was derived from the predicted Cenp-C proteins of seven *Drosophila* species (*D. ananassae*, *D. erecta*, *D. melanogaster*, *D. pseudoobscura*, *D. simulans*, *D. virilis*, *D. yakuba*) and found to deviate from the consensus sequence derived from fungal, plant, and other metazoan Cenp-C proteins (Talbert et al. 2004), in particular toward the C-terminal end.

ing this region (deletion of amino acids 36–546) fail to localize to the centromere (Fig. 3A; data not shown).

Three other small regions of *D. melanogaster* Cenp-C displayed similarities to nuclear localization signals (amino acids 1058–1075) (Fig. 3A, NLS) and to AT hooks, which can mediate binding to the minor grove of DNA (amino acids 593–612 and amino acids 1207–1219) (Fig. 3A, AT1 and AT2). These regions showed limited conservation among Drosophilids and were found to be dispensable for centromere localization (Fig. 3A; data not shown).

While the regions NLS, AT1, AT2, and the N-terminal domain with the regions R and DH are dispensable for centromere localization, all except AT1 appear to provide other essential functions. Cenp-C versions lacking these regions were unable to prevent phenotypic abnormalities in *Cenp-C* mutant embryos when expressed from appropriate transgenes (data not shown). In contrast, analogous expression of wild-type Cenp-C or Cenp-C lacking AT1 was sufficient to prevent phenotypic abnormalities in *Cenp-C* mutant embryos (Figs. 3A, 6A [below]).

We also analyzed the consequences of overexpression of wild-type and mutant Cenp-C versions during eye and wing development. Overexpression of the minimally conserved middle region had no effect (Fig. 5, E-M). Overexpression of full-length Cenp-C resulted in an aberrant phenotype but only in wings and not in eyes (Fig. 5, FL and E-FL). Stronger defects were observed after expression of the N-terminal region containing the maximally conserved R and DH blocks (Fig. 5, E-N). The strongest defects were caused by expression of C-terminal regions containing the centromere localization domain (Fig. 5, E-C and E-CN). Therefore, we assume that the overexpressed fragments capable of centromere binding displace wild-type Cenp-C. Similarly, we propose that overexpression of the region with the maximally conserved N-terminal R and DH blocks, as well as an excess of wild-type and thus noncentromeric Cenp-C, might titrate away other components, perhaps kinetochore proteins normally recruited by centromeric wild-type Cenp-C during mitosis.

Is Cenp-C involved in sister-chromatid separation?

To define the Cenp-C function in further detail, we analyzed the consequences of loss-of-function mutations. In particular, since our identification of *Cenp-C* by genetic interactions argued for a functional cooperation between separase regulatory subunits and this centromere protein, we were interested in whether the *Cenp-C* mutant phenotype provides evidence for a direct interaction.

The two available *Cenp-C* alleles (*prl41* and *IR35*) both behaved as recessive lethal mutations. Homozygous and trans-heterozygous embryos, as well as embryos carrying either of the two alleles over a deficiency (*Df(3R)p25*) did not hatch. Immunolabeling with antibodies against Cyclin B and a DNA stain indicated striking abnormalities within the central nervous system (CNS) during the second half of embryogenesis (Fig. 6A, *Cenp-C*$^{-}$). The CNS of *Cenp-C* mutant embryos included many oversize cells with abnormally high levels of Cyclin B. In addition, pycnotic nuclei characteristic of apoptotic cells were more frequent within the *Cenp-C* mutant CNS, which overall contained far fewer cells than the CNS of wild-type embryos. In contrast, other tissues of *Cenp-C* mutant embryos appeared to be relatively normal. These findings indicated that initial development of *Cenp-C* mutant embryos is normal, presumably reflecting the presence of the maternal *Cenp-C*$^{+}$ contribution, which can be demonstrated by immunofluorescence (Fig. 2C), RT–PCR, and immunoblotting experiments (data not shown). However, this maternal *Cenp-C*$^{+}$ contribution evidently is no longer sufficient to support the extended cell proliferation known to occur during CNS development, where continued cell cycle progression despite chromosome segregation defects might result in oversize cells and apoptosis in the *Cenp-C* mutants. Accordingly, the observation that the CNS is most severely affected in the *Cenp-C* mutants suggests that Cenp-C is only required in dividing cells. This notion is also supported by the observed correlation between Cenp-C expression and mitotic proliferation (Fig. 2B,C).

To characterize the *Cenp-C* mutant phenotype in fur-

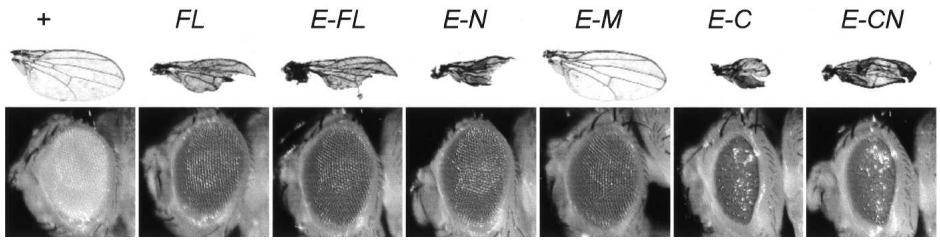

Figure 5. Distinct Cenp-C regions cause defects after overexpression. *MS1096* and *GMR-GAL4* were used to drive overexpression of various *UAS-Cenp-C* transgene variants during wing (*top* row) and eye (*bottom* row) development, respectively. Wild-type wings and eyes are present in control flies (+) with a *GAL4* transgene but without an *UAS* transgene. Aberrant wing and eye phenotypes were observed to variable degrees in flies with either *UAS-Cenp-C* II.2 (*FL*), *UAS-EGFP-Cenp-C* II.2 (E-FL), *UAS-EGFP-Cenp-C-N* II.1 (E-N), *UAS-EGFP-Cenp-C-M* III.2 (E-M), *UAS-EGFP-Cenp-C-C* II.1 (E-C), or *UAS-EGFP-Cenp-CN* II.2 (E-CN) in combination with a *GAL4* transgene. The strongest defects were observed after overexpression of N-terminally truncated Cenp-C fragments containing the centromere localization domain (E-C and E-CN). However, aberrant wings and eyes were also caused by the N-terminal region, which does not localize to the centromere (E-N), while the middle region did not have an effect (E-M). Several independent insertions of each transgene variant were analyzed and found to behave similarly to those shown.

ther detail at a cellular level, we focused on the onset of phenotypic abnormalities. Analyses with the two alleles in homo-, hemi-, or trans-heterozygous embryos gave similar results. Starting during embryonic cycle 15, immunolabeling revealed declining Cenp-C levels in *Cenp-C*-deficient embryos compared with sibling controls (data not shown). Based on double-labeling with a DNA stain and scoring of mitotic figures, the division completing cycle 15 appeared still largely normal in the mutants. At the stage of mitosis 16, residual maternally derived Cenp-C levels were further reduced, but still above background at least in some of the mutant embryos (Fig. 2C). However, mitosis 16 was severely affected. Metaphase figures appeared relatively normal, but anaphase and telophase figures frequently displayed abnormal chromatin bridges (Fig. 6B). Labeling with antibodies against Cid/Cenp-A revealed centromere signals of normal intensity in the *Cenp-C* mutants. Interestingly, in 70% of the chromatin bridges, Cid/Cenp-A signals were observed in the middle (Fig. 6C, *Cenp-C*$^{-}$). Chromatin bridges appearing during mitosis 15 in *Cap-G* mutant embryos almost never displayed comparable central centromere signals (Fig. 6C, *Cap-G*$^{-}$). Cap-G is a subunit of the condensin complex and provides a major function required for sister-chromatid resolution during mitosis. Interestingly, Cap-G has recently been shown to interact genetically and physically with the centromere component Cid/Cenp-A (Jäger et al. 2005). However, the

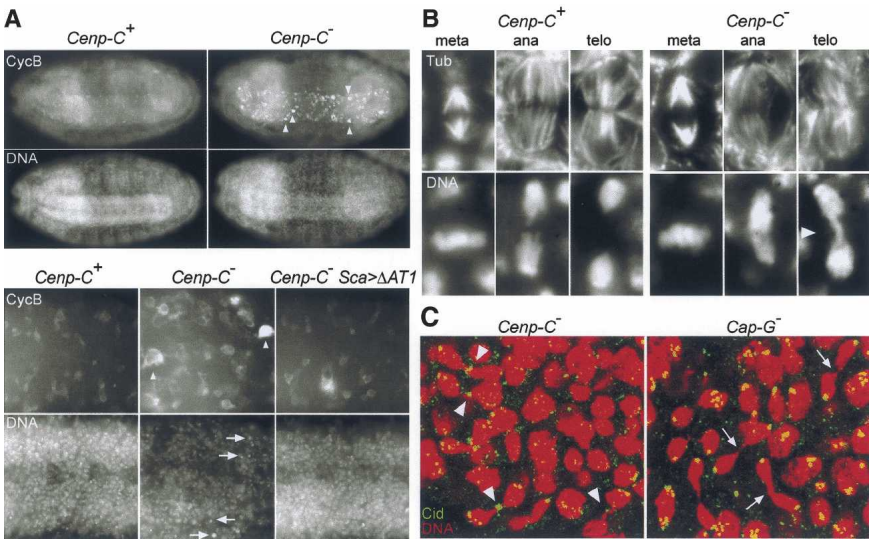

Figure 6. *Cenp-C* mutant phenotype. (*A*) Embryos after germ-band retraction, when mitotic cell proliferation is restricted to the nervous system, were labeled with antibodies against Cyclin B (CycB) and a DNA stain (DNA). While the entire embryos are shown in the two *top* rows, high-magnification views of CNS regions are shown in the two *bottom* rows. In comparison to sibling control embryos (*Cenp-C*$^{+}$), *Cenp-C*^{prl41}/*Df(3R)p25* embryos (*Cenp-C*$^{-}$) contain fewer but often much larger cells expressing Cyclin B at very high levels in the central nervous system (arrowheads). In addition, considerably higher numbers of apoptotic cells with pycnotic nuclei are present in these embryos (arrows). *Sca-GAL4*-mediated expression of *UAS-EGFP-Cenp-C* (data not shown) or *UAS-EGFP-Cenp-C-ΔAT1* in the *Cenp-C* mutant embryos (*Cenp-C*$^{-}$ *Sca* > *ΔAT1*) prevents these abnormalities almost completely. (*B*) Epidermal cells during mitosis 16 from either sibling control embryos (*Cenp-C*$^{+}$) or *Cenp-C*^{prl41} mutant embryos (*Cenp-C*$^{-}$) are presented after labeling with antibodies against tubulin (Tub) and a DNA stain (DNA). While metaphase cells (meta) appear to be indistinguishable, anaphase (ana) and telophase (telo) cells frequently displayed chromatin bridges (arrowhead). (*C*) Epidermal regions after labeling with antibodies against Cid/Cenp-A (Cid, green) and a DNA stain (DNA, red) contain late mitotic cells with chromatin bridges in both *Cenp-C*^{prl41}/*Cenp-C*^{IR35} (*Cenp-C*$^{-}$) and *Cap-G*^{6}/*Df(2R)vg56* (*Cap-G*$^{-}$) mutant embryos. However, while the majority of the chromatin bridges in *Cenp-C*$^{-}$ embryos display anti-Cid/Cenp-A signals at the midpoint (arrowheads), bridges in *Cap-G*$^{-}$ embryos are devoid of such signals (arrows).

early phenotypic consequences of mutations in *Cenp-C* and *Cap-G* are evidently distinct.

Our observations in fixed mutant embryos indicated that Cenp-C is particularly important for separation of sister centromeres during mitosis and/or for segregation of sister chromatids to the poles. A distinct increase in the number of phospho-histone H3-positive cells was observed after incubation in colchicine, demonstrating that the mitotic spindle checkpoint is still functional in *Cenp-C* mutants, at least in most cells at the stage of mitosis 16. Nevertheless, immunolabeling with an antibody against the checkpoint component BubR1 already revealed less intense signals at the kinetochores during prometaphase 16 in *Cenp-C* mutants compared with sibling controls (data not shown). Moreover, the relatively normal appearance and number of metaphase plates during mitosis 16 in the *Cenp-C* mutants also argued that most kinetochores are still quite functional, allowing for chromosome attachment to the mitotic spindle, chromosome congression into the metaphase plate, and spindle checkpoint silencing.

Since kinetochore functionality in *Cenp-C* mutants would be surprising and a strong argument for a sister separation defect as an underlying cause of the observed anaphase defects, we applied in vivo imaging for a more careful analysis of kinetochore functionality, in particular in sister-chromatid pairs that fail to become segregated during mitosis 16 in *Cenp-C* mutants. Therefore, we crossed transgenes driving expression of mRFP fused to histone H2Av and EGFP fused to Cid/Cenp-A into the *Cenp-C* mutant background. Time-lapse analysis of progression through mitosis 16 (Fig. 7) clearly revealed that chromosome congression into a metaphase plate is slightly delayed in the mutants. The period from the onset of chromosome condensation until the metaphase-to-anaphase transition lasted for ~5.6 min in the *Cenp-C* mutants, compared with 4.4 min in sibling controls (Fig. 7B). This delay occurred during prometaphase. Moreover, the metaphase frame acquired just before the onset of anaphase usually revealed a more irregular centromere positioning than in the straight metaphase plates characteristically observed in sibling control embryos (Fig. 7A). After the metaphase-to-anaphase transition, some mutant cells failed to achieve timely separation and/or

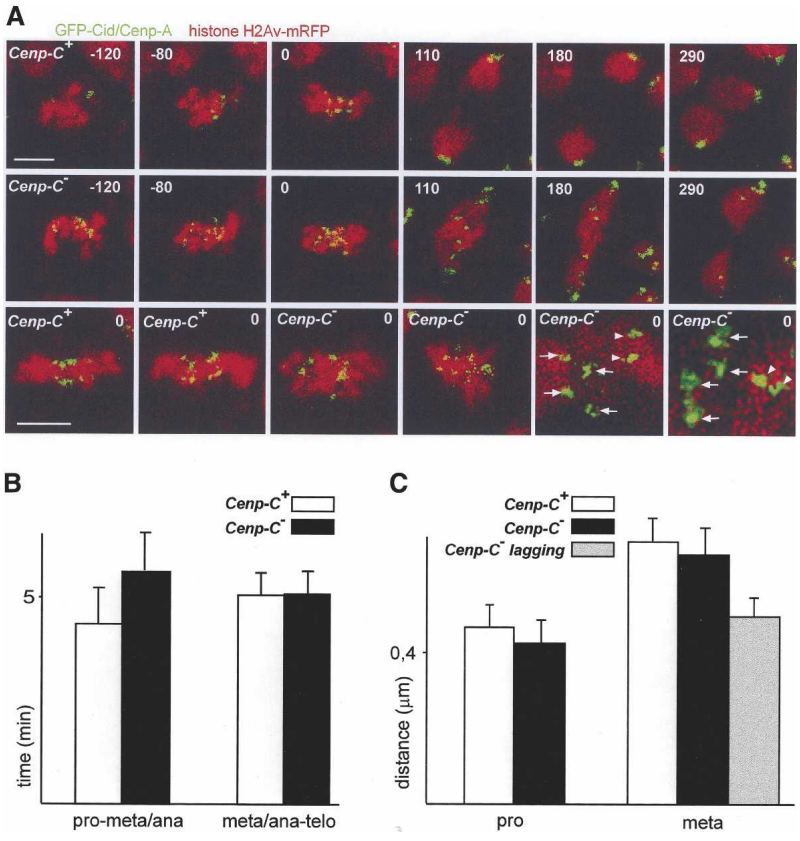

Figure 7. Mitotic chromosome segregation in *Cenp-C* mutant embryos. (*A*) Mitotic divisions in *Cenp-C*$^+$ (*Cenp-C*$^+$) or *Cenp-C*$^-$ (*Cenp-C*$^-$) embryos expressing *gcid-EGFP-cid* (GFP-Cid/Cenp-A) and *His2Av-mRFP1* (histone H2Av-mRFP) were analyzed by time-lapse in vivo imaging. The time (in seconds) relative to the last frame before the onset of anaphase, which was set to 0, is indicated in each frame. All frames in the *top* row are from a cell progressing through mitosis 16 in a *Cenp-C*$^+$ sibling control embryo and all frames in the *middle* row from a *Cenp-C*$^-$ embryo at the same stage. Magnification in the *top* two rows is indicated by the white bar in the *upper left* panel, which corresponds to 3 µm. Various metaphase plates are shown in the *bottom* row always in the same orientation with the bar corresponding to 3 µm illustrating the magnification shown in the first four panels. Even higher magnifications are shown in the two *right*-most panels in which sister centromeres of lagging chromosomes in *Cenp-C*$^-$ embryos are indicated by white arrowheads and those of nonlagging chromosomes by white arrows. Chromosomes that were subsequently lagging behind during anaphase in *Cenp-C*$^-$ embryos did not only have more closely spaced sister centromeres than nonlagging chromosomes (see also *C*) but were also often not oriented in the axis of the spindle, as evident in the *right*-most panel in the *bottom* row. (*B*) The average time (in minutes) from the onset of mitosis 16 until the last frame before the onset of anaphase (pro-meta/ana), as well as from the onset of anaphase until telophase (meta/ana-telo), was determined after time-lapse analysis of embryos that were either *Cenp-C*$^+$ (*Cenp-C*$^+$, white bars) or *Cenp-C*$^-$ (*Cenp-C*$^-$, black bars). At least 20 mitoses from more than four embryos were analyzed. (*C*) The distance between sister centromeres (in micrometers) was determined during prophase (pro) and immediately before the onset of anaphase (meta) after time-lapse analysis of embryos at the stage of mitosis 16. Average values obtained with *Cenp-C*$^+$ embryos are represented by white bars. Values obtained for chromosomes that were subsequently lagging behind during anaphase in *Cenp-C*$^-$ embryos are indicated by the gray bar, while the values observed in *Cenp-C*$^-$ embryos during prophase and before the metaphase-to-anaphase transition in case of nonlagging chromosomes are given by black bars. At least 11 chromosomes from more than four embryos were analyzed.

segregation of one or two chromosomes (Fig. 7A). Measuring the distance between the sister kinetochores just before the metaphase-to-anaphase transition indicated that these late or nonsegregating chromosomes were not attached to the spindle in a normal bipolar fashion. Bipolar attachment results in a significant increase in the intersister kinetochore distance, as confirmed by comparing the values in sibling control embryos during prophase and metaphase (Fig. 7C). This increase was also observed in the *Cenp-C* mutants but only in the normally segregating chromosomes. In contrast, in the nonsegregating chromosomes, the intersister kinetochore distance at the metaphase-to-anaphase transition was not greater than the average distance observed during prophase (Fig. 7C). These findings indicate that Cenp-C is required for normal bipolar kinetochore attachment.

Discussion

Our identification of *Drosophila* Cenp-C closes a prominent gap in the arguments for homologous centromere organization. Centromeric DNA sequences have evolved extremely rapidly and appear to have driven the coevolution of centromeric proteins during eukaryote evolution (Henikoff et al. 2001; Talbert et al. 2004). The resulting low sequence similarity between centromeric proteins has effectively concealed the existence of a common set of constitutive eukaryotic centromere proteins until very recently. The first features demonstrated to be shared among fungal, plant, and animal centromeres were centromere-specific histone H3 variants (Sullivan et al. 1994; Stoler et al. 1995; Buchwitz et al. 1999; Henikoff et al. 2000; Takahashi et al. 2000; Talbert et al. 2002). In addition to these Cenp-A homologs, only one further constitutive centromere component, Cenp-C, has so far been shown to be present in each of the three main eukaryotic branches (Saitoh et al. 1992; Brown 1995; Meluh and Koshland 1995; Dawe et al. 1999; Moore and Roth 2001; Talbert et al. 2004). Our findings now also establish the existence of *Drosophila* Cenp-C, which had previously escaped detection by careful bioinformatics genome analyses (Talbert et al. 2004) because of its very limited sequence similarity. In combination with the recent identification of related Cenp-H-, Cenp-I-, and Mis12-like proteins in both vertebrates and yeast (Nishihashi et al. 2002; Goshima et al. 2003; Westermann et al. 2003; Cheeseman et al. 2004; Obuse et al. 2004), our results provide strong support for the notion of a common set of constitutive centromere proteins. These proteins, which are centromeric throughout the cell cycle, appear to provide a foundation for kinetochore assembly and spindle attachment during mitosis by recruiting several distinct multisubunit complexes that also contain highly diverged proteins (Wigge and Kilmartin 2001; De Wulf et al. 2003; Westermann et al. 2003; Cheeseman et al. 2004).

The extensive sequence divergence characteristically observed among homologous eukaryotic centromere and kinetochore proteins is striking, especially in the light of their common fundamental cellular function. The average amino acid identity observed in a genome-wide comparison of *D. melanogaster* and *D. pseudoobscura* ortholog pairs is 77% (Richards et al. 2005) and only 38% in case of the *Cenp-C* pair. Moreover, based on the ratio between radical charge mutations and conservative substitutions in *D. melanogaster* and *D. pseudoobscura* ortholog pairs, *Cenp-C* is one of 44 genes likely to have evolved under positive selection (Richards et al. 2005). Except for a few very restricted regions (data not shown), our comparison of *D. melanogaster Cenp-C* with the orthologs from *D. erecta* and *D. yakuba*, which are closer relatives than *D. pseudoobscura* and thus amenable to d_N/d_S analyses (Comeron 1999), did not reveal strong evidence for positive selection, in contrast to the recent findings in plant and mammalian lineages (Talbert et al. 2004). However, we point out that these d_N/d_S analyses ignore insertions and deletions (indels), which have occurred considerably more often during *Cenp-C* evolution in Drosophilids than in the mammalian lineage. Most of the indels are observed within the minimally conserved central regions of Drosophilid Cenp-C. Similar variabilities resulting from recurrent exon duplications have been observed in the central region of the plant Cenp-C genes (Talbert et al. 2004).

The adaptively evolving regions of mammalian Cenp-C have been shown to bind to DNA in vitro, consistent with the proposed coevolution of centromeric DNA and protein sequences (Talbert et al. 2004). However, this DNA binding in vitro is not sequence-specific (Sugimoto et al. 1994), suggesting that interactions with centromere-specific proteins contribute to centromere localization of Cenp-C. As in other organisms (Howman et al. 2000; Moore and Roth 2001; Oegema et al. 2001; Van Hooser et al. 2001; Westermann et al. 2003), Cid/Cenp-A is also required for centromere localization of Cenp-C in *Drosophila*. High-resolution light microscopy of mitotic chromosomes has indicated that human Cenp-C covers the poleward-oriented peripheral region of the Cenp-A-containing centromeric chromatin (Blower et al. 2002). Direct interactions between Cenp-A and Cenp-C have not yet been demonstrated in any organism. Our attempts with yeast two-hybrid experiments were also unsuccessful (R. Schittenhelm, S. Heeger, and C.F. Lehner, unpubl.).

The CENPC motif has recently been identified as the only region conserved among the Cenp-C orthologs from fungi, plant, and animals (Talbert et al. 2004). In Drosophilids, even this short motif of ~24 amino acids is not fully conserved in its C-terminal part. Our results suggest that this CENPC motif is crucial for centromere localization. We demonstrate that a single-point mutation affecting one of the invariant positions in the CENPC motif interferes with centromere localization of the C-terminal domain of Cenp-C in our transfection assay. This mutation was identified as the only missense mutation interfering with centromere localization after extensive random mutagenesis. Further experiments will reveal whether and how the CENPC motif contacts Cid/Cenp-A nucleosomes. We would like to emphasize, however, that also in *Drosophila* Cenp-C, other regions

than the CENPC motif clearly contribute to efficient centromere localization. Centromere localization of the CN subregion (1009–1205), for instance, is only detected in our transfection assay in live but not in fixed cells, while centromere localization of the larger C region (1009–1411) is resistant to fixation.

The highest conservation among Drosophilid Cenp-C proteins is observed within the N-terminal third, which is neither required nor sufficient for normal centromere localization. Nevertheless, prolonged overexpression of this domain in proliferating eye and wing imaginal disc cells results in severe defects. The conserved N-terminal Cenp-C domains (R and DH) might bind to kinetochore proteins and titrate these away from the centromere when overexpressed. Biochemical and genetic characterizations in *Saccharomyces cerevisiae* and *Caenorhabditis elegans* have suggested that Cenp-C is not only associated with Cenp-A, but that it also recruits the next layer of kinetochore proteins, in particular the Mis12/Mtw1 and Ndc80 complexes, which remain to be identified in *Drosophila* (De Wulf et al. 2003; Pinsky et al. 2003; Westermann et al. 2003; Cheeseman et al. 2004).

As in yeast (Meluh and Koshland 1995), chicken (Fukagawa and Brown 1997; Fukagawa et al. 1999), and mice (Kalitsis et al. 1998), *Cenp-C* is also an essential gene in *Drosophila*. Antibody microinjection experiments in mammalian cells (Tomkiel et al. 1994); RNA interference in *C. elegans* (Moore and Roth 2001; Oegema et al. 2001); and phenotypic analysis in yeast (Brown et al. 1993), chicken cells (Fukagawa et al. 2001), and mutant *Drosophila* embryos demonstrate that Cenp-C is required for normal chromosome segregation during mitosis. Our in vivo imaging in *Cenp-C* mutant embryos discloses these defects in detail. Previously, in vivo imaging has also been applied in *C. elegans CENP-C(RNAi)* embryos (Moore and Roth 2001; Oegema et al. 2001). The formation of holocentric chromosomes and transient Cenp-C recruitment only during mitosis differentiates *C. elegans* from other metazoans like *Drosophila* and mammalian cells. Moreover, in contrast to the findings in *C. elegans*, chromosome congression into a central plane is still observed in the *Drosophila Cenp-C* mutants. Presumably, this chromosome congression reflects the function of residual maternally provided Cenp-C, which is still detectable at the stage of our analyses. Moreover, our time-lapse analyses demonstrate that chromosome congression is not entirely normal in the *Cenp-C* mutant embryos. Metaphase plate formation is delayed and often does not lead to the highly ordered arrangement of all chromosomes characteristically observed before anaphase onset in wild type. Occasional chromosomes fail to achieve bipolar attachment in the *Cenp-C* mutants. These chromosomes do not segregate normally during anaphase. Cenp-C is, therefore, clearly required for normal attachment of kinetochores to the mitotic spindle.

Evidently, the insufficiently attached chromosomes in *Cenp-C* mutant embryos are unable to inhibit the onset of anaphase, even though the mitotic spindle checkpoint appears to be at least partially functional in *Cenp-C* mutants at the analyzed stage. However, assembly of mitotic spindle checkpoint proteins might fail, particularly on the kinetochores of those chromosomes that do not attach correctly to the mitotic spindle.

In principle, the chromosome segregation defects observed in the *Cenp-C* mutants might not only reflect impaired interactions between kinetochores and spindle. Segregation of sister chromatids to the spindle poles also depends on complete resolution of sister-chromatid cohesion at the metaphase-to-anaphase transition. This final separation of sister chromatids is thought to be achieved by separase-mediated cleavage of the Scc1/Rad21 subunit of those cohesin complexes that perdure in the pericentromeric region until the metaphase-to-anaphase transition. Several observations are consistent with the idea that a localized full activation of separase might be assisted by centromeric proteins (see above). Accordingly, mutations in *Cenp-C* might reduce separase activity and thereby explain the genetic interactions with the regulatory separase subunits Pim/securin and Thr that led to our identification of *Drosophila* Cenp-C. We have failed to observe coimmunoprecipitation of Cenp-C with separase complex proteins and have been unable to detect effects of *Cenp-C* mutations on Pim and Thr levels (O. Leismann and C.F. Lehner, unpubl.). Our analysis has, therefore, not exposed clear evidence for separase activation at centromeres. On the other hand, Cenp-C is clearly required for normal chromosome attachment to the mitotic spindle, and thus the observed genetic interactions most likely reflect a summation of negative effects on the efficiency of sister-chromatid separation (by separase) and segregation (by the spindle). However, we would like to emphasize that our results certainly do not rule out a local activation of separase within the centromeric region.

Materials and methods

Fly stocks

We used the *GAL4* driver lines *GMR-GAL4*, *MS1096*, *Sca-GAL4*, *2xsev-Hs-GAL4* 332.5. *UAS-pim-myc* (Leismann et al. 2000), and *UAS-cid* (Jäger et al. 2005) have been described previously. For the generation of *GMR-thrΔC* lines, we used a pGMR construct (Hay et al. 1994) containing the same insert fragment including the myc-epitope region as present in *UAS-thr1-930-myc* (Jäger et al. 2001). The deficiency kit, as well as *Df(3R)Exel6149*, was obtained from the Bloomington *Drosophila* Stock Center. Its composition at the time of our screen, as well as a list of the deficiencies that were identified as dominant modifiers of the adult rough eye phenotype resulting from *GMR-thrΔC* or *GMR-GAL4 UAS-pim-myc* expression is given in the Supplemental Material. $l(3)85Aa^{prl41}$ (Jones and Rawls 1988) was also obtained from the Bloomington *Drosophila* Stock Center. $l(3)85Aa^{IR35}$ was kindly provided by K. Dej and T. Orr-Weaver (The Whitehead Institute, Cambridge, MA). $cid^{12\text{-}1}$ and $cid^{22\text{-}4}$ were generously provided by Thom Kaufman (Indiana University, Bloomington) and used for the analysis of Cenp-C localization in trans-heterozygous embryos. $Cap\text{-}G^{6}$ (Jäger et al. 2005) was crossed over *Df(2R)vg56* for the phenotypic comparison with *Cenp-C* mutants. The *His2Av-mRFP1*

and the *gcid-EGFP-cid* transgenic lines, which express functional fusion proteins as assessed by mutant rescue experiments, will be described in detail elsewhere.

Lines carrying genomic fragments from the 85A region were constructed for the identification of the locus interacting with eye-specific *pim* and *thrΔC* overexpression, using insert DNA derived from the BAC clone R48A14 (Hoskins et al. 2000) and pCaSpeR4 followed by standard P element germline transformation. Three olfactory receptor genes (*Or85b*, *Or85c*, *Or85d*) within the region delimited by deficiency breakpoints were excluded from further analysis. A transgene containing a 15-kb fragment with the predicted genes *CG11737*, *CG31454*, and *CG31259* did not prevent the lethality of the $l(3)85Aa^{prl41}$ mutants. The *abcd* transgene contained a 14.6-kb NdeI–XbaI fragment including *CG31453*, *mRpS18C*, *CG31460*, and *Cenp-C*. The same fragment after filling and religation of a SalI site within exon 5 of *Cenp-C* was used in the $abcd^{m}$ transgene. The proximal 6.4-kb NdeI–EcoRI subfragment lacking *Cenp-C* was used in the *abc* transgene, and the *d* transgene contained the distal 8.7-kb PmlI–XbaI subfragment including only *Cenp-C*.

For the expression of *Cenp-C* fused to EYFP or 10 copies of the myc epitope under control of the *Cenp-C* regulatory region, we modified the *d* transgene construct for the generation of the *gEYFP-Cenp-C* and *gmyc-Cenp-C* lines. A slightly larger subfragment (10.3-kb StuI–XbaI fragment) was used for the *gCenp-C-EGFP* and *gCenp-C-myc* lines. While *gCenp-C-EGFP*, *gmyc-Cenp-C*, and *gCenp-C-myc* insertions were unable to confer full rescue when crossed into *Cenp-C* mutant backgrounds, *gEYFP-Cenp-C* allowed *Cenp-C* mutant development to the adult stage.

The vector pUAST (Brand and Perrimon 1993) and the EST clone RE27988 (Berkeley *Drosophila* Genome Project), which contains a full-length *Cenp-C* cDNA insert according to our sequence analyses, were used for the generation of transgenic lines allowing *GAL4*-dependent expression of wild-type and mutant *Cenp-C* versions (Fig. 3). Moreover, the EGFP coding sequence was introduced into these transgenes immediately after the start codon.

Mutagenesis and transfection

The GeneMorph II random mutagenesis kit (Stratagene) was used for the enzymatic amplification of a *Cenp-C* cDNA region under mutagenic conditions using the primers mf (5′-ACGAGCTGTACAAGCTTGCC-3′) and mr (5′-GCAACCGAAGATATCATAGGC-3′) and the plasmid pRS1 as template. This pBluescript KS+ derivative contained the Gal4-binding sites and the basal *Hsp70Bb* promoter region isolated from pUAST upstream of the *EGFP-Cenp-C-C* (amino acids 1009–1411) fusion gene. The amplification products were digested with HindIII and EcoRV and used to replace the corresponding 668-bp region in pRS1, resulting in a mutant clone library after electroporation of *Escherichia coli DH10B* cells. The QIAprep 96 Turbo Miniprep kit (QIAGEN) was used for the preparation of plasmid DNA from 394 random clones.

Expression of the mutant library was achieved by transfection of *Drosophila* SR+ cells (Yanagawa et al. 1998). These cells were cultured at 26°C in Schneider's *Drosophila* Medium (GIBCO) containing 10% fetal bovine serum, 1% penicillin, and 1% streptomycin. Before transfection, we plated 10^5 cells/well of a μClear 96 well plate (GIBCO) in 0.2 mL of medium. After 24 h, medium was exchanged with 0.16 mL of fresh medium and 0.04 mL of transfection mix containing 0.25 μg of a given mutant library plasmid, 0.75 μg of pBluescript KS+ as carrier DNA, and 3 μL of FuGene6 (Roche) in Dulbecco's Modified Eagle's Medium (GIBCO). EGFP signals were analyzed 24 h after transfection in live cells using an inverted confocal laser scanning microscope (Leica DM IRBE TCS SP1) with a 40× oil immersion objective. Initial experiments involving transfection of the same pUAST-EGFP-Cenp-C constructs that had previously been analyzed after *Drosophila* germline transformation indicated that the subcellular localization of these mutant Cenp-C versions (FL, N, M, C, CN, CM, CC, ΔN, ΔAT1, ΔNLS, ΔAT2) (see Fig. 3) in SR+ cells was identical as in transgenic embryos. In initial experiments, cotransfection of pUAST-EGFP-Cenp-C constructs with an Act5c-GAL4 plasmid resulted in very high levels of expression, which obscured centromere localization in many cases. The Act5c-GAL4 plasmid was therefore omitted in subsequent experiments, and basal expression of the pUAST derivatives proved to be sufficient for detection of centromere localization.

In vivo imaging and immunofluorescence

Syncytial blastoderm-stage embryos of a *gEYFP-Cenp-C* II.1; *His2Av-mRFP1* III.1 line were analyzed by in vivo imaging essentially as described previously (Pandey et al. 2005). Moreover, embryos obtained from a cross of *His2Av-mRFP1* II.2, *gcid-EGFP-cid* II.1; $Cenp\text{-}C^{prl41}$/*TM3*, *Sb*, *Kr-GAL4*, *UAS-GFP* females with $Cenp\text{-}C^{IR35}$/*TM3*, *Sb*, *Kr-GAL4*, *UAS-GFP* males were analyzed analogously at the stage when the epidermal cells progress through mitosis 16.

Immunofluorescence and DNA labeling of fixed embryos was performed essentially as described previously (Leismann et al. 2000). Affinity-purified rabbit antibodies against Cid/Cenp-A (Jäger et al. 2005), Cyclin B (Jacobs et al. 1998), and GFP (Molecular Probes Inc.), and mouse monoclonal antibodies against α-tubulin DM1A (Sigma) were used at a dilution of 1:500, 1:500, 1:5000, and 1:8000, respectively. An affinity-purified rabbit antibody against *Drosophila* Cenp-C was generated with a bacterially expressed protein fragment (amino acids 502–939) with a His-tag and used at a dilution of 1:5000. For the analysis of the CNS phenotype, 12–14-h embryos were collected from a cross of *Sca-GAL4; Df(3R)p25/TM3*, *Sb*, *P{35Ubx-lacZ}2* males and $Cenp\text{-}C^{prl41}$/*TM3*, *Sb*, *P{35Ubx-lacZ}2* females with or without a *UAS-EGFP-Cenp-C* transgene. $Cenp\text{-}C^{prl41}$/*Df(3R)p25* embryos were identified after double-labeling with antibodies against β-galactosidase.

Sequence comparisons

The VISTA Browser (Couronne et al. 2003) and the *Drosophila* Species Genome Web pages (http://bugbane.bio.indiana.edu:7151) were used for the identification of *Cenp-C* genes in genome sequences of *D. ananassae*, *D. erecta*, *D. pseudoobscura*, *D. simulans*, *D. virilis*, and *D. yakuba* (prepublication data from Agencourt Bioscience Corporation and Genome Sequencing Center at Washington University; Richards et al. 2005). Alignments of coding and amino acid sequences were performed using the European Bioinformatics Institute CLUSTAL W Server (Thompson et al. 1994). Cenp-C-box consensus motifs were displayed using the Logos program on the Blocks WWW Server (http://blocks.fhcrc.org). K-estimator (Comeron 1999) was used for d_N/d_S analyses that estimate and compare the rate of nonsynonymous and synonymous exchanges in *Cenp-C* gene pairs from closely related species. Prior to analysis, insertions were removed from the coding sequences.

Acknowledgments

We are most grateful to Kim Dej and Terry Orr-Weaver for communicating unpublished information and generously providing

the IR35 allele. We are also indebted to Thom Kaufman for unpublished information and the *cid* mutant strains. We thank Buzz Baum for providing the SR+ cells, as well as Matthias Fischer and Rahul Pandey for their contributions during preparation of anti-Cenp-C antibodies and immunoblotting, and many other lab members for additional help. This work was supported by a grant from the Deutsche Forschungsgemeinschaft (DFG Le 987/3-3) and by the Fonds der Deutschen Chemie.

References

Blower, M.D., Sullivan, B.A., and Karpen, G.H. 2002. Conserved organization of centromeric chromatin in flies and humans. *Dev. Cell* **2:** 319–330.

Brand, A.H. and Perrimon, N. 1993. Targeted gene expression as a means of altering cell fates and generating dominant phenotypes. *Development* **118:** 401–415.

Brown, M.T. 1995. Sequence similarities between the yeast chromosome segregation protein Mif2 and the mammalian centromere protein CENP-C. *Gene* **160:** 111–116.

Brown, M.T., Goetsch, L., and Hartwell, L.H. 1993. MIF2 is required for mitotic spindle integrity during anaphase spindle elongation in *Saccharomyces cerevisiae*. *J. Cell Biol.* **123:** 387–403.

Buchwitz, B.J., Ahmad, K., Moore, L.L., Roth, M.B., and Henikoff, S. 1999. A histone-H3-like protein in *C. elegans*. *Nature* **401:** 547–548.

Cheeseman, I.M., Niessen, S., Anderson, S., Hyndman, F., Yates III, J.R., Oegema, K., and Desai, A. 2004. A conserved protein network controls assembly of the outer kinetochore and its ability to sustain tension. *Genes & Dev.* **18:** 2255–2268.

Chestukhin, A., Pfeffer, C., Milligan, S., DeCaprio, J.A., and Pellman, D. 2003. Processing, localization, and requirement of human separase for normal anaphase progression. *Proc. Natl. Acad. Sci.* **100:** 4574–4579.

Ciosk, R., Zachariae, W., Michaelis, C., Shevchenko, A., Mann, M., and Nasmyth, K. 1998. An ESP1/PDS1 complex regulates loss of sister chromatid cohesion at the metaphase to anaphase transition in yeast. *Cell* **93:** 1067–1076.

Comeron, J.M. 1999. K-Estimator: Calculation of the number of nucleotide substitutions per site and the confidence intervals. *Bioinformatics* **15:** 763–764.

Couronne, O., Poliakov, A., Bray, N., Ishkhanov, T., Ryaboy, D., Rubin, E., Pachter, L., and Dubchak, I. 2003. Strategies and tools for whole-genome alignments. *Genome Res.* **13:** 73–80.

Dawe, R.K., Reed, L.M., Yu, H.G., Muszynski, M.G., and Hiatt, E.N. 1999. A maize homolog of mammalian CENPC is a constitutive component of the inner kinetochore. *Plant Cell* **11:** 1227–1238.

De Wulf, P., McAinsh, A.D., and Sorger, P.K. 2003. Hierarchical assembly of the budding yeast kinetochore from multiple subcomplexes. *Genes & Dev.* **17:** 2902–2921.

Earnshaw, W.C. and Rothfield, N. 1985. Identification of a family of human centromere proteins using autoimmune sera from patients with scleroderma. *Chromosoma* **91:** 313–321.

Fukagawa, T. and Brown, W.R. 1997. Efficient conditional mutation of the vertebrate CENP-C gene. *Hum. Mol. Genet.* **6:** 2301–2308.

Fukagawa, T., Pendon, C., Morris, J., and Brown, W. 1999. CENP-C is necessary but not sufficient to induce formation of a functional centromere. *EMBO J.* **18:** 4196–4209.

Fukagawa, T., Regnier, V., and Ikemura, T. 2001. Creation and characterization of temperature-sensitive CENP-C mutants in vertebrate cells. *Nucleic Acids Res.* **29:** 3796–3803.

Funabiki, H., Kumada, K., and Yanagida, M. 1996. Fission yeast Cut1 and Cut2 are essential for sister separation, concentrate along the metaphase spindle and form large complexes. *EMBO J.* **15:** 6617–6628.

Goshima, G., Kiyomitsu, T., Yoda, K., and Yanagida, M. 2003. Human centromere chromatin protein hMis12, essential for equal segregation, is independent of CENP-A loading pathway. *J. Cell Biol.* **160:** 25–39.

Hay, B.A., Wolff, T., and Rubin, G.M. 1994. Expression of baculovirus p35 prevents cell-death in *Drosophila*. *Development* **120:** 2121–2129.

Henikoff, S., Ahmad, K., Platero, J.S., and van Steensel, B. 2000. Heterochromatic deposition of centromeric histone H3-like proteins. *Proc. Natl. Acad. Sci.* **97:** 716–721.

Henikoff, S., Ahmad, K., and Malik, H.S. 2001. The centromere paradox: Stable inheritance with rapidly evolving DNA. *Science* **293:** 1098–1102.

Herzig, A., Lehner, C.F., and Heidmann, S. 2002. Proteolytic cleavage of the THR subunit during anaphase limits *Drosophila* separase function. *Genes & Dev.* **16:** 2443–2454.

Hoskins, R.A., Nelson, C.R., Berman, B.P., Laverty, T.R., George, R.A., Ciesiolka, L., Naeemuddin, M., Arenson, A.D., Durbin, J., David, R.G., et al. 2000. A BAC-based physical map of the major autosomes of *Drosophila melanogaster*. *Science* **287:** 2271–2274.

Howman, E.V., Fowler, K.J., Newson, A.J., Redward, S., MacDonald, A.C., Kalitsis, P., and Choo, K.H. 2000. Early disruption of centromeric chromatin organization in centromere protein A (Cenpa) null mice. *Proc. Natl. Acad. Sci.* **97:** 1148–1153.

Jacobs, H.W., Knoblich, J.A., and Lehner, C.F. 1998. *Drosophila* Cyclin B3 is required for female fertility and is dispensable for mitosis like Cyclin B. *Genes & Dev.* **12:** 3741–3751.

Jäger, H., Herzig, A., Lehner, C.F., and Heidmann, S. 2001. *Drosophila* separase is required for sister chromatid separation and binds to PIM and THR. *Genes & Dev.* **15:** 2572–2584.

Jäger, H., Herzig, B., Herzig, A., Sticht, H., Lehner, C.F., and Heidmann, S. 2004. Structure predictions and interaction studies indicate homology of separase N-terminal regulatory domains and *Drosophila* THR. *Cell Cycle* **3:** 182–188.

Jäger, H., Rauch, M., and Heidmann, S. 2005. The *Drosophila melanogaster* condensin subunit Cap-G interacts with the centromere-specific histone H3 variant CID. *Chromosoma.* **113:** 350–361.

Jensen, S., Segal, M., Clarke, D.J., and Reed, S.I. 2001. A novel role of the budding yeast separin Esp1 in anaphase spindle elongation: Evidence that proper spindle association of Esp1 is regulated by Pds1. *J. Cell Biol.* **152:** 27–40.

Jones, W.K. and Rawls Jr., J.M. 1988. Genetic and molecular mapping of chromosome region 85A in *Drosophila melanogaster*. *Genetics* **120:** 733–742.

Kalitsis, P., Fowler, K.J., Earle, E., Hill, J., and Choo, K.H. 1998. Targeted disruption of mouse centromere protein C gene leads to mitotic disarray and early embryo death. *Proc. Natl. Acad. Sci.* **95:** 1136–1141.

Kumada, K., Nakamura, T., Nagao, K., Funabiki, H., Nakagawa, T., and Yanagida, M. 1998. Cut1 is loaded onto the spindle by binding to Cut2 and promotes anaphase spindle movement upon Cut2 proteolysis. *Curr. Biol.* **8:** 633–641.

Lanini, L. and McKeon, F. 1995. Domains required for CENP-C assembly at the kinetochore. *Mol. Biol. Cell* **6:** 1049–1059.

Leismann, O., Herzig, A., Heidmann, S., and Lehner, C.F. 2000. Degradation of *Drosophila* PIM regulates sister chromatid separation during mitosis. *Genes & Dev.* **14:** 2192–2205.

Meeks-Wagner, D., Wood, J.S., Garvik, B., and Hartwell, L.H. 1986. Isolation of two genes that affect mitotic chromosome

transmission in *S. cerevisiae*. *Cell* **44:** 53–63.
Meluh, P.B. and Koshland, D. 1995. Evidence that the MIF2 gene of *Saccharomyces cerevisiae* encodes a centromere protein with homology to the mammalian centromere protein CENP-C. *Mol. Biol. Cell* **6:** 793–807.
Moore, L.L. and Roth, M.B. 2001. HCP-4, a CENP-C-like protein in *Caenorhabditis elegans*, is required for resolution of sister centromeres. *J. Cell Biol.* **153:** 1199–1208.
Nasmyth, K. 2002. Segregating sister genomes: The molecular biology of chromosome separation. *Science* **297:** 559–565.
Nishihashi, A., Haraguchi, T., Hiraoka, Y., Ikemura, T., Regnier, V., Dodson, H., Earnshaw, W.C., and Fukagawa, T. 2002. CENP-I is essential for centromere function in vertebrate cells. *Dev. Cell* **2:** 463–476.
Obuse, C., Iwasaki, O., Kiyomitsu, T., Goshima, G., Toyoda, Y., and Yanagida, M. 2004. A conserved Mis12 centromere complex is linked to heterochromatic HP1 and outer kinetochore protein Zwint-1. *Nat. Cell Biol.* **6:** 1135–1141.
Oegema, K., Desai, A., Rybina, S., Kirkham, M., and Hyman, A.A. 2001. Functional analysis of kinetochore assembly in *Caenorhabditis elegans*. *J. Cell Biol.* **153:** 1209–1226.
Pandey, R., Heidmann, S., and Lehner, C.F. 2005. Epithelial reorganization and dynamics of progression through mitosis in *Drosophila* separase complex mutants. *J. Cell Sci.* **118:** 733–742.
Pinsky, B.A., Tatsutani, S.Y., Collins, K.A., and Biggins, S. 2003. An Mtw1 complex promotes kinetochore biorientation that is monitored by the Ipl1/Aurora protein kinase. *Dev. Cell* **5:** 735–745.
Richards, S., Liu, Y., Bettencourt, B.R., Hradecky, P., Letovsky, S., Nielsen, R., Thornton, K., Hubisz, M.J., Chen, R., Meisel, R.P., et al. 2005. Comparative genome sequencing of *Drosophila pseudoobscura*: Chromosomal, gene, and *cis*-element evolution. *Genome Res.* **15:** 1–18.
Saitoh, H., Tomkiel, J., Cooke, C.A., Ratrie III, H., Maurer, M., Rothfield, N.F., and Earnshaw, W.C. 1992. CENP-C, an autoantigen in scleroderma, is a component of the human inner kinetochore plate. *Cell* **70:** 115–125.
Shibata, F. and Murata, M. 2004. Differential localization of the centromere-specific proteins in the major centromeric satellite of *Arabidopsis thaliana*. *J. Cell Sci.* **117:** 2963–2970.
Song, K., Gronemeyer, B., Lu, W., Eugster, E., and Tomkiel, J.E. 2002. Mutational analysis of the central centromere targeting domain of human centromere protein C (CENP-C). *Exp. Cell Res.* **275:** 81–91.
Stoler, S., Keith, K.C., Curnick, K.E., and Fitzgerald-Hayes, M. 1995. A mutation in *CSE4*, an essential gene encoding a novel chromatin-associated protein in yeast, causes chromosome nondisjunction and cell-cycle arrest at mitosis. *Genes & Dev.* **9:** 573–586.
Sugimoto, K., Yata, H., Muro, Y., and Himeno, M. 1994. Human centromere protein C (CENP-C) is a DNA-binding protein which possesses a novel DNA-binding motif. *J. Biochem. (Tokyo)* **116:** 877–881.
Sullivan, K.F., Hechenberger, M., and Masri, K. 1994. Human CENP-A contains a histone H3 related histone fold domain that is required for targeting to the centromere. *J. Cell Biol.* **127:** 581–592.
Takahashi, K., Chen, E.S., and Yanagida, M. 2000. Requirement of Mis6 centromere connector for localizing a CENP-A-like protein in fission yeast. *Science* **288:** 2215–2219.
Talbert, P.B., Masuelli, R., Tyagi, A.P., Comai, L., and Henikoff, S. 2002. Centromeric localization and adaptive evolution of an *Arabidopsis* histone H3 variant. *Plant Cell* **14:** 1053–1066.
Talbert, P.B., Bryson, T.D., and Henikoff, S. 2004. Adaptive evolution of centromere proteins in plants and animals. *J. Biol.* **3:** 18.
Thompson, J.D., Higgins, D.G., and Gibson, T.J. 1994. CLUSTAL W: Improving the sensitivity of progressive multiple sequence alignment through sequence weighting, position-specific gap penalties and weight matrix choice. *Nucleic Acids Res.* **22:** 4673–4680.
Tomkiel, J., Cooke, C.A., Saitoh, H., Bernat, R.L., and Earnshaw, W.C. 1994. CENP-C is required for maintaining proper kinetochore size and for a timely transition to anaphase. *J. Cell Biol.* **125:** 531–545.
Van Hooser, A.A., Ouspenski, I.I., Gregson, H.C., Starr, D.A., Yen, T.J., Goldberg, M.L., Yokomori, K., Earnshaw, W.C., Sullivan, K.F., and Brinkley, B.R. 2001. Specification of kinetochore-forming chromatin by the histone H3 variant CENP-A. *J. Cell Sci.* **114:** 3529–3542.
Westermann, S., Cheeseman, I.M., Anderson, S., Yates III, J.R., Drubin, D.G., and Barnes, G. 2003. Architecture of the budding yeast kinetochore reveals a conserved molecular core. *J. Cell Biol.* **163:** 215–222.
Wigge, P.A. and Kilmartin, J.V. 2001. The Ndc80p complex from *Saccharomyces cerevisiae* contains conserved centromere components and has a function in chromosome segregation. *J. Cell Biol.* **152:** 349–360.
Yanagawa, S., Lee, J.S., and Ishimoto, A. 1998. Identification and characterization of a novel line of *Drosophila* Schneider S2 cells that respond to wingless signaling. *J. Biol. Chem.* **273:** 32353–32359.
Yang, C.H., Tomkiel, J., Saitoh, H., Johnson, D.H., and Earnshaw, W.C. 1996. Identification of overlapping DNA-binding and centromere-targeting domains in the human kinetochore protein CENP-C. *Mol. Cell. Biol.* **16:** 3576–3586.

Genetic interactions of Separase regulatory subunits reveal the diverged Drosophila Cenp-C homolog

Sebastian Heeger[1)], Oliver Leismann[1,2)], Ralf Schittenhelm, Oliver Schraidt, Stefan Heidmann and Christian F. Lehner[3)]

Department of Genetics, BZMB, University of Bayreuth, 95440 Bayreuth, Germany

1) these two authors made equal contributions

2) present address: Laboratory of Chromosome & Cell Biology, Rockefeller University, 1230 York Avenue, New York, NY 10021, USA

3) corresponding author: Department of Genetics, University of Bayreuth, 95440 Bayreuth, Germany, chle@uni-bayreuth.de

Supplementary Material

The screen for deficiencies which dominantly modify the rough adult eye phenotype resulting from *GMR-thrΔC* and *GMR-GAL4 UAS-pim-myc* expression was performed with the Bloomington deficiency kit. The chromosomal aberrations contained in this kit at the time of the screen were: *Df(1)BA1, Df(1)sc-J4, Df(1)64c18, Df(1)JC19, Df(1)N-8, Df(1)dm75e19, Df(1)A113, Df(1)JC70, Df(1)C149, Df(1)N73, Df(1)dx81, Df(1)Sxl-bt, Df(1)ct-J4, Df(1)ct4b1, Df(1)C128, Df(1)RA2, Df(1)KA14, Df(1)lz-90b24, Df(1)C52, Df(1)v-L15, Df(1)v-N48, Df(1)KA7, Df(1)HA85, Df(1)N105, Df(1)JA26, Df(1)C246, Df(1)N12, Df(1)g, Df(1)RK2, Df(1)RK4, Df(1)sd72b, Df(1)4b18, Df(1)r-D1, Df(1)B25, Df(1)B, Df(1)BK10, Df(1)N19, Df(1)JA27, Df(1)HF396, Df(1)DCB1-35b, Df(1)A209, Df(2L)net-PMF, Df(2L)al, Df(2L)ast2, Df(2L)dp-79b, Df(2L)C144, Df(2L)JS32, Df(2L)23C, Df(2L)S2590, Df(2L)ed1, Df(2L)sc19-8, Df(2L)sc19-4, Df(2L)cl-h3, Df(2L)E110, Df(2L)Dwee-delta5, Df(2L)J-H, Df(2L)spd, Df(2L)XE-2750, Df(2L)w67c23, Df(2L)TE29Aa-11, Df(2L)N22-14,*

Df(2L)s1402, Df(2L)Mdh, Df(2L)J39, Df(2L)Prl, Df(2L)prd1.7, Df(2L)b87e25, Df(2L)TE35BC-24, Df(2L)r10, Df(2L)cact-255rv64, Df(2L)H20, Df(2L)TW137, Df(2L)TW50, Df(2L)TW161, Df(2L)C', Df(2R)M41A4, Df(2R)nap9, Df(2R)ST1, Df(2R)pk78s, Df(2R)cn9, Df(2R)H3C1, Df(2R)H3E1, Df(2R)Np5, Df(2R)w45-30n, Df(2R)B5, Df(2R)X1, Df(2R)stan2, Df(2R)E3363, Df(2R)en-A, Df(2R)en30, Df(2R)CB21, Df(2R)vg135, Df(2R)vg-C, Df(2R)CX1, Df(2R)trix, Df(2R)knSA3, Df(2R)Jp1, Df(2R)Jp8, Df(2R)Pcl7B, Df(2R)PC4, Df(2R)P34, Df(2R)017, Df(2R)AA21, Df(2R)Pu-D17, Df(2R)X58-7, Df(2R)X58-12, Df(2R)59AD, Df(2R)or-BR6, Df(2R)bw, Df(2R)Chi[g230], Df(2R)Px2, Df(2R)M60E, Df(2R)ES1, Df(2R)Kr10, Df(3L)emc-E12, Df(3L)Ar14-8, Df(3L)Aprt-1, Df(3L)R-G7, Df(3L)M21, Df(3L)HR119, Df(3L)GN24, Df(3L)ZN47, Df(3L)XDI98, Df(3L)pbl-X1, Df(3L)66C-G28, Df(3L)h-i22, Df(3L)Scf-R6, Df(3L)Rdl-2, Df(3L)29A6, Df(3L)AC1, Df(3L)1xd6, Df(3L)vin2, Df(3L)vin5, Df(3L)vin7, Df(3L)iro-2, In(3LR)C190, Df(3L)fz-GF3b, Df(3L)fz-M21, Df(3L)BK10, Df(3L)brm11, Df(3L)st-fl13, Df(3L)81k19, Df(3L)W10, Df(3L)Cat, Df(3L)VW3, Df(3L)kto2, Df(3L)XS-533, Df(3L)rdgC-co2, Df(3L)ri-79c, Df(3L)ME107, Df(3L)31A, Df(3L)Pc-2q, Df(3L)Ten-m-Al29, Df(3L)Delta1AK, Df(3L)ME15, Df(3R)6-7, Df(3R)3-4, Df(3R)Tpl10, Df(3R)Scr, Df(3R)Antp17, Df(3R)p712, Df(3R)p-XT103, Df(3R)by10, Df(3R)by62, Df(3R)M-Kx1, Df(3R)T-32, Df(3R)ry615, Df(3R)ry506-85C, Df(3R)ea, Df(3R)P115, Df(3R)DG2, Df(3R)C4, Df(3R)Cha7, Df(3R)Dl-BX12, Df(3R)H-B79, Df(3R)e-R1, Df(3R)e-N19, Df(3R)mbc-30, Df(3R)mbc-R1, Df(3R)crb-F89-4, Df(3R)crb87-5, Df(3R)slo[8], Df(3R)Tl-P, Df(3R)D605, Df(3R)3450, Df(3R)Dr-rv1, Df(3R)L127, Df(3R)B81, Df(3R)awd-KRB, Df(3R)faf-BP, Df(4)M101-62f, C(4)RM, Df(4)G

The following table lists deficiencies of the kit as well as their chromosomal breakpoints which were recognized as specific dominant enhancers or suppressors. Strong interactions are indicated by bold print, moderate interactions by regular print. Deficiencies which did not only act as dominant enhancers or suppressors of *GMR-thrΔC* or *GMR-GAL4 UAS-pim-myc* expression but also of *GMR-otd* or *GMR-GAL4 UAS-otd* were not considered as specific interactors.

deficiency	breakpoints	GMR-GAL4 UAS-PIM	GMR-thrΔC
Df(1)64c18	002E01-02; 003C02	**Enhancer**	**Enhancer**
Df(1)JC19	002F06; 003C05	**Enhancer**	**Enhancer**
Df(1)Sxl-bt	006E02; 007A06		Enhancer
Df(1) lz-90b24	008B05-06; 008D08-09 or 008D01-02; 008E01-02	**Enhancer**	
Df(1)RK4	012F05-06; 013A09-B01	**Enhancer**	
Df(1)sd72b	013F01; 014B01	**Enhancer**	
Df(1)r-D1	014C02-04; 015B02-C01		**Enhancer**
Df(1)B25	015D03; 016A04-06		Enhancer
Df(1)B	016A02; 016A06		**Enhancer**
Df(1) DCB1-35b	019F01-02; 020E-F	Enhancer	
Df(2L)JS32	023C03-05; 023D01-02	**Enhancer**	
Df(2L)Dwee-delta5	027A; 028A	Suppressor	
Df(2L) XE-2750	028B02; 028D03	Enhancer	Enhancer
Df(2L)Pr1	032F01-03; 033F01-02	**Enhancer**	**Enhancer**
Df(2R) H3C1	043F; 044D03-08		Suppressor
Df(2R) H3E1	044D01-04; 044F12		**Suppressor**
Df(2R) vg135	049A-B; 049D-E	**Enhancer**	**Enhancer**
Df(2R)vg-C	049A04-13; 049E07-F01	Enhancer	
Df(2R)CX1	049C01-04; 050C23-D02	**Enhancer**	**Enhancer**
Df(2R)Jp1	051C03; 052F05-09	**Suppressor**	
Df(2R)017	056F05; 056F015		**Suppressor**
Df(2R) AA21	056F09-17; 057D11-12	**Suppressor**	**Suppressor**
Df(3L) Scf-R6	066E01-06; 066F01-06	**Enhancer**	**Enhancer**
Df(3L) AC1	067A02; 067D07-13 or 067A05; 067D09-13	Suppressor	Suppressor
Df(3L)vin5	068A02-03; 069A01-03		Enhancer
Df(3L)vin7	068C08-11; 069B04-05	**Suppressor**	Enhancer
In(3LR)C190^{L} Ubx^{42TR}	069F03-04; 070C03-04 + 089;089	Suppressor	
Df(3L) brm11	071F01-04; 072D01-10	Enhancer	
Df(3L) XS-533	076B04; 077B	**Enhancer**	**Enhancer**

Df(3L) ri-79c	077B-C; 077F-78A	Enhancer	Enhancer
Df(3L) Delta1AK	079F; 080A	Enhancer	Enhancer
Df(3R) ME15	081F03-06; 082F05-07		**Suppressor**
Df(3R) p712	084D04-06; 085B06	**Enhancer**	**Enhancer**
Df(3R) p-XT103	085A02; 085C01-02	**Enhancer**	**Enhancer**
Df(3R) M-Kx1	086C01; 087B01-05	**Suppressor**	**Suppressor**
Df(3R)DG2	089E01-F04; 091B01-B02	**Suppressor**	Suppressor
Df(3R)C4	089E03-04; 090A01-07	Enhancer	**Enhancer**
Df(3R) Cha7	090F01-F04; 091F05		Suppressor
Df(3R) crb87-5	095F07; 096A17-18	Suppressor	Suppressor
Df(3R) Dr-rv1	099A01-02; 099B06-11	Suppressor	Suppressor
Df(3R) awd-KRB	100C; 100D		**Enhancer**
Df(3R) faf-BP	100D; 100F05		**Suppressor**

Teilarbeit B

Ralf Schittenhelm*, Sebastian Heeger*, Friederike Althoff, Anne Walter, Stefan Heidmann, Karl Mechtler and Christian F. Lehner

Spatial organization of kinetochore proteins in native *Drosophila* chromosomes revealed at unprecedented resolution by fluorescent fusion protein imaging

Manuskript noch nicht eingereicht

* beide Autoren haben im selben Maße zu dieser Arbeit beigetragen

Darstellung des Eigenanteils

Die Etablierung der Methodik sowie alle Experimente zur Vermessung des CKC und die statistische Beschreibung der Daten sind meine Arbeit (Fig. 3, S4, S5 und S6 sowie Tab. 1 und 2).

Geschrieben wurde diese Teilarbeit von Christian F. Lehner mit Beiträgen von Ralf Schittenhelm und mir.

Spatial organization of kinetochore proteins in native *Drosophila* chromosomes revealed at unprecedented resolution by fluorescent fusion protein imaging

Ralf Schittenhelm[1]*, Sebastian Heeger[1]*, Friederike Althoff[1], Anne Walter[1], Stefan Heidmann[1], Karl Mechtler[2] and Christian F. Lehner[1,3]

1) Department of Genetics, BZMB, University of Bayreuth, 95440 Bayreuth, Germany

2) Institute of Molecular Biotechnology GmbH, IMBA, Dr. Bohr-Gasse 3, 1030 Vienna, Austria

3) author for correspondence:

Christian Lehner

Department of Genetics

University of Bayreuth

Universitaetsstr. 30

95447 Bayreuth

Germany

e-mail: chle@uni-bayreuth.de

phone: +49 921 55 2701

fax: +49 921 55 2710

*equal contributions

running title: kinetochore map

Summary

Centromere and kinetochore proteins in different eukaryotic lineages show surprisingly little conservation at the primary sequence level despite their fundamental biological role. The *Drosophila* Ndc80 complex components (Ndc80, Nuf2, Spc25) and the putative MIND complex components (Mis12, Nsl1, Nnf1a, Nnf1b) described here represent the most diverged orthologs reported so far. Their identification confirms the existence of a shared set of homologous kinetochore complexes in eukaryotes. Using transgenic *Drosophila* strains co-expressing combinations of red and green fluorescent fusion proteins, fully capable of providing the essential wild-type functions, we have analyzed the spatial arrangement of kinetochore components. Early syncytial embryos allowed a simple and efficient analysis of native mitotic chromosomes. In these, we localized Cenp-A/Cid, Cenp-C, Mis-12 and the Ndc80 complex subunits Nuf2 and Spc25 along the spindle axis with unprecedented spatial resolution using light microscopy in combination with statistical analyses. Thereby, Cenp-C and the Ndc80 complex were found to have a polar orientation within the kinetochore with the former bridging a space between the innermost kinetochore component Cenp-A/Cid and the Ndc80 and MIND complexes.

Key words: Ndc80/Hec1 complex, MIND complex, Cenp-A, Cenp-C, centromere, kinetochore

Introduction

The kinetochore which is formed within the centromeric region of eukaryotic chromosomes is crucial for faithful segregation of genetic information during mitotic and meiotic divisions. Its composition changes during the division cycle. In prometaphase it allows the attachment of

chromosomes to spindle fibers. Moreover, it is associated with a number of checkpoint proteins which monitor chromosome integration into the spindle and prevent progression into anaphase unless a correct bipolar chromosome orientation has been reached.

Despite their fundamental biological role, centromeric DNA and primary sequences of associated proteins have evolved very rapidly (for recent reviews see (Cleveland et al. 2003; De Wulf et al. 2003; Kline-Smith et al. 2005; Schueler and Sullivan 2006; Vos et al. 2006)). Until recently, therefore, it has been difficult to integrate findings from different model organisms into a general model for kinetochore organization in eukaryotes. However, rapid progress has dramatically improved the recognition of shared elements of centromere kinetochore complexes (CKC). The basis of CKC assembly in eukaryotes appears to be formed by specialized chromatin containing nucleosomes with a centromere-specific histone H3 variant (Vos et al. 2006). Cenp-A/Cid, the *Drosophila* centromere-specific histone H3 variant, is found at the centromere throughout the division cycles (Henikoff et al. 2000), as also true in other organisms (Vos et al. 2006). Cenp-C homologs represent another ubiquitous CKC component with a constitutive centromere localization (apart from the mitosis-specific association observed in C. elegans) (Moore and Roth 2001; Oegema et al. 2001; Heeger et al. 2005; Vos et al. 2006). Four multi-protein complexes (COMA, MIND, Spc105, Ndc80) which were originally identified in budding yeast have also been characterized, at least partially, in a wide range of eukaryotes (Kline-Smith et al. 2005; Meraldi et al. 2006; Vos et al. 2006). Their centromere association in human cells appears to vary from constitutive (COMA) (McAinsh et al. 2006), constitutive except for telophase (MIND) (Kline et al. 2006; McAinsh et al. 2006), to mitosis-specific (Ndc80)(Chen et al. 1997; Martin-Lluesma et al. 2002; Kline-Smith et al. 2005). Moreover, a number of mitotic spindle checkpoint proteins are conserved and present at high concentrations at kinetochores which are either not attached to the spindle or not exposed to the physical tension resulting from bipolar attachment (Vos et al. 2006). Apart from these proteins, about 50 additional CKC components have been

described in various experimental systems and the identification of diverged orthologs in other eukaryotes is progressing in many cases (Meraldi et al. 2006; Vos et al. 2006).

Initial insights into the details of the structural CKC organization were obtained by electron microscopy (Rieder 1982; Vos et al. 2006). In *Drosophila*, kinetochore ultrastructure is similar to the appearance of vertebrate kinetochores (Maiato et al. 2006), in particular during prometaphase when the hemispherical organization is transformed into a disk with a distinct outer plate of about 40 nm thickness. This outer plate is separated by a gap of about 30 nm from another electron-dense inner plate. In *Drosophila*, this inner plate is poorly resolved from the underlying amorphous inner chromatin mass. On the other side, i.e. distal to the outer plate, prometaphase kinetochores have a fibrous corona of variable depth (up to 200 nm). We point out that kinetochore ultrastructure is known to change significantly from prophase to metaphase (Rieder 1982) (Maiato et al. 2006) and that certain aspects like the distinction of the inner plate might reflect artefactual chromatin shrinking during fixation (McEwen et al. 1998).

Only a few CKC components have been localized by immuno electron microscopy at an ultrastructural level. Thereby, vertebrate Cenp-C has been assigned to the inner plate (Saitoh et al. 1992) and the Ndc80 complex components Ndc80/Hec1 and Nuf2 to the outer plate (DeLuca et al. 2005). Moreover, Cenp-E has been located within the outer corona (Cooke et al. 1997; DeLuca et al. 2005). Based on double immunofluorescence comparisons with these well-studied proteins, almost all other CKC components have been tentatively classified as present either in the inner chromatin, the inner or outer plate, or the fibrous corona. Moreover, several studies have characterized kinetochore ultrastructure after RNA interference-mediated depletion of CKC components (DeLuca et al. 2005; Liu et al. 2006). RNA interference mostly in combination with fluorescence microscopy has also been used extensively to analyze dependencies in the CKC assembly process (see for instance (Liu et al. 2006) and references in (Vos et al. 2006)). In general, inner components were found to be required for the later

assembly of outer components, even though certain inconsistencies point to a higher complexity (Liu et al. 2006). Finally, light microscopic analyses have been performed with stretched chromatin fibers which have argued for a lateral association of repeating units into a kinetochore disk (Blower et al. 2002; Sullivan and Karpen 2004).

The methods used for kinetochore characterizations of course have their disadvantages and limitations. Here, we apply a light-microscopic approach with unprecedented spatial resolution. This approach exploits some unique advantages of the model organism *Drosophila* melanogaster. Genetic complementation tests were used to establish the functionality of CKC proteins fused to fluorescent proteins. These fluorescent proteins, the enhanced green fluorescent protein (EGFP) and monomeric red fluorescent protein (mRFP), provide localization tags which are considerably smaller than antibodies. The cylindrical β-barrels formed by EGFP and mRFP have a diameter of 2.4 nm and a height of 4.2 nm (Ormo et al. 1996; Yang et al. 1996). In contrast, indirect immunolocalization involves detection by two antibodies, each being more than fivefold larger than EGFP/mRFP, in combination with colloidal gold in the case of electron microscopy. In addition, fluorescent proteins eliminate potential problems with antibody specificity and antigen accessibility. Moreover, potential fixation artifacts can be avoided by imaging unfixed specimens. In *Drosophila*, the rapid syncytial division cycles of early embryogenesis result in a very high physiological mitotic index approaching 50% which allows a very efficient isolation of native mitotic chromosomes. After our identification of components of the *Drosophila* Ndc80 and the putative MIND complex, we analyzed their localization in comparison to the previously described Cenp-A/Cid (Henikoff et al. 2000) and Cenp-C proteins (Heeger et al. 2005). By averaging the data obtained with hundreds of native chromosomes released from embryos co-expressing a red and a green fluorescent CKC component, we were able to improve spatial resolution well beyond the light diffraction limit. Thereby, we localized Cenp-C to a gap between the innermost Cenp-A/Cid and the outer Mis12 and Ndc80 complexes. Moreover,

both Cenp-C and the rod-like Ndc80 complex appear to have a defined, polar orientation along the spindle axis.

Results and Discussion

Identification of the *Drosophila* Ndc80 and MIND complexes

Bioinformatic analysis revealed similarities between known Ndc80/Hec1 proteins and the predicted *Drosophila CG9938* product (data not shown). Similar findings from a systematic bioinformatic search for eukaryotic kinetochore proteins were described while this work was in progress (Meraldi et al. 2006). However, the observed similarities were only very limited and not correlated with evolutionary descent. Vertebrate Ndc80/Hec1proteins were clearly more similar to fungal and plant homologs than to *CG9938*. To confirm therefore that the diverged *CG9938* indeed encodes the *Drosophila* Ndc80 homolog, we expressed an EGFP fusion protein in *Drosophila* S2R+ cells. The subcellular localization of the EGFP signals was found to correspond to the known behavior (Chen et al. 1997; Martin-Lluesma et al. 2002) of human Ndc80/Hec1 (data not shown). Moreover, the expected localization was subsequently also observed in transgenic embryos expressing EGFP-CG9938 fusion protein (Fig. 1A). During interphase we did not observe signals above background (Fig. 1A). However, during mitosis distinct signals were present at the kinetochore from prometaphase until late anaphase. The kinetochore signals were in close proximity to those obtained after double labeling with antibodies against the constitutive centromere protein Cenp-C (Fig. 1A). Based on this and the following evidence, we conclude that *CG9938* represents the *Drosophila Ndc80* gene.

In a genome-wide yeast two hybrid screen, *Drosophila* Ndc80 was reported to support a high confidence interaction with the predicted *CG8902* product (Giot et al. 2003). Moreover, this *CG8902* protein has a very limited similarity to the Ndc80 complex component Nuf2 (Meraldi et al. 2006). To evaluate whether this most distant Nuf2 family member displayed

the expected kinetochore localization during mitosis, it was also expressed as an EGFP fusion protein in S2R+ cells. Its subcellular localization was found to be indistinguishable from that of vertebrate Ndc80 components (data not shown). In addition, the same localization behavior was also observed in transgenic embryos expressing EGFP-CG8902 (Fig. 1B). We conclude that *CG8902* represents the *Drosophila Nuf2* gene.

An additional *Drosophila* Ndc80 interactor (Giot et al. 2003), the *CG7242* product, was observed to have limited similarity to the Ndc80 complex component Spc25. This gene was also identified as a most distant Spc25 family member by Meraldi et al. (2006). Analysis of the intracellular localization of an EGFP fusion protein confirmed the expected kinetochore localization also in this case, both in transfected S2R+ cells (data not shown) and in transgenic embryos (Fig. 1C). We conclude that *CG7242* encodes Drosophila Spc25.

Apart from Ndc80 complex members, the bioinformatic search had revealed an additional putative *Drosophila* CKC component. CG18156 was found to have very limited sequence similarity to fungal and metazoan Mis12 proteins (Meraldi et al. 2006). Mis12 was originally identified in fission yeast and subsequently found to be a component of a conserved CKC complex called MIND which contains three additional proteins (Takahashi et al. 1994; De Wulf et al. 2003; Goshima et al. 2003; Obuse et al. 2004; Kline et al. 2006). Our localization studies after transfection of S2R+ cells with an EGFP-CG18156 expression construct revealed centromere localization. EGFP signals were found to be co-localized with Cenp-A/Cid at the centromere in interphase cells (Suppl. Fig. 1A). This localization behavior corresponds to the findings observed for human Mis12 which is centromeric throughout interphase except for a brief period in late telophase and early G1 (Kline et al. 2006; McAinsh et al. 2006). In transgenic embryos expressing EGFP-CG18156, we observed the centromeric signals only during mitosis (Fig. 1D). Primary and secondary sequence comparison as well as the kinetochore localization strongly support that *CG18156* encodes the *Drosophila* Mis12 homolog.

To demonstrate that the identified putative *Drosophila* Ndc80 complex components Ndc80, Nuf2 and Spc25 are indeed present in a complex in vivo, we used mass spectrometry to analyze the proteins co-precipitated with functional EGFP-Nuf2 from embryo extracts. EGFP-Nuf2 was expressed from a transgene (*gEGFP-Nuf2*) under the control of the *Nuf2* regulatory region. Antibodies against EGFP were used for immunoprecipitation. SDS-PAGE of the immunoprecipitates followed by silver staining revealed the presence of proteins specifically co-precipitated by EGFP-Nuf2 but not by an unrelated control EGFP fusion protein (Fig. 2). Mass spectrometry revealed the identity of these proteins. Among the co-immunoprecipitated proteins were *Drosophila* Ndc80 and Spc25, as expected from the Ndc80 complex characterizations in yeast and vertebrates (Kline-Smith et al. 2005). Moreover, *Drosophila* Mis12 was also co-immunoprecipitated. Physical interactions between the Ndc80 and the MIND complex have previously been observed in other organisms (Cheeseman et al. 2004; Obuse et al. 2004; Liu et al. 2005).

In addition to Ndc80, Spc25 and Mis12, we also detected the products of the uncharacterized genes *CG1558* and *CG13434* in the EGFP-Nuf2 immunoprecipitates (Fig. 2). Expression of EGFP fusion proteins in S2R+ cells revealed a centromere localization during interphase and mitosis in both cases (Suppl. Fig. 1B,C). Based on primary and secondary sequence comparisons, these genes appear to encode additional components of the MIND complex. However, the observed similarities were very limited, precluding an unequivocal definition of orthologous relationships in particular in case of *CG1558*. The following designation of *CG1558* as *Nsl1* and *CG13434* as *Nnf1* will have to remain tentative. Interestingly, the sequenced genomes of melanogaster subgroup species (*D. melanogaster*, *D. simulans*, *D. sechellia*, *D. erecta*, *D. yakuba*) all encode a *CG13434* paralog, resulting from an apparent duplication of the primordial *CG13434* ortholog at the start of the melanogaster subgroup lineage (Suppl. Fig. 2A,B). An EGFP fusion of this paralog, *CG31658*, was also observed to localize to the centromere during interphase and mitosis (Suppl. Fig. 1D).

Therefore, we will designate *CG13434* as *Nnf1a* and *CG31658* as *Nnf1b*. RT-PCR experiments suggested co-expression of the Nnf1 paralogs at least during early *Drosophila* development (Suppl. Fig. 2C) An analogous co-immunoprecipitation experiment using *gSpc25-mRFP* embryo extracts and anti-mRFP antibodies confirmed co-immunoprecipitation of the Ndc80 complex components Ndc80, Nuf2 and Spc25 with Mis12, Nsl1, Nnf1a and also Nnf1b (data not shown). However, in both the EGFP-Nuf2 and mRFP-Spc25 immunoprecipitates we were unable to detect a homolog of Spc24, which is present as a fourth subunit in both yeast and mammalian Ndc80 complexes. In addition, we also did not detect a homolog of Dsn1, which is present as a fourth subunit in both the mammalian and yeast Mis12 complexes. More extensive purification of the *Drosophila* Ndc80 and MIND complexes will be required for their complete characterization.

Essential functions of *Drosophila* MIND and Ndc80 complex components can be provided by fluorescent fusion protein variants

To define the functions of the *Drosophila* Ndc80 complex and Mis12 genetically, we identified and characterized mutations in the *Nuf2*, *Spc25* and *Mis12* genes (for a schematic illustration of gene models, mutations and transgenes see Suppl. Fig. 3). A P element insertion in *Nuf2* had been isolated in a transposon mutagenesis screen for recessive lethal mutations (Oh et al. 2003). The insertion SH2276 was confirmed to be located 11 bp upstream of the initiation codon in the 5' UTR of *Nuf2*. The insertion leads to a partial loss of function. *Nuf2*^{SH2276} homozygotes were found to develop to the late pupal stages and to die either as pharate adults or soon after eclosion. The *gEGFP-Nuf2* transgene was found to prevent the lethality of early *Nuf2*^{SH2276} adults. Our findings demonstrate that *Drosophila Nuf2* is an essential gene. Moreover, they indicate that the EGFP-Nuf2 fusion protein is functional.

The piggyBac transposon insertion c00064 (Thibault et al. 2004) was mapped 38 bp upstream of the initiation codon in the 5' UTR of *Spc25*. *Spc25*^{c00064} homozygotes were found

to die during the late larval stages. Compared to sibling control larvae, the mutants had only rudimentary imaginal discs and small brains, suggesting that Spc25 is required in mitotically proliferating cells. The late larval lethality of *Spc25*^{c00064} homozygotes was prevented by a transgene driving expression of a Spc25-mRFP fusion protein under control of the *Spc25* regulatory region (*gSpc25-mRFP*). This transgene also complemented the recessive lethality of *Spc25*$^{A34-1}$, another independent allele previously isolated as a recessive lethal mutation (Hilliker et al. 1980). Based on these observations we conclude that *Drosophila Spc25* is an essential gene. In addition, the Spc25-mRFP fusion protein must be functional.

The collection of transposon insertions of Thibault et al. (2004) also includes a line (f03756) with a piggyBac WH insertion in the first intron of the *Drosophila* gene encoding the MIND component Mis12. *Mis12*^{f03756} hemizygotes were found to die during embryogenesis. This embryonic lethality was prevented by a transgene allowing expression of an EGFP-Mis12 fusion protein under control of the *Mis12* regulatory region (*gEGFP-Mis12*). *Drosophila Mis12* is therefore also an essential gene. In addition, the EGFP-Mis12 fusion protein is functional as well.

Mapping of centromere and kinetochore proteins in native chromosomes at high resolution

The accuracy of distance measurements can be increased beyond the diffraction-limited resolution of light microscopy by analyzing the spatial separation between signals from two different fluorophores (Stelzer 1998; Shimogawa et al. 2006). To exploit this approach for the analysis of the organization of the CKC, we prepared native chromosomes from embryos expressing functional fluorescent fusion proteins. We used a number of strains which co-expressed both a green and a red fluorescent CKC component. Eggs were collected from these strains and aged to the syncytial blastoderm stage where thousands of nuclei progress synchronously through mitoses. Embryos were gently squashed in a buffer containing a DNA

stain. Chromosomes released from mitotic embryos were analyzed by wide-field fluorescence microscopy (Fig. 3A-C). Analyses with embryos expressing a green fluorescent microtubule binding protein and red fluorescent Cenp-A/Cid demonstrated that spindles did not survive the squashing procedure and that the sister kinetochores of the released chromosomes were not under tension (Suppl. Fig. 4). Green and red signals in chromosomes released from embryos expressing two different fluorescent CKC components were captured with a cooled CCD camera. Pixel intensities were quantified along the axis connecting the two sister CKCs in chromosomes released from prometa- or metaphase embryos. The distance between the intensity maxima in the two sister CKC was determined. The difference between the distances separating the green ($d_{GGinter}$) and red ($d_{RRinter}$) fluorescent maxima, respectively, was calculated and divided by two to obtain an estimate for the distance ($d_{RGintra}$) between the red and the green fluorescent component within a CKC (Fig. 3D). Independent estimates for $d_{RGintra}$ from at least 100 different chromosomes were averaged to yield an estimate of the distance which separates a given pair of CKC proteins (Table 1). These pair separation values are represented by double arrows in Fig. 3E. Moreover, as another estimate for the spatial arrangement of the CKC proteins, we determined the average of all the $d_{GGinter}$ and $d_{RRinter}$ values obtained in our analyses for a given CKC protein. For instance, in the case of Cenp-A/Cid, the 500 $d_{RRinter}$ measurements and 200 $d_{GGinter}$ measurements resulted in an average value for the separation of the two sister kinetochore Cenp-A/Cid signal maxima of 460 nm. From the separation differences apparent when different CKC components were compared (Table 2), the CKC components were positioned along the centromere-spindle axis as indicated by the vertical colored lines in Fig. 3E.

To determine the position of a spindle checkpoint protein in native chromosomes, we used a strain co-expressing red fluorescent Cenp-A/Cid and green fluorescent Bub3. Various mitotic spindle checkpoint components have been reported to localize to the outermost, fibrous corona region of the kinetochore in intact cells (Vos et al. 2006). In our native chromosome

preparations, the localization of EGFP-Bub3 was found to be highly variable on different kinetochores (Suppl. Fig. 5), precluding a precise mapping.

The following control experiments support the accuracy of our CKC map. We generated a strain in which one of the two transgenes generated green and the other red fluorescent Cenp-A/Cid. In native chromosomes prepared from this strain (Fig. 3A,B), the red or green fluorescent proteins are expected to be perfectly co-localized. Our distance measurement resulted in $d_{RGintra}$ = 5 nm (Table 1). In an analogous analysis with a strain co-expressing red or green fluorescent Spc25, we obtained the expected $d_{RGintra}$ = 0 nm (Table 1). These distances were far smaller than the $d_{RGintra}$ values obtained for pairs of different proteins (Table 1). Finally, the additive behavior of different $d_{RGintra}$ values corresponded closely to the expectations. For instance, the sum of the measured distances between Cenp-A/Cid and Spc25 ($d_{RGinter}$ = 49 nm) on the one hand and Spc25 and Nuf2 ($d_{RGinter}$ = 15 nm) on the other hand is only 5 nm different from the measured separation between Cenp-A/Cid and Nuf2 ($d_{RGinter}$ = 69 nm). Based on all these findings, we expect the correct signal maxima to be within +/- 5 nm of the positions indicated in Fig. 3E.

Based on previous analyses, Cenp-A, Cenp-C and Mis12 are thought to be components of the inner plate of the characteristic trilaminar kinetochore structure apparent in the EM (Kline et al. 2006; Vos et al. 2006). However, our analyses indicate a significant separation between the inner most CKC component Cenp-A and all other CKC components analyzed here. Recently, Cenp-A nucleosomes purified from human cells were found to be intimately associated with the six proteins Cenp-M, -N, -T, -U, -H in addition to Cenp-C (Foltz et al. 2006; Izuta et al. 2006; Okada et al. 2006). The apparent space between Cenp-A and Cenp-C might therefore be occupied by some of those proteins. Here, Cenp-C is shown to spread in a polar orientation across a central CKC region. The C-terminal domain of Cenp-C, which contains the most conserved region of this rapidly evolving protein (Talbert et al. 2004; Heeger et al. 2005), points towards the centromeric DNA. These C-terminal sequences are

connected via a minimally conserved spacer to the N-terminal domain which is oriented towards the kinetochore spindle fibers. The N-terminal region of *D. melanogaster* Cenp-C contains some blocks which are highly conserved among Drosophilids (Heeger et al. 2005). These blocks might be involved in recruiting the next layer of kinetochore proteins which we suggest to include the Ndc80 and MIND complexes. We find the MIND component Mis12 to be close to the N-terminal Cenp-C region. Moreover, the Ndc80 complex component Spc25 appears to be even a bit closer but well separated by about 20 nm from the other Ndc80 component Nuf2. Apart from a polar Cenp-C orientation, our analyses therefore also indicate a polar orientation for the Ndc80 complex.

The tetrameric Ndc80 complex has a highly elongated, rod-like structure in vitro (Ciferri et al. 2005; Wei et al. 2005). The globular N-terminal domains of Ndc80 and Nuf2 are present on one end of the rod. The remainder of these two subunits forms an extended coiled coil which is further prolonged at its C-terminal end by binding to the N-terminal coiled coil region of the Spc24/Spc25 dimer. Closely associated C-terminal globular domains of Spc24 and Spc25 form the other end of the rod. SFM and EM analyses indicate that the coiled coil region separating the globular domains at the end of the Ndc80 complex has an extension of about 50 nm (Ciferri et al. 2005; Wei et al. 2005). This is over twofold longer than the distance which we have observed between fluorescent proteins at the N- and C-terminus of Nuf2 and Spc25 in kinetochores of native chromosomes. Many of the elongated Ndc80 complexes might not be perfectly oriented along the spindle axis, especially since the kinetochores in our preparations are not under tension. Such a non-uniform orientation could result in spatial distributions of the N- and C-terminus of Nuf2 and Spc25, respectively, with signal maxima that are more closely spaced than their separation within an isolated complex. An analysis of the positions of CKC components in chromosomes which are bi-oriented within the spindle and under tension would clearly be of interest. However, the increased background levels present in living embryos have so far precluded such analyses.

Our observed polar orientation of the Ndc80 complex within the kinetochore is consistent with earlier proposals. In budding yeast, the Ndc80 complex is though to function as a connection between the innermost components (CBF3 complex and Cenp-A/Cse4 nucleosome) and the DASH complex which forms a ring around a single attaching microtubule (Cheeseman et al. 2006; Westermann et al. 2006). The observation that Ndc80 and Nuf2 kinetochore localization is no longer observed in the absence of Spc24 or Spc25 (Bharadwaj et al. 2004) is consistent but does not prove an orientation of the complex with inner Spc24/25 and outer Ndc80/Nuf2 globular domains, because absence of Spc24 or Spc25 for instance might simply result in an instability of other complex components, as often observed in the case of stable complexes.

We also point out that the results of a detailed immunolocalization study comparing the distribution of Cenp-A and Cenp-C in human kinetochores (Blower et al. 2002) are largely consistent with our findings. These authors observed surprisingly little overlap between Cenp-A and Cenp-C, with the latter extending over top and bottom of a Cenp-A cylinder (Blower et al. 2002). However, problems with antigen accessibility, which in principle might also explain a marginal overlap, were not excluded by Blower et al. (2002) in contrast to our study. Moreover, many immunolocalization studies, including a recent study with *Drosophila* cells (Maiato et al. 2006), have failed to detect a comparable extensive spatial separation between Cenp-A/Cid and Cenp-C using comparable methodology as Blower et al. (2003).

In conclusion, we emphasize that our work provides a highly resolved structural framework, which contains the most widely studied ubiquitous CKC components, and a precise method for a future integration of additional proteins.

Materials and Methods

Fly strains

Drosophila stocks with the mutations *Nuf2*^{SH2276} (Oh et al. 2003) and *l(3)A34-1* (synonym: *l(3)87Da*^{2}) (Hilliker et al. 1980) or the deficiencies *Df(2L)ade3*, *Df(3L)XDI98*, and *Df(3R)ry75* were obtained from the Bloomington stock center. The PiggyBac insertion lines *Spc25*^{c00064} and *Mis12*^{f03756} (Thibault et al. 2004) were kindly provided by the Harvard Medical School stock collection.

Nuf2^{SH2276} appears to be a hypomorphic allele. Hemizygotes with *Nuf2*^{SH2276} over *Df(2L)ade3*, which deletes *Nuf2*, were found to die during the late pupal stages, i.e. earlier than *Nuf2*^{SH2276} homozygotes.

The EMS-induced recessive lethal mutation *l(3)A34-1* which had genetically been mapped to a chromosomal region including *Spc25* (Hilliker et al. 1980) failed to complement *Spc25*^{c00064}. Moreover, the lethality of *l(3)A34-1* in trans over the deficiency *Df(3R)ry75*, which deletes *Spc25*, was rescued by the *gmRFP-Spc25* transgene. *Spc25*^{c00064} homozygotes and hemizygotes (in trans over the deficiency *Df(3R)ry75*) displayed an indistinguishable phenotype which was more severe than that of *l(3)A34-1* hemizygotes. Therefore, *Spc25*^{c00064} appears to be an amorphic and *l(3)A34-1* a hypomorphic allele.

The gene trap line *G147* expresses a microtubule-binding EGFP fusion protein (Morin et al. 2001). Transgenic strains expressing kinetochore proteins fused to fluorescent proteins were generated by standard P element-mediated germ line transformation. Lines expressing functional Cenp-A/Cid with an internal EGFP (*gcid-EGFP-cid*) or mRFP (*gcid-mRFP-cid*) insertion 11 amino acids before the start of the histone fold domain have been described before (Schuh et al. 2006), as well as lines expressing Cenp-C with an N-terminal EYFP extension (*gEYFP-Cenp-C*) or with a C-terminal EGFP extension (*gCenp-C-EGFP*) (Heeger et al. 2005). *gBub3* lines have also been described recently (Pandey et al. manuscript

submitted). Additional lines were generated with the constructs described below. Lines with combinations of transgenes resulting in the expression of a red and a green fluorescent CKC component were generated by standard crosses. We analyzed lines with *gcid-mRFP-cid* II.1 in combination with either *gcid-EGFP-cid* III.2, *gEYFP-Cenp-C* II.1, *gCenp-C-EGFP* III.2, *gEGFP-Nuf2* II.1, *gMis12-EGFP* II.1, *gEGFP-Bub3*, or *G147*. In addition, we also analyzed lines with *gSpc25-mRFP* II.1 in combination with either *gSpc25-EGFP* II.1, *gcid-EGFP-cid* III.2, *gEYFP-Cenp-C* II.1, *gCenp-C-EGFP* III.2, *gEGFP-Nuf2* II.1, or *gMis12-EGFP* II.1. All transgenic lines had a *w* mutant background.

Plasmid constructions

pPUAST constructs containing cDNAs fused to the EGFP coding sequence were used for transfection of *Drosophila* S2R+ cells. For these constructions, we first generated two pPUAST variants for either N- or C-terminal EGFP fusions. For the former variant, the EGFP coding sequence was amplified using the primers RaS42 (5'-C GAATTC ATG GTG AGC AAG GGC GAG-3') and RaS43 (5'-TGGATTTCTG GCGGCCGC CTT GTA CAG CTC GTC CAT G-3') which introduce an *Eco*RI and a *Not*I site before the initiation codon or the stop codon, respectively. This PCR fragment was introduced into the corresponding polylinker sites in pPUAST. For the latter variant, the EGFP coding sequence was amplified with the primers RaS79 (5'-GC GGTACC ATG GTG AGC AAG GGC GAG-3') and RaS80 (5'-GG TCTAGA TTA CTT GTA CAG CTC GTC CAT G-3') which introduce a *Kpn*I and an *Xba*I site upstream of the initiation codon and after the stop codon, respectively. The resulting fragment was introduced into the corresponding polylinker sites of pPUAST. The restriction sites remaining in the polylinker of the pPUAST variants were used for the insertion of cDNA fragments amplified from EST plasmids characterized by the *Drosophila* genome project (Stapleton et al. 2002). The following EST plasmids were used: LD33040 (*Ndc80*), SD05495 (*Nuf2*), LD37196 (*Spc25*), RE19545 (*Mis12*), RE03006 (*Nsl1*), RE42502

(*Nnf1a*). *Nnf1b* was amplified from genomic DNA. Primers used for amplification were: RaS74 (5'-GG GAATTC AT GCGGCCGC G ATG TCG CAC CTG ATG CC-3') and RaS75 (5'-GG TCTAGA CTA ATG ATT CTT GAT GGC ATC TAG-3') for *pPUAST-EGFP-Ndc80*, RaS77 (5'-GATTAAAACT GCGGCCGC A ATG GCG TTA TCA GTC GAA ATT-3') and RaS78 (5'-TC TCTAGA TTA AGT GGA ATT CAT CTG CC-3') for *pPUAST-EGFP-Nuf2*, RaS81 (5'-GG GGTACC GGT GTG GCT CAT CGG CG-3') and RaS82 (5'-AG AGATCT ATG GCA ATT ATT ATG ACT GAA TC-3') for *pPUAST-Spc25-EGFP*, RaS113 (5'-GTTA GCGGCCGC A ATG GAC TTC AAT AGC CTA GC-3') in combination with RaS114 (5'-AGTT GGTACC ATC AGT CTC CTT CTT TAT CTG-3') or RaS115 (5'-G TCTAGA TTA ATC AGT CTC CTT CTT TAT C-3') for *pPUAST-Mis12-EGFP* or *pPUAST-EGFP-Mis12*, AnW28 (5'-ACGA GCGGCCGC T ATG GAG CCA GCC GAA AGT C-3') and AnW29 (5'-GC GGTACC TCA CCG TTG GTT GGC CAT AT-3') for *pPUAST-EGFP-Nsl1*, AnW25 (5'-CAAA GCGGCCGC T ATG GAG GAT TCG GAA GCC G-3') and AnW26 (5'-A CTCGAG TCA GAA GTC GTT CAA TGC-3') for *pPUAST-EGFP-Nnf1a*, AnW36 (5'-TGTG GCGGCCGC A ATG AAT AAT ATT GAA GAG GAC AC-3') and AnW37 (5'-TT GGTACC TTA CAT TTC TTC CTG CAC ATA C-3') for *pPUAST-EGFP-Nnf1b*.

pP{CaSpeR-4} constructs were made for the expression of kinetochore proteins fused to fluorescent proteins under control of the corresponding genomic regulatory region. Genomic fragments were amplified from BAC clones characterized by the *Drosophila* genome project (BACR30C16 for *Ndc80*, BACR39J17 for *Nuf2*, BACR17F05 for *Spc25*, BACR14L10 for *Mis12*) (Hoskins et al. 2000). The sequences of the primers were: AnW20 (5'-G GAATTC GTA GAA TCG TTT GGA AAT GC-3') and AnW21 (5'-G GGATCC CTT GGC GTT ATT GAA ACT AC-3') for the 5' part of *Ndc80*, AnW22 (5'-C TCTAGA ATG TCG CAC CTG ATG CCC-3') and AnW23 (5'-CATTGT AGGCCT ACG TTA GCA CTA TCG GGG-3') for the 3' part of *Ndc80*; RaS83 (5'-CACCCAGTTC GCGGCCGC ATG TAT CAA ATG TGT

CGC C-3') and RaS84 (5'-GA GGATCC CAT TCA ATC CAG AGT TTT AAT-3') for the 5' part of *Nuf2*, RaS87 (5'-TG TCTAGA ATG GCG TTA TCA GTC GAA A-3') and RaS88 (5'-A AGGCCT TGC CCC AGA TAA GGA AAA GG-3') for the 3' part of *Nuf2*; RaS93 (5'-GTTTAGATGG GCGGCCGC GCC GAT GAT CAG GAC CGG-3') and RaS94 (5'-GG GGATCC GGT GTG GCT CAT CGG CG-3') for the 5' part of *Spc25*; RaS95 (5'-AC TCTAGA CTT CCG ATT AAC TGA TTT AC-3') and RaS96 (5'-G AGGCCT CGA TTA ACA CCG GCC G-3') for the 3' part of *Spc25*; RaS125 (5'-AGC GAATTC GCT TCC TTT GTT TGT TCG GG-3') and RaS126 (5'-GTT GGATCC ATC AGT CTC CTT CTT TAT CTG-3') for the 5' part of *Mis12*, RaS127 (5'-ACT TCTAGA ATA AAC TAA CTG GAT CAA GTT TT-3') and RaS128 (5'-TCTCCCA AGGCCT CAG GCT TAT AGC AAA ATA TAC G-3') for the 3' part of *Mis12*. The PCR fragments with the 5' and 3' parts of a given gene were introduced into polylinker sites of pP{CaSpeR-4}. Moreover, a PCR fragment containing the coding sequences of either *mRFP1* or *EGFP* was introduced into the *Bam*H1 and *Xba*I sites between the 5' and 3' parts. The primers for the amplification of the coding sequences of the fluorescent proteins were: RaS85 (5'-GC GGATCC ATG GTG AGC AAG GGC GAG-3') and RaS86 (5'-TC TCTAGA CTT GTACAG CTC GTC CAT G-3') for *EGFP* in *gEGFP-Ndc80* and *gEGFP-Nuf2*, RaS85 and RaS80 (5'-GG TCTAGA TTA CTT GTA CAG CTC GTC CAT G-3') for *EGFP* in *gMis12-EGFP*, RaS91 (5'-AG GGATCC ATG GCC TCC TCC GAG GAC-3') and RaS92 (AA TCTAGA TTA GGC GCC GGT GGA GTG-3') for *mRFP1* in *gSpc25-mRFP*, RaS91 and AnW24 (5'-AA TCTAGA GGC GCC GGT GGA GTG G-3') for *mRFP1* in *gmRFP-Ndc80*.

Immunoprecipitation

For the coimmunoprecipitation experiments, we collected 5-8 hour embryos from either *w^1;P{w^+, gNuf2-EGFP} II.1* or *w^1; P{w+, sryα-Gal4} II.1, P{w^+, UAS-EGFP-CG11743} II.1* flies at 25°C. After dechorionization in 50% Klorix, eggs were shock frozen in liquid nitrogen

and stored at -80°C. 1 ml packed embryos were homogenized in 4 ml lysis buffer (50 mM HEPES at pH 7.5, 60 mM NaCl, 3 mM $MgCl_2$, 1 mM $CaCl_2$, 0.2% Triton X-100, 0.2% Nonidet NP-40, 10% glycerol, 1 mM DTT) containing 0.2 ml protease inhibitor cocktail (P 8340, Sigma). The extracts were cleared by centrifugation (20 min, 14000 x g). For further clearing, supernatants were incubated with 0.15 ml Protein-A-Sepharose beads (Affi-Prep, BIO-RAD) during 1 hour followed by another centrifugation. 25 µl Protein-A-Sepharose beads to which about 25 µg affinity-purified rabbit antibodies against GFP (J. Dürr and S. H., unpublished) had been crosslinked with dimethyl pimelidate (Harlow and Lane 1988) were used for immunoprecipitation from the supernatant. Immunoprecipitates were washed four times with lysis buffer. During the third and fourth washes, 0.5% Nonidet NP-40 and 0.5% Triton-X-100 were present in the lysis buffer. Moreover, during the fourth wash 300 mM NaCl was also present in the lysis buffer. Immunoprecipitated proteins were eluted for five minutes at 37°C with 0.04 ml 2% sodium dodecyl sulfate (SDS), 50 mM Tris-HCl, pH 7.5, followed by another elution at 94°C. SDS-PAGE sample buffer was added and the immunoprecipitated proteins were resolved on a large 12% Tris-HCl precast gel (BIO-RAD). Silver staining was performed essentially as described (Blum et al. 1987). Fixation was done in 30% ethanol, 10% acetic acid. After a wash in 30% ethanol, water was used for an additional 20 minute wash. 0.02% and 0.05% formaldehyde were included in the silver nitrate solution and the developer, respectively. Staining was terminated in 5% acetic acid. Note that Fig. 2 displays proteins eluted at 37°C. The majority of EGFP-Nuf2 was only eluted during the second elution at 94°C. Excised bands were rinsed in water and analysed by mass spectrometry essentially as described previously (Riedel et al. 2006).

Preparation and analysis of native chromosomes

Eggs were collected on apple juice agar plates and aged to the syncytial blastoderm stages. After chorion removal with 50% bleach and extensive washing in water, eggs were returned

to apple juice agar plates. Three eggs were lined up on a glass slide and 3.5 µl of phosphate buffered saline containing 2 µg/ml Hoechst 33258 were added. Embryos were squashed by capillary forces after adding a coverslip (24 x 32 mm). Microscopic analyses were started within a few minutes, after turbulent mixing within the specimen had settled. Single focal planes were acquired with a Zeiss Axioplan 2 Imaging system using a 100x PlanApo NA 1.4 objective, an AxioCam MRm camera and AxioVision software. With this setup, a camera pixel represents about a 68 nm square region of the object. Extent of movement within the unfixed sample was controlled by comparing the spatial distribution of the DNA staining acquired before and after acquisition of the red and green signals. Chromosomes which had moved more than 0.2 µm during acquisition were excluded from the analyses. In addition, chromosomes which did not clearly display two distinct sister kinetochores signals were also excluded from the analyses. Thereby, chromosomes from anaphase embryos, as well as chromosomes from prometa- and metaphase embryos with an orientation of the axis between sister kinetochores perpendicular (or nearly perpendicular) to the slide were eliminated. The majority of chromosomes (about 70%, n = 436) from prometaphase and metaphase embryos displayed two distinct sister kinetochores. The squashing procedure therefore appears to result in a preferred planar orientation of the two sister kinetochore on the slide. For evaluation, signal intensities along a line connecting the two sister kinetochores were determined using ImageJ software and transferred to MS Excel software for further analysis. The $d_{RRinter}$, $d_{GGinter}$ and $d_{RGintra}$ values for a given pair of CKC components (see Fig. 3D and Table 1), as well as the d_{inter} values obtained for a given CKC component by pooling the corresponding data from the pairwise analyses (Table 2), were not normally distributed, as expected since chromosomes with closely spaced, overlapping sister kinetochore signals were excluded from the analyses for instance. An adequate statistical error analysis was further complicated by unexplored potential biological (kinetochore variation in chromosome 2, 3, 4, X and Y, or precise mitotic stage), experimental (chromosome orientation and extent of

stretch/compression) and instrumental variability (pixelation, background noise). The distribution of all the measured data is therefore shown in Suppl. Fig. 6.

Acknowledgements

We thank Brigitte Jaunich for technical help. This work was supported by a grant from the Deutsche Forschungsgemeinschaft (DFG Le 987/3-3 and 3-4) and by the Fonds der Deutschen Chemie.

References

Bharadwaj, R., Qi, W., and Yu, H. 2004. Identification of two novel components of the human NDC80 kinetochore complex. *J Biol Chem* **279**(13): 13076-13085.

Blower, M.D., Sullivan, B.A., and Karpen, G.H. 2002. Conserved organization of centromeric chromatin in flies and humans. *Dev Cell* **2**(3): 319-330.

Blum, H., Beier, H., and Gross, H.J. 1987. Improved silver staining of plant proteins, RNA and DNA in polyacrylamide gels. *Electrophoresis* **8**: 93-99.

Cheeseman, I.M., Chappie, J.S., Wilson-Kubalek, E.M., and Desai, A. 2006. The Conserved KMN Network Constitutes the Core Microtubule-Binding Site of the Kinetochore. *Cell* **127**(5): 983-997.

Cheeseman, I.M., Niessen, S., Anderson, S., Hyndman, F., Yates, J.R., 3rd, Oegema, K., and Desai, A. 2004. A conserved protein network controls assembly of the outer kinetochore and its ability to sustain tension. *Genes Dev* **18**(18): 2255-2268.

Chen, Y., Riley, D.J., Chen, P.L., and Lee, W.H. 1997. HEC, a novel nuclear protein rich in leucine heptad repeats specifically involved in mitosis. *Mol Cell Biol* **17**(10): 6049-6056.

Ciferri, C., De Luca, J., Monzani, S., Ferrari, K.J., Ristic, D., Wyman, C., Stark, H., Kilmartin, J., Salmon, E.D., and Musacchio, A. 2005. Architecture of the human ndc80-hec1 complex, a critical constituent of the outer kinetochore. *J Biol Chem* **280**(32): 29088-29095.

Cleveland, D.W., Mao, Y., and Sullivan, K.F. 2003. Centromeres and kinetochores: from epigenetics to mitotic checkpoint signaling. *Cell* **112**(4): 407-421.

Cooke, C.A., Schaar, B., Yen, T.J., and Earnshaw, W.C. 1997. Localization of CENP-E in the fibrous corona and outer plate of mammalian kinetochores from prometaphase through anaphase. *Chromosoma* **106**(7): 446-455.

De Wulf, P., McAinsh, A.D., and Sorger, P.K. 2003. Hierarchical assembly of the budding yeast kinetochore from multiple subcomplexes. *Genes Dev* **17**(23): 2902-2921.

DeLuca, J.G., Dong, Y., Hergert, P., Strauss, J., Hickey, J.M., Salmon, E.D., and McEwen, B.F. 2005. Hec1 and nuf2 are core components of the kinetochore outer plate essential for organizing microtubule attachment sites. *Mol Biol Cell* **16**(2): 519-531.

Foltz, D.R., Jansen, L.E., Black, B.E., Bailey, A.O., Yates, J.R., 3rd, and Cleveland, D.W. 2006. The human CENP-A centromeric nucleosome-associated complex. *Nat Cell Biol* **8**(5): 458-469.

Giot, L., Bader, J.S., Brouwer, C., Chaudhuri, A., Kuang, B., Li, Y., Hao, Y.L., Ooi, C.E., Godwin, B., Vitols, E., Vijayadamodar, G., Pochart, P., Machineni, H., Welsh, M., Kong, Y., Zerhusen, B., Malcolm, R., Varrone, Z., Collis, A., Minto, M., Burgess, S., McDaniel, L., Stimpson, E., Spriggs, F., Williams, J., Neurath, K., Ioime, N., Agee, M., Voss, E., Furtak, K., Renzulli, R., Aanensen, N., Carrolla, S., Bickelhaupt, E., Lazovatsky, Y., DaSilva, A., Zhong, J., Stanyon, C.A., Finley, R.L., Jr., White, K.P., Braverman, M., Jarvie, T., Gold, S., Leach, M., Knight, J., Shimkets, R.A., McKenna, M.P., Chant, J., and Rothberg, J.M. 2003. A protein interaction map of Drosophila melanogaster. *Science* **302**(5651): 1727-1736. Epub 2003 Nov 1726.

Goshima, G., Kiyomitsu, T., Yoda, K., and Yanagida, M. 2003. Human centromere chromatin protein hMis12, essential for equal segregation, is independent of CENP-A loading pathway. *J Cell Biol* **160**(1): 25-39.

Harlow, E. and Lane, D. 1988. *Antibodies. A Laboratory Manual*. Cold Spring Harbor Laboratory Press.

Heeger, S., Leismann, O., Schittenhelm, R., Schraidt, O., Heidmann, S., and Lehner, C.F. 2005. Genetic inteactions of Separase regulatory subunits reveal the diverged Drosophila Cenp-C homolog. *Genes Dev* **19**(17): 2041-2053.

Henikoff, S., Ahmad, K., Platero, J.S., and van Steensel, B. 2000. Heterochromatic deposition of centromeric histone H3-like proteins. *Proc Natl Acad Sci U S A* **97**(2): 716-721.

Hilliker, A.J., Clark, S.H., Chovnick, A., and Gelbart, W.M. 1980. Cytogenetic analysis of the chromosomal region immediately adjacent to the rosy locus in Drosophila melanogaster. *Genetics* **95**(1): 95-110.

Hoskins, R.A., Nelson, C.R., Berman, B.P., Laverty, T.R., George, R.A., Ciesiolka, L., Naeemuddin, M., Arenson, A.D., Durbin, J., David, R.G., Tabor, P.E., Bailey, M.R., DeShazo, D.R., Catanese, J., Mammoser, A., Osoegawa, K., de Jong, P.J., Celniker, S.E., Gibbs, R.A., Rubin, G.M., and Scherer, S.E. 2000. A BAC-based physical map of the major autosomes of Drosophila melanogaster. *Science* **287**(5461): 2271-2274.

Izuta, H., Ikeno, M., Suzuki, N., Tomonaga, T., Nozaki, N., Obuse, C., Kisu, Y., Goshima, N., Nomura, F., Nomura, N., and Yoda, K. 2006. Comprehensive analysis of the ICEN (Interphase Centromere Complex) components enriched in the CENP-A chromatin of human cells. *Genes Cells* **11**(6): 673-684.

Kline-Smith, S.L., Sandall, S., and Desai, A. 2005. Kinetochore-spindle microtubule interactions during mitosis. *Curr Opin Cell Biol* **17**(1): 35-46.

Kline, S.L., Cheeseman, I.M., Hori, T., Fukagawa, T., and Desai, A. 2006. The human Mis12 complex is required for kinetochore assembly and proper chromosome segregation. *J Cell Biol* **173**(1): 9-17.

Liu, S.T., Rattner, J.B., Jablonski, S.A., and Yen, T.J. 2006. Mapping the assembly pathways that specify formation of the trilaminar kinetochore plates in human cells. *J Cell Biol* **175**(1): 41-53.

Liu, X., McLeod, I., Anderson, S., Yates, J.R., 3rd, and He, X. 2005. Molecular analysis of kinetochore architecture in fission yeast. *Embo J* **24**(16): 2919-2930.

Maiato, H., Hergert, P.J., Moutinho-Pereira, S., Dong, Y., Vandenbeldt, K.J., Rieder, C.L., and McEwen, B.F. 2006. The ultrastructure of the kinetochore and kinetochore fiber in Drosophila somatic cells. *Chromosoma* **115**(6): 469-480.

Martin-Lluesma, S., Stucke, V.M., and Nigg, E.A. 2002. Role of Hec1 in spindle checkpoint signaling and kinetochore recruitment of Mad1/Mad2. *Science* **297**(5590): 2267-2270.

McAinsh, A.D., Meraldi, P., Draviam, V.M., Toso, A., and Sorger, P.K. 2006. The human kinetochore proteins Nnf1R and Mcm21R are required for accurate chromosome segregation. *Embo J* **25**(17): 4033-4049.

McEwen, B.F., Hsieh, C.E., Mattheyses, A.L., and Rieder, C.L. 1998. A new look at kinetochore structure in vertebrate somatic cells using high-pressure freezing and freeze substitution. *Chromosoma* **107**(6-7): 366-375.

Meraldi, P., McAinsh, A.D., Rheinbay, E., and Sorger, P.K. 2006. Phylogenetic and structural analysis of centromeric DNA and kinetochore proteins. *Genome Biol* **7**(3): R23.

Moore, L.L. and Roth, M.B. 2001. HCP-4, a CENP-C-like protein in Caenorhabditis elegans, is required for resolution of sister centromeres. *J Cell Biol* **153**(6): 1199-1208.

Morin, X., Daneman, R., Zavortink, M., and Chia, W. 2001. A protein trap strategy to detect GFP-tagged proteins expressed from their endogenous loci in Drosophila. *Proc Natl Acad Sci U S A* **98**(26): 15050-15055.

Obuse, C., Iwasaki, O., Kiyomitsu, T., Goshima, G., Toyoda, Y., and Yanagida, M. 2004. A conserved Mis12 centromere complex is linked to heterochromatic HP1 and outer kinetochore protein Zwint-1. *Nat Cell Biol* **6**(11): 1135-1141.

Oegema, K., Desai, A., Rybina, S., Kirkham, M., and Hyman, A.A. 2001. Functional analysis of kinetochore assembly in Caenorhabditis elegans. *J Cell Biol* **153**(6): 1209-1226.

Oh, S.W., Kingsley, T., Shin, H.H., Zheng, Z., Chen, H.W., Chen, X., Wang, H., Ruan, P., Moody, M., and Hou, S.X. 2003. A P-element insertion screen identified mutations in 455 novel essential genes in Drosophila. *Genetics* **163**(1): 195-201.

Okada, M., Cheeseman, I.M., Hori, T., Okawa, K., McLeod, I.X., Yates, J.R., 3rd, Desai, A., and Fukagawa, T. 2006. The CENP-H-I complex is required for the efficient incorporation of newly synthesized CENP-A into centromeres. *Nat Cell Biol* **8**(5): 446-457.

Ormo, M., Cubitt, A.B., Kallio, K., Gross, L.A., Tsien, R.Y., and Remington, S.J. 1996. Crystal structure of the Aequorea victoria green fluorescent protein. *Science* **273**(5280): 1392-1395.

Richards, S., Liu, Y., Bettencourt, B.R., Hradecky, P., Letovsky, S., Nielsen, R., Thornton, K., Hubisz, M.J., Chen, R., Meisel, R.P., Couronne, O., Hua, S., Smith, M.A., Zhang, P., Liu, J., Bussemaker, H.J., van Batenburg, M.F., Howells, S.L., Scherer, S.E., Sodergren, E., Matthews, B.B., Crosby, M.A., Schroeder, A.J., Ortiz-Barrientos, D., Rives, C.M., Metzker, M.L., Muzny, D.M., Scott, G., Steffen, D., Wheeler, D.A., Worley, K.C., Havlak, P., Durbin, K.J., Egan, A., Gill, R., Hume, J., Morgan, M.B., Miner, G., Hamilton, C., Huang, Y., Waldron, L., Verduzco, D., Clerc-Blankenburg, K.P., Dubchak, I., Noor, M.A., Anderson, W., White, K.P., Clark, A.G., Schaeffer, S.W., Gelbart, W., Weinstock, G.M., and Gibbs, R.A. 2005. Comparative genome sequencing of Drosophila pseudoobscura: chromosomal, gene, and cis-element evolution. *Genome Res* **15**(1): 1-18.

Riedel, C.G., Katis, V.L., Katou, Y., Mori, S., Itoh, T., Helmhart, W., Galova, M., Petronczki, M., Gregan, J., Cetin, B., Mudrak, I., Ogris, E., Mechtler, K., Pelletier, L., Buchholz, F., Shirahige, K., and Nasmyth, K. 2006. Protein phosphatase 2A protects centromeric sister chromatid cohesion during meiosis I. *Nature* **441**(7089): 53-61.

Rieder, C.L. 1982. The formation, structure, and composition of the mammalian kinetochore and kinetochore fiber. *Int Rev Cytol* **79**: 1-58.

Saitoh, H., Tomkiel, J., Cooke, C.A., Ratrie, H., 3rd, Maurer, M., Rothfield, N.F., and Earnshaw, W.C. 1992. CENP-C, an autoantigen in scleroderma, is a component of the human inner kinetochore plate. *Cell* **70**(1): 115-125.

Schueler, M.G. and Sullivan, B.A. 2006. Structural and functional dynamics of human centromeric chromatin. *Annu Rev Genomics Hum Genet* **7**: 301-313.

Schuh, M., Lehner, C.F., and Heidmann, S. 2006. Incorporation of Drosophila Cid/Cenp-A and Cenp-C into centromeres during early embryonic anaphase. *Curr Biol* **in press**.

Shimogawa, M.M., Graczyk, B., Gardner, M.K., Francis, S.E., White, E.A., Ess, M., Molk, J.N., Ruse, C., Niessen, S., Yates, J.R., 3rd, Muller, E.G., Bloom, K., Odde, D.J., and Davis, T.N. 2006. Mps1 phosphorylation of Dam1 couples kinetochores to microtubule plus ends at metaphase. *Curr Biol* **16**(15): 1489-1501.

Stapleton, M., Carlson, J., Brokstein, P., Yu, C., Champe, M., George, R., Guarin, H., Kronmiller, B., Pacleb, J., Park, S., Wan, K., Rubin, G.M., and Celniker, S.E. 2002. A Drosophila full-length cDNA resource. *Genome Biol* **3**(12): RESEARCH0080.

Stelzer, E.H. 1998. Contrast, resolution, pixelation, dynamic range and signal-to-noise ratio: fundamental limits to resolution in fluorescence light microscopy. *J Microscopy* **189**: 15-24.

Sullivan, B.A. and Karpen, G.H. 2004. Centromeric chromatin exhibits a histone modification pattern that is distinct from both euchromatin and heterochromatin. *Nat Struct Mol Biol* **11**(11): 1076-1083.

Takahashi, K., Yamada, H., and Yanagida, M. 1994. Fission yeast minichromosome loss mutants mis cause lethal aneuploidy and replication abnormality. *Mol Biol Cell* **5**: 1145-1158.

Talbert, P.B., Bryson, T.D., and Henikoff, S. 2004. Adaptive evolution of centromere proteins in plants and animals. *J Biol* **3**(4): 18.

Thibault, S.T., Singer, M.A., Miyazaki, W.Y., Milash, B., Dompe, N.A., Singh, C.M., Buchholz, R., Demsky, M., Fawcett, R., Francis-Lang, H.L., Ryner, L., Cheung, L.M., Chong, A., Erickson, C., Fisher, W.W., Greer, K., Hartouni, S.R., Howie, E., Jakkula, L., Joo, D., Killpack, K., Laufer, A., Mazzotta, J., Smith, R.D., Stevens, L.M., Stuber, C., Tan, L.R., Ventura, R., Woo, A., Zakrajsek, I., Zhao, L., Chen, F., Swimmer, C., Kopczynski, C., Duyk, G., Winberg, M.L., and Margolis, J. 2004. A complementary transposon tool kit for Drosophila melanogaster using P and piggyBac. *Nat Genet* **36**(3): 283-287.

Thompson, J.D., Higgins, D.G., and Gibson, T.J. 1994. CLUSTAL W: improving the sensitivity of progressive multiple sequence alignment through sequence weighting, position-specific gap penalties and weight matrix choice. *Nucleic Acids Res* **22**(22): 4673-4680.

Vos, L.J., Famulski, J.K., and Chan, G.K. 2006. How to build a centromere: from centromeric and pericentromeric chromatin to kinetochore assembly. *Biochem Cell Biol* **84**(4): 619-639.

Wei, R.R., Sorger, P.K., and Harrison, S.C. 2005. Molecular organization of the Ndc80 complex, an essential kinetochore component. *Proc Natl Acad Sci U S A* **102**(15): 5363-5367.

Westermann, S., Wang, H.W., Avila-Sakar, A., Drubin, D.G., Nogales, E., and Barnes, G. 2006. The Dam1 kinetochore ring complex moves processively on depolymerizing microtubule ends. *Nature* **440**(7083): 565-569.

Yang, F., Moss, L.G., and Phillips, G.N., Jr. 1996. The molecular structure of green fluorescent protein. *Nat Biotechnol* **14**(10): 1246-1251.

Figure legends

Figure 1. Localization of *Drosophila* Ndc80 complex components and Mis12.
Transgenic embryos expressing EGFP fused to either Ndc80 (A), Nuf2 (B), Spc25 (C) or Mis12 (D) were fixed at the stage when some cells progress through the fourteenth asynchronous round of mitosis. Cells in interphase (left panels) and metaphase (right panels) after double labeling with an antibody against Cenp-C (Cenp-C) and a DNA stain (DNA) illustrate that the EGFP fusion proteins were only associated with centromeres during mitosis. Bar = 5 μm.

Figure 2. Co-immunoprecipitation of Ndc80 and MIND complex components
Antibodies against GFP were used for immunoprecipitation from extracts of embryos expressing either EGFP-Nuf2 (Nuf2) or another unrelated EGFP fusion protein (Con) for control. After SDS-PAGE and silver staining, bands enriched in the EGFP-Nuf2 immunoprecipitates were characterized by mass spectrometry. Stars denote bands containing only highly abundant cellular proteins (mostly ribosomal proteins) presumably reflecting non-specific contaminations. Arrowheads denote bands which also contained rare proteins (as measured by their representation in EST data bases) which are either components of the Ndc80 complex or putative MIND components, as indicated by the names on the left margin. The numbers on the right margin indicate the molecular weight (kDa) of the proteins in the marker lane (MW).

Figure 3. Axial positions of different kinetochore proteins along the spindle axis.
(A) Native chromosomes released from syncytial embryos co-expressing a red and a green fluorescent CKC component were labeled with a DNA stain. The appearance of the native chromosomes with red (rCenp-A) and green (gCenp-A) fluorescent Cenp-A/Cid is illustrated

at low magnification. Bar = 5 μm. (B) The fourth chromosome indicated by the white arrows in A is shown at high magnification. Bar = 0.5 μm. (C) A fourth chromosome from an embryo expressing red fluorescent Cenp-A/Cid (rCenp-A) and green fluorescent Nuf2 (gNuf2) is shown at the same magnification as in B. These high magnification views (B,C) display the pixel resolution as acquired. (D) For an estimation of the spatial separation between a red and a green fluorescent CKC component, signal intensities were quantified along the axis running through the two sister kinetochores, as illustrated by the white line in C. The displayed intensity profiles are from the chromosome shown in C. The spatial separation ($d_{RGintra}$) was calculated by halving the difference between the distances separating the red ($d_{RRinter}$) and green ($d_{GGinter}$) signal maxima of the sister kinetochores, as indicated by the equation.

(E) The scheme summarizes the positions of the analyzed CKC components along the spindle axis. Double arrows represent the spatial separation as revealed by the pairwise analyses outlined in A-D with hundreds of native chromosomes (see also Table 1). Arrows above the dashed line are from experiments comparing the distance between red fluorescent Cenp-A/Cid and various green fluorescent CKC components. Analogous analyses of the distance between red fluorescent Spc25 and green fluorescent CKC components are represented by the arrows below the dashed line. Color coding specifies the green fluorescent component in these pairwise analyses. The vertical lines indicate the position of CKC components as revealed by pooling all $d_{RRinter}$ and $d_{GGinter}$ values obtained for a given CKC component during the pairwise analyses (see Table 2). The numbers indicate the spatial separation (nm) from the innermost centromere component Cenp-A/Cid which was set to zero. Cenp-C was analyzed with EGFP fused to either the N-terminus (Cenp-C(N)) or the C-terminus (Cenp-C(C)).

Supplementary Figure 1. Localization of *Drosophila* Mis12 and putative MIND complex components.

S2R+ cells were transfected with constructs allowing expression of EGFP fused to either Mis12 (A), Nsl1 (B), Nnf1a (C) or Nnf1b (D). Fixed cells in interphase (left panels) and metaphase (right panels) after double labeling with an antibody against Cenp-A/Cid (Cenp-A) and a DNA stain (DNA) illustrate that association of EGFP fusion proteins with centromeres is not restricted to mitosis. Bar = 5 μm.

Supplementary Figure 2. *Nnf1* gene duplication in the melanogaster subgroup.
(A) A phylogenetic tree was constructed after aligning the predicted amino acids sequences encoded by *Nnf1*-like genes identified by BLAST searches in Drosophilid genomes using CLUSTALW (Thompson et al. 1994; Richards et al. 2005)(prepublication data from Agencourt Bioscience Corporation and Genome Sequencing Center at Washington University(Richards et al. 2005)). An *Nnf1* gene duplication resulting in the two paralogs *Nnf1a* and *Nnf1b* early after the divergence of the melanogaster subgroup lineage provides the most parsimonious explanation for the observed branching pattern. *D. melanogaster* (Dmel), *D. simulans* (Dsim), *D. sechellia* (Dsec), *D. yakuba* (Dyak), *D. erecta* (Dere), *D. ananassae* (Dana), *D. persimilis* (Dper), *D. pseudoobscura* (Dpse), *D. willistoni* (Dwil).
(B) Alignment of the genome regions flanking the *Nnf1* paralogs in *D. melanogaster* (D mel) with *D. pseudoobscura* (D pse) genome regions reveals that *Nnf1a* (upper panel) but not *Nnf1b* (lower panel) is present in a syntenic region. Black arrows point to *Nnf1a/CG14434* and *Nnf1b/CG31658*. Syntenic regions are shaded with identical colors. Dashed lines indicate the first and last orthologous gene in syntenic regions flanking *Nnf1b*. In *D. pseudoobscura* these regions are followed by sequences which are unlinked in *D. melanogaster*. The cytological positions of these regions in *D. melanogaster* are indicated at the bottom of the colored *D. pseudoobscura* segments.
(C) The developmental expression pattern of *D. melanogaster Nnf1a* and *Nnf1b* was analyzed by RT-PCR experiments. The stages analyzed were: embryos 0-2 (0-2), 2-4 (2-4), 4-8 (4-8),

and 8-16 (8-16) hours after egg deposition; larval stages (L1, L2, L3), pupae (P), adult males (M) and females (F). Control amplifications (G) from a cloned *Nnf1a* cDNA and an intron containing genomic *Nnf1b* fragment, as well as amplifications (N) with mock reverse transcribed mRNA demonstrated that the RT-PCR products were not derived from contaminating genomic DNA. The results are consistent with *Nnf1a* expression being correlated with mitotic proliferation and *Nnf1b* expression being germline-specific.

Supplementary Figure 3. Genetic characterization of Ndc80 and putative MIND complex components.

Gene models are shown for *Ndc80/CG9938* (A), *Nuf2/CG8902* (B), *Spc25/CG7242* (C), *Mis12/CG18156* (D), *Nsl1/CG1558* (E), *Nnf1a/CG13434* (F), and *Nnf1b/CG31658* (G). Moreover, transposon insertions present in mutant alleles are indicated by triangles above the gene models. In addition, the genomic fragment used for transgene constructions are indicated by the solid lines below the gene models. The position where the EGFP coding sequence was inserted in these transgenes is illustrated by the triangles below the gene models.

Supplementary Figure 4. Spindle association of released native chromosomes.

To evaluate whether and how kinetochores from released native chromosomes interact with spindle remnants, we performed experiments with embryos expressing a green fluorescent microtubule binding protein (G147) and red fluorescent Cenp-A/Cid (Cenp-A). 82.4% of the chromosomes (n = 319) had kinetochores which showed no association with microtubules, as illustrated by the inset in the upper left corner which displays the kinetochores indicated by the filled arrowhead at high magnification. 16.6% had kinetochores with a lateral association with microtubules, as illustrated by the inset in the lower right corner which displays the kinetochores indicated by the open arrowhead. 0.3% had kinetochores with a monopolar end-on attachment. 0.6% appeared to have a bipolar attachment with microtubules which however

appeared to be so disorganized that the attachment presumably did not result in significant tension across the sister kinetochores.

Supplementary Figure 5. Localization of the mitotic spindle checkpoint protein Bub3 on native chromosomes.

Native chromosomes were prepared from embryos expressing red fluorescent Cenp-A/Cid and green fluorescent Bub3. In contrast to Cenp-A/Cid, the localization of EGFP-Bub3 in kinetochores from different chromosomes was found to be highly variable, as illustrated by the kinetochores indicated by numbered arrowheads in the top panels and shown at high magnification in the lower panels. Bar = 5 μm.

Supplementary Figure 6. Distribution of distance measurements.

Histogram curves illustrate the distribution of the $d_{RGintra}$ values (see Fig. 3 and Table 1) obtained in the pairwise analyses with chromosomes from embryos expressing red fluorescent Cenp-A/Cid and green CKC components (A), as well as in the analogous analyses with red fluorescent Spc25 in combination with green CKC components (B). Moreover, the distribution of the d_{inter} values, i.e. all the $d_{RRinter}$ and $d_{GGinter}$ measurements obtained for a given CKC components (see Table 2) are displayed as well (C).

Table 1. Pairwise mapping of CKC components

red protein	green protein	$d_{RRinter}$ [a] (nm)	$d_{GGinter}$ [a] (nm)	$d_{RGintra}$ [a] (nm)
Cenp-A/Cid	Cenp-A/Cid	445	455	5
	Cenp-C(C) [b]	460	490	15
	Cenp-C(N) [b]	463	547	42
	Mis12	472	574	51
	Nuf2	451	589	69
Spc25	Cenp-A/Cid	573	475	- 49
	Cenp-C(C) [b]	556	511	- 23
	Cenp-C(N) [b]	539	512	- 14
	Mis12	503	516	7
	Nuf2	547	576	15
	Spc25	531	531	0

a) Native chromosomes (n = 100) from embryos co-expressing a red and a green fluorescent CKC component were analyzed. Average values for the distances separating the red fluorescent signal maxima of sister kinetochores ($d_{RRinter}$) and the distances separating the green fluorescent signal maxima of sister kinetochores ($d_{GGinter}$) were used for the calculation of the distance separating the two components within a sister kinetochore ($d_{RGintra}$) (see also Fig. 3D and Material and Methods).

b) Cenp-C was expressed as a fusion with GFP either at the N-terminus (Cenp-C(N)) or at the C-terminus (Cenp-C(C)).

Table 2. Axial positions of CKC components from pooled data

protein	n	d_{inter} [a)] (nm)	axial position [b)] (nm)
Cenp-A/Cid	700	460	0
Cenp-C(C)	200	500	20
Cenp-C(N)	200	530	35
Spc25	700	540	40
Mis12	200	545	43
Nuf2	200	584	62

a) All $d_{RRinter}$ and $d_{GGinter}$ measurements obtained for a given CKC in the analyses after pairwise expression of red and green fusion proteins (see Table 1) were summed and averaged to estimate the distance separating the signal maxima of sister kinetochores (d_{inter}). The differences between the d_{inter} values obtained for different CKC components were found to be significant according to Mann-Whitney U tests ($p < 0.05$), except for the closely clustered Cenp-C(N), Spc25 and Mis12.

c) The separation of CKC components from Cenp-A/Cid along the spindle axis in a kinetochore was estimated by halving the difference between the d_{inter} values obtained for Cenp-A/Cid and a given CKC component. Axial separation is given relative to Cenp-A/Cid which was set to zero.

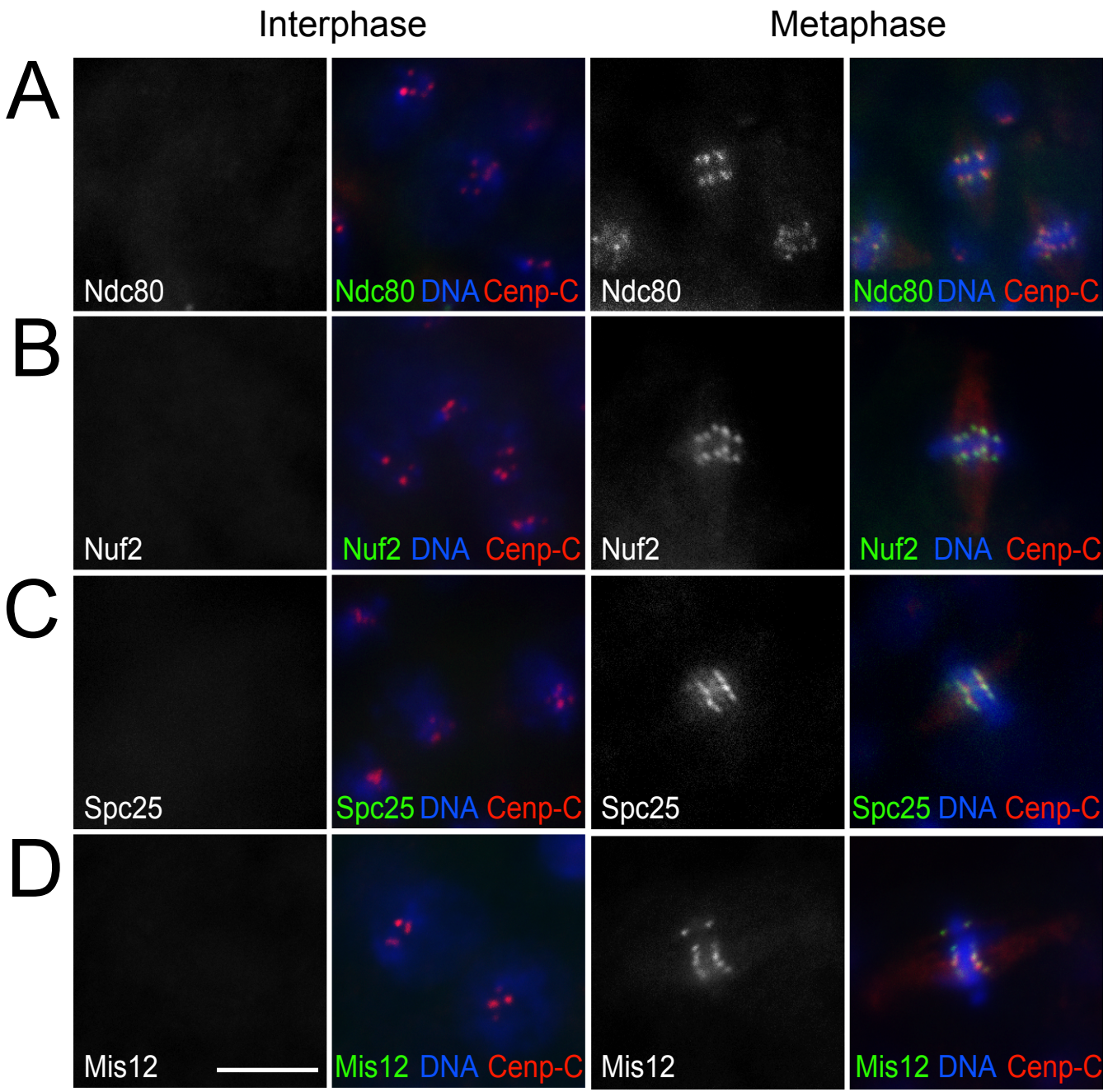
Interphase
Metaphase
A
Ndc80
Ndc80 DNA Cenp-C
Ndc80
Ndc80 DNA Cenp-C
B
Nuf2
Nuf2 DNA Cenp-C
Nuf2
Nuf2 DNA Cenp-C
C
Spc25
Spc25 DNA Cenp-C
Spc25
Spc25 DNA Cenp-C
D
Mis12
Mis12 DNA Cenp-C
Mis12
Mis12 DNA Cenp-C

Schittenhelm et al., Fig. 2

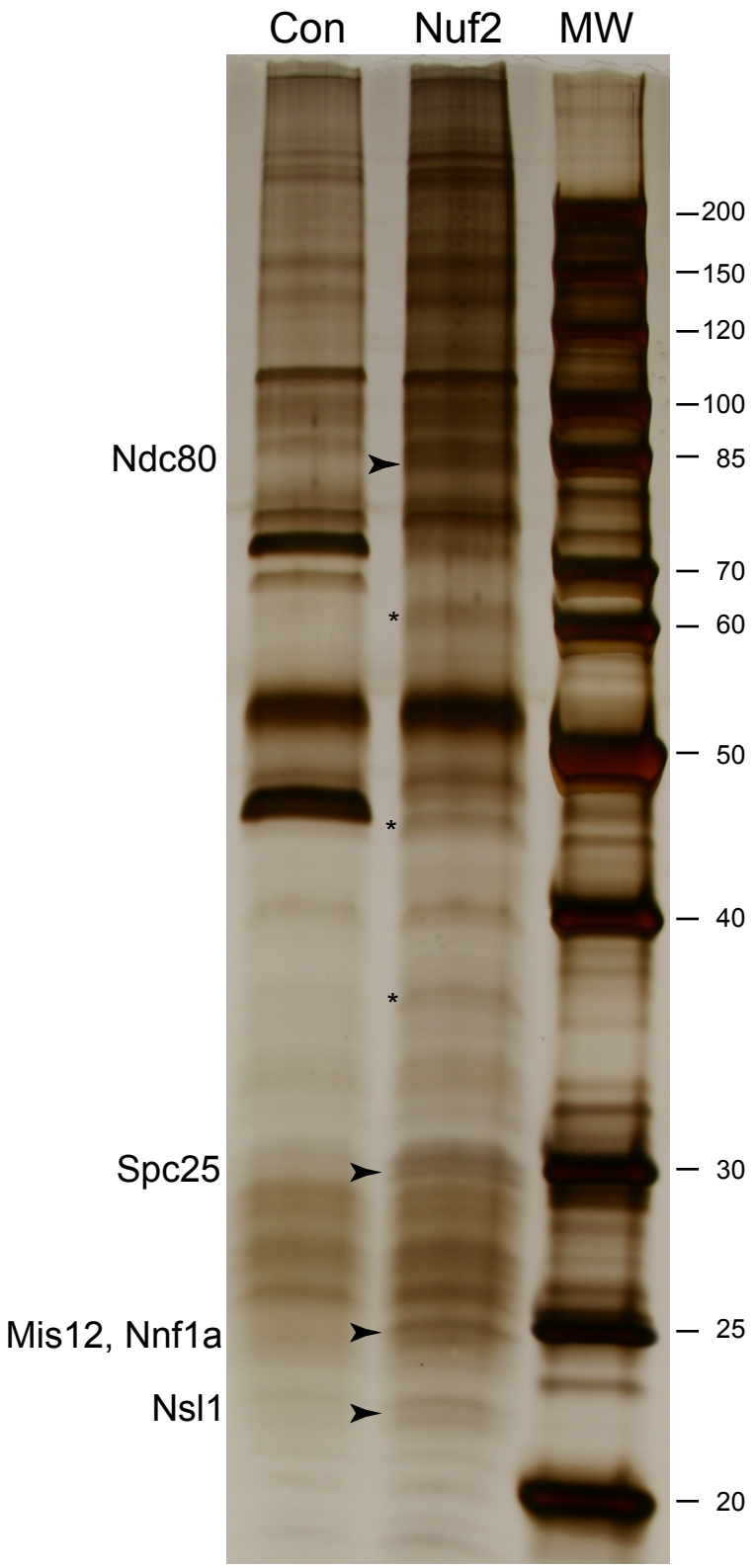

Schittenhelm et al., Fig. 3

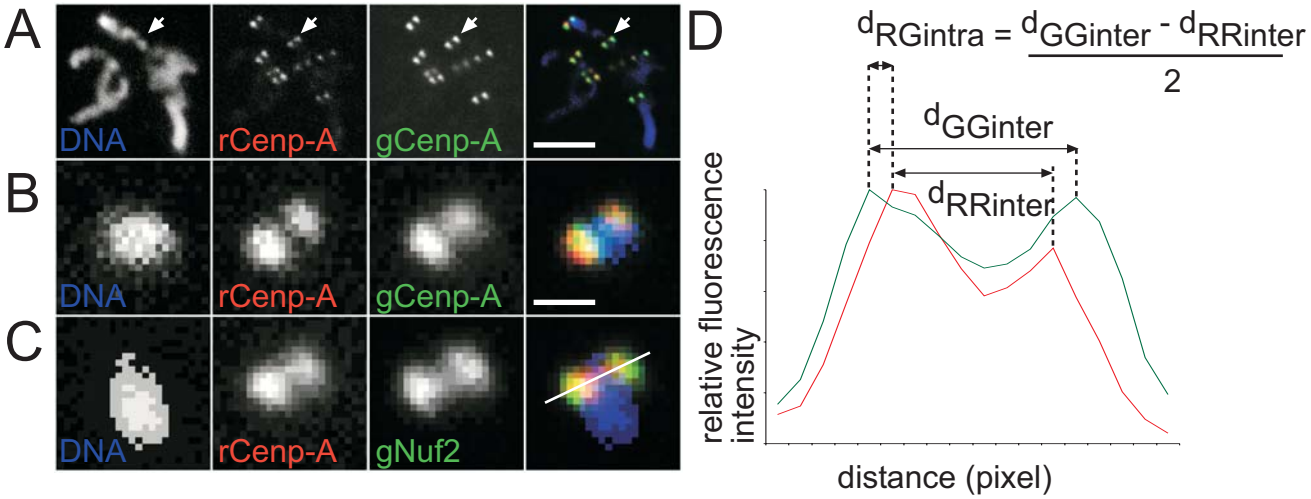

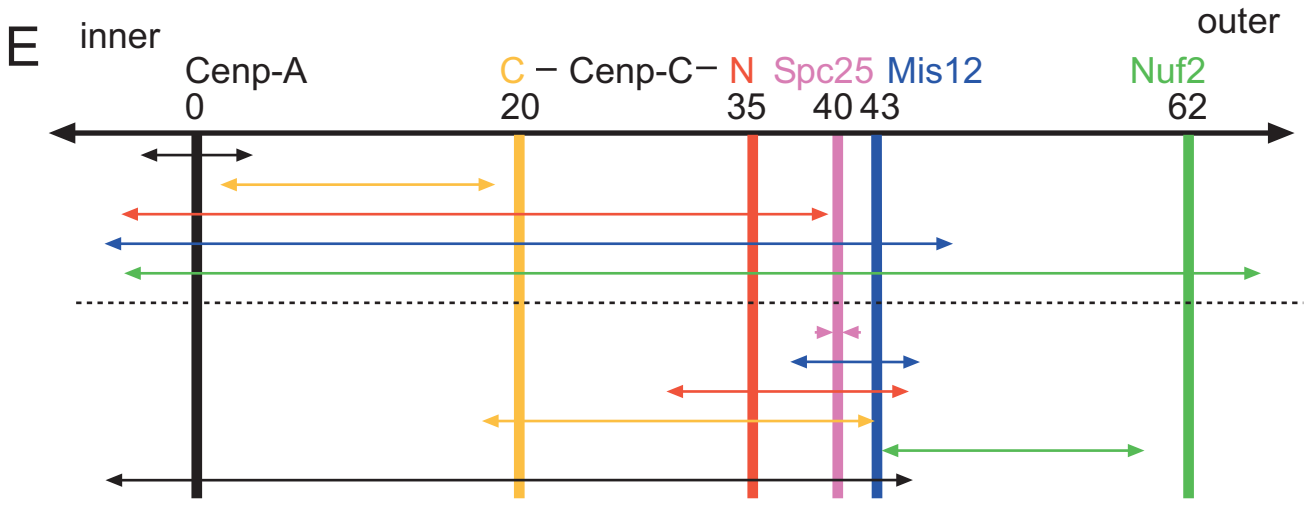

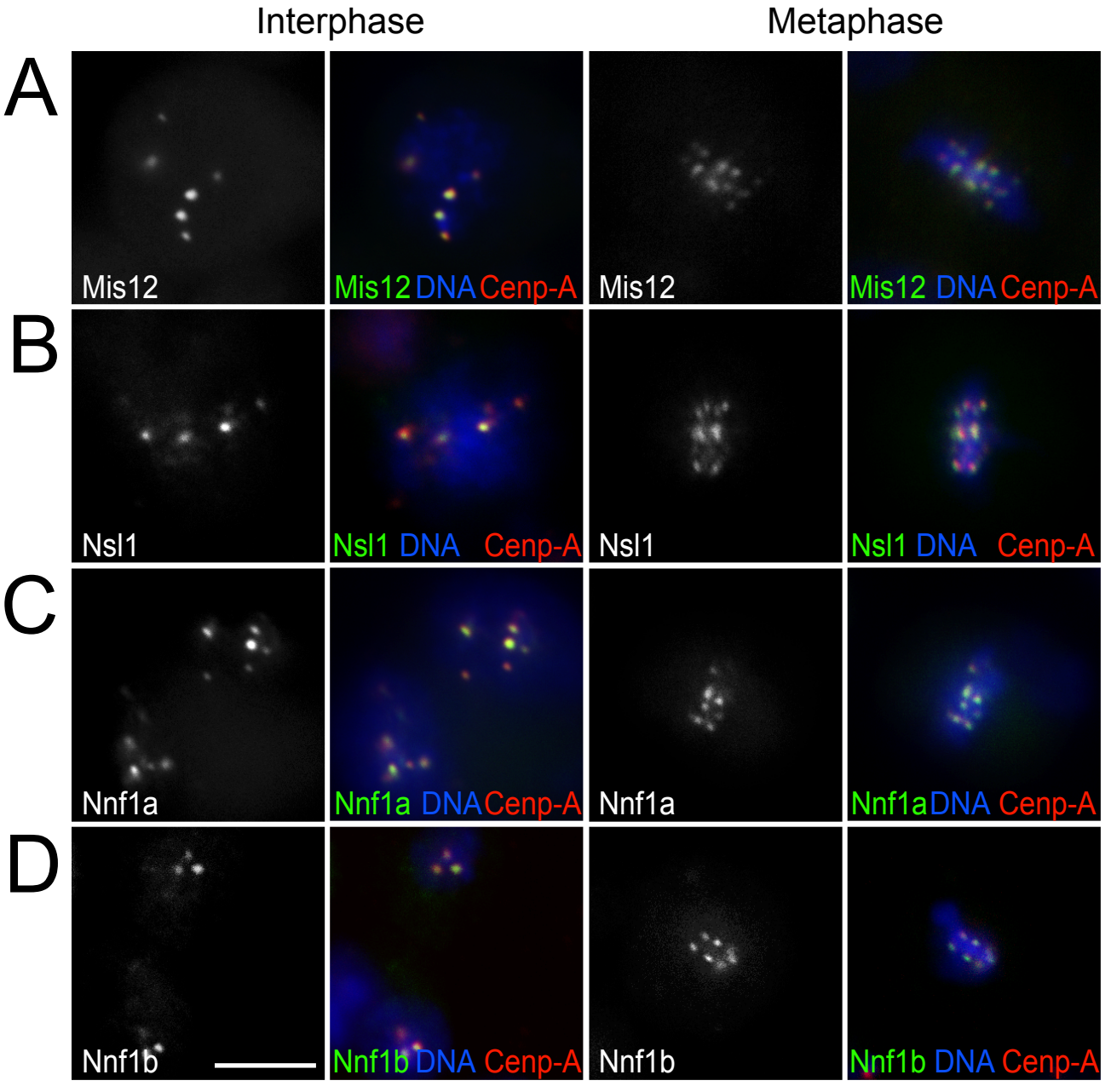
Interphase
Metaphase
A
Mis12
Mis12 DNA Cenp-A
Mis12
Mis12 DNA Cenp-A
B
Nsl1
Nsl1 DNA Cenp-A
Nsl1
Nsl1 DNA Cenp-A
C
Nnf1a
Nnf1a DNA Cenp-A
Nnf1a
Nnf1a DNA Cenp-A
D
Nnf1b
Nnf1b DNA Cenp-A
Nnf1b
Nnf1b DNA Cenp-A

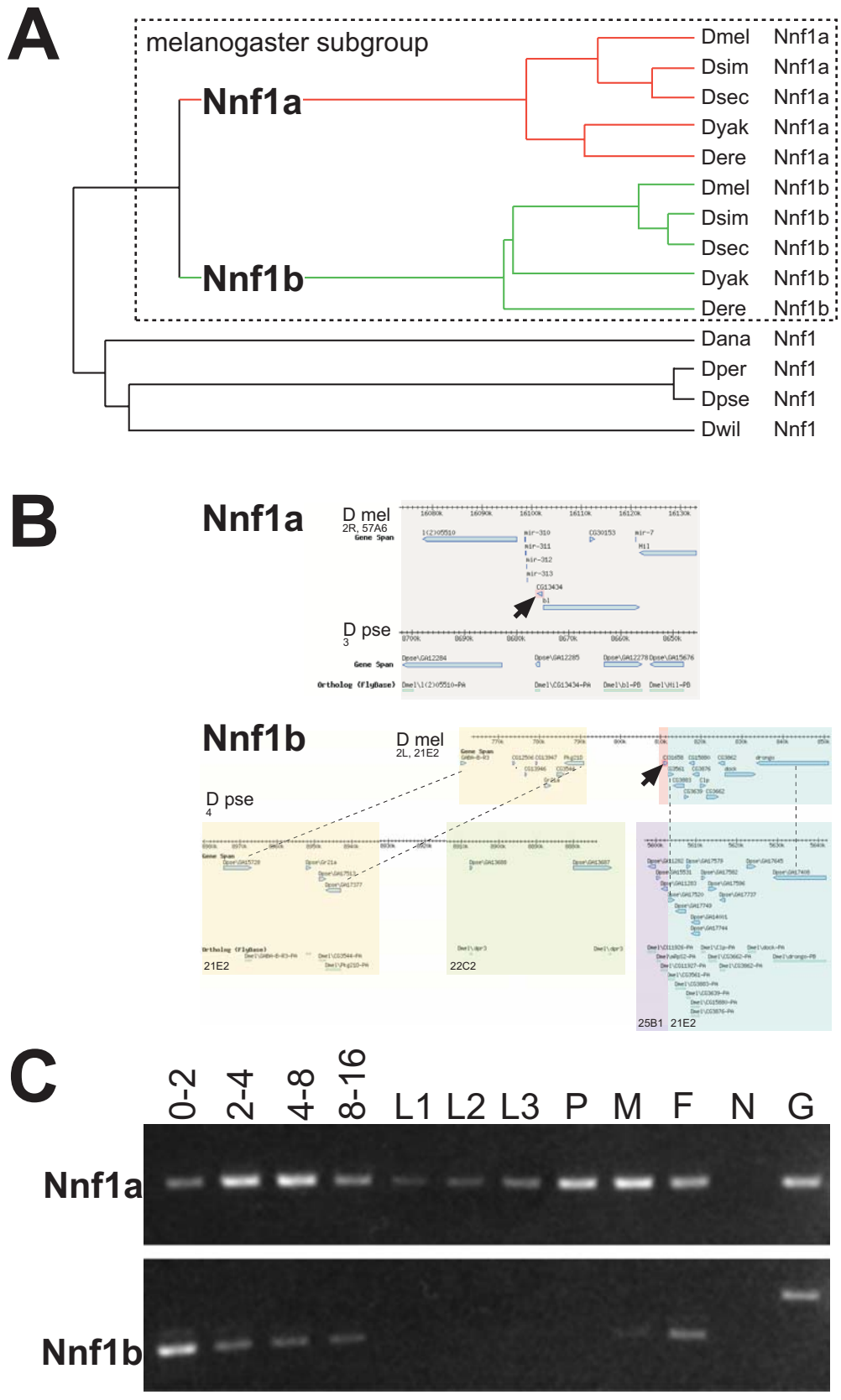
A
melanogaster subgroup
Nnf1a
Nnf1b
Dmel Nnf1a
Dsim Nnf1a
Dsec Nnf1a
Dyak Nnf1a
Dere Nnf1a
Dmel Nnf1b
Dsim Nnf1b
Dsec Nnf1b
Dyak Nnf1b
Dere Nnf1b
Dana Nnf1
Dper Nnf1
Dpse Nnf1
Dwil Nnf1
B
Nnf1a
D mel
2R, 57A6
D pse
3
Nnf1b
D mel
2L, 21E2
D pse
4
21E2
22C2
25B1 21E2
C
0-2
2-4
4-8
8-16
L1 L2 L3 P M F N G
Nnf1a
Nnf1b

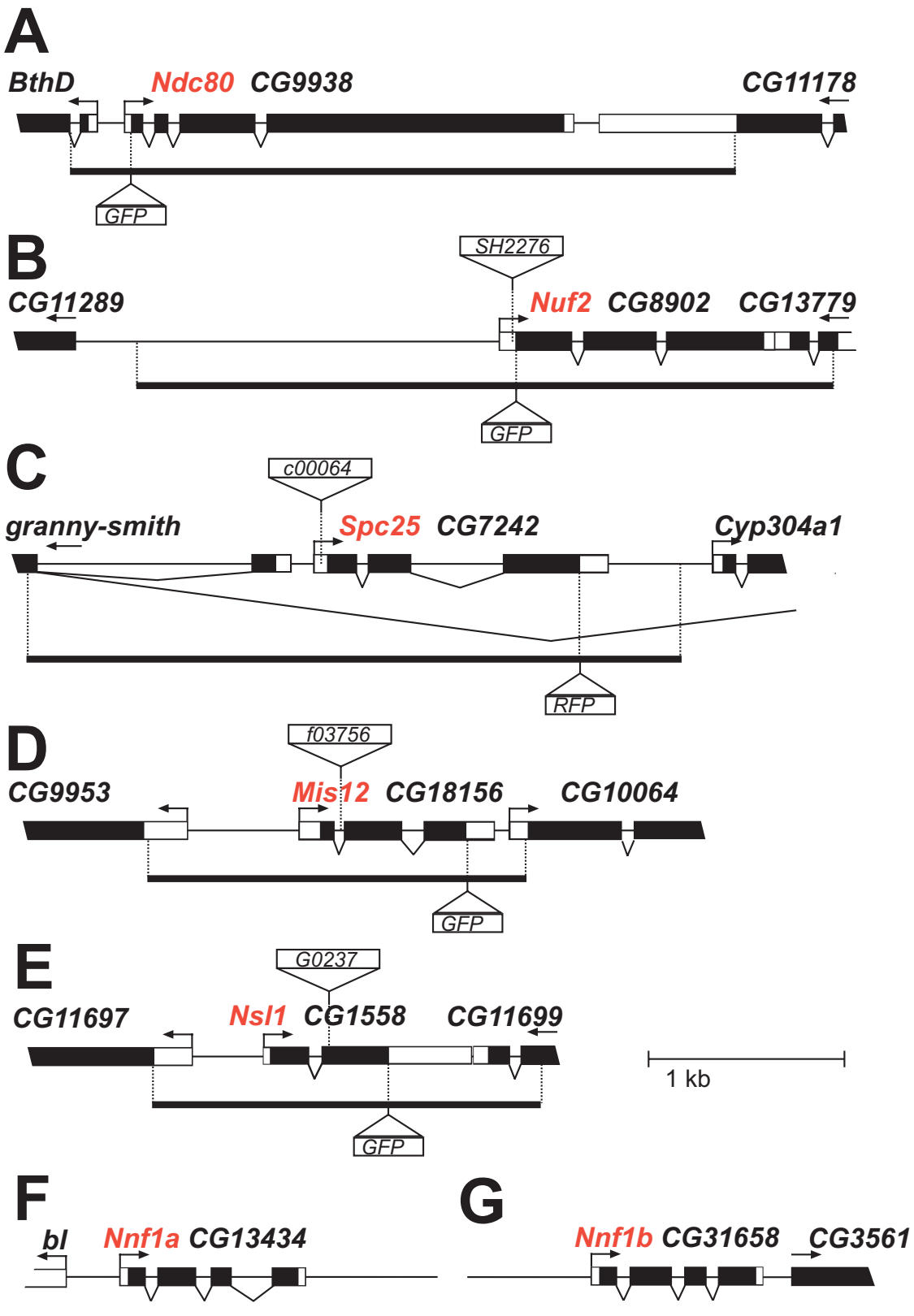
A
BthD
Ndc80
CG9938
CG11178
GFP
B
SH2276
CG11289
Nuf2
CG8902
CG13779
GFP
C
c00064
granny-smith
Spc25
CG7242
Cyp304a1
RFP
D
f03756
CG9953
Mis12
CG18156
CG10064
GFP
E
G0237
CG11697
Nsl1
CG1558
CG11699
GFP
1 kb
F
bl
Nnf1a
CG13434
G
Nnf1b
CG31658
CG3561

Schittenhelm et al., Suppl. Fig. 4

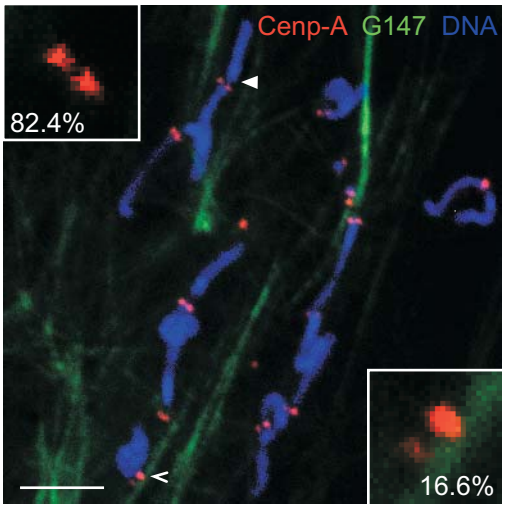

Schittenhelm et al., Suppl. Fig. 5

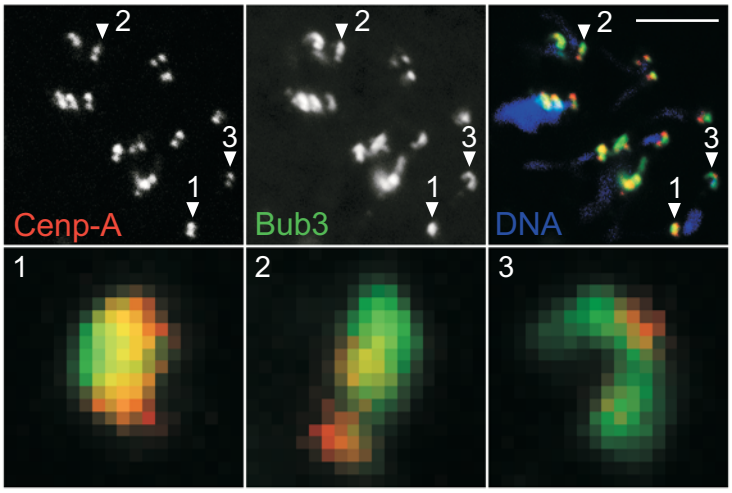

Schittenhelm et al., Suppl. Fig. 6

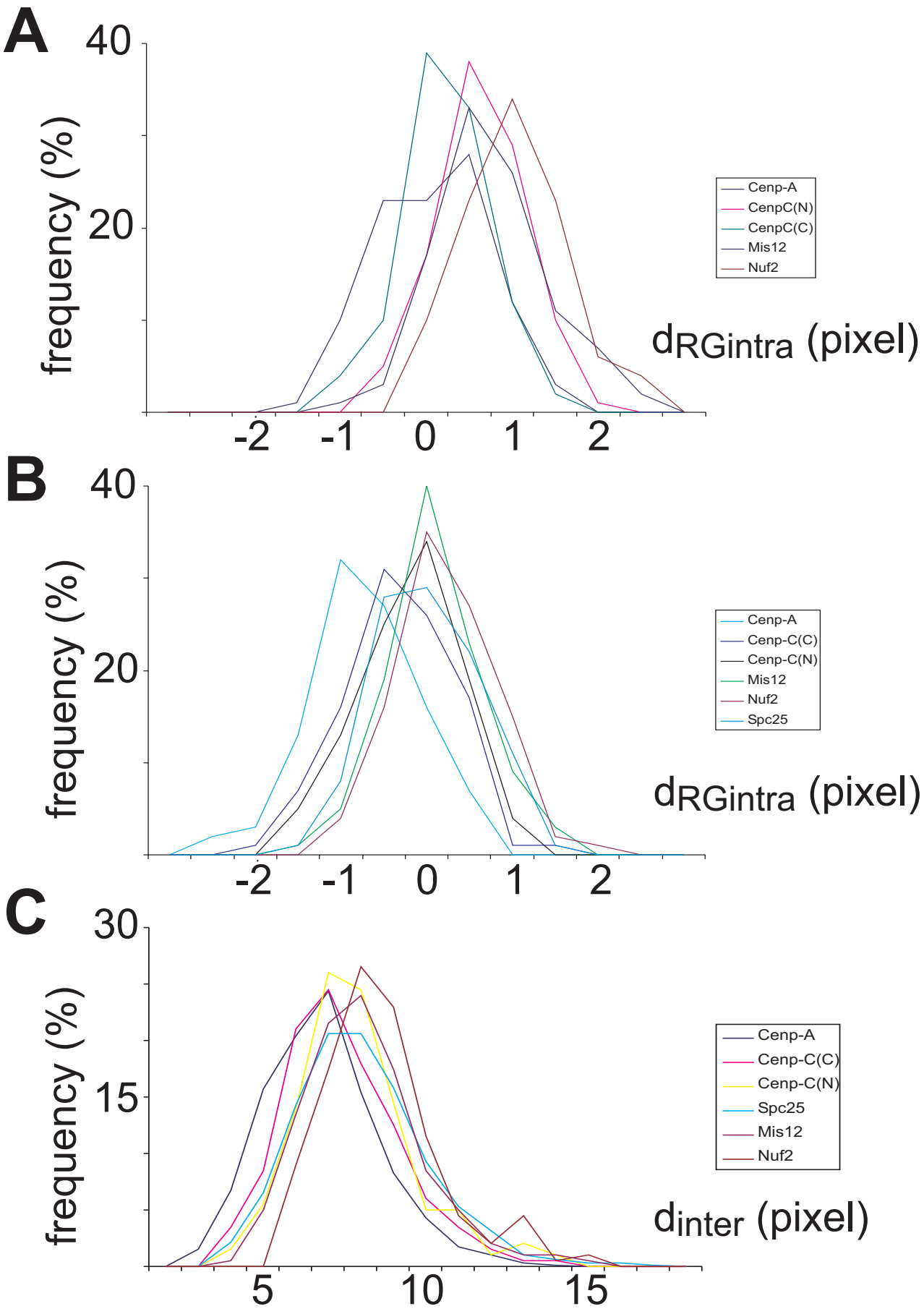

Teilarbeit C

Matthias G. Fischer, Sebastian Heeger, Udo Häcker and Christian F. Lehner (2004)

The Mitotic Arrest in Response to Hypoxia and of Polar Bodies during Early Embryogenesis Requires *Drosophila* Mps1

Curr Biol **14**: 2019–2024

Darstellung des Eigenanteils

Die Generierung des Kontrukts *gEGFP-Mps1* und die Etablierung von transgenen Linien in *D. melanogaster* habe ich vorgenommen (Fig. 1A).

Geschrieben wurde diese Teilarbeit von Christian F. Lehner mit Beiträgen der anderen Autoren.

Current Biology, Vol. 14, 2019–2024, November 23, 2004, ©2004 Elsevier Ltd. All rights reserved. DOI 10.1016/j.cub.2004.11.008

The Mitotic Arrest in Response to Hypoxia and of Polar Bodies during Early Embryogenesis Requires *Drosophila* Mps1

Matthias G. Fischer,[1] Sebastian Heeger,[1] Udo Häcker,[2] and Christian F. Lehner[1,*]
[1]BZMB
Department of Genetics
University of Bayreuth
94440 Bayreuth
Germany
[2]Department of Cell and Molecular Biology
BMC B13
Lund University
22184 Lund
Sweden

Summary

Mps1 kinase plays an evolutionary conserved role in the mitotic spindle checkpoint [1–8]. This system precludes anaphase onset until all chromosomes have successfully attached to spindle microtubules via their kinetochores [9]. Mps1 overexpression in budding yeast is sufficient to trigger a mitotic arrest, which is dependent on the other mitotic checkpoint components, Bub1, Bub3, Mad1, Mad2, and Mad3 [3]. Therefore, Mps1 might act at the top of the mitotic checkpoint cascade. Moreover, in contrast to the other mitotic checkpoint components, Mps1 is essential for spindle pole body duplication in budding yeast [10]. Centrosome duplication in mammalian cells might also be controlled by Mps1 [6, 11], but the fission yeast homolog is not required for spindle pole body duplication [4]. Our phenotypic characterizations of *Mps1* mutant embryos in *Drosophila* do not reveal an involvement in centrosome duplication, while the mitotic spindle checkpoint is defective in these mutants. In addition, our analyses reveal novel functions. We demonstrate that Mps1 is also required for the arrest of cell cycle progression in response to hypoxia. Finally, we show that Mps1 and the mitotic spindle checkpoint are responsible for the developmental cell cycle arrest of the three haploid products of female meiosis that are not used as the female pronucleus.

Results and Discussion

The *Drosophila* gene *CG7643* encodes a Mps1 homolog. The predicted amino acid sequence of *Drosophila* Mps1 has a higher similarity to vertebrate as compared to yeast orthologs. Similarities are found predominantly in the C-terminal protein kinase domains. Using a *piggyBac* transposon with an insertion preference clearly distinct from the widely used P elements, we identified an insertion in the *Drosophila Mps1* gene in a recent mutagenesis experiment [12]. In the following, this allele will be designated as $Mps1^{1}$. The *piggyBac* insertion disrupts the codon of amino acid 26 within the first exon. It is therefore predicted to cause an extensive gene product truncation that removes most of the N-terminal regulatory region and the entire C-terminal kinase domain (Figure 1A). In principle, aberrantly spliced readthrough transcripts or transcripts starting within the *piggyBac* transposon might allow expression of N-terminally truncated Mps1 protein. Quantitative RT-PCR experiments indicated that the abundance of such aberrant transcripts in $Mps1^{1}$ mutants, which span the first exon junction downstream of the *piggyBac* insertion, reached at most 2.5% of the wild-type *Mps1* transcript levels. Moreover, we point out that deletion analyses with human Mps1 have revealed that N-terminal truncations abolish the normal kinetochore localization [13, 14]. Therefore, we conclude that $Mps1^{1}$ is very likely a null allele.

$Mps1^{1}$ homozygous progeny of heterozygous parents was found to develop up to the pupal stages. The great majority of the $Mps1^{1}$ homozygotes died as pharate adults, but a small fraction eclosed with rough eyes and bent wings (0.03% at 25°C, 0.15% at 18°C). The premature lethality of $Mps1^{1}$ homozygotes was completely prevented by a transgene (*gEGFP-Mps1*) driving expression of an EGFP-Mps1 fusion protein under the control of the *Mps1* regulatory region (Figure 1A; data not shown). The recessive lethality associated with $Mps1^{1}$ therefore reflects a lack of Mps1 function. Moreover, EGFP-Mps1 is a functional protein.

The relatively late stage of $Mps1^{1}$ lethality suggested that Mps1 is not absolutely essential for progression through the cell division cycle. However, phenotypic consequences in $Mps1^{1}$ homozygotes might also have been masked by a maternal $Mps1^{+}$ contribution. Therefore, we generated $Mps1^{1}$ germline clones and analyzed $Mps1^{1}$ mutants lacking both maternal and zygotic function. Forty-five percent of these mutants still developed up to the pupal stages, suggesting that cell proliferation can proceed substantially in the absence of *Mps1* function. In contrast, embryonic lethality was found to result from a mutation in zebrafish *mps1* [8].

Since $Mps1^{1}$ mutant cells are able to progress through division cycles, it appeared unlikely that centrosome duplication was affected. To directly analyze centrosome behavior in progeny of $Mps1^{1}$ germline clones, we immunolabeled embryos with an antibody against γ-tubulin. These stainings did not reveal centrosome abnormalities (data not shown). Moreover, we introduced a *D-TACC-GFP* transgene, which expresses a centrosomal protein [15], into the $Mps1^{1}$ mutant background and analyzed centrosome duplication during the early embryonic, syncytial cell cycles by in vivo imaging. Again, centrosome behavior was found to be normal (Figure 1B).

While the mouse Mps1 homolog (ESK/mMps1) has been proposed to be important for centrosome duplication [6], an initial study of human Mps1 (TTK/PYT/hMps1) did not confirm such an involvement [7]. Subsequent work has pointed to a higher hMps1 requirement for the mitotic spindle checkpoint than for normal centrosome

*Correspondence: chle@uni-bayreuth.de

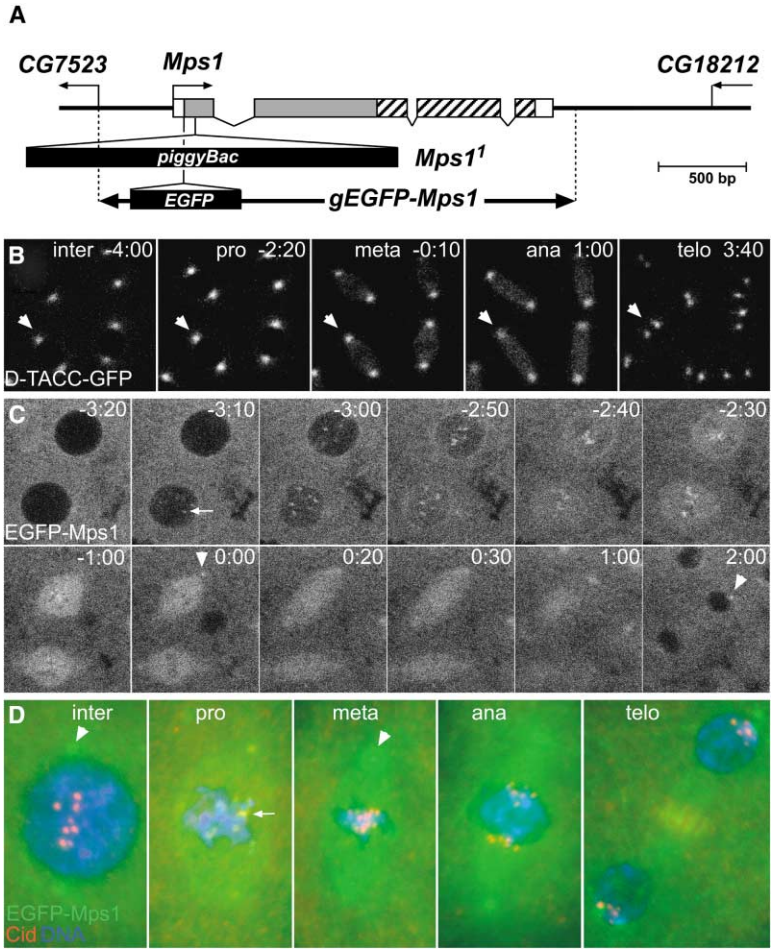

Figure 1. The *Drosophila* Mps1 Homolog

(A) The structure of the *Mps1* gene, which is flanked by the predicted genes *CG7523* and *CG18212*, is schematically illustrated. Thin arrows indicate the direction of transcription. Exons are boxed, and translated regions are filled. Gray filling indicates the N-terminal regulatory domain, and hatching indicates the C-terminal protein kinase domain. The *piggyBac* insertion in the *Mps1*^{1} allele is indicated by the upper black triangle. The genomic region present in the *gEGFP-Mps1* transgene is indicated by the thick double arrow, and the N-terminal *EGFP* insertion is indicated with the lower black triangle.

(B) Centrosome duplication in *Mps1* mutants. Selected frames from a time-lapse analysis of the behavior of a centrosomal GFP marker protein (D-TACC-GFP) in embryos derived from females with *Mps1*^{1} germline clones indicate that centrosome duplication is not dependent on Mps1. The cell cycle phases (inter-, pro-, meta-, ana-, and telophase) are indicated in each frame as well as the time (min:s) relative to the metaphase-to-anaphase transition, which was set as zero. Superficial sections with a region from a syncytial blastoderm embryo during mitosis 11 are shown. Arrows point to the same centrosome, which has duplicated in the last frame.

(C) Selected frames from a time-lapse analysis illustrate the behavior of a functional EGFP-Mps1 fusion protein in vivo. A region from the surface of a syncytial blastoderm embryo during mitosis 11 is shown. The time (min:s) relative to the metaphase-to-anaphase transition is given in each frame. The white arrow indicates kinetochore labeling, which starts during prophase. The arrowheads indicate centrosome labeling, which is observed from metaphase until prophase.

(D) Double labeling of fixed embryos during the syncytial blastoderm stage with an antibody against the centromere protein Cid (red) and a DNA stain (blue) confirms that EGFP-Mps1 (green) is present on kinetochores during prophase (white arrow). Arrowheads indicate centrosome labeling. Single nuclei from embryos during inter- (inter), pro- (pro), meta- (meta), ana- (ana), and telophase (telo) before and during mitosis 11 are shown.

behavior [11]. Residual Mps1 function allowing centrosome duplication in the *Drosophila Mps1*^{1} mutant is not ruled out. However, as the expression of Mps1 function is rather difficult to envisage in the light of our characterization of the *Mps1*^{1} allele, it is readily conceivable that, like the fission yeast homolog, *Drosophila* Mps1 is not required for normal spindle pole behavior.

While all analyzed Mps1 homologs localize to kinetochores during prometaphase, conflicting observations have been reported concerning centrosome and nuclear envelope localization in human cells [11, 13, 14]. To evaluate the localization of *Drosophila* Mps1, we analyzed *gEGFP-Mps1* embryos by in vivo imaging (Figure 1C) and immunolabeling (Figure 1D). During interphase in syncytial blastoderm stage embryos, EGFP-Mps1 was excluded from the nucleus and enriched on centrosomes. During prophase, centrosome signals weakened. In parallel, signals appeared on kinetochores, as confirmed by double labeling with an antibody against the centromere protein Cid, the *Drosophila* Cenp-A homolog (Figure 1D). Until the metaphase-to-anaphase transition, EGFP-Mps1 gradually disappeared again from kinetochores and became increasingly enriched on spindles and spindle poles. In anaphase, kinetochore signals were no longer detected. Very similar observations were also made in embryos after cellularization (data not shown).

Consistent with the observed kinetochore localization during early mitosis, *Drosophila* Mps1 was found to be required for the mitotic spindle checkpoint, as previously described for all the other analyzed homologs. Inhibition of mitotic spindle formation by colcemid failed to induce a mitotic arrest in the progeny of *Mps1*^{1} germline clones (see Figures S1 and S2 in the Supplemental Data available with this article online).

We also analyzed whether Mps1 regulates the dynamics of progression through mitosis in unperturbed conditions. Time-lapse analyses with *Mps1*^{1} germline clone progeny expressing *histone H2AvD-GFP* demonstrated that the metaphase-to-anaphase transition occurred prematurely during the syncytial cycles (Figure S4). Analyses with cultured vertebrate cells have indicated that elimination of Mad2 and BubR1 (but not of Mad1, Bub1, and Bub3) also results in a premature onset of

anaphase and severe chromosome segregation defects in most cells [16, 17]. In the *Drosophila Mps1*^{1} mutants, chromosome segregation was still normal in most cells. Nevertheless, an increased frequency of occasional division failures of individual nuclei was readily detected in syncytial embryos. During these aberrant mitoses, some or even all chromosomes failed to display poleward movements during anaphase (Figure S4), suggesting that they had not yet been properly attached to the spindle by the time of the premature metaphase-to-anaphase transition. These mitotic division failures eventually resulted in the elimination of aberrant nuclei from the superficial nuclear layer—a characteristic process during the syncytial blastoderm cycles that prevents formation of aneuploid cells during cellularization [18]. Analyses of fixed embryos confirmed that about 45% of the fertilized embryos displayed severely reduced numbers of nuclei with a highly irregular distribution and appearance, preventing syncytial and cellular blastoderm formation. Another 45% of the fertilized embryos appeared to progress successfully beyond cellularization with no or few irregularities in the distribution and appearance of nuclei or mitotic figures. These irregularities were observed predominantly within the polar regions.

Inhibition of the mitotic checkpoint by overexpression of a dominant-negative BubR1 kinase in cultured human cells has previously been shown to advance not only the onset of anaphase but also cyclin B1 degradation so that this mitotic cyclin was degraded at the same time as cyclin A [19, 20]. Immunolabeling of cellularized *Mps1*^{1} germline clone progeny also revealed a simultaneous disappearance of Cyclin A and B (Figure S4). In contrast, in unperturbed human cells [21], as well as in cellularized *Drosophila* embryos [22] and other organisms, the mitotic degradation of A-type cyclins occurs before that of the B-type cyclins. Our observations indicate therefore that in addition to BubR1, Mps1 is also required for the delay of B-type cyclin degradation relative to A-types. The difference in the dynamics of *Drosophila* Cyclin B and B3 degradation [23, 24] did not appear to be affected in the *Mps1*^{1} mutants (data not shown).

An RNA interference screen for genes required for survival of anoxia in *C. elegans* has recently led to the identification of the *san-1* gene, which encodes a Mad3 homolog involved in the mitotic spindle checkpoint [25]. In addition, the Mad2 homolog *mdf-2* was similarly found to be required for the mitotic spindle checkpoint and anoxia survival [25]. Anoxia arrests mitotic cells not only in *C. elegans* embryos [25], but also in *Drosophila* embryos [26, 27]. In *Drosophila*, precellularization embryos that are confronted with oxygen limitation during prophase arrest cell cycle progression rapidly and reversibly in metaphase. Hypoxic conditions imposed during all other cell cycle stages induce a reversible arrest in interphase, which is accompanied by abnormal chromatin condensation. It is not known whether the metaphase arrest resulting from hypoxia in *Drosophila* embryos depends on the function of mitotic spindle checkpoint proteins. Moreover, since the *C. elegans* genome sequence does not contain a Mps1 homolog, it appeared to be of particular interest to evaluate whether *Drosophila* Mps1

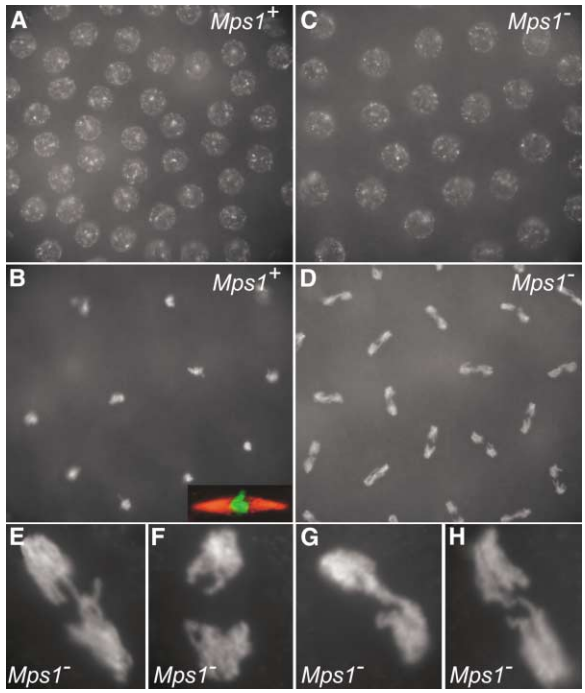

Figure 2. *Drosophila* Mps1 Is Required for Metaphase Arrest in Response to Hypoxia

Embryos (1–2 hr) collected from *histone H2AvD-GFP* females (*Mps1*$^{+}$; [A and B]) and females with *Mps1*^{1} germline clones (*Mps1*$^{-}$; [C–H]) were mixed, dechorionated, and incubated in degassed medium before fixation and DNA labeling. In *Mps1*$^{+}$ embryos, hypoxia resulted in a cell cycle arrest during either interphase (A) or metaphase (B), as previously described [26]. Double labeling with antibodies against phospho-histone H3 and tubulin confirmed that mitotic *Mps1*$^{+}$ embryos arrest during metaphase (inset in [B]). In contrast, while hypoxia still resulted in an interphase arrest (C), it failed to trigger a metaphase arrest in *Mps1*$^{-}$ embryos. *Mps1*$^{-}$ embryos during anaphase were therefore readily observed (D), although anaphase figures were usually abnormal, as indicated by the high-magnification views (E–H).

is required for the hypoxia-induced metaphase arrest. Therefore, we mixed stage 5 embryos derived from *Mps1*^{1} germline clones with *Mps1*$^{+}$ control embryos expressing a *histone H2AvD-GFP* transgene and incubated aliquots of the resulting embryo mixture for 20 min in hypoxic or normoxic conditions, respectively, before fixation and DNA labeling. Confirming previous analyses [26], hypoxic *Mps1*$^{+}$ control embryos (GFP-positive) were arrested either in interphase with abnormally condensed chromosomes or in mitosis with clusters of hypercondensed chromosomes within a mitotic spindle (Figures 2A and 2B). Most importantly, we did not observe *Mps1*$^{+}$ embryos where all nuclei were in ana- or telophase in a total of 57 analyzed embryos. In contrast, *Mps1*^{1} embryos (GFP-negative) were frequently observed to be in anaphase or telophase (24% of the 161 analyzed embryos; Figure 2D), demonstrating that Mps1 is required for the hypoxia-induced metaphase arrest.

While ana- and telophase figures were clearly recognizable in the hypoxic *Mps1*^{1} mutants, we emphasize that these mitotic figures were almost always highly aberrant with frequent chromatin bridges (Figures 2E–

2H). Moreover, chromosome arms, which appear as straight lines during wild-type anaphase, had a wavy appearance in hypoxic *Mps1*^{1} anaphase figures, hinting at reduced spindle pulling forces.

The dramatic difference in the frequencies of embryos during exit from mitosis (anaphase, telophase), which was apparent in the comparison of hypoxic *Mps1*$^{+}$ and *Mps1*^{1} embryos, was not observed when the normoxic embryos were compared (data not shown). However, we also observed the dramatic difference in hypoxic mixtures in which the embryos derived from *Mps1*^{1} germline clones were marked with *histone H2AvD-GFP* instead of the *Mps1*$^{+}$ control embryos. We conclude, therefore, that Mps1 is required for the metaphase arrest that results in response to hypoxic conditions imposed during prophase. Mps1 does not appear to play a role in the hypoxia-induced cell cycle arrest during interphase. A comparable high fraction of *Mps1*$^{+}$ and *Mps1*^{1} embryos arrested in interphase with the characteristic abnormal chromatin appearance was observed in the hypoxic embryo mixture (Figures 2A and 2C).

In vertebrates, the mitotic spindle checkpoint is known to be involved in the physiological arrest of mature oocytes during metaphase of the second meiotic division [28]. In *Drosophila*, mature oocytes arrest during metaphase of the first meiotic division. The early developmental arrest during cycle 1 or 2, which was apparent in 9% of the fertilized embryos derived from *Mps1*^{1} female germline clones, might therefore reflect defective regulation of the female meiotic divisions. However, the physiological arrest during metaphase of meiosis I did not appear to be compromised in *Mps1*^{1} mutant oocytes. DNA labeling of mass isolated mature *Mps1*^{1} mutant oocytes [29] did not reveal abnormalities (data not shown). Moreover, after in vitro activation [29], we observed normal meiotic figures in *Mps1*^{1} mutants (data not shown). While we cannot exclude the possibility that all or some *Mps1*^{1} mutant oocytes are subtly affected, these observations suggest that Mps1 is required neither for the physiological arrest of mature oocytes during metaphase I nor for completion of the meiotic divisions after release from this metaphase I arrest.

While female meiosis appeared to be largely successful, the subsequent behavior of the three haploid meiotic nuclei, which are segregated away from the female pronucleus, was found to be abnormal in eggs derived from *Mps1*^{1} female germline clones. This abnormal behavior was observed in all of the *Mps1*^{1} progeny, irrespective of whether the zygotic nuclei succeeded at progressing through the syncytial cycles or not. During wild-type development, the innermost one of the four haploid nuclei generated by female meiosis develops into the pronucleus, whereas the peripheral, outer three polar body nuclei become reorganized into a characteristic condensed chromosome bouquet [30]. In the *Drosophila* egg, where cytokinesis is omitted until after cellularization, these chromosomes are not extruded. Chromosome condensation in the polar body nuclei occurs concomitantly with entry into mitosis 1 after the first round of DNA replication. Condensation of the polar body chromatin is not accompanied by assembly of bipolar mitotic spindles, while the duplicated, sperm-derived centrosomes organize such a spindle around the female and male pronuclei chromosomes. In wild-type embryos, we observed a very strong enrichment of the mitotic spindle checkpoint components EGFP-Mps1 (Figure 3C), BubR1 (data not shown), Mad2-GFP (Figure 3D), and GFP-Fizzy (data not shown) within the pericen-

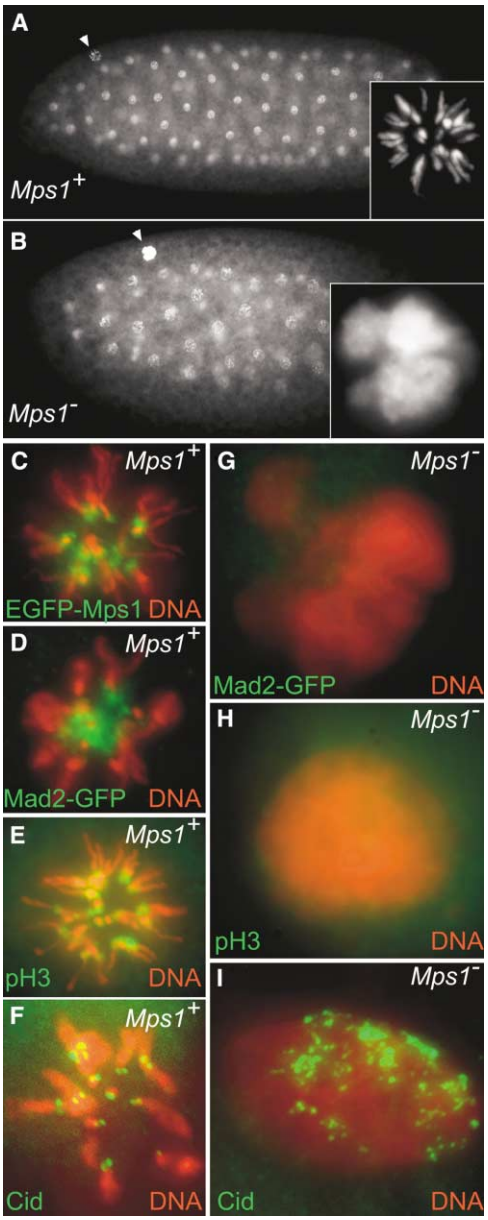

Figure 3. The Cell Cycle Arrest of the Haploid Polar Body Nuclei Requires Mps1 Function

Embryos (0–1 hr) were collected from either *w* females (*Mps1*$^{+}$; [A and C–F]) or females with *Mps1*^{1} germline clones (*Mps1*$^{-}$; [B and G–I]). Moreover, these females carried transgenes driving the expression of either EGFP-Mps1 ([C]; green) or Mad2-GFP ([D and G]; green). Embryos were labeled with a DNA stain ([A and B]; red in [C]–[I]) and with antibodies against phospho-histone H3 ([E and H]; green) or Cid ([F and I]; green). Arrowheads in the embryos shown in (A) and (B) point to the polar body nuclei, which are shown at the same higher magnification in the insets. High-magnification views of the polar body nuclei are also shown in (C)–(I). See text for further explanations.

tromeric regions of the condensed polar body chromosomes. Moreover, anti-pH3 labeling was also strikingly intense within this chromosomal region (Figure 3E). Phosphorylation of histone H3 is thought to result from kinase activity of the Survivin-Incenp-Aurora B complex, which is known to be required for kinetochore localization of mitotic spindle checkpoint components [31]. Immunolabeling with antibodies against Aurora B and Incenp indicated that these proteins were also strongly enriched within the pericentromeric region of the bouquet chromosomes (Figure S5). This prominent enrichment of checkpoint components and pH3 on polar body chromosomes perdured in wild-type embryos throughout the early syncytial stages. During these stages, the polar bodies remain condensed, while the zygotic nuclei progress through mitotic cycles. These observations suggested that polar bodies might be kept inactive and arrested in mitosis by the mitotic spindle checkpoint in wild-type embryogenesis. Consistent with this notion, we also observed an enrichment of Cyclin B in the central domain of the bouquet (Figure S5). Moreover, this notion predicts that the polar body chromosomes escape from the arrest in *Mps1*^{1} mutants. Indeed, instead of the bouquet-like arrangement of condensed polar body chromosomes that is characteristic for wild-type embryos (Figures 3A and 3C–3F), we observed one or two giant nuclei in all of the progeny derived from *Mps1*^{1} germline clone females (Figures 3B and 3G–3I). These giant nuclei contained decondensed chromatin, which was not labeled with anti-BubR1 (data not shown), Mad2-GFP (Figure 3G), and anti-pH3 (Figure 3H) in the great majority of the embryos. We point out that, during the syncytial blastoderm cycles in the zygotic nuclei, the behavior of BubR1 was not affected by the *Mps1*^{1} mutation (data not shown), in contrast to the findings observed with immunodepleted *Xenopus* extracts [31]. The absence of mitotic spindle checkpoint components from the abnormal giant nuclei in the *Mps1*^{1} mutants therefore presumably results indirectly from the failure to arrest during mitosis 1. The intensity of the DNA labeling indicated that the giant nuclei had undergone overreplication. Labeling with an antibody against the constitutive centromere protein CID/Cenp-A resulted in an excessive number of signals, and these were generally located in the outer periphery of the decondensed chromatin (Figure 3I), while the expected 12 pairs of centromere signals were detected in the center of wild-type bouquets (Figure 3F). Based on estimates of centromere signal numbers, at least four rounds of overreplication had occurred in the analyzed *Mps1*^{1} embryos.

Conclusions

Our characterization of Mps1 function in *Drosophila* has uncovered a previously unknown involvement in the hypoxia stress response. These observations extend recent findings obtained in *C. elegans*, which does not have an obvious Mps1 homolog but requires other mitotic spindle checkpoint components for efficient protection against aneuploidies resulting from progression through mitosis when oxygen is absent [25]. The mitotic spindle checkpoint is therefore likely of general importance for protection against hypoxia-induced genetic damage in metazoans. In humans, such a role of the mitotic spindle checkpoint might further augment its relevance in the context of tumor progression where angiogenesis is crucial for the elimination of the insufficient blood (and oxygen) supply during initial tumor growth.

Moreover, our analyses have revealed a novel, developmental role of Mps1 during early embryogenesis when it is required for the cell cycle arrest of those three haploid products of female meiosis that are segregated away from the female pronucleus. In *Drosophila*, these discarded meiotic products are not extruded. They arrest during M phase of the first mitotic cycle and are transformed into a cluster of radially arranged condensed chromosomes. It remains to be clarified why the interdigitated microtubules are not focused into the characteristic, centrosome-free, tapered bipolar spindle, which is organized by chromosomes during the preceding female meiotic divisions. However, the failure to form a functional bipolar spindle might be linked to the activation of the mitotic spindle checkpoint, which keeps the bouquet chromosomes from further cell cycle progression. While our findings provide an initial molecular insight, the important mechanisms that differentiate the female pronucleus from the other haploid products of female meiosis are far from being understood.

Supplemental Data

Supplemental Data including five additional figures and the description of the Experimental Procedures are available at http://www.current-biology.com/cgi/content/full/14/22/2019/DC1/.

Acknowledgments

We thank Ralf Schittenhelm for assisting during transgene construction; Rahul Pandey for some of the immunolabelings; and Jordan Raff, Bill Earnshaw, David Glover, Claudio Sunkel, and Stefan Heidmann for providing fly strains, antibodies, and comments on the manuscript. This work was supported by grants from the Swedish Research Council VR and the Swedish Cancer Foundation to U.H. and by grants from the German-Israeli Research Foundation (GIF 658) and the Deutsche Forschungsgemeinschaft (DFG Le987/3-3) to C.F.L.

Received: July 29, 2004
Revised: September 6, 2004
Accepted: September 21, 2004
Published: November 23, 2004

References

1. Fisk, H.A., Mattison, C.P., and Winey, M. (2004). A field guide to the Mps1 family of protein kinases. Cell Cycle *3*, 439–442.
2. Weiss, E., and Winey, M. (1996). The Saccharomyces cerevisiae spindle pole body duplication gene MPS1 is part of a mitotic checkpoint. J. Cell Biol. *132*, 111–123.
3. Hardwick, K.G., Weiss, E., Luca, F.C., Winey, M., and Murray, A.W. (1996). Activation of the budding yeast spindle assembly checkpoint without mitotic spindle disruption. Science *273*, 953–956.
4. He, X., Jones, M.H., Winey, M., and Sazer, S. (1998). Mph1, a member of the Mps1-like family of dual specificity protein kinases, is required for the spindle checkpoint in S. pombe. J. Cell Sci. *111*, 1635–1647.
5. Abrieu, A., Magnaghi-Jaulin, L., Kahana, J.A., Peter, M., Castro, A., Vigneron, S., Lorca, T., Cleveland, D.W., and Labbe, J.C. (2001). Mps1 is a kinetochore-associated kinase essential for the vertebrate mitotic checkpoint. Cell *106*, 83–93.

6. Fisk, H.A., and Winey, M. (2001). The mouse Mps1p-like kinase regulates centrosome duplication. Cell *106*, 95–104.
7. Stucke, V.M., Sillje, H.H., Arnaud, L., and Nigg, E.A. (2002). Human Mps1 kinase is required for the spindle assembly checkpoint but not for centrosome duplication. EMBO J. *21*, 1723–1732.
8. Poss, K.D., Nechiporuk, A., Hillam, A.M., Johnson, S.L., and Keating, M.T. (2002). Mps1 defines a proximal blastemal proliferative compartment essential for zebrafish fin regeneration. Development *129*, 5141–5149.
9. Cleveland, D.W., Mao, Y., and Sullivan, K.F. (2003). Centromeres and kinetochores: From epigenetics to mitotic checkpoint signaling. Cell *112*, 407–421.
10. Winey, M., Goetsch, L., Baum, P., and Byers, B. (1991). MPS1 and MPS2: Novel yeast genes defining distinct steps of spindle pole body duplication. J. Cell Biol. *114*, 745–754.
11. Fisk, H.A., Mattison, C.P., and Winey, M. (2003). Human Mps1 protein kinase is required for centrosome duplication and normal mitotic progression. Proc. Natl. Acad. Sci. USA *100*, 14875–14880.
12. Hacker, U., Nystedt, S., Barmchi, M.P., Horn, C., and Wimmer, E.A. (2003). piggyBac-based insertional mutagenesis in the presence of stably integrated P elements in Drosophila. Proc. Natl. Acad. Sci. USA *100*, 7720–7725.
13. Liu, S.T., Chan, G.K., Hittle, J.C., Fujii, G., Lees, E., and Yen, T.J. (2003). Human MPS1 kinase is required for mitotic arrest induced by the loss of CENP-E from kinetochores. Mol. Biol. Cell *14*, 1638–1651.
14. Stucke, V.M., Baumann, C., and Nigg, E.A. (2004). Kinetochore localization and microtubule interaction of the human spindle checkpoint kinase Mps1. Chromosoma *113*, 1–15.
15. Gergely, F., Kidd, D., Jeffers, K., Wakefield, J.G., and Raff, J.W. (2000). D-TACC: A novel centrosomal protein required for normal spindle function in the early Drosophila embryo. EMBO J. *19*, 241–252.
16. Meraldi, P., Draviam, V.M., and Sorger, P.K. (2004). Timing and checkpoints in the regulation of mitotic progression. Dev. Cell *7*, 45–60.
17. Michel, L., Diaz-Rodriguez, E., Narayan, G., Hernando, E., Murty, V.V., and Benezra, R. (2004). Complete loss of the tumor suppressor MAD2 causes premature cyclin B degradation and mitotic failure in human somatic cells. Proc. Natl. Acad. Sci. USA *101*, 4459–4464.
18. Takada, S., Kelkar, A., and Theurkauf, W.E. (2003). *Drosophila* checkpoint kinase 2 couples centrosome function and spindle assembly to genomic integrity. Cell *113*, 87–99.
19. Geley, S., Kramer, E., Gieffers, C., Gannon, J., Peters, J.M., and Hunt, T. (2001). Anaphase-promoting complex/cyclosome-dependent proteolysis of human cyclin A starts at the beginning of mitosis and is not subject to the spindle assembly checkpoint. J. Cell Biol. *153*, 137–148.
20. den Elzen, N., and Pines, J. (2001). Cyclin A is destroyed in prometaphase and can delay chromosome alignment and anaphase. J. Cell Biol. *153*, 121–136.
21. Pines, J., and Hunter, T. (1991). Human cyclin A and cyclin B1 are differentially located in the cell and undergo cell cycle dependent nuclear transport. J. Cell Biol. *115*, 1–17.
22. Lehner, C.F., and O'Farrell, P.H. (1990). The roles of *Drosophila* cyclin A and cyclin B in mitotic control. Cell *61*, 535–547.
23. Jacobs, H.W., Knoblich, J.A., and Lehner, C.F. (1998). Drosophila Cyclin B3 is required for female fertility and is dispensable for mitosis like Cyclin B. Genes Dev. *12*, 3741–3751.
24. Sigrist, S., Jacobs, H., Stratmann, R., and Lehner, C.F. (1995). Exit from mitosis is regulated by *Drosophila fizzy* and the sequential destruction of cyclins A, B and B3. EMBO J. *14*, 4827–4838.
25. Nystul, T.G., Goldmark, J.P., Padilla, P.A., and Roth, M.B. (2003). Suspended animation in C. elegans requires the spindle checkpoint. Science *302*, 1038–1041.
26. DiGregorio, P.J., Ubersax, J.A., and O'Farrell, P.H. (2001). Hypoxia and nitric oxide induce a rapid, reversible cell cycle arrest of the Drosophila syncytial divisions. J. Biol. Chem. *276*, 1930–1937.
27. Foe, V.E., and Alberts, B.M. (1985). Reversible chromosome condensation induced in Drosophila embryos by anoxia: Visualization of interphase nuclear organization. J. Cell Biol. *100*, 1623–1636.
28. Tunquist, B.J., and Maller, J.L. (2003). Under arrest: Cytostatic factor (CSF)-mediated metaphase arrest in vertebrate eggs. Genes Dev. *17*, 683–710.
29. Page, A.W., and Orr-Weaver, T.L. (1997). Activation of the meiotic divisions in Drosophila oocytes. Dev. Biol. *183*, 195–207.
30. Foe, V.E., Odell, G.M., and Edgar, B.A. (1993). Mitosis and morphogenesis in the Drosophila embryo. In The Development of Drosophila melanogaster, Volume 1 (Cold Spring Harbor, NY: Cold Spring Harbor Laboratory Press), pp. 149–300.
31. Vigneron, S., Prieto, S., Bernis, C., Labbe, J.C., Castro, A., and Lorca, T. (2004). Kinetochore localization of spindle checkpoint proteins: Who controls whom? Mol. Biol. Cell *15*, 4584–4596.

The Mitotic Arrest in Response to Hypoxia and of Polar Bodies during Early Embryogenesis Requires *Drosophila* Mps1

Matthias G. Fischer, Sebastian Heeger, Udo Häcker, and Christian F. Lehner

Supplemental Results

To assess whether *Drosophila* Mps1 functions in the mitotic spindle checkpoint, we studied cell cycle progression at the stage of mitosis 14 in embryos derived from *Mps1*^{1} germline clones after incubation in colcemid. This drug inhibits mitotic spindle formation. Therefore, it triggers the mitotic spindle checkpoint in wild-type embryos. Incubation in colcemid resulted in the expected, dramatic enrichment of mitotic cells in *Mps1*$^{+}$ control embryos, as revealed by immunolabeling with an antibody against phosphorylated histone H3 (pH3), an excellent marker for mitotic cells (Figure S1, compare S1B and S1E). In contrast, incubation in colcemid did not result in an enrichment of mitotic cells in *Mps1*^{1} mutants (Figure S1, compare S1H and S1K). Moreover, double labeling with a DNA stain and an antibody against Cyclin B, which is known to be stable in the mitotic checkpoint arrest, confirmed that *Mps1*^{1} mutant cells progress through mitosis 14 also in the presence of colcemid. While the pH3-positive cells enriched by colcemid in *Mps1*$^{+}$ embryos were all Cyclin B positive and contained condensed DNA (Figure S1F), we did not observe an increase of Cyclin B-positive cells in colcemid-treated *Mps1*^{1} embryos, and some Cyclin B-negative cells were found to contain decondensing DNA with decreasing levels of anti-pH3 labeling in these mutant embryos (Figure S1L, arrows). These findings demonstrate therefore that the mitotic spindle checkpoint is defective in *Mps1*^{1} mutants.

A comparison of sibling progeny of *Mps1*^{1} germline clones that had inherited either the *Mps1*^{1} or the *Mps1*$^{+}$ allele from the father further confirmed that *Drosophila* Mps1 is required for the mitotic spindle checkpoint. While colcemid resulted in a drastic enrichment of mitotic cells in the paternally rescued embryos at the stage of mitosis 16, mitotic cells were not increased in siblings with the paternal *Mps1*^{1} allele (Figure S2).

The paternal rescue of mitotic spindle checkpoint function in progeny of *Mps1*^{1} germline clones indicated

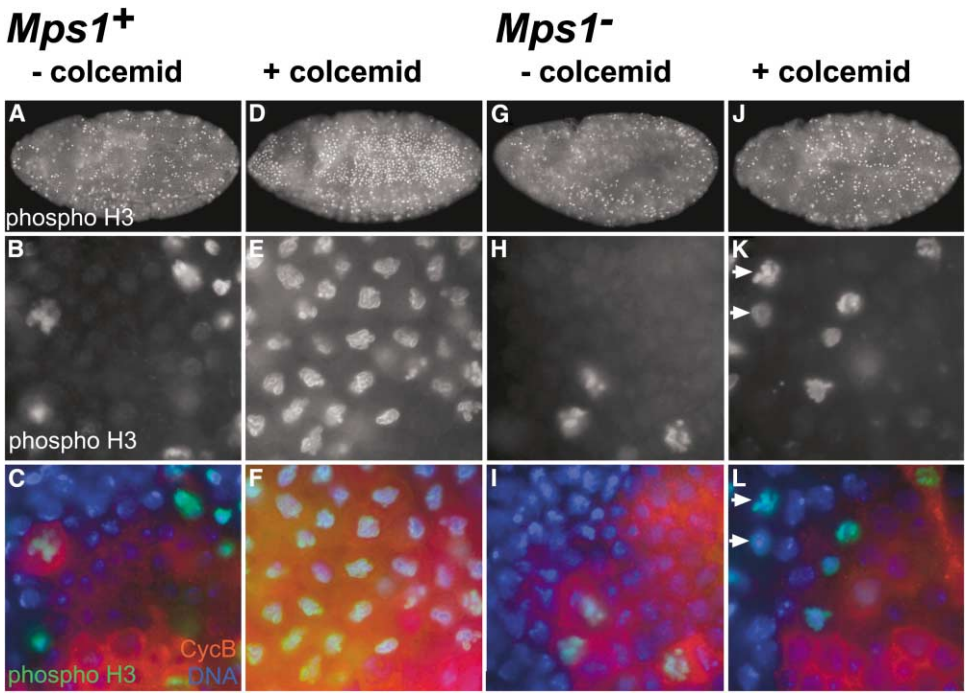

Figure S1. *Drosophila* Mps1 Is Required for the Mitotic Spindle Checkpoint

Embryos (3–4 hr) derived either from *w* females (*Mps1*$^{+}$; [A–F]) or from females with *Mps1*^{1} germline clones (*Mps1*$^{-}$; [G–L]) were incubated for 30 min without (− colcemid; [A–C and G–I]) or with colcemid (+ colcemid; [D–F and J–L]) before fixation and immunolabeling with antibodies against phospho-histone H3 (phospho H3; [A, B, D, E, G, H, J, and K]; green in [C], [F], [I], and [L]) and Cyclin B (CycB; red in [C], [F], [I], and [L]) and a DNA stain (DNA; blue in [C], [F], [I], and [L]). While lateral views of the entire embryos are shown in the top row, the two bottom rows display representative epidermal regions at higher magnification. Colcemid results in a dramatic increase of mitotically arrested cells (phospho H3-positive) in *Mps1*$^{+}$ but not in *Mps1*$^{-}$ embryos, where cells exit from mitosis, as indicated by absence of Cyclin B labeling and decondensing chromatin (white arrows).

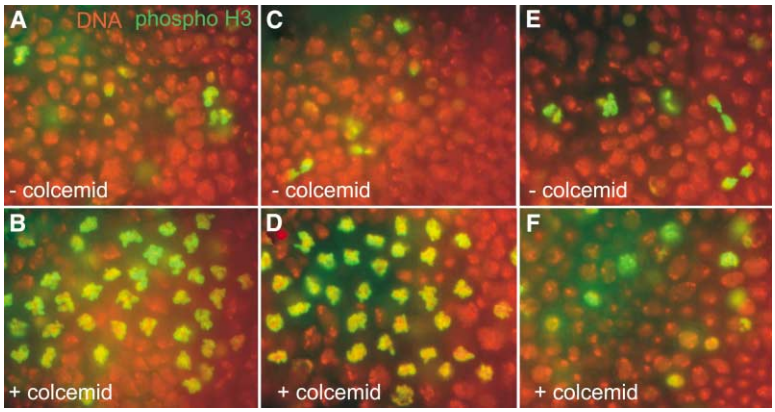

Figure S2. Paternal Rescue of the Mitotic Spindle Checkpoint in *Mps1*^{1} Germline Clone Progeny

Eggs were collected either from wild-type parents (A and B) or from females with *Mps1*^{1} germline clones mated with *Mps1*^{1} heterozygous males (C–F). After aging to the stage of mitosis 16, embryos were incubated for 20 min without (− colcemid; [A, C, and E]) or with colcemid (+ colcemid; [B, D, and F]) before fixation and immunolabeling with antibodies against phospho-histone H3 (phospho H3; green), a DNA stain (DNA; red), and antibodies against β-galactosidase (data not shown). The anti-β-galactosidase labeling allowed the distinction of *Mps1*^{1} germline clone progeny with either a paternal *Mps1*$^{+}$ (C and D) or a paternal *Mps1*^{1} allele (E and F). While the latter did not display an enrichment of mitotic, phospho-histone H3-positive cells after incubation in colcemid, the former revealed a comparable increase in mitotic, phospho-histone H3-positive cells as also observed in the wild-type embryos. A paternal *Mps1*$^{+}$ allele is therefore sufficient to restore the mitotic spindle checkpoint in *Mps1*^{1} germline clone progeny at the stage of mitosis 16.

an onset of zygotic *Mps1* expression before the onset of mitosis 16. Further experiments with *Mps1*^{1} mutant embryos derived from *Mps1*^{1} heterozygous parents demonstrated that the maternal *Mps1* contribution perdures beyond the onset of zygotic *Mps1* expression. Colcemid induced a comparable enrichment of mitotic cells in both *Mps1*^{1} mutant and *Mps1*$^{+}$ sibling embryos at the stage when epidermal cells within the thoracic region progress through mitosis 17 (Figure S3).

To clarify whether Mps1, which is clearly involved in the arrest of mitosis in response to spindle damage and hypoxia, affects the dynamics of progression through mitosis in unperturbed conditions, we performed in vivo imaging with progeny of *Mps1*^{1} germline clones expressing *histone H2AvD-GFP*. In *Mps1*^{1} progeny, metaphase was found to be shortened by 35%–40%, and anaphase occurred about 1 min earlier than in *Mps1*$^{+}$ control embryos (Figure S4A; $p < 0.001$ in a Student's t test). Prophase also appeared to be slightly shortened in *Mps1*^{1} embryos, although statistical significance was not apparent in this case (data not shown). In contrast, the duration of anaphase was slightly, but again statistically insignificantly, extended in *Mps1*^{1} embryos (Figure S4A; $p > 0.14$). Also in the case of all other cell cycle phases, we did not detect significant differences between *Mps1*^{1} and control embryos. Therefore, we conclude that Mps1 specifically delays the onset of anaphase in unperturbed conditions.

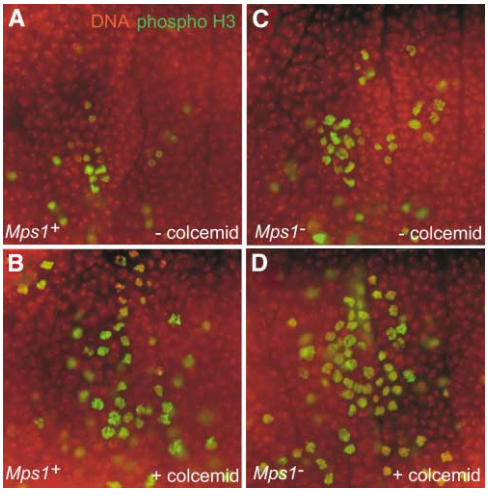

Figure S3. Perdurance of the Maternal Mps1 Contribution

Eggs were collected from *Mps1*^{1} heterozygous parents and aged. At the stage when the epidermal cells in the prospective anterior spiracle region progress through mitosis 17, we incubated the embryos for 20 min either without (− colcemid; [A and C]) or with colcemid (+ colcemid; [B and D]) before fixation and immunolabeling with antibodies against phospho-histone H3 (phospho H3; green), a DNA stain (DNA; red), and antibodies against β-galactosidase (data not shown). The anti-β-galactosidase labeling allowed the distinction of *Mps1*^{1} mutant (C and D) and *Mps1*$^{+}$ sibling embryos (A and B). However, a comparable enrichment of mitotic, phospho-histone H3-positive cells was observed after exposure to colcemid in both mutant and sibling controls, suggesting that the maternal Mps1 contribution is still sufficient for mitotic spindle checkpoint activation in *Mps1*^{1} mutants at the stage of mitosis 17.

As already indicated by the analyses of fixed embryos, in vivo imaging with *Mps1*^{1} embryos confirmed an increased frequency of occasional division failures of individual nuclei. During these aberrant mitoses, individual chromosomes (Figure S4B, top), or sometimes even all chromosomes (Figure S4B, bottom), failed to display poleward movements during anaphase, suggesting that they had not yet been properly attached to the spindle by the time of the premature metaphase-to-anaphase transition. These mitotic division failures were followed by an elimination of the affected nuclei from the superficial layer of nuclei.

To evaluate whether *Drosophila* Mps1 is required for a delay of Cyclin B degradation relative to that of Cyclin A, we analyzed progeny of *Mps1*^{1} germline clones and *Mps1*$^{+}$ control embryos at the stage of mitosis 14, the first asynchronous cell division following cellularization. Double labeling of *Mps1*^{1} progeny with antibodies against Cyclin A and Cyclin B did not reveal metaphase cells that were Cyclin A negative and Cyclin B positive, while such cells were clearly present in *Mps1*$^{+}$ control embryos (Figure S4C), as expected [S1]. These observations indicated that Mps1 is required for the delay of Cyclin B degradation relative to Cyclin A degradation.

Mps1 is enriched on the pericentromeric region of those chromosomes that are discarded as polar bodies

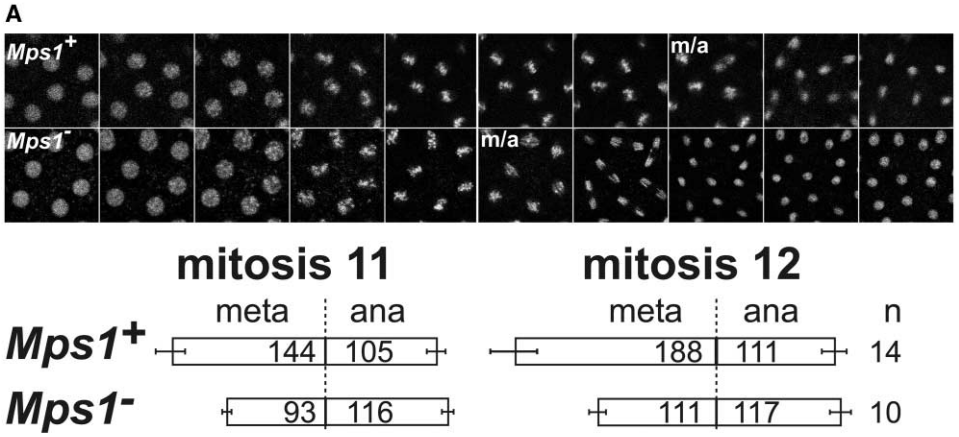

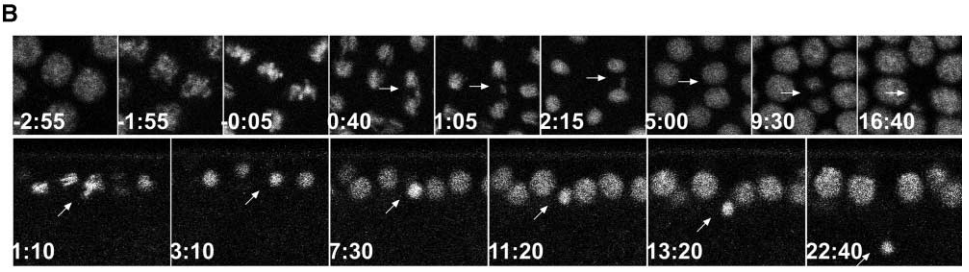

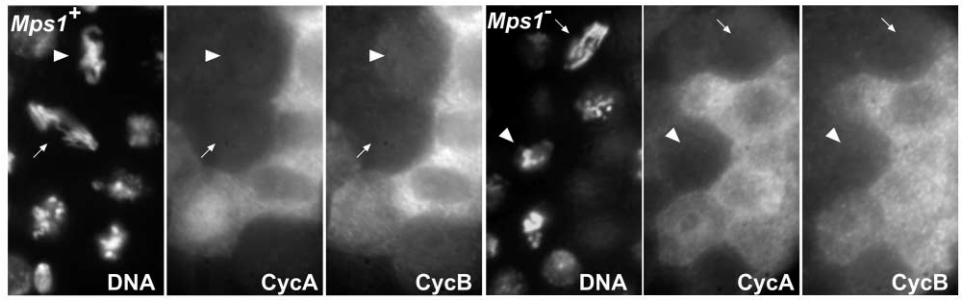

Figure S4. Mps1 Delays Anaphase Onset and Cyclin B Degradation during Unperturbed Mitoses

(A) Embryos expressing a histone-GFP fusion protein were isolated either from *Mps1*$^{+}$ females (*Mps1*$^{+}$) or from females with *Mps1*^{1} germline clones (*Mps1*$^{-}$). Time-lapse imaging was used to determine the dynamics of progression through the syncytial cycles 11 and 12. The metaphase-to-anaphase transition (m/a) was found to be significantly advanced in *Mps1*^{1} embryos, as demonstrated by representative frame sequences (top; frames acquired at 30 s intervals) and statistical analyses (bottom; duration of metaphase and anaphase in seconds with bars indicating standard deviations).

(B) Occasional division errors observed by in vivo imaging of *Mps1*^{1} embryos expressing a histone-GFP fusion protein during the syncytial blastoderm cycles. The top frame sequence illustrates a mitosis with a lagging chromosome (arrow) with superficial focal planes, and the bottom frame sequence illustrates a mitosis where all chromosomes of a nucleus fail to separate during anaphase (arrow) with tangential sections (embryo surface up and embryo interior down). The time (min:s) relative to the metaphase-to-anaphase transition, which was set as zero, is given in each frame.

(C) Embryos (3–4 hr), which progress through mitosis 14, the first asynchronous cell division after cellularization, were collected either from *w* females (*Mps1*$^{+}$; left three panels) or from females with *Mps1*^{1} germline clones (*Mps1*$^{-}$; right three panels). After fixation, embryos were double labeled with antibodies against Cyclin A (CycA) and Cyclin B (CycB) and a DNA stain (DNA). Representative epidermal regions are shown at high magnification. CycA-negative metaphase cells (arrowheads) with anti-CycB signals clearly above the level observed in anaphase cells (arrows) are present in *Mps1*$^{+}$ embryos (left), but not in *Mps1*$^{-}$ embryos (right).

during female meiosis. Moreover, Mps1 is required for the cell cycle arrest of these chromosomes. Therefore, an analysis of the distribution of Incenp and Aurora B kinase appeared to be of interest. A complex containing the proteins Survivin, Incenp, and Aurora B is known to localize to the centromeric region of mitotic chromo-

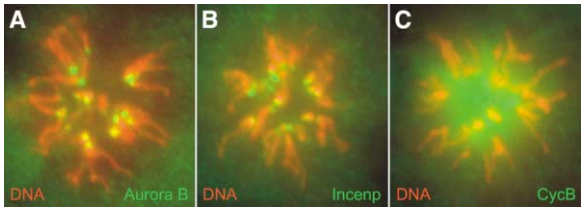

Figure S5. Enrichment of Aurora B, Incenp, and Cyclin B in Polar Bodies

Embryos (0–1 hr) were fixed with methanol and labeled with antibodies against Aurora B ([A], green), Incenp ([B], green), and Cyclin B ([C], green) and a DNA stain ([A]–[C], red). Maximum projections of the polar body regions are shown.

somes during prophase and has recently been shown to be required for the subsequent centromeric localization of mitotic spindle checkpoint components including Mps1 [S2]. Immunolabeling of wild-type embryos with antibodies against Incenp (Figure S5A) and Aurora B (Figure S5B) revealed a comparable enrichment of the antigens within the pericentromeric region of the polar body chromosomes, as also observed for Mps1 and other mitotic spindle checkpoint components.

All our observations indicate that the mitotic spindle checkpoint is activated within the pericentromeric region of the polar body chromosomes. Since this checkpoint inhibits the degradation of Cyclin B, this protein might be enriched within the region of the polar body chromosomes. Immunolabeling of methanol-fixed wild-type embryos with a rabbit antibody against *Drosophila* Cyclin B resulted in elevated signal intensities within a sphere that included the pericentromeric regions of the polar body chromosomes (Figure S5C).

Supplemental Experimental Procedures

Fly Strains

The generation of the *P{FRT(w[hs])}2A P{neoFRT}82B Mps1*^{1}*=Mps1*$^{Bac\{3xP3\text{-}EYFP,\ p\text{-}Gal4D\text{-}K10\}715}$*/TM3, Sb P{35UZ}2* stock has been described [S3]. Inverse PCR and sequence analysis with the primer PRF [S3] revealed that the *Bac{3xP3-EYFP, p-Gal4D-K10}* transposon of *Mps1*^{1} is inserted within codon 26 after a TTAA sequence, as expected in the light of the known insertion site sequence specificity of the *piggyBac* transposon. We point out that mobilization of *piggyBac* insertions has never been observed to result in imprecise excisions, preventing a simple isolation of intragenic *Mps1* deletions. The available deficiencies within the Mps1 region result in a dominant reduction of viability. Therefore, our observation that adult escapers were no longer observed when *Mps1*^{1} was crossed over the deficiency *Df(3R)G2*, while homozygous *Mps1*^{1} escapers occurred at a low frequency ($<$0.2%), does not necessarily rule out the possibility that *Mps1*^{1} is a null allele.

Mps1^{1} germline clones were generated by crossing virgin females from this stock with *P{hsFLP}22, y w; P{neoFRT}82B P{ovoD1-18}3R/TM3, Sb* males [S4] and exposing progeny at day 7–9 after egg deposition and development at 18°C each day for 2 hr to 37°C. Adult female progeny lacking the *TM3* balancer chromosome was crossed to *P{FRT(w[hs])}2A P{neoFRT}82B Mps1*^{1}*/TM3, Sb P{35UZ}2* males before collection and analysis of their eggs. For the analysis of various GFP fusion proteins in embryos derived from females with *Mps1*^{1} germline clones, we crossed appropriate transgene insertions on chromosome I or II into the *P{FRT(w[hs])}2A P{neoFRT}82B Mps1*^{1}*/TM3, Sb P{35UZ}2* background. *P{Ubi-fzy.GFP}* [S5], *P{Ubi-tacc.GFP}* [S6], *His2AvD-GFP* [S7] have been described, and *P{Ubi-Mad2.GFP}* was kindly provided by Jordan Raff (Cancer UK, Cambridge).

For the construction of the *gEGFP-Mps1* transgene, the 5′ region was enzymatically amplified from BAC RPC1-98 21K3 DNA, which includes the genomic *Mps1* region, with the primers RaS3 (5′-TGGAT GCGGCCGC ACT GCC AAA ATA TTG C-3′) and RaS4 (5′-CTT GGATCC CGA TTT ATT CTG CCC GAC-3′) introducing a NotI and a BamHI site, respectively. In addition, the subsequent genomic *Mps1* region was amplified from the same template using the primers RaS5 (5′-TGCA CCATGG CCACGC CTG TGC CCC GC-3′) and RaS6 (5′-AT GGTACC TAT CTT ATA AGT AAA CGC AA-3′), introducing a NcoI and a KpnI site, respectively. This introduction of a NcoI site around the *Mps1* start codon also changed the second codon resulting in a T2A mutation. The two genomic *Mps1* fragments were eventually inserted into pPCaSpeR4 together with an intervening BamH1-NcoI fragment, which contained the EGFP coding region and a 6 bp linker. Germline transformation with the resulting transgene construct was done according to standard procedures after confirmation of its expected structure by DNA sequencing. Since transgenes and *Mps1* mutation were present in a *w* mutant background, we used *w* flies for some control experiments.

In Vivo Imaging and Immunofluorescence

Embryos expressing GFP fusion proteins were aged to the syncytial blastoderm stages after collection on apple juice agar plates. Dechorionated embryos were lined up, immobilized on a coverslip, and covered with halocarbon oil. Time-lapse confocal laser scanning microscopy was performed with a Leica TCS SP1 system in combination with an inverted microscope at 22°C–24°C in a temperature-controlled room. Light damage was prevented by minimizing the laser intensity and opening the pinhole. Frames were collected at either 10 or 30 s intervals. The results shown in Figure 1C were obtained with embryos from a stock homozygous for two independent *gEGFP-Mps1* insertions on chromosome II. Slightly lower signals with indistinguishable temporal and spatial dynamics were obtained with stocks carrying single transgene insertion (data not shown).

Before immunofluorescence labeling, embryos were aged to the appropriate stages and either fixed in methanol (Figure 1D, Figure 2, and Figure 3) or in 4% formaldehyde (Figures S1–S3 and Figure S4C) according to standard procedures [S8]. For the analysis of the spindle checkpoint response, we incubated progeny from females with *Mps1*^{1} germline clones or from *w* control females for 30 min on a rotating wheel in a 1:1 mixture of octane and Schneider's tissue culture medium either without or with 10 μM demecolcine (Sigma) before fixation. For the analysis of the hypoxia response, we incubated embryos for 20 min on a rotating wheel in either aerated or extensively degassed 0.7% NaCl, 0.07% Triton X-100 before fixation.

For immunolabeling, we used the following antibodies: mouse monoclonal GTU-88 against γ-tubulin (Sigma) at 1:500; mouse monoclonal antibody DM1A against α-tubulin (Sigma) at 1:40,000; mouse monoclonal antibodies 7.1 and 13.1 against GFP (Roche) at 1:100; affinity-purified rabbit antibodies against Cid (kindly provided by S. Heidmann, University of Bayreuth) at 1:500; rabbit antiserum against BubR1 [S9] at 1:500; mouse monoclonal antibodies against β-galactosidase (Promega) at 1:250; rabbit antibodies against phospho-histone H3 (Upstate Biotechnology) at 1:400; mouse monoclonal AX-D5 against a *Drosophila* sperm tail protein [S10] at 1:3; mouse monoclonal antibodies F2 against *Drosophila* Cyclin B [S11] at 1:3; rabbit antiserum against *Drosophila* Cyclin A and B [S12, S13] at 1:500 and 1:10,000, respectively; rabbit antiserum against *Drosophila* Incenp [S14] at 1:500; and rabbit antiserum against *Drosophila* Aurora B [S15] at 1:500. The staining of polar body chromosomes with anti-phospho-histone H3 was found to be affected by the fixation procedure. While an intense labeling throughout the entire polar body chromosomes was observed after formaldehyde fixation, weaker signals with a striking maximum within the pericentromeric regions were seen after methanol fixation. In contrast, only the latter distribution of anti-Incenp labeling was observed after both formaldehyde and methanol fixation. Anti-Aurora B signals were found to be sensitive to formaldehyde fixation. DNA was la-

beled with 1 μg/ml Hoechst 33258. Single focal planes or Z stacks were acquired with a Zeiss Axioplan 2 Imaging system using Zeiss AxioVision software. Adobe Photoshop was used for the preparation of the figures.

Quantitative RT-PCR

A QuickPrep micro mRNA purification kit (Amersham) was used for mRNA isolation from 0–3 hr *w* and *Mps1*^{1} germline clone progeny. SuperScript III reverse transcriptase (Invitrogen) was used for the preparation of first strand cDNA, which was used as template in the quantitative RT-PCR assays after RNase H treatment. TaqMan technology (Applied Biosystems) in combination with an ABI Prism 7000 sequence detection system was used for the quantification of *Mps1* transcript levels. In addition, *RpL32* transcript levels were determined and used for normalization. Additional details on the quantitative RT-PCR assays will be provided upon request. Three mRNA preparations for both genotypes were analyzed independently. Results were found to be similar and are given as an average in the text. An estimation of the absolute mRNA levels involving titration assays with known amounts of cloned *Mps1* cDNA indicated the presence of one million mRNA copies per wild-type embryo.

Supplemental References

S1. Lehner, C.F., and O'Farrell, P.H. (1990). The roles of *Drosophila* cyclin A and cyclin B in mitotic control. Cell *61*, 535–547.

S2. Vigneron, S., Prieto, S., Bernis, C., Labbe, J.C., Castro, A., and Lorca, T. (2004). Kinetochore localization of spindle checkpoint proteins: Who controls whom? Mol. Biol. Cell *15*, 4584–4596.

S3. Hacker, U., Nystedt, S., Barmchi, M.P., Horn, C., and Wimmer, E.A. (2003). piggyBac-based insertional mutagenesis in the presence of stably integrated P elements in Drosophila. Proc. Natl. Acad. Sci. USA *100*, 7720–7725.

S4. Chou, T.B., and Perrimon, N. (1996). The autosomal FLP-DFS technique for generating germline mosaics in Drosophila melanogaster. Genetics *144*, 1673–1679.

S5. Raff, J.W., Jeffers, K., and Huang, J.Y. (2002). The roles of Fzy/Cdc20 and Fzr/Cdh1 in regulating the destruction of cyclin B in space and time. J. Cell Biol. *157*, 1139–1149.

S6. Gergely, F., Kidd, D., Jeffers, K., Wakefield, J.G., and Raff, J.W. (2000). D-TACC: A novel centrosomal protein required for normal spindle function in the early Drosophila embryo. EMBO J. *19*, 241–252.

S7. Clarkson, M., and Saint, R. (1999). A His2AvDGFP fusion gene complements a lethal His2AvD mutant allele and provides an in vivo marker for Drosophila chromosome behavior. DNA Cell Biol. *18*, 457–462.

S8. Rothwell, W.F., and Sullivan, W. (2000) Fluorescent analysis of Drosophila embryos. In Drosophila Protocols, W. Sullivan, M. Ashburner, R.S. Hawley, eds. (Cold Spring Harbor, NY: Cold Spring Harbor Laboratory Press), pp. 141–158.

S9. Logarinho, E., Bousbaa, H., Dias, J.M., Lopes, C., Amorim, I., Antunes-Martins, A., and Sunkel, C.E. (2004). Different spindle checkpoint proteins monitor microtubule attachment and tension at kinetochores in Drosophila cells. J. Cell Sci. *117*, 1757–1771.

S10. Karr, T.L. (1991). Intracellular sperm egg interactions in Drosophila: A 3-dimensional structural analysis of a paternal product in the developing egg. Mech. Dev. *34*, 101–111.

S11. Knoblich, J.A., and Lehner, C.F. (1993). Synergistic action of *Drosophila* cyclin A and cyclin B during the G2-M transition. EMBO J. *12*, 65–74.

S12. Lehner, C.F., and O'Farrell, P.H. (1989). Expression and function of *Drosophila* cyclin A during embryonic cell cycle progression. Cell *56*, 957–968.

S13. Jacobs, H.W., Knoblich, J.A., and Lehner, C.F. (1998). Drosophila Cyclin B3 is required for female fertility and is dispensable for mitosis like Cyclin B. Genes Dev. *12*, 3741–3751.

S14. Adams, R.R., Maiato, H., Earnshaw, W.C., and Carmena, M. (2001). Essential roles of Drosophila inner centromere protein (INCENP) and aurora B in histone H3 phosphorylation, metaphase chromosome alignment, kinetochore disjunction, and chromosome segregation. J. Cell Biol. *153*, 865–880.

S15. Giet, R., and Glover, D.M. (2001). Drosophila aurora B kinase is required for histone H3 phosphorylation and condensin recruitment during chromosome condensation and to organize the central spindle during cytokinesis. J. Cell Biol. *152*, 669–682.

Teilarbeit D

Rahul Pandey, Sebastian Heeger and Christian F. Lehner

Rapid effects of acute anoxia on spindle kinetochore interactions activate the mitotic spindle checkpoint

eingereicht bei *Mol Cell Biol*

Darstellung des Eigenanteils

Mein Beitrag zu dieser Arbeit war die Charakterisierung des Verhaltens von Cenp-C nach Sauerstoffentzug (Fig. 5A).

Geschrieben wurde das Manuskript von Christian F. Lehner mit Beiträgen der anderen Autoren.

Rapid effects of acute anoxia on spindle kinetochore interactions activate the mitotic spindle checkpoint

Rahul Pandey, Sebastian Heeger and Christian F. Lehner[*)]

Department of Genetics, BZMB, University of Bayreuth, 95440 Bayreuth, Germany

running title: anoxia-induced spindle checkpoint arrest

[*)] Corresponding author. Mailing address: Department of Genetics, University of Bayreuth, Universitätsstrasse 30, 95447 Bayreuth, Germany. Phone: 49 921 55 2701. Fax: 49 921 55 2710. E-mail: chle@uni-bayreuth.de.

word counts: Material and Methods (1007), Introduction, Results, Discussion (5651)

Abstract

The dramatic chromosome instability in tumor cells might reflect a synergy of spindle checkpoint defects and hypoxia. Spindle checkpoint function has already been shown to protect effectively from anoxia-induced chromosome missegregation in *C. elegans* and *D. melanogaster*. Our analyses with syncytial *D. melanogaster* embryos demonstrate that oxygen deprivation affects microtubule organization rapidly and reversibly within minutes. In addition, motor proteins (dynein, Kin-8), centrosomal proteins (Cnn, TACC) and kinetochore proteins (Cenp-C, Nuf2) are rapidly re-localized. Kinetochores congress ineffectively into the metaphase plate and are not exposed to normal pulling forces. Consequentially, the spindle checkpoint remains active, resulting in a drastic accumulation of checkpoint proteins mainly within the equatorial region. These rapid cellular effects of anoxia presumably result from reduced ATP levels since they are mimicked by inhibitors of oxidative phosphorylation. Yet the ATP decrease does not prevent motor protein and kinase activity at least initially; and in checkpoint-deficient embryos, mitosis is still completed, although accompanied by massive chromosome missegregation. The chromosome segregation machinery is therefore a more sensitive anoxia target than spindle checkpoint activity which involves ATP-consuming protein kinases. This allows the spindle checkpoint to provide protection from aneuploidies in response to acute anoxia.

Introduction

Oxygen plays a decisive role in metabolism and is particularly important in metazoans for efficient ATP production by oxidative phosphorylation. Diverse and highly adapted mechanisms have evolved to cope with oxygen limitation during development and adult life.

A well-known pathway triggered by acute and chronic hypoxia involves the activation of the HIF-1 transcription factor. This pathway has been shown to operate in a conserved manner in vertebrates and invertebrates like *C. elegans* and *D. melanogaster* (13). In addition,

experiments with these invertebrate model organisms have revealed the importance of alternative pathways especially in anoxia when oxygen levels are even further decreased. Not only nematode (37) and insect embryos (12) but also some vertebrates (38) tolerate extended periods of anoxia. In response to anoxia, they enter a state of suspended animation from which they can rapidly recover upon re-oxygenation. HIF-1 is not required in *C. elegans* for survival of anoxia, while it is clearly crucial for survival of hypoxia (24, 37). However, a screen for *C. elegans* genes required for survival of anoxia has led to the identification of *san-1* which encodes a homolog of budding yeast Mad3 (36). Mad3 is a component of the mitotic spindle checkpoint, a surveillance pathway known to monitor the bipolar integration of chromosomes into the mitotic spindle. Moreover, experiments in *D. melanogaster* demonstrated that Mps1 protein kinase, which also functions in the spindle checkpoint, is required for the mitotic arrest resulting from severe hypoxia (11).

The mitotic spindle checkpoint acts during mitosis and prevents progression into anaphase until all chromosomes are bi-oriented (for reviews see (28, 30, 40, 47)). It is activated during prometaphase of normal mitoses by kinetochores which are either not yet attached to spindle microtubules or not under physical tension. Several proteins are known to function in the spindle checkpoint. Apart from the components introduced above (Mad3, Mps1), additional protein kinases (Bub1, BubR1) and scaffold proteins (Mad1, Bub3) are involved. Moreover, in metazoans, the kinesin Cenp-E and the Rod/Zw10/Zwilch (RZZ) complex which recruits dynein-dynactin and Mad2 to the kinetochore have also been implicated in the spindle checkpoint. The molecular interactions that lead to spindle checkpoint activation are not yet understood in detail. However, it is clear that spindle checkpoint activity prevents Fzy/Cdc20-APC/C ubiquitin ligase from marking securin and B-type cyclins for rapid proteasomal degradation. Securin inhibits separase, a protease that cleaves the Scc1 subunit of the cohesin complex. Therefore, as long as the spindle checkpoint remains active, sister chromatids are

kept together by the cohesin linkage and anaphase cannot proceed. Moreover, high levels of B-type cyclin cdk activity maintain the mitotic state in the spindle checkpoint arrest.

The spindle checkpoint protects against aneuploidies. Spindle checkpoint dysfunction has been proposed to be involved in tumor formation, because excessive chromosome instability is a hallmark of a large fraction of solid human tumors. Evidence supporting this notion is increasing (28). Moreover, the spindle checkpoint might be of particular importance in tumor cells because their growth is known to be severely constrained by oxygen limitation (19, 41). As a result, areas with very low (down to zero) oxygen partial pressures exist in solid tumors, occurring either acutely or chronically (19). Based on the initial analyses in *C. elegans* and *D. melanogaster*, it is readily conceivable that it is the combination of spindle checkpoint dysfunction and severe hypoxia which generates the remarkable chromosome instability typically observed in tumor cells. At least in the two model organisms, this combination clearly results in mitotic chromosome segregation defects (11, 36). A more detailed analysis of the functional connections between anoxia and the spindle checkpoint should therefore be of interest.

The synchronous cell cycle progression of thousands of nuclei which occur during the syncytial blastoderm stage of early *Drosophila* embryogenesis provides many advantages for experimental studies. Zalokar and Erk already observed that anoxia leads to a rapid and reversible developmental arrest during these stages in wild type (50). The studies of Foe and Alberts (1985) and DiGregorio et al. (2001) clearly revealed that anoxia triggers chromatin condensation in interphase nuclei and blocks further cell cycle progression within few minutes (7, 12). Embryos which have already entered mitosis at the time of anoxia induction become arrested either in metaphase or in late telophase. A metaphase arrest is observed when anoxia is induced before the metaphase to anaphase transition, and late telophase arrest thereafter.

In principle, it is conceivable that the early and rapid activation of the mitotic spindle checkpoint in response to anoxia involves an unknown dedicated pathway directly targeting one of the spindle checkpoint components. Such a pathway would appear especially beneficial if the error-free execution of post-metaphase processes were to be more sensitive to oxygen shortage than the initial mitotic processes. In this case, spindle assembly and chromosome attachment might still occur normally after oxygen deprivation, but progression into the more oxygen-dependent anaphase would be inhibited by a dedicated anoxia-sensing spindle checkpoint activation pathway. Alternatively, the process of chromosome attachment to the mitotic spindle might be more sensitive to ATP shortage than activation of the mitotic spindle checkpoint which involves ATP-consuming protein kinases. Accordingly, already a relatively minor drop in ATP levels would result in free kinetochores or reduce tension between sister kinetochores and thereby activate the spindle checkpoint. Our analyses support this latter notion. We demonstrate that spindle and kinetochore function are indeed very rapidly affected by oxygen deprivation. Crucial components of centrosomes and spindles as well as kinetochore proteins including Cenp-C which is thought to localize exclusively and constitutively to the centromere are rapidly and dramatically re-distributed in response to anoxia.

Results

Anoxia has rapid effects on mitotic spindles

Previous analyses have demonstrated that oxygen deprivation from the normal 21% to below 2% triggers a rapid cell cycle arrest in syncytial *Drosophila* embryos (7, 9, 12). In the following, we will use the term anoxia for these conditions even though our experimental procedures do not eliminate oxygen completely. We use this term to clearly distinguish our relatively severe conditions from milder hypoxia (5-3% O_2) which although sufficient for

HIF-1 activation does not trigger rapid cell cycle and developmental arrest during *Drosophila* development (29).

Mitotic spindles and chromosomes in metaphase plates have been shown to be present in syncytial embryos arrested by anoxia induction during early mitosis (i.e. before the metaphase to anaphase transition) (7, 9, 11). However, a careful comparison revealed that the mitotic spindles present in arrested embryos fixed after a 20 minute incubation in degassed buffer were different from metaphase spindles in normoxic embryos (Fig. 1A). After anti-α-tubulin labeling, centrosomes were either not or only hardly detectable in anoxic embryos. Moreover, asters were greatly reduced or absent. In addition, spindles were narrow and contained few and only short microtubule fibers which did not extend far away from the metaphase plates. The extent of these spindle abnormalities was somewhat variable. In the majority of the anoxic embryos, abnormalities were at least as severe as in the example shown in Fig. 1A. In contrast to the mitotic spindles, we did not observe clear differences in the metaphase plate arrangement of the condensed chromosomes when comparing normoxic and anoxic embryos.

To analyze how fast spindle abnormalities develop in anoxia, we fixed embryos after a two or five minute incubation in degassed buffer. Spindles were observed to be affected already after two minutes of anoxia (Fig. 1A). After five minutes, abnormalities were more severe but still minor than after 20 minutes of anoxia. Apart from a partial centrosome detachment and a reduction of astral and centrosome-proximal spindle fibers (Fig. 1A), spindle length appeared to be slightly extended in anoxia (Fig. 1B).

To study the effects of anoxia on spindle behavior, we also performed in vivo imaging with embryos expressing GFP-α-tubulin (15). These embryos were made anoxic by applying a flow of N_2 (Fig. 1C) or Ar gas (data not shown). As previously described (7, 9), we observed a rapid mitotic arrest after oxygen deprivation during early mitosis. We were unable to observe clear spindle abnormalities already after two minutes, in contrast to our findings with fixed embryos. Moreover, even after prolongation of anoxia up to 20 minutes, we never

observed the almost complete elimination of spindles which was frequently apparent after 20 minutes of incubation in degassed buffer followed by fixation and anti-α-tubulin labeling. Therefore, microtubule destabilizing effects of fixation (26) might enhance the apparent effects of anoxia on spindle organization. However, after prolonged anoxia, the reduction of centrosome-proximal spindle fibers was also evident in the in vivo imaging experiments (Fig. 1C). A very similar spindle response to prolonged anoxia has also previously been observed using in vivo imaging of Ncd-GFP, a fluorescent spindle-associated *Drosophila* kinesin-14 protein (9, 44).

In vivo imaging allowed an observation of spindle behavior during recovery from anoxia. Re-oxygenation was followed by a prominent increase in the density of microtubules around centrosomes (Fig. 1C). Subsequently, the centrosomes were pulled towards the spindle resulting in a distinct shortening of spindle length (Fig. 1C). Thereafter the spindle adopted an essentially normal metaphase appearance (Fig. 1C) followed rapidly by anaphase onset (not shown). In vivo imaging with embryos expressing the centrosomal protein GFP-D-TACC (2) confirmed the characteristic spindle shortening preceding anaphase during recovery from anoxia (Fig. 1D). Spindles shortened transiently to a length below that of normoxic metaphase spindles but comparable to prophase spindles. The defective poles of metaphase spindles in anoxic embryos therefore appear to be extensively rebuilt after re-oxygenation.

The rapid spindle malfunction in response to oxygen deprivation is independent of the spindle checkpoint

To address whether the observed rapid effects of oxygen deprivation on the spindle might be cause or consequence of spindle checkpoint activation, we incubated checkpoint-deficient embryos lacking *Mps1* function (11) for 5 minutes in degassed buffer followed by fixation and anti-α-tubulin labeling. Anoxic *Mps1* mutant embryos with metaphase plates (Fig. 2A, lower panel) were found to display the same abnormalities as observed with checkpoint-

competent control embryos (Fig. 1A). Moreover, we emphasize that normoxic *Mps1* mutant embryos (Fig. 2A, upper panel) did not display the metaphase spindle abnormalities which are characteristically observed in anoxic embryos. We conclude, therefore, that the rapid initial anoxia effects on spindle organization occur independently of spindle checkpoint activation.

In vivo imaging of *Mps1* mutant embryos, in which completion of mitosis is not blocked by oxygen deprivation, allowed an analysis of the function of the mitotic apparatus in anoxia. To monitor chromosome congression and segregation, we used embryos expressing green fluorescent Cenp-A/Cid centromere protein and red fluorescent histone H2Av (17). These experiments revealed that anoxia severely impaired chromosome congression during prometaphase. Congression proved to be slow and incomplete after oxygen deprivation, while it occurred far more effectively in normoxic *Mps1* mutants (Fig. 2B)(11). Moreover, in anoxic *Mps1* mutant embryos, anaphase appeared to start with a delay but still before normal metaphase plates had formed (Fig. 2B). Anaphase was also significantly slower in anoxia. The leading centromeres moved towards the poles with an average speed of about 2.5 μm min^{-1} in anoxic *Mps1* mutants compared to about 4 μm min^{-1} in normoxic ones (in both cases s.d. = 0.25 μm min^{-1} and n = 12 mitotic figures from a total of 3 different embryos). Consistent with the observed pronounced congression defects, lagging chromosomes were far more frequently observed during anaphase in anoxic *Mps1* mutants (Fig. 2B)(11). These observations suggest that spindle attachment of kinetochores is impaired by anoxia.

To confirm the impaired spindle attachment of kinetochores, we compared the average separation of sister kinetochores in normoxic and hypoxic metaphase plates after immunolabeling $Mps1^{+}$ embryos with antibodies against α-tubulin and Cenp-A/Cid (Fig. 2C). As previously established in cultured *Drosophila* cells and cellularized embryos (17, 31), chromosome bi-orientation in normoxic syncytial embryos was also found to be accompanied by an increase in the average separation of sister kinetochores, from 0.42 μm in prophase to 0.71 μm in metaphase (Fig. 2D). However, in anoxic metaphase plates, the average distance

between sister kinetochores (0.63 μm) was slightly (12 %) but significantly shorther than in the normoxic controls (Fig. 2D). Tension generated by the mitotic spindle, therefore, appears to be reduced in anoxia. Alternatively, it is not excluded that anoxia leads to tighter cohesion between sister chromatids. Apart from the reduced inter sister kinetochore distances, the α-tubulin and Cenp-A/Cid double labeling also demonstrated that the anoxic spindles were largely composed of kinetochore fibers which are known to be the most stable spindle fibers (32).

Effects of anoxia on centrosomal components and motor proteins

According to our microtubule analyses, the mitotic apparatus is rapidly affected by oxygen deprivation. Anoxia induction leads to a reduction of centrosome-proximal spindle fibers, centrosome detachment and slight spindle lengthening. Therefore, the centrosome appears to be especially sensitive to anoxia. To characterize centrosome behavior in response to anoxia in further detail, we examined the centrosome components Aurora A, γ-tubulin, Centrosomin (Cnn) and D-TACC. Anoxia had only a subtle effect on Aurora A and γ-tubulin (Fig. 3A). In the resulting mitotic arrest the centrosomal pool of these proteins had a more doughnut-shaped appearance with sharp outer borders while in normoxic metaphase the signal maxima were present in the centrosome center with a more graded decline towards the periphery (Fig. 3A, compare insets). These localization differences between anoxic and normoxic metaphases were far more pronounced in the case of Cnn (Fig. 3B). The characteristic flares of Cnn, which represent transport away from and back to the centrosome primarily on dynamic astral microtubules (33), were absent in anoxia. Cnn flaring on astral microtubules is known to be more extensive in interphase compared to metaphase (33). Accordingly, the anoxia-induced elimination of Cnn flares was even more striking in interphase embryos (Fig. 3C). D-TACC localization was also strongly affected by oxygen deprivation (Fig. 3D). However, D-TACC localization, which is known to stimulate astral microtubule plus end growth (2, 27, 39), was

affected in a manner opposite to Aurora A, γ-tubulin and Cnn. D-TACC was found to be far less focused to centrosomes in anoxia (Fig. 3D). By in vivo imaging using embryos expressing GFP-D-TACC (data not shown), we analyzed the dynamics of D-TACC re-localization in response to oxygen deprivation. These analyses revealed that the striking D-TACC spikes were gradually built up after oxygen deprivation during prophase. At the time when anaphase onset would have occurred in normoxic conditions, D-TACC re-distribution was subtle at most. During recovery from anoxia, GFP-D-TACC spikes were compacted back into the normal distribution within the period where centrosome fiber re-growth was apparent in the GFP-α-tubulin imaging experiments (Fig. 1C). D-TACC function at the centrosome has been shown to be regulated by Aurora A which phosphorylates an identified site on D-TACC (2). An antibody against this phospho-epitope (2) resulted in signal intensities which were not clearly altered by oxygen deprivation (data not shown), suggesting that Aurora A activity is not inhibited by anoxia.

Similar effects on spindle organization as those triggered by anoxia have been observed in Schneider cells after knock-down of the kinesin family member Kin-8 (Klp67A) or dynein heavy chain 64C, while knock-down of many other components of the mitotic apparatus resulted in additional, structurally different spindle responses (14). Therefore, we analyzed whether oxygen deprivation affects the localization of these motor proteins. Both motor proteins appeared to be rapidly and strongly affected. Oxygen deprivation induced a rapid reduction of Kin-8 levels within the equatorial spindle region already within 2 minutes (Fig. 4A). After 5 minutes of anoxia, Kin-8 spindle association was almost undetectable (Fig. 4A). With an antibody recognizing the *Drosophila* dynein light intermediate chain (D-LIC), we followed the response of dynein to anoxia. In normoxic metaphase, D-LIC was predominantly associated with the pseudo-cleavage furrows (Fig. 4B), as previously reported for dynein heavy chain (6, 45). After oxygen deprivation, D-LIC accumulated within minutes on spindle fibers in the vicinity of the kinetochores (Fig. 4B). The same behavior in response to anoxia

was also observed by in vivo imaging embryos expressing a functional D-LIC version fused to GFP (data not shown). In these experiments, we also observed D-LIC-GFP particle movement on spindle fibers towards the pole (see below), suggesting that the dynein motor activity is not eliminated, at least during the initial minutes of anoxia.

Outer and constitutive inner kinetochore proteins are re-localized in response to anoxia. Kin-8 and dynein which are rapidly affected by anoxia are thought to provide important functions at the kinetochore (43, 46). Therefore, we characterized the response of centromere kinetochore complex components to oxygen deprivation. We did not observe rapid effects on the behavior of Cenp-A/Cid, a centromeric histone H3 variant which acts at the top of the centromere kinetochore assembly process (Fig. 2C). Surprisingly, however, the localization of Cenp-C, another constitutive centromere protein of the inner kinetochore plate, was found to be severely affected by anoxia. An anoxia-induced re-distribution of Cenp-C was observed by immunofluorescence after fixation (Fig. 5A), as well as by in vivo imaging (data not shown) of a functional EYFP-Cenp-C variant (17). Cenp-C immunolabeling with two different affinity-purified rabbit antibodies indicated that a fraction of Cenp-C is spindle-associated even in normoxic syncytial embryos (Fig. 5A, and data not shown). In anoxic embryos, this Cenp-C pool appeared to be increased and re-distributed to the centrosome-proximal spindle region (Fig. 5A). Interestingly, we observed a similar anoxia-induced re-distribution predominantly to the centrosome-proximal spindle region also for the outer kinetochore plate Ndc80/Hec1 complex component Nuf2 when analyzing the localization of a functional *Drosophila* EGFP-Nuf2 version (Fig. 5B). Therefore, we conclude that oxygen deprivation affects some important kinetochore proteins.

Kinetochore attachment to spindle fibers is thought to be regulated by the chromosomal passenger complex which includes Aurora B kinase and INCENP (48). Using antibodies against *Drosophila* INCENP (1), we were unable to detect an extensive re-localization after

anoxia induction during mitosis comparable to that observed for Cenp-C and Nuf2 (data not shown). However, we cannot exclude that anoxia affects Aurora B kinase activity.

The response of spindle checkpoint proteins to anoxia

Since anoxia has rapid effects on the mitotic apparatus, we analyzed the response of mitotic spindle checkpoint proteins. Oxygen was deprived from embryos expressing functional EGFP fusion proteins and their localization was analyzed by in vivo imaging as well as after fixation.

During normoxic metaphase some EGFP-Mps1 has been shown to be enriched on centrosomes and spindles and only weakly on kinetochores (11). Apart from these localized signals, diffuse specific signals are observed as well. In response to oxygen deprivation, EGFP-Mps1 strongly accumulated at kinetochores and even more pronounced in the spindle fiber overlap zone in the equatorial region (Fig. 6A, arrows). Interestingly, in about 5% of the embryos, impressive filamentous EGFP-Mps1 structures formed in the vicinity of the centrosomes in addition to the equatorial concentration (Fig. 6A, arrowheads). EGFP-Mps1 re-localization started within minutes after oxygen deprivation and reached a maximum after about 8 minutes. Recovery from anoxia (Fig. 6A) was accompanied by a return to the normal metaphase distribution before anaphase onset. We point out that the comparatively weaker signals of kinetochore- and spindle-associated EGFP-Mps1 before oxygen deprivation, as well as after re-oxygenation, were not detectable with the confocal microscope settings adjusted for detection of the drastic EGFP-Mps1 enrichment within the equatorial region during anoxia, as apparent in Fig. 6A.

While the EGFP-Mps1 filaments close to centrosomes were only formed in some of the anoxic metaphase embryos, we observed EGFP-Mps1 aggregation far more frequently in the cortical region of anoxic pre-blastoderm embryos where nuclei have not yet migrated out to the egg periphery. EGFP-Mps1 aggregation occurred in about 80% of the anoxic pre-

blastoderm embryos, usually in the form of bright dots but occasionally also in filamentous structures (Fig. 6D).

EGFP-BubR1 behavior in response to anoxia was very similar to EGFP-Mps1. In mitotic cells, enrichment also occurred within the equatorial region (Fig. 6E), although apparently less pronounced than with EGFP-Mps1. After oxygen deprivation, we also observed EGFP-BubR1 aggregation within the cortical region of pre-blastoderm embryos (data not shown), as well as filament formation around centrosomes in syncytial blastoderm embryos during mitosis (Fig. 6E), at comparable frequencies as with EGFP-Mps1. Double labeling indicated co-localization of BubR1 and EGFP-Mps1 within these aggregates (Fig. 6F). Co-localization was not perfect, however, perhaps reflecting antibody accessibility problems.

To analyze the behavior of *Drosophila* Bub3 in response to anoxia, we established an *gEGFP-Bub3* transgene which was found to rescue the recessive lethality associated with a newly identified *Bub3* mutation. Similar to EGFP-Mps1 and EGFP-BubR1, we also observed an enrichment of EGFP-Bub3 within the equatorial region in response to oxygen deprivation (Fig. 6G). However, aggregation in dots or filaments was not detected with anoxic *gEGFP-Bub3* embryos.

In metazoans, the RZZ complex which includes the Rod protein has been implicated in the mitotic spindle checkpoint and shown to recruit the Mad2 checkpoint protein to kinetochores and spindle fibers (4, 25). In response to anoxia, EGFP-Rod was strongly enriched on metaphase spindles, in particular within the equatorial region (Fig. 6H). As expected, the behavior of EGFP-Mad2 in response to anoxia was highly similar to EGFP-Rod (data not shown). The RZZ complex is also known to interact with the dynein/dynactin motor protein complex which mediates the shedding of Mad2 and presumably other spindle checkpoint proteins away from bi-oriented kinetochore along kinetochore fibers. As observed in normoxic larval neuroblasts (3), dynein behavior (Fig. 4B) appeared to be similar but not identical to the RZZ complex and Mad2 in anoxic embryos. Interestingly, with D-LIC-GFP

and EGFP-Rod (data not shown), as well as with EGFP-Mps1 (Fig. 6B), we observed particle transport along spindle fibers during the anoxia-induced metaphase arrest, suggesting that dynein motor activity is not abolished.

Spindle checkpoint activation results in Fzy/Cdc20 inhibition via Mad2 and BubR1. This inhibition prevents the APC/C-mediated degradation of securin and B-type cyclins and thereby anaphase onset. Consistent with the proposed complex formation between Fzy and activated Mad2 and BubR1, anoxia was found to result in an enrichment of EGFP-Fzy on metaphase spindles (Fig. 6I), similar to the other analyzed mitotic spindle checkpoint components. In addition, EGFP-Fzy was also found on centrosomes in anoxic metaphase embryos.

Interestingly, some spindle checkpoint components were not only re-distributed during mitosis in response to oxygen deprivation, but also during interphase. In normoxic interphase embryos, EGFP-Mps1 is very weakly enriched on centrosomes (Fig. 6C)(11). After oxygen deprivation, EGFP-Mps1 was observed in very bright and highly focused spots (Fig. 6C) which were closely associated with interphase centrosomes and possibly represent centriolar structures. The same behavior was also observed with EGFP-BubR1 (data not shown). Similarly, EGFP-Bub3 enrichment on centrosomes was not detected in normoxic but occurred strongly in anoxic interphase embryos (data not shown).

The observed re-localization of EGFP-Mps1 and EGFP-Bub3 in anoxic interphase embryos raised the possibility that oxygen deprivation activates the spindle checkpoint not only during mitosis but also during interphase. Spindle checkpoint activation in various experimental systems is correlated with an electrophoretic mobility shift of several components including *Drosophila* Mps1. Therefore, we analyzed whether oxygen deprivation during interphase leads to an Mps1 mobility shift. However, we did not detect such a shift, even though it was clearly observed during prometaphase of normal mitosis and in the anoxic metaphase arrest (Fig. 7).

From our characterization of spindle checkpoint components (Mps1, BubR1, Bub3, Rod, Mad2) and the final target (Fzy), we conclude that anoxia rapidly affects their behavior (even during interphase in the case of Mps1 and Bub3) and activates the checkpoint pathway during mitosis.

Comparison of the consequences of anoxia and metabolic inhibitors

The drop in ATP levels after oxygen deprivation has been shown to be less than 10% within the time sufficient to induce a metaphase arrest (7). This modest drop is not expected to have pronounced effects on protein kinase and motor protein activities based on biochemical analyses in vitro. Our in vivo studies strongly support the notion that these enzymes retain at least some activity after oxygen deprivation at least within the first minutes. Mitotic spindle checkpoint activation which occurs in anoxic embryos involves protein kinase activities (Mps1, BubR1) and dynein/dynactin-mediated transport. Moreover, motor activity of the *Drosophila* kinesin-14 Ncd has recently been described in oxygen-deprived embryos (44). It is conceivable, therefore, that anoxia might activate the mitotic spindle checkpoint independent of its effect on oxidative phosphorylation and ATP levels. Accordingly, inhibition of oxidative phosphorylation in the presence of oxygen would not be expected to result in spindle checkpoint activation. To address whether inhibition of oxidative phosphorylation in the presence of oxygen results in spindle checkpoint activation, we incubated syncytial embryos in medium containing azide (data not shown) or cyanide (Fig. 8). These cytochrome oxidase inhibitors were observed to have rapid effects on metaphase spindle organization and EGFP-Mps1 localization (Fig. 8A). Moreover, the effects appeared to be indistinguishable from those induced by oxygen deprivation. In addition, the metabolic inhibitors also mimicked the effects of oxygen deprivation on chromatin condensation and centrosomal EGFP-Mps1 during interphase (Fig. 8B). Therefore we conclude that spindle

checkpoint activation by anoxia is presumably caused by inhibition of oxidative phosphorylation.

Discussion

Anoxia in combination with spindle checkpoint defects drastically enhances chromosome instability in *C. elegans* and *D. melanogaster* and possibly during cancer development in humans as well. A functional spindle checkpoint has been shown to protect the model organisms very effectively from anoxia-induced aneuploidy. Our analyses with syncytial *Drosophila* embryos provide insights into the mechanism of spindle checkpoint activation by anoxia. Oxygen deprivation is shown to affect microtubule organization rapidly and reversibly within minutes. The spindle association of the motor proteins dynein and Kin-8 was changed quickly. Strikingly, the kinetochore proteins Cenp-C and Nuf2 are re-localized as well. Kinetochores congress ineffectively into the metaphase plate and do not appear to experience a normal tension. We propose that therefore the spindle checkpoint remains active, resulting in the observed massive accumulation of checkpoint proteins within the equatorial region. Since inhibitors of oxidative phosphorylation have the same effects as anoxia, it appears that spindle defects and consequential checkpoint activation and mitotic arrest result from a decrease in ATP levels. Importantly, however, ATP levels after anoxia induction are still sufficiently high, allowing motor protein and protein kinase activities at least initially. Moreover, in the absence of mitotic spindle checkpoint function, anaphase and completion of mitosis still proceed although accompanied by massive chromosome missegregation. Thus faithful chromosome segregation during mitosis appears to be exquisitely sensitive to ATP reduction, far more than spindle checkpoint activation which involves ATP-consuming protein kinases. As a consequence spindle checkpoint activation in response to acute anoxia can provide protection from aneuploidies.

Anoxia effects on spindle organization have been reported previously (9, 16, 44). However, the spindle abnormalities described in these studies were observed after prolonged exposure to anoxia of 30 minutes or longer. Our analyses in checkpoint-deficient *Mps1* mutant embryos demonstrate that the spindle abnormalities are not simply the consequence of the anoxia-induced mitotic arrest. Moreover, our description of rapid effects strongly suggests that spindle abnormalities are a cause of the mitotic arrest. While spindle abnormalities were clearly apparent in fixed embryos already after two minutes of anoxia, we did not observe them equally early by in vivo imaging. We explain this discrepancy by the lower signal to noise ratio and lower spatial resolution of our in vivo imaging experiments compared to the analyses with fixed material. Moreover, the methanol fixation applied in our experiments is known to disturb some aspects of the microtubule organization (26) and thereby it seems to enhance the apparent defects. Nevertheless, the apparent differences between mitotic spindles fixed after two minutes of incubation in either normoxic or anoxic media provide clear evidence that oxygen deprivation has rapid effects on spindles. Only rapid effects can cause a mitotic spindle checkpoint arrest in syncytial embryos because of the speed of the mitotic divisions during these developmental stages. To cause a mitotic arrest, anoxia has to be induced after entry into mitosis (otherwise it leads to an interphase arrest) and the consequences must be sensed in the embryo before the metaphase to anaphase transition which occurs only 4.5 minutes after mitosis onset (34).

The spindle abnormalities which develop within minutes after oxygen deprivation are accompanied by a reduced separation of sister kinetochores in metaphase plates. The inter-kinetochore distance in metaphase is thought to reflect the pulling forces exerted by the spindle on bi-oriented chromosomes. Accordingly, anoxia appears to reduce these pulling forces. It should be pointed out, however, that the observed decrease in the inter-kinetochore distance might also be explained by reduced chromosome elasticity. Since oxygen deprivation induces a substantial chromatin condensation at least in interphase (12), a contribution by

increased stiffness of anoxic metaphase chromosomes should not be discounted prematurely. Nevertheless, the notion of reduced pulling forces is further supported by the observation that the speed of chromosome congression in prometaphase and segregation to the poles in anaphase in the checkpoint-deficient *Mps1* mutant embryos is markedly slower during anoxic compared to normoxic mitoses.

The rapid effects of oxygen deprivation on spindles and chromosome attachment, readily explain why mitotic spindle checkpoint activity is maintained in anoxia. All the mitotic spindle checkpoint proteins analyzed (Mps1, BubR1, Bub3, Rod, Mad2) as well as their target Fzy/Cdc20 accumulate strongly on anoxic spindles, predominantly in the equatorial region. A similar accumulation has been observed in normoxic embryos in response to taxol in experiments with EGFP-BubR1, EGRFP-Rod and EGFP-Mad2 (4). Moreover, Mps1 has a low electrophoretic mobility in anoxic metaphase extracts, as also observed in normoxic metaphase and in colchicine arrest (data not shown). Interestingly, some mitotic spindle checkpoint proteins (Mps1 and Bub3) were also observed to re-localize in interphase in response to anoxia. However, based on the Mps1 behavior revealed in our immunoblotting experiments, anoxia does not appear to activate the mitotic spindle checkpoint during interphase. This further argues against a physiological link that would allow mitotic spindle checkpoint activation by anoxia independent of the effects on the mitotic apparatus.

The anoxia response of Mps1 and Bub3 during interphase might also reflect effects on microtubules. The same interphase response was also induced by the inhibitors of oxidative phosphorylation KCN and NaN_3. A rapid reduction of microtubule asters induced by these various treatments therefore occurs during both mitosis and interphase. Aster reduction might reflect increased microtubule instability or reduced centrosomal nucleation activity. The centrosomal components Cnn and TACC are clearly re-organized after anoxia induction during interphase, while other components (γ-tubulin and Aurora A) were only subtly affected. Moreover, the Cnn-containing flares of pericentrosomal material, which are moved

by microtubule dynamics independent of motors during normoxia (33), are eliminated by anoxia.

We note that an opposite response of aster microtubules has been observed with mitotic mammalian cells in culture after treatment with cyanide and 2-deoxyglucose (49). These conditions are expected to induce a more drastic reduction in ATP levels because they inhibit glycolysis in addition to oxidative phosphorylation. With regard to the precise experimental conditions, we would also like to add that CO_2 was found to have slightly different consequences when it was used instead of N_2 or Ar for air displacement during in vivo imaging. In the wild, *Drosophila* deposits eggs into fermenting yeast on decaying fruits. Anoxia resulting from high CO_2 concentration is therefore likely to be of physiological relevance. After CO_2 application in prophase, we also observed a rapid and reversible arrest in metaphase. Interestingly, however, metaphase arrest occurred also in checkpoint-deficient *Mps1* mutant embryos, in contrast to the experiments with N_2, Ar or degassed buffer. Moreover, the mobility of checkpoint protein particles was found to be strongly reduced in the CO_2-induced mitotic arrest.

In addition to centrosomal proteins, anoxia affects the localization of spindle-associated protein Kin-8/KLP67A and dynein. Our observations are in accord with those of others (22, 44) and argue against the possibility that the rapid effects on these proteins reflect an inhibition of their motor activity. Similarly, our observations argue that the activity of protein kinases (like Mps1, BubR1, Aurora A) is not inhibited during the initial response to anoxia. We consider it to be likely, therefore, that the observed anoxia-induced re-localization of the proteins analyzed in our studies and including the kinetochore proteins Cenp-C and Nuf2 results from altered microtubule dynamics. However, the rapid chromatin condensation which is induced by anoxia during interphase (12) is very unlikely to be linked with microtubule dynamics, indicating the existence of sensitive anoxia targets other than microtubules.

Our finding that metabolic inhibitors (CN^-, N_3^-) and anoxia have indistinguishable early effects both in interphase and mitosis is consistent with the notion that the sensitive targets respond already to relatively minor changes in ATP levels. We also point out that the recovery dynamics of ATP levels after re-oxygenation was found to be closely correlated to resumption of mitosis (7). The behavior of the highly abundant cellular component tubulin is directly regulated by GTP which is generated from ATP. It is conceivable, therefore, that microtubule dynamics responds rather immediately to changes in ATP levels. However, further analysis will certainly be required for the identification of the sensitive targets of anoxia and the molecular details of their response.

Materials and methods

Fly stocks

The following fly strains have been described before: *Mps1*^{1} and *P{gEGFP-Mps1}* (11), *P{gcid-EGFP-cid}*, *P{gEYFP-Cenp-C}* and *P{His2Av-mRFP1}* (17), *w*^{1118}*; P{w*$^{+mC}$*=GAL4::VP16-nos.UTR}MVD1*, *P{w*$^{+mC}$*=UASp-GFPS65C-alphaTub84B}3* (15), *G147* (35), *P{gEGFP-Rod}*, *P{gEGFP-BubR1}*, and *P{gEGFP-Mad2}* (4), *P{Ubi-EGFP-Fzy}* (42), *P{Ubi-TACC-GFP}* (2). *P{Ubi-DLIC-GFP}* was kindly provided by Jordan Raff before publication. *P{gEGFP-Nuf2 }* will be described in detail elsewhere. We used *w*^{1} for control experiments because all the analyzed mutations and transgenes were in a *w* mutant background. Females with *Mps1*^{1} germ line clones were generated using the FLP-DFS method (5) as described previously (11), and the term "*Mps1* mutant embryos" refers to the progeny derived from these females.

P{gEGFP-Bub3} lines were obtained by standard germ line transformation using a pP{CaSpeR-4} construct. For its construction, we amplified the genomic *Bub3* region from BAC RPC1-98 10L12 (21) using the primers RaS7 (5'-GAT GAATTC AGGGGAAGGACGAACTGG-3') and RaS8 (5'-ACGA TCTAGA ATGCTTGGGCAACA ATTCCGA-3') which introduced an *Eco*RI and an *Xba*I site, respectively. After digestion with *Eco*RI and *Xba*I, the amplification product was inserted into the corresponding sites of pP{CaSpeR-4} to generate *P{gBub3}* lines. To insert the EGFP coding sequence just before the initiation codon, we subcloned an *Eco*RI-*Bgl*II fragment from the *P{gBub3}* construct into pLitmus28Δ*Eco*RV-*Stu*I. Into the resulting cloning intermediate, we introduced restriction sites for *Bam*HI, *Sma*I and *Not*I immediately upstream of the *Bub3* initiation codon by inverse PCR using the primers RP23 (5'-TGGG CCCGGGATCC TGTCAAGTTTTCTGC TAGCA-3') and RP24 (5'-GCAG CCCGGGCGGCCGC ATG CGTCCCCCAGAGTTCAA-3'). The *Bam*HI-*Not*I fragment including the *Sma*I site was subsequently replaced with a *Bam*HI-*Not*I fragment containing the complete EGFP coding sequence. Finally, the recombinant *Eco*RI-

*Bgl*II fragment with the EGFP sequence was used to replace the corresponding region in *P{gBub3}*. After sequence confirmation, several independent *P{gBub3}* and *P{gEGFP-Bub3}* lines were established. Complementation tests using $Bub3^{233}$ mutant flies indicated that both transgenes, *P{gBub3}* and *P{gEGFP-Bub3}*, were functional. $Bub3^{233}$ carries a *pBac{tTA}* mutator element (20) within the 5' UTR of *Bub3* resulting in recessive lethality at the larval/pupal interphase. $Bub3^{233}$ homozygotes carrying *P{gBub3}* or *P{gEGFP-Bub3}* were found to be fully viable and fertile.

In vivo imaging

Embryos were aged to the syncytial blastoderm stages after collection on apple juice agar plates. Dechorionated embryos were lined up, immobilized on coverslips and covered with halocarbon oil. Time lapse confocal laser scanning microscopy was performed with a Leica TCS SP1 system in combination with an inverted microscope at 22-24°C in a temperature controlled room. To avoid light damage, excitation laser intensity was minimized and the pinhole was opened. In most experiments, two frames (1024 x 1024 pixels) were acquired and averaged, at 15 second intervals using a 63x glycerol immersion objective, sometimes in combination with four-fold electronic zoom magnification.

For induction of anoxia, we covered the embryos mounted under halocarbon oil on the glass coverslip with a glass cylinder (20 mm diameter, 30 mm high), which was closed on one side except for two small openings (2 mm diameter), using silicon grease for air tight sealing. Air in the glass cylinder was then displaced by applying a flow of nitrogen, argon or carbon dioxide gas via silicon tubing connected to one of the top openings and a gas bottle on the other end. Re-oxygenation was achieved by stopping the gas flow.

Immunofluorescence

Embryos were collected and aged to the appropriate developmental stage before chorion removal. To induce anoxia, half of the embryos were subsequently incubated in extensively degassed 0.7% NaCl 0.07% Triton-X-100 (NaCl-Tx) for 2 to 20 minutes. The other half of the embryos was incubated at the same time in normal NaCl-Tx for normoxic control experiments. For the inhibitor experiments, we incubated half of the de-chorionated embryos in 4 mM KCN or 4 mM NaN_3 in phosphate buffered saline (PBS) for 5 to 15 minutes. For control experiments, the other half of the embryos was incubated in 4 mM KCl in PBS for the same time. Embryos were rapidly fixed and de-vitellinized after these incubations by replacing NaCl-Tx or PBS with a 1:1 mixture of heptane and methanol. The concentration of the inhibitors of oxidative phosphorylation was chosen because 4 mM of NaCN has previously been shown to reduce ATP levels with comparable kinetics as oxygen deprivation (7).

For immunofluorescent staining we used mouse monoclonal antibody DM1A anti-α-tubulin (Sigma) at 1:8000, affinity-purified rabbit anti-Cenp-A/Cid (23) at 1:1000, affinity-purified rabbit anti Cenp-C (17) at 1:2000, rabbit anti-BubR1 (kindly provided by C. Sunkel, Universidade do Porto, Portugal) at 1:2000, rabbit anti-INCENP (1) at 1:500, rabbit anti-KLP67A (43) at 1:50, mouse monoclonal 74.1 anti-dynein intermediate chain (8)(Abcam) at 1:300, rabbit anti-Aurora A (2) at 1:250, rabbit anti-phospho-TACC (2) at 1:500, rabbit anti-Centrosomin (18) at 1:200, and mouse monoclonal GTU-88 anti-γ-tubulin (Sigma) at 1:500. DNA was labeled with 1 µg/ml Hoechst 33258. Single focal planes or Z stacks were acquired with a Zeiss Axioplan 2 Imaging system using Zeiss AxioVision software. Adobe Photoshop was used for preparation of the figures.

Immunoblotting

Embryos were collected and aged to the syncytial blastoderm stage before chorion removal. Aliquots of embryos were incubated in either NaCl-Tx, or Schneider's *Drosophila* cell culture

medium containing 10 μM colcemid (N-Deacetyl-N-methylcolchizin, Sigma) or in extensively de-gassed NaCl-Tx for 20 minutes. After methanol fixation and DNA staining, interphase or metaphase embryos were selected with the help of an inverted microscope and pooled before extract preparation (10). Extracts were resolved by SDS polyacrylamide gel electrophoresis. For production of rabbit antibodies against *Drosophila* Mps1, we expressed an Mps1 fragment (amino acids 150-630) in *E. coli* with an N-terminal His_6 extension. Ni-NTA chromatography was used for purification of the immunogen. Antibodies were affinity-purified after immobilization of the immunogen on CNBr-activated Sepharose (Sigma). Immunoblots were probed with affinity-purified rabbit anti-Mps1 at 1:5000 and affinity-purified rabbit anti-EGFP (kindly provided by S. Heidmann, University of Bayreuth) at 1:3000 using Hybond-ECL membranes and ECL-detection (Amersham Biosciences).

Acknowledgments

We thank F. Althoff, U. Großkinsky and R. Schittenhelm for providing reagents and help during initial experiments. We are also grateful to W. Earnshaw, D. Glover, R. Karess, T. Kaufman, J. Raff and C. Sunkel for antibodies and fly stocks. Moreover, we thank S. Heidmann for comments on the manuscript.

This work was supported by the Deutsche Forschungsgemeinschaft (DFG LE 987/4-1).

References

1. **Adams, R. R., H. Maiato, W. C. Earnshaw, and M. Carmena.** 2001. Essential roles of *Drosophila* inner centromere protein (INCENP) and aurora B in histone H3 phosphorylation, metaphase chromosome alignment, kinetochore disjunction, and chromosome segregation. J Cell Biol **153:**865-80.
2. **Barros, T. P., K. Kinoshita, A. A. Hyman, and J. W. Raff.** 2005. Aurora A activates D-TACC-Msps complexes exclusively at centrosomes to stabilize centrosomal microtubules. J Cell Biol **170:**1039-46.
3. **Basto, R., F. Scaerou, S. Mische, E. Wojcik, C. Lefebvre, R. Gomes, T. Hays, and R. Karess.** 2004. In vivo dynamics of the rough deal checkpoint protein during *Drosophila* mitosis. Curr Biol **14:**56-61.
4. **Buffin, E., C. Lefebvre, J. Huang, M. E. Gagou, and R. E. Karess.** 2005. Recruitment of Mad2 to the kinetochore requires the Rod/Zw10 complex. Curr Biol **15:**856-61.
5. **Chou, T. B., and N. Perrimon.** 1996. The autosomal FLP-DFS technique for generating germline mosaics in *Drosophila melanogaster*. Genetics **144:**1673-1679.
6. **Cytrynbaum, E. N., P. Sommi, I. Brust-Mascher, J. M. Scholey, and A. Mogilner.** 2005. Early spindle assembly in *Drosophila* embryos: role of a force balance involving cytoskeletal dynamics and nuclear mechanics. Mol Biol Cell **16:**4967-81.
7. **DiGregorio, P. J., J. A. Ubersax, and P. H. O'Farrell.** 2001. Hypoxia and nitric oxide induce a rapid, reversible cell cycle arrest of the *Drosophila* syncytial divisions. J Biol Chem **276:**1930-7.
8. **Dillman, J. F., 3rd, and K. K. Pfister.** 1994. Differential phosphorylation in vivo of cytoplasmic dynein associated with anterogradely moving organelles. J Cell Biol **127:**1671-81.

9. **Douglas, R. M., T. Xu, and G. G. Haddad.** 2001. Cell cycle progression and cell division are sensitive to hypoxia in *Drosophila melanogaster* embryos. Am J Physiol Regul Integr Comp Physiol **280:**R1555-63.

10. **Edgar, B. A., D. A. Lehman, and P. H. O'Farrell.** 1994. Transcriptional regulation of string(cdc25): a link between developmental programming and the cell cycle. Development **120:**3131-3143.

11. **Fischer, M. G., S. Heeger, U. Hacker, and C. F. Lehner.** 2004. The mitotic arrest in response to hypoxia and of polar bodies during early embryogenesis requires *Drosophila* Mps1. Curr Biol **14:**2019-24.

12. **Foe, V. E., and B. M. Alberts.** 1985. Reversible chromosome condensation induced in *Drosophila* embryos by anoxia: visualization of interphase nuclear organization. J Cell Biol **100:**1623-36.

13. **Gorr, T. A., M. Gassmann, and P. Wappner.** 2006. Sensing and responding to hypoxia via HIF in model invertebrates. J Insect Physiol **52:**349-64.

14. **Goshima, G., R. Wollman, N. Stuurman, J. M. Scholey, and R. D. Vale.** 2005. Length control of the metaphase spindle. Curr Biol **15:**1979-88.

15. **Grieder, N. C., M. de Cuevas, and A. C. Spradling.** 2000. The fusome organizes the microtubule network during oocyte differentiation in *Drosophila*. Development **127:**4253-64.

16. **Hajeri, V. A., J. Trejo, and P. A. Padilla.** 2005. Characterization of sub-nuclear changes in Caenorhabditis elegans embryos exposed to brief, intermediate and long-term anoxia to analyze anoxia-induced cell cycle arrest. BMC Cell Biol **6:**47.

17. **Heeger, S., O. Leismann, R. Schittenhelm, O. Schraidt, S. Heidmann, and C. F. Lehner.** 2005. Genetic inteactions of Separase regulatory subunits reveal the diverged *Drosophila* Cenp-C homolog. Genes Dev **19:**2041-53.

18. **Heuer, J. G., K. J. Li, and T. C. Kaufman.** 1995. The *Drosophila* homeotic target gene centrosomin (cnn) encodes a novel centrosomal protein with leucine zippers and maps to a genomic region required for midgut morphogenesis. Development **121:**3861-3876.

19. **Hockel, M., and P. Vaupel.** 2001. Tumor hypoxia: definitions and current clinical, biologic, and molecular aspects. J Natl Cancer Inst **93:**266-76.

20. **Horn, C., N. Offen, S. Nystedt, U. Hacker, and E. A. Wimmer.** 2003. piggyBac-Based Insertional Mutagenesis and Enhancer Detection as a Tool for Functional Insect Genomics. Genetics **163:**647-61.

21. **Hoskins, R. A., C. R. Nelson, B. P. Berman, T. R. Laverty, R. A. George, L. Ciesiolka, M. Naeemuddin, A. D. Arenson, J. Durbin, R. G. David, P. E. Tabor, M. R. Bailey, D. R. DeShazo, J. Catanese, A. Mammoser, K. Osoegawa, P. J. de Jong, S. E. Celniker, R. A. Gibbs, G. M. Rubin, and S. E. Scherer.** 2000. A BAC-based physical map of the major autosomes of *Drosophila melanogaster*. Science **287:**2271-4.

22. **Howell, B. J., B. F. McEwen, J. C. Canman, D. B. Hoffman, E. M. Farrar, C. L. Rieder, and E. D. Salmon.** 2001. Cytoplasmic dynein/dynactin drives kinetochore protein transport to the spindle poles and has a role in mitotic spindle checkpoint inactivation. J Cell Biol **155:**1159-72.

23. **Jäger, H., M. Rauch, and S. Heidmann.** 2005. The *Drosophila melanogaster* condensin subunit Cap-G interacts with the centromere-specific histone H3 variant CID. Chromosoma **113**:350-361.

24. **Jiang, H., R. Guo, and J. A. Powell-Coffman.** 2001. The Caenorhabditis elegans hif-1 gene encodes a bHLH-PAS protein that is required for adaptation to hypoxia. Proc Natl Acad Sci U S A **98:**7916-21.

25. **Karess, R.** 2005. Rod-Zw10-Zwilch: a key player in the spindle checkpoint. Trends Cell Biol **15:**386-92.

26. **Kellogg, D. R., T. J. Mitchison, and B. M. Alberts.** 1988. Behaviour of microtubules and actin filaments in living *Drosophila* embryos. Development **103:**675-86.

27. **Kinoshita, K., T. L. Noetzel, L. Pelletier, K. Mechtler, D. N. Drechsel, A. Schwager, M. Lee, J. W. Raff, and A. A. Hyman.** 2005. Aurora A phosphorylation of TACC3/maskin is required for centrosome-dependent microtubule assembly in mitosis. J Cell Biol **170:**1047-55.

28. **Kops, G. J., B. A. Weaver, and D. W. Cleveland.** 2005. On the road to cancer: aneuploidy and the mitotic checkpoint. Nat Rev Cancer **5:**773-85.

29. **Lavista-Llanos, S., L. Centanin, M. Irisarri, D. M. Russo, J. M. Gleadle, S. N. Bocca, M. Muzzopappa, P. J. Ratcliffe, and P. Wappner.** 2002. Control of the hypoxic response in *Drosophila* melanogaster by the basic helix-loop-helix PAS protein similar. Mol Cell Biol **22:**6842-53.

30. **Lew, D. J., and D. J. Burke.** 2003. The spindle assembly and spindle position checkpoints. Annu Rev Genet **37:**251-82.

31. **Logarinho, E., H. Bousbaa, J. M. Dias, C. Lopes, I. Amorim, A. Antunes-Martins, and C. E. Sunkel.** 2004. Different spindle checkpoint proteins monitor microtubule attachment and tension at kinetochores in *Drosophila* cells. J Cell Sci **117:**1757-71.

32. **McIntosh, J. R., E. L. Grishchuk, and R. R. West.** 2002. Chromosome-microtubule interactions during mitosis. Annu Rev Cell Dev Biol **18:**193-219.

33. **Megraw, T. L., S. Kilaru, F. R. Turner, and T. C. Kaufman.** 2002. The centrosome is a dynamic structure that ejects PCM flares. J Cell Sci **115:**4707-18.

34. **Minden, J. S., J. W. Agard, J. W. Sedat, and B. M. Alberts.** 1989. Direct cell lineage analysis in *Drosophila melanogaster* by time lapse three dimensional optical microscopy of living embryos. J. Cell Biol. **109:**505-516.

35. **Morin, X., R. Daneman, M. Zavortink, and W. Chia.** 2001. A protein trap strategy to detect GFP-tagged proteins expressed from their endogenous loci in *Drosophila*. Proc Natl Acad Sci U S A **98:**15050-5.

36. **Nystul, T. G., J. P. Goldmark, P. A. Padilla, and M. B. Roth.** 2003. Suspended animation in C. elegans requires the spindle checkpoint. Science **302:**1038-41.

37. **Padilla, P. A., T. G. Nystul, R. A. Zager, A. C. Johnson, and M. B. Roth.** 2002. Dephosphorylation of cell cycle-regulated proteins correlates with anoxia-induced suspended animation in Caenorhabditis elegans. Mol Biol Cell **13:**1473-83.

38. **Padilla, P. A., and M. B. Roth.** 2001. Oxygen deprivation causes suspended animation in the zebrafish embryo. Proc Natl Acad Sci U S A **98:**7331-5.

39. **Peset, I., J. Seiler, T. Sardon, L. A. Bejarano, S. Rybina, and I. Vernos.** 2005. Function and regulation of Maskin, a TACC family protein, in microtubule growth during mitosis. J Cell Biol **170:**1057-66.

40. **Pinsky, B. A., and S. Biggins.** 2005. The spindle checkpoint: tension versus attachment. Trends Cell Biol **15:**486-93.

41. **Pouyssegur, J., F. Dayan, and N. M. Mazure.** 2006. Hypoxia signalling in cancer and approaches to enforce tumour regression. Nature **441:**437-43.

42. **Raff, J. W., K. Jeffers, and J. Y. Huang.** 2002. The roles of Fzy/Cdc20 and Fzr/Cdh1 in regulating the destruction of cyclin B in space and time. J Cell Biol **157:**1139-49.

43. **Savoian, M. S., M. K. Gatt, M. G. Riparbelli, G. Callaini, and D. M. Glover.** 2004. *Drosophila* Klp67A is required for proper chromosome congression and segregation during meiosis I. J Cell Sci **117:**3669-77.

44. **Sciambi, C. J., D. J. Komma, H. N. Skold, K. Hirose, and S. A. Endow.** 2005. A bidirectional kinesin motor in live *Drosophila* embryos. Traffic **6:**1036-46.

45. **Sharp, D. J., H. M. Brown, M. Kwon, G. C. Rogers, G. Holland, and J. M. Scholey.** 2000. Functional coordination of three mitotic motors in *Drosophila* embryos. Mol Biol Cell **11:**241-53.

46. **Sharp, D. J., G. C. Rogers, and J. M. Scholey.** 2000. Cytoplasmic dynein is required for poleward chromosome movement during mitosis in *Drosophila* embryos. Nat Cell Biol **2:**922-30.

47. **Taylor, S. S., M. I. Scott, and A. J. Holland.** 2004. The spindle checkpoint: a quality control mechanism which ensures accurate chromosome segregation. Chromosome Res **12:**599-616.

48. **Vader, G., R. H. Medema, and S. M. Lens.** 2006. The chromosomal passenger complex: guiding Aurora-B through mitosis. J Cell Biol **173:**833-7.

49. **Wadsworth, P., and E. D. Salmon.** 1988. Spindle microtubule dynamics: modulation by metabolic inhibitors. Cell Motil Cytoskeleton **11:**97-105.

50. **Zalokar, M., and I. Erk.** 1976. Division and migration of nuclei during early embryogenesis of *Drosophila* melanogaster. J.Microbiol.Cell. **25:**97-109.

Figure Legends

FIG. 1. Mitotic spindle organization in anoxia.

(A) Early *Drosophila* embryos during the synchronous syncytial blastoderm cycles were incubated in either normoxic ($+O_2$) or anoxic ($-O_2$) buffer for 2, 5 or 20 minutes (2', 5', 20') before fixation and labeling with anti-α-tubulin (Tub) and a DNA stain (DNA). Metaphase embryos reveal an increasing reduction of centrosome-proximal spindle fibers during anoxia. Bar = 10 μm.

(B) The pole to pole distances in metaphase spindles (in μm on y-axis +/- s.d.) after incubation (2 minutes) in either normoxic (white bars) or anoxic (black bars) buffer before fixation and immunolabeling (see A) was measured during mitosis 10, 11, 12 and 13. At least 25 different spindles from at least 5 different embryos were measured and averaged for each bar.

(C) Selected frames are shown after time lapse in vivo imaging of embryos expressing α-tubulin-GFP. Time in minutes after prometaphase onset is indicated in the lower left corners. In the presence of oxygen ($+O_2$, top row), the last metaphase frame is reached after 3.5 minutes, followed by anaphase (not shown). In the embryo made anoxic at the start of mitosis ($-O_2$, lower row), a metaphase arrest is maintained until after re-oxygenation ($+O_2$, lower row). The last frame before re-oxygenation at 15 minutes reveals the loss of centrosome-proximal spindle fibers (arrowheads) and a reduced spindle width (dashed lines) in comparison to normoxic metaphase spindles. Re-oxygenation is followed by a pronounced increase in centrosomal fibers (18 minutes, arrow) and spindle shortening (21 minutes) before an apparently normal metaphase spindle (27 minutes) precedes anaphase (not shown).

(D) The intercentrosomal distance in mitotic spindles was determined after in vivo imaging of embryos expressing GFP-D-TACC starting in prophase. Anaphase onset in normoxic conditions (x-x) is indicated by the open arrow. During the metaphase arrest in anoxic

conditions (o-o), the intercentrosomal distance extends slightly beyond normoxic metaphase values. Re-oxygenation (indicated by arrowhead $+O_2$) is followed by a pronounced shortening and eventual anaphase onset (black arrow). The given distances at each time point are average values of five different spindles observed in representative embryos.

FIG. 2. Mitotic spindle function in anoxia.

(A) Spindle checkpoint-deficient embryos lacking Mps1 protein kinase function were incubated during the synchronous syncytial blastoderm cycles in either normoxic ($+O_2$) or anoxic ($-O_2$) buffer for 5 minutes before fixation and labeling with anti-α-tubulin (Tub) and a DNA stain (DNA). The effects of anoxia on metaphase spindles do not depend on spindle checkpoint function (compare with Fig. 1A). Bar = 10 μm.

(B) Progression through mitosis was analyzed by in vivo imaging of *Mps1* mutant embryos expressing a green fluorescent Cenp-A/Cid centromere protein (Cenp-A) and a red fluorescent histone H2A variant (Histone H2Av) in either normoxic ($+O_2$, top row) or anoxic ($-O_2$, bottom row) conditions. Time in minutes starting in early prometaphase is indicated in the lower left corners of the selected frames. Chromosome congression in anoxia is slow and incomplete at the time of anaphase onset. Subsequent chromosome segregation is also slow. Some of the frequent lagging centromeres are indicated by arrowheads. Bar = 10 μm.

(C,D) Spindle checkpoint-competent embryos were incubated during the synchronous syncytial blastoderm cycles in either normoxic ($+O_2$) or anoxic ($-O_2$) buffer for 5 minutes before fixation and labeling with antibodies against α-tubulin (Tub), Cenp-A (Cenp-A) and a DNA stain (DNA). The relative resistance of kinetochore fibers against anoxia-induced depolymerization is illustrated with representative metaphase figures (C). Bar = 5 μm. Moreover, inter sister kinetochore distances were measured (n = 125 sister kinetochore pairs from at least 18 different embryos) and the average (in μm +/- s.d.) in prophase (pro) or

metaphase (meta) is given in (D). The average distance in normoxic ($+O_2$) and anoxic ($-O_2$) metaphase was found to be distinct ($p< 0.0001$ in t test; n=125). We did not detect significant variation in the average sister kinetochore separation with developmental stage (mitosis 11-13).

FIG. 3. Centrosome structure in anoxia.

Syncytial blastoderm embryos were incubated (20 minutes) in either normoxic ($+O_2$) or anoxic ($-O_2$) buffer before fixation and immunolabeling.

(A) anti-Aurora A kinase (AurA), anti-γ-tubulin (γ-Tub) and DNA (DNA) during metaphase

(B) anti-Centrosomin (Cnn) and DNA (DNA) during metaphase and (C) during interphase

(D) GFP-D-TACC (TACC), anti-γ-tubulin (γ-Tub) and DNA (DNA) during metaphase.

Insets in the lower left corners show a representative centrosome at higher magnification after labeling with anti-AurA (A) and anti-Cnn (B and C). Bars = 10 μm.

FIG. 4. Motor proteins in anoxia.

Syncytial blastoderm embryos were incubated in either normoxic ($+O_2$) or anoxic ($-O_2$) buffer for 2 or 5 minutes before fixation and immunolabeling.

(A) anti-Kinesin 8/Klp67A (KLP67A), anti-α-tubulin (Tub) and DNA stain (DNA). Klp67A decreases rapidly in the central spindle region in response to anoxia.

(B) dynein light intermediate chain-GFP (DLIC) and DNA. Dynein accumulates rapidly at metaphase plates (arrowhead) in response to anoxia. Bars = 10 μm.

FIG. 5. Kinetochore proteins in anoxia.

Syncytial blastoderm embryos were incubated in either normoxic ($+O_2$) or anoxic ($-O_2$) buffer for 20 minutes before fixation and immunolabeling.

(A) anti-Cenp-C (Cenp-C) and DNA stain (DNA).

(B) EGFP-Nuf2 (Nuf2) and DNA stain (DNA) in *gEGFP-Nuf2* embryos.

In response to anoxia, Cenp-C and EGFP-Nuf2 accumulate on spindles predominantly in the centrosome-proximal region. Bar = 10 μm.

FIG. 6. Spindle checkpoint proteins in anoxia.

(A) Selected frames after in vivo imaging of an embryo expressing EGFP-Mps1 (Mps1) and histone H2Av-mRFP (H2Av). Time in minutes is indicated in the frames showing the merged images in the bottom panel. Anoxia ($-O_2$) was induced at t = 1.75 minutes after the onset of chromosome condensation during entry into mitosis. The resulting EGFP-Mps1 accumulation within the equatorial region of metaphase figures (arrows) and in centrosome-associated filaments (arrowheads) is indicated. The embryo was re-oxygenated ($+O_2$) at t = 9.75 minutes during the metaphase arrest, resulting in EGFP-Mps1 disappearance and completion of mitosis. Bar = 10 μm.

(B) Frames showing EGFP-Mps1 at high magnification within the equatorial region of a metaphase figure during the anoxia-induced mitotic arrest. Time in seconds is indicated within each frame. An EGFP-Mps1 particle moving along the spindle is indicated by arrowheads.

(C) High magnification views of single nuclei from syncytial *gEGFP-Mps1* embryos during interphase. The embryos were fixed and labeled with anti-γ-tubulin (γ-Tub) and DNA stain (DNA) after a 20 minute incubation in either normoxic ($+O_2$) or anoxic ($-O_2$) buffer. The weak centrosomal EGFP-Mps1 (Mps1) signals in normoxic embryos (arrowhead), as well as the strong signals in sub-centrosomal dots in anoxic embryos (arrow) are indicated. Bar = 10 μm.

(D) EGFP-Mps1 signals (Mps1) in cortical regions of pre-blastoderm embryos which were fixed after a 20 minute incubation in either normoxic ($+O_2$) or anoxic ($-O_2$) buffer. Anoxia induced filamentous or dot-like EGFP-Mps1 aggregates. Bar = 5 μm.

(E) *EGFP-BubR1* embryos were fixed and labeled with anti-γ-tubulin (γ-Tub) and DNA stain (DNA) after a 20 minute incubation in either normoxic ($+O_2$) or anoxic ($-O_2$) buffer. In response to anoxia, EGFP-BubR1 (BubR1) accumulates within the equatorial region of metaphase figures and in peri-centrosomal filaments (arrowhead). Bar = 5 μm.
(F) *gEGFP-Mps1* embryos were fixed and labeled with anti-BubR1 (BubR1) and DNA stain (DNA) after a 20 minute incubation in anoxic ($-O_2$) buffer. EGFP-Mps1 (Mps1) and anti-BubR1 signals largely overlap in the in peri-centrosomal filaments (arrowhead).
(G,H,I) *EGFP-Bub3* (G), *EGFP-Rod* (H), or *EGFP-Fzy* (I) embryos were fixed after a 20 minute incubation in either normoxic ($+O_2$) or anoxic ($-O_2$) buffer and labeled with a DNA stain (G-I; DNA) and anti-α-tubulin (H; Tub). Bar = 5 μm.

FIG. 7. Mps1 modification in response to anoxia.
gEGFP-Bub3 embryos were fixed and labeled with DNA stain (DNA) after a 20 minute incubation in either normoxic ($+O_2$) or anoxic ($-O_2$) buffer. Syncytial blastoderm embryos during interphase (i) or metaphase (m) were sorted using a microscope. Anoxic interphase embryos were further sorted into early interphase (ie) and late interphase (il) based on the appearance of chromatin which is condensed into a meshwork during early interphase and into distinct chromatids during late interphase. Sorted embryos were used for extract preparation and immunoblotting with anti-Mps1 (Mps1) and anti-GFP (Bub3).

FIG. 8. Spindle checkpoint activation by cytochrome oxidase inhibitor.
gEGFP-Mps1 embryos were incubated in either absence (- CN) or presence (+ CN) of cyanide for 5 (A) or 15 (B) minutes before fixation and labeling with anti-α-tubulin (Tub) and a DNA stain (DNA). Cyanide induces re-organization of EGFP-Mps1 (Mps1), microtubules and chromatin during metaphase (A) and interphase (B) which is indistinguishable from the effects of anoxia. Bar = 5 μm.

Figure 1

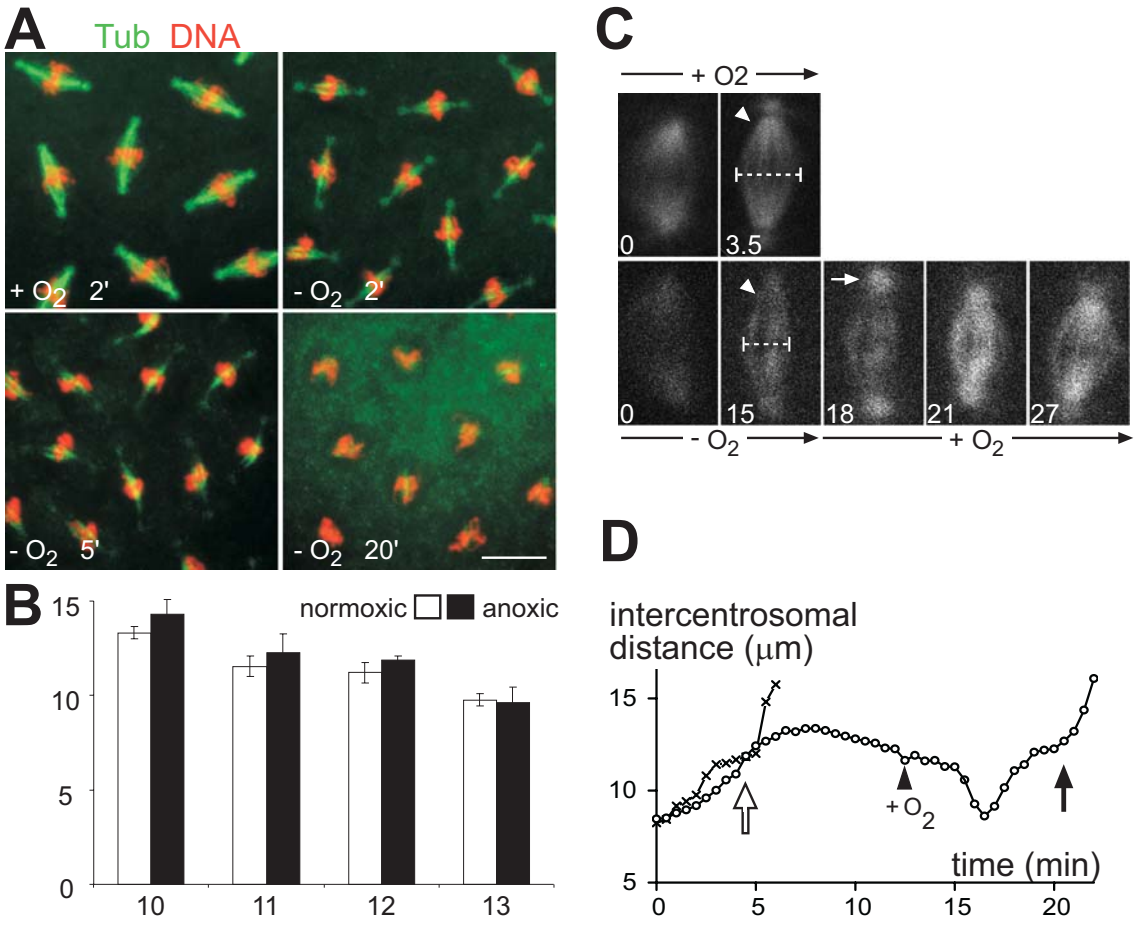
A
Tub DNA
+ O2 2'
- O2 2'
- O2 5'
- O2 20'
B
normoxic
anoxic
15
10
5
0
10
11
12
13
C
+ O2
0
3.5
0
15
18
21
27
- O2
+ O2
D
intercentrosomal distance (μm)
15
10
5
+ O2
time (min)
0
5
10
15
20

Figure 2

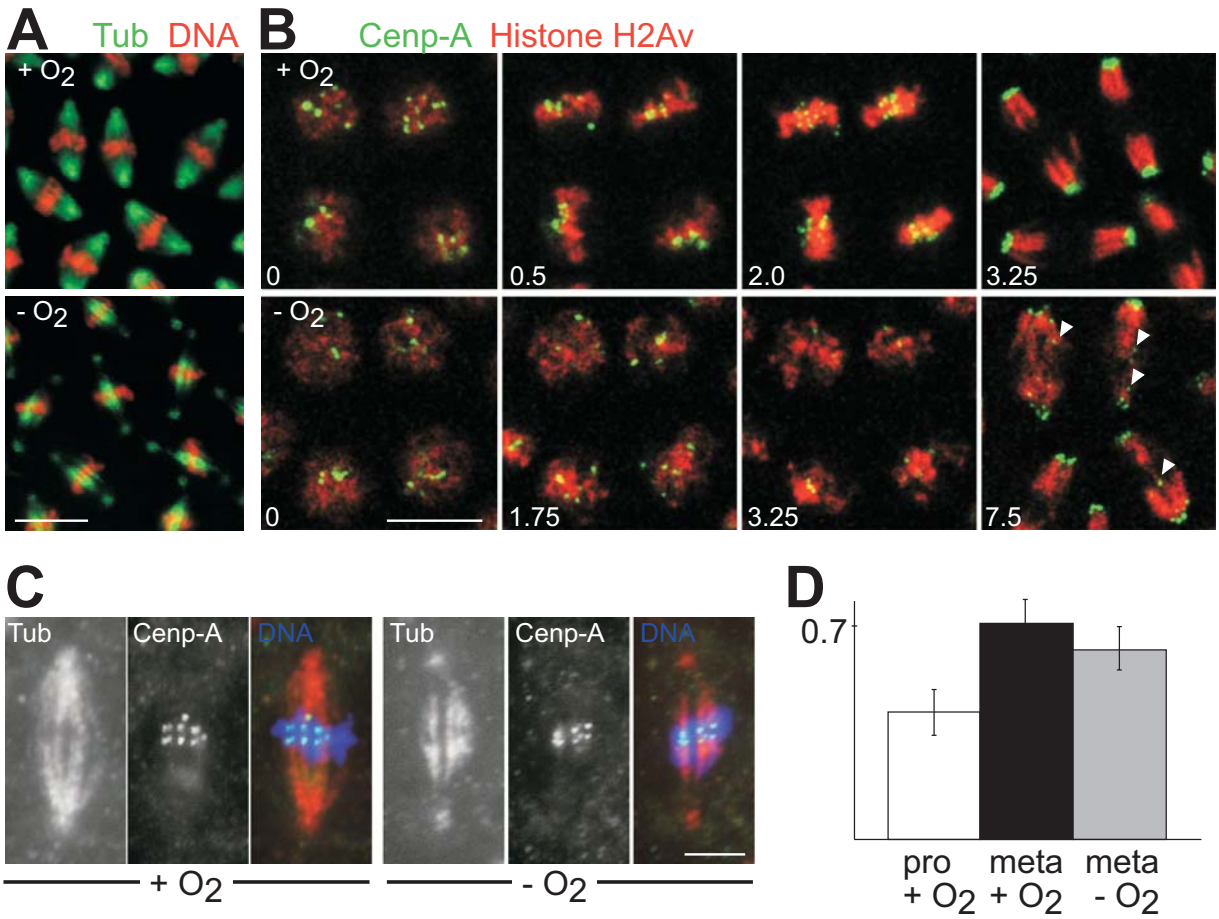
A
Tub DNA
+ O2
- O2
B
Cenp-A Histone H2Av
+ O2
- O2
0
0.5
2.0
3.25
0
1.75
3.25
7.5
C
Tub
Cenp-A
DNA
Tub
Cenp-A
DNA
+ O2
- O2
D
0.7
pro + O2
meta + O2
meta - O2

Figure 3

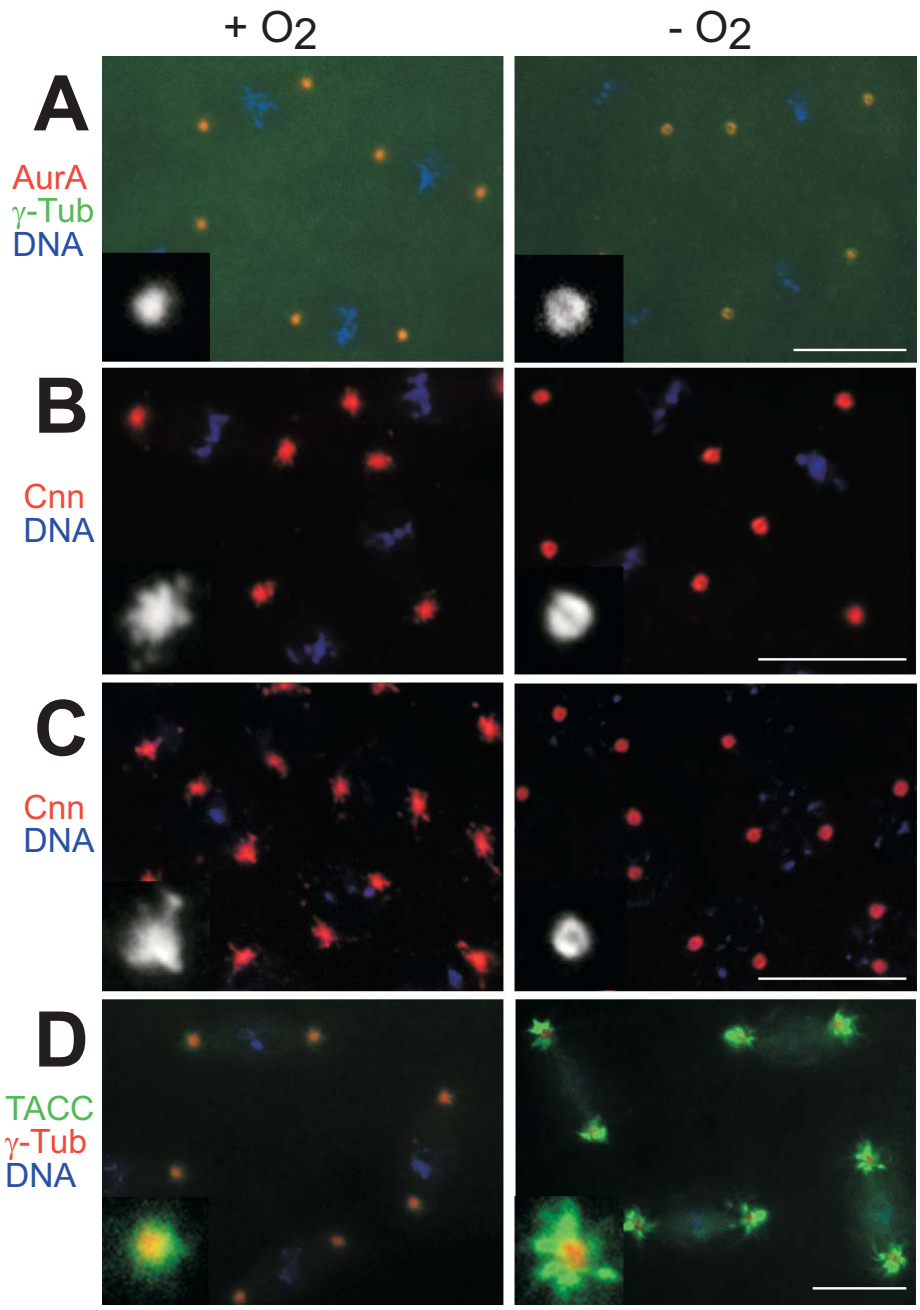

Figure 4

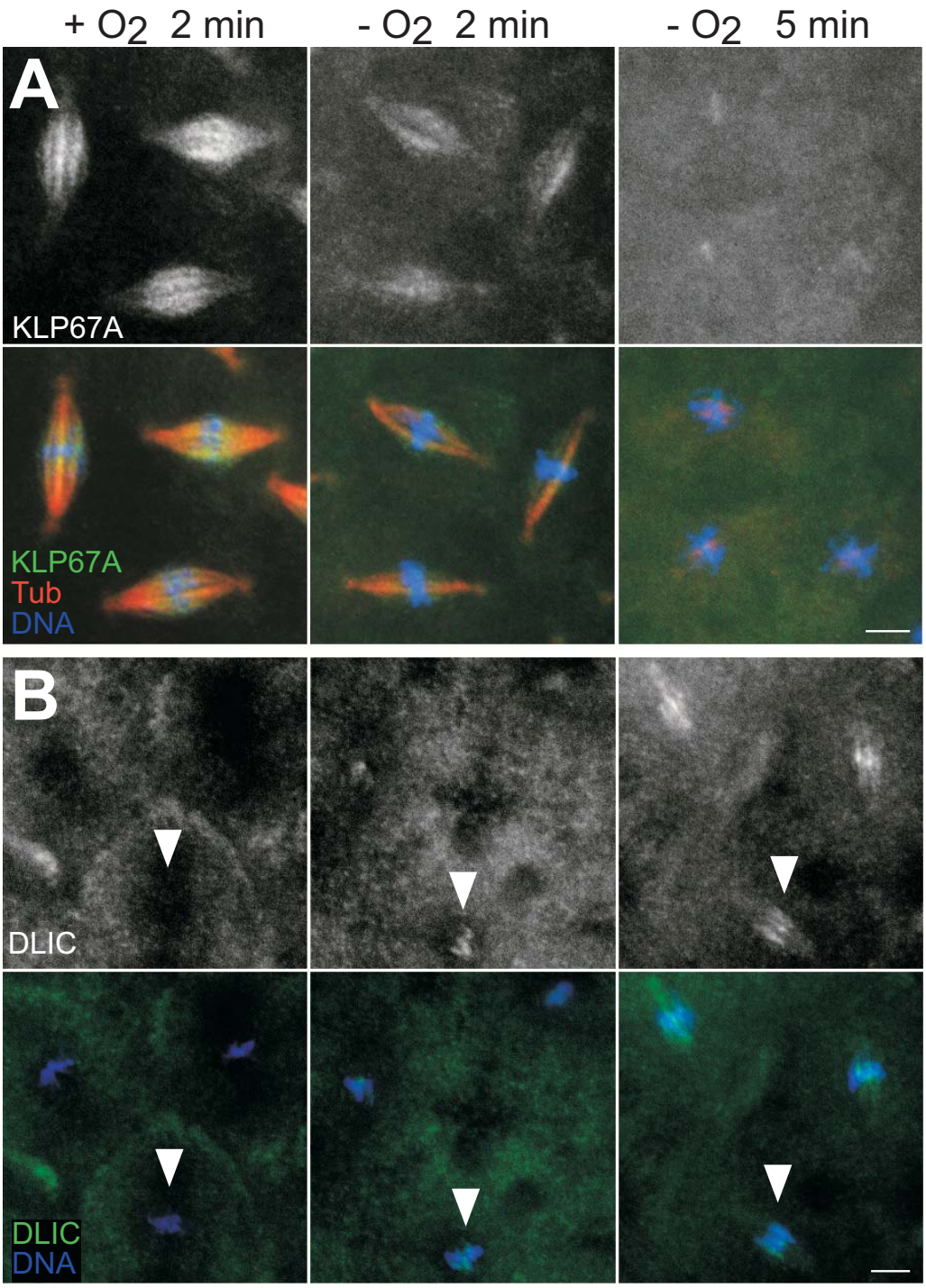

Figure 5

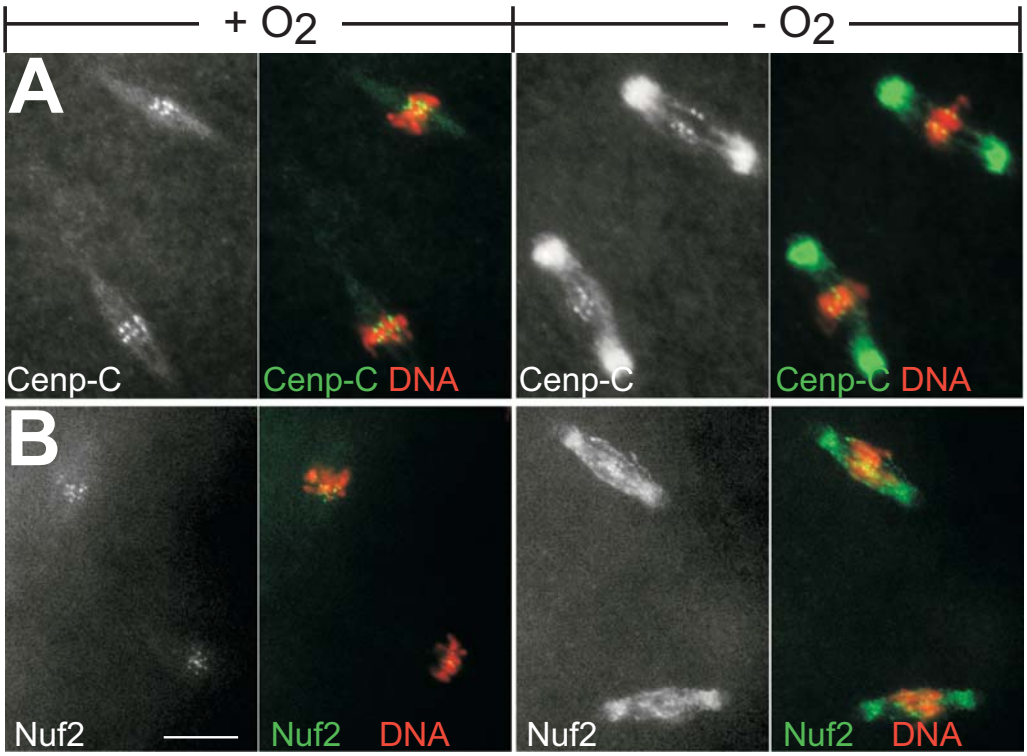
+ O2
- O2
A
Cenp-C
Cenp-C DNA
Cenp-C
Cenp-C DNA
B
Nuf2
Nuf2 DNA
Nuf2
Nuf2 DNA

Figure 6

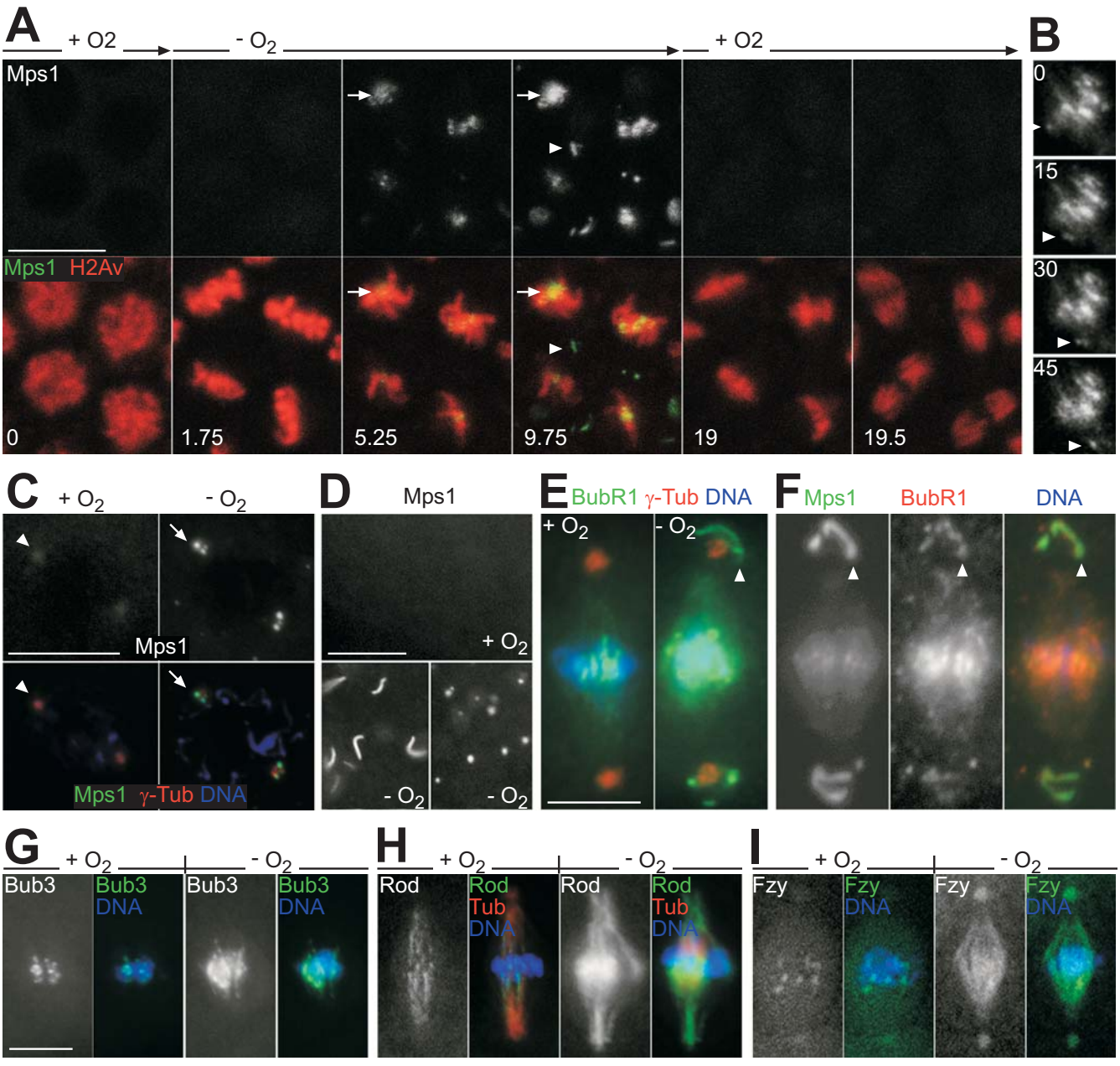
A
+ O2
- O2
+ O2
Mps1
Mps1 H2Av
0
1.75
5.25
9.75
19
19.5
B
0
15
30
45
C
+ O2
- O2
Mps1
Mps1 γ-Tub DNA
D
Mps1
+ O2
- O2
- O2
E
BubR1 γ-Tub DNA
+ O2
- O2
F
Mps1
BubR1
DNA
G
+ O2
- O2
Bub3
Bub3 DNA
Bub3
Bub3 DNA
H
+ O2
- O2
Rod
Rod Tub DNA
Rod
Rod Tub DNA
I
+ O2
- O2
Fzy
Fzy DNA
Fzy
Fzy DNA

Figure 7

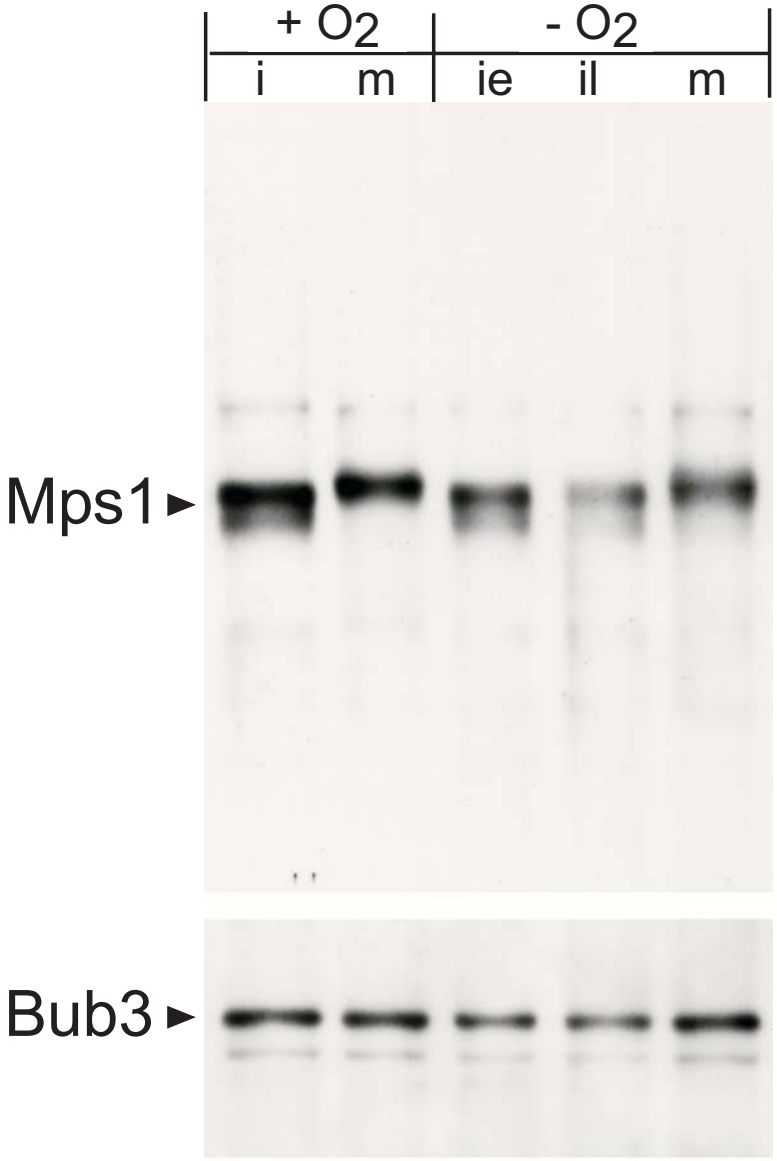

Figure 8

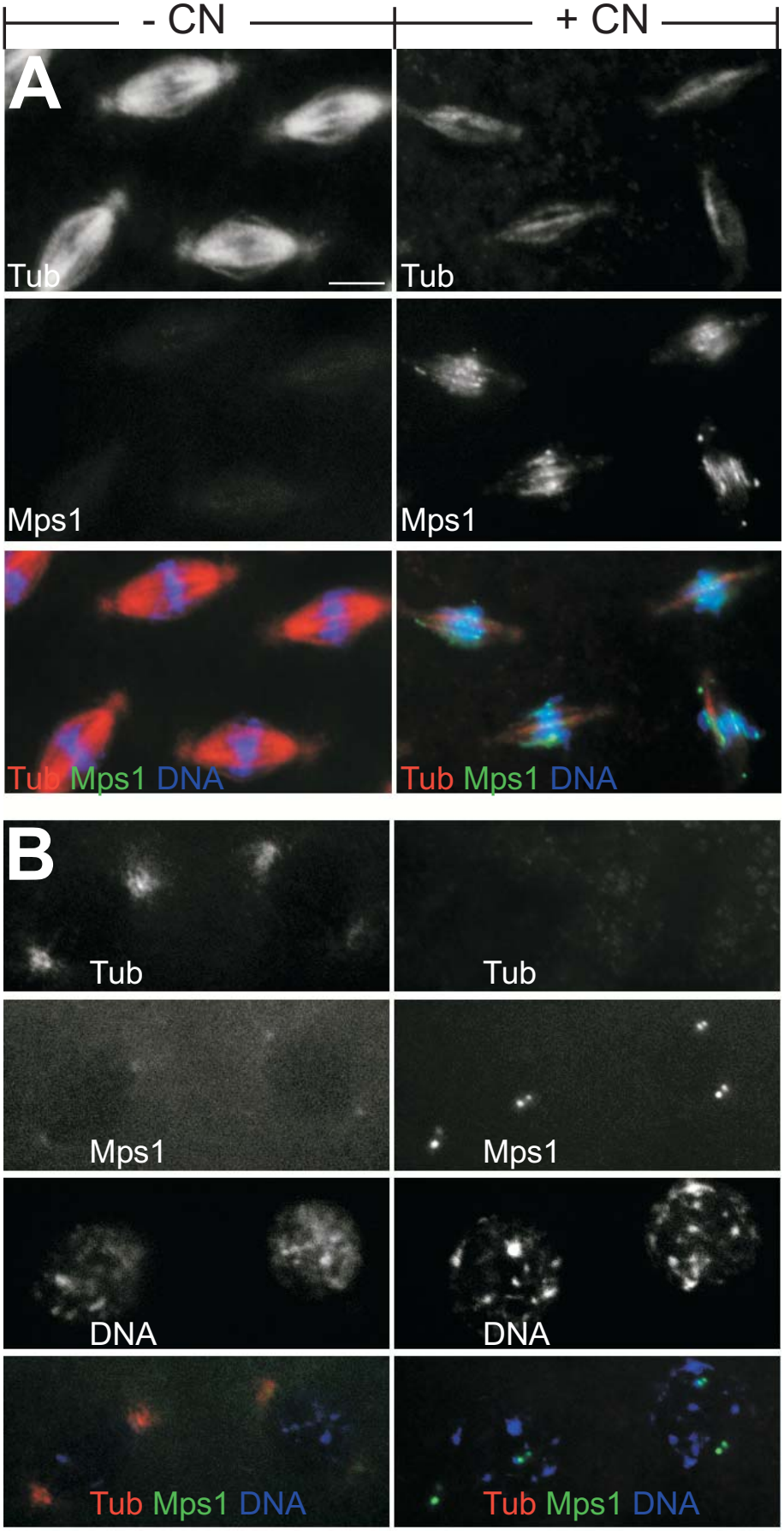
- CN
+ CN
A
Tub
Tub
Mps1
Mps1
Tub Mps1 DNA
Tub Mps1 DNA
B
Tub
Tub
Mps1
Mps1
DNA
DNA
Tub Mps1 DNA
Tub Mps1 DNA

Erklärung

Hiermit versichere ich, die vorliegende Arbeit selbständig verfaßt und keine anderen als die von mir angegebenen Quellen und Hilfsmittel benutzt zu haben.

Ferner erkläre ich, daß ich weder an der Universität Bayreuth noch an einer anderen Hochschule versucht habe, eine Dissertation einzureichen, oder mich einer Promotionsprüfung zu unterziehen.

Sebastian Heeger

Bayreuth, 01.12.2006